THE SYNTHESIS, REACTIVITY & MAGNETISM OF LANTHANIDE ORGANOMETALLIC & COORDINATION COMPLEXES

A thesis submitted to the University of Manchester for the degree of Doctor of Philosophy in the Faculty of Science and Engineering

---

2017

Richard Grindell

School of Chemistry

Table of Contents

Word Count – 41,423

List of Figures

List of Schemes

List of Tables

List of Equations

List of Common Terms and Abbreviations

9-BBN -9-borabicyclo[3.3.1]nonane

Bipy – 2,2'-bipyridine

Cp – cyclopentadienyl

Cp* - pentamethyl(cyclopentadienyl)

Cp^{Me4} - tetramethyl(cyclopentadienyl)

Cp^{Me} - methyl(cyclopentadienyl)

Cp' - trimethylsilyl(cyclopentadienyl)

Cp'' – bis(trimethylsilyl)cyclopentadienyl

DME – dimethoxyethane

E – element

HAN - hexaazatrinapthalene

HOMO – highest occupied molecular orbital

IMes – 1,3-bis(2,4,6-trimethylphenyl)imidazol-2-ylidene

IPr – 1,3-bis-(2,6-diisopropylphenyl)imidazol-2-ylidene

IR – infrared

I^{t}Bu – 1,3-bis-(tert-butyl)imidazol-2-ylidene

KC_8 – potassium graphite

KD – Kramers doublet

Ln – lanthanide and/or rare-earth metal

LUMO - lowest unoccupied molecular orbital

M – metal

Mes – mesityl

NMR – nuclear magnetic resonance

QTM – quantum tunnelling of magnetisation

RT – room temperature

SMM – single molecule magnet

THF – tetrahydrofuran

TM – transition metal

Trisox – tris(oxazolinyl)ethane

UV – ultra violet

XRD – X-ray diffraction

Abstract

This project was focused on the synthesis and reactivity of rare-earth ^{n}butyl complexes of the formula $[Cp^{Me}_2M(\mu\text{-}^{n}Bu)]_2$ (where M = Y, Dy). Dysprosium was used as it has a large magnetic moment which is favourable for producing single molecule magnets (SMMs). Yttrium was used as a diamagnetic analogue to examine the reactivity of $[Cp^{Me}_2Y(\mu\text{-}^{n}Bu)]_2$ in solution, and provide further characterisation of isolated complexes with NMR spectroscopy. Another goal of the project was to establish the reactivity of $[Cp^{Me}_2M(\mu\text{-}^{n}Bu)]_2$ with respect to the commonly used alkylating reagent ^{n}butyllithium (^{n}BuLi).

It was found that the ^{n}butyl complexes are remarkably stable in solution and the solid state, allowing for the synthesis to be scaled up and for the ^{n}butyl complexes to be used as starting materials. The reactivity of $[Cp^{Me}_2M(\mu\text{-}^{n}Bu)]_2$ towards ferrocene was investigated. The product was a ferrocenyl-bridged dimer of the formula $[Cp^{Me}_2M(\mu\text{-}(C_5H_4)FeCp)]_2$ resulting from a single deprotonation of ferrocene. The reactivity of $[Cp^{Me}_2M(\mu\text{-}^{n}Bu)]_2$ towards N-heterocyclic carbenes (NHCs) was also investigated. No reaction occurred between $[Cp^{Me}_2Y(\mu\text{-}^{n}Bu)]_2$ and 1,3-bis-(2,6-diisopropylphenyl)imidazol-2-ylidene (IPr), a reaction did occur between $[Cp^{Me}_2Y(\mu\text{-}^{n}Bu)]_2$ and 1,3-bis-(tert-butyl)imidazol-2-ylidene (I^{t}Bu) but no crystalline product could be obtained. $[Cp^{Me}_2M(\mu\text{-}^{n}Bu)]_2$ reacts with 1,3-bis(2,4,6-trimethylphenyl)imidazol-2-ylidene (IMes) to form a monomeric, benzyl tethered carbene complex $[Cp^{Me}_2M(IMes')]$. An *ortho*-methyl group on one of the mesityl substituents is deprotonated generating an asymmetric functionalised carbene. A control experiment between Cp^{Me}_3M (M = Dy, Y) and IMes resulted in the formation of the abnormal, rearranged carbene complexes $[Cp^{Me}_3M(aIMes)]\cdot C_6H_6$. Structural analysis revealed a very short C-H---π interaction between neighbouring molecules. The mechanism of carbene rearrangement was probed by ^{1}H NMR spectroscopy (M = Y). Magnetic susceptibility measurements revealed that $[Cp^{Me}_2Dy(\mu\text{-}^{n}Bu)]_2$, $[Cp^{Me}_2Dy(\mu\text{-}(C_5H_4)FeCp)]_2$, $[Cp^{Me}_2Dy(IMes')]$ and $[Cp^{Me}_3Dy(aIMes)]\cdot C_6H_6$ are not SMMs.

$[Cp^{Me}_2M(\mu\text{-}^{n}Bu)]_2$ activates sulfur and selenium to form hexanuclear clusters of the formula $[Cp^{Me}_{10}M((E_3)_2E_2]$ (M = Dy, Y; E = S, Se). $[Cp^{Me}_{10}M((S_3)_2S_2]$ is an SMM with an energy barrier to magnetisation reversal, U_{eff}, of 73 cm^{-1}. The analogous selenium cluster could be characterised by single crystal X-ray diffraction however separation from unreacted selenium proved difficult without using coordinating solvent. Extraction of $[Cp^{Me}_{10}Y((Se_3)_2Se_2]$ with THF resulted in the crystallisation of the ion pair $[Cp^{Me}_2Y(THF)_3][\{Cp^{Me}Y(Se_2)\}_6Se]$ and $[\{Cp^{Me}_2Y(THF)\}(\mu\text{-}Se_2)]$.

A trimetallic dysprosium coordination complex containing a hexaazatrinapthalene (HAN) bridging ligand is reported. Magnetic measurements on $[\{(thd)_3Dy\}_3HAN]$ (Dy_3HAN) show that it is an SMM in zero field and two magnetic relaxation mechanisms are present. An optimised DC field of 1 kOe allowed for better resolution of the two relaxation processes and an energy barrier for each process could be extracted. The U_{eff} barriers are 42 and 52 cm^{-1}. *Ab initio* theoretical analysis revealed the magnetic anisotropy axes are nearly collinear precluding the presence of a toroidal magnetic moment. The ground state of Dy_3HAN was found to be frustrated.

Declaration

No portion of the work referred to in the thesis has been submitted in support of an application for another degree or qualification of this or any other university or other institute of learning.

Copyright Statement

i. The author of this thesis (including any appendices and/or schedules to this thesis) owns certain copyright or related rights in it (the "Copyright") and s/he has given The University of Manchester certain rights to use such Copyright, including for administrative purposes.

ii. Copies of this thesis, either in full or in extracts and whether in hard or electronic copy, may be made only in accordance with the Copyright, Designs and Patents Act 1988 (as amended) and regulations issued under it or, where appropriate, in accordance with licensing agreements which the University has from time to time. This page must form part of any such copies made.

iii. The ownership of certain Copyright, patents, designs, trade marks and other intellectual property (the "Intellectual Property") and any reproductions of copyright works in the thesis, for example graphs and tables ("Reproductions"), which may be described in this thesis, may not be owned by the author and may be owned by third parties. Such Intellectual Property and Reproductions cannot and must not be made available for use without the prior written permission of the owner(s) of the relevant Intellectual Property and/or Reproductions.

iv. Further information on the conditions under which disclosure, publication and commercialisation of this thesis, the Copyright and any Intellectual Property and/or Reproductions described in it may take place is available in the University IP Policy (see http://documents.manchester.ac.uk/DocuInfo.aspx?DocID=487), in any relevant Thesis

restriction declarations deposited in the University Library, The University Library's regulations (see http://www.manchester.ac.uk/library/aboutus/regulations) and in The University's policy on Presentation of Theses

Acknowledgements

I'd like to take the opportunity to thank Prof Richard Layfield for giving me the opportunity to pursue a career in research and EPSRC for the funding that makes the chemistry happen. I've been able to gain understanding and bounce ideas off many people in the Layfield group and thanks go to those members past and present for their insight and support throughout the last three and a half years. I've learnt a lot about X-ray crystallography from Dr Ben Day and a lot about single molecule magnetism from our resident magnetochemist Dr Fu-Sheng Guo, their advice has been invaluable.

On the personal side thanks go to my family and friends who have experienced second hand the trials, tribulations and very occasionally the sheer ecstasy of being an academic researcher. Special thanks go to my wonderful girlfriend Mary and her family who always have a morale-boosting word to help perk me up through those difficult times we academics often face.

Chapter 1

Introduction to Organo-Lanthanide Chemistry

1 Introduction to Trivalent Organo-Lanthanide Chemistry

The chemistry of the lanthanides (also known as rare-earth metals which include scandium, yttrium and lanthanum) is dominated by the +3 oxidation state. This is due primarily to the radially contracted nature of the 4f valence orbital set and the relative ease of removing the two electrons in the 6s orbital (for La and the lanthanides) and the 5s orbital (for Y). The main exception is Ce which can exist in the +4 oxidation state, samarium, europium, thulium and ytterbium can also adopt the +2 oxidation state. Recently, it has been found that all the lanthanides can be stabilised in the +2 oxidation state using cyclopentadienyl ligands.[1] For the early lanthanides the 5d orbitals are relatively low in energy and cerium has a ground state electron configuration of $[Xe]4f^{1}5d^{1}6s^{2}$ as opposed to $[Xe]4f^{2}6s^{2}$. The fourth ionisation energies of all the lanthanides are large thus limiting redox behaviour. As a result the chemistry of trivalent lanthanide complexes is dominated by just a few types of reactivity, the most prominent being; salt metathesis, σ-bond metathesis, Lewis acid-base interactions, deprotonation and ligand-based reduction. The lanthanide contraction also plays a key role in reactivity, it is a phenomenon that arises from an increasing effective nuclear charge as the 4f orbital is filled across the period. The result is a larger than expected decrease in ionic radius across the series from La^{3+} to Lu^{3+} due to relativistic effects.

The inception of lanthanide organometallic chemistry was brought about by the discovery of the tris(cyclopentadienyl) lanthanide complexes ($LnCp_3$) by Wilkinson *et. al.* in 1954.[2] This followed the discovery of the structure of ferrocene in the same group in the early 1950s.[3] At the time, no organometallic compounds of the rare-earth metals were known, so this was a very important study which helped establish many facts about the lanthanide ions and their reactivity.

The complexes $LnCp_3$ (where Ln = Sc, Y, La, Ce, Pr, Nd, Sm and Gd) were synthesised by a

salt metathesis reaction between the corresponding lanthanide trichloride and cyclopentadienyl sodium. A key discovery here was that the products were volatile and could be isolated as pure crystalline solids by sublimation at high temperature (200-250°C) under vacuum. They are also thermally stable up to 400°C and decompose on contact with air and moisture.

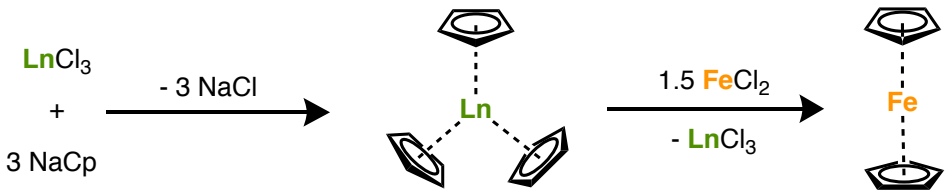

Scheme 1.1. Synthesis of $LnCp_3$ reported by Wikinson *et. al.* Ionic nature of the lanthanides demonstrated by formation of ferrocene upon reaction of $LnCp_3$ with $FeCl_2$.[2]

It is common knowledge today that the bonding of rare-earth metals is almost completely ionic, due to the radially contracted nature of the 4f orbital manifold. The $LnCp_3$ complexes were found to behave in this way by reacting them with $FeCl_2$ in THF, which gave ferrocene in quantitative yield.

1.1 Organo-Rare Earth Alkyl Complexes: Structure and Reactivity

1.1.1 Tris(alkyl) Rare-Earth Complexes

Some of the most reactive metal-carbon bonds are Ln—C bonds due to relatively long bond distances, with respect to TM—C bonds, and the ionic nature of the bonding. In 1973 Lappert *et. al*. reported the synthesis of the first alkyl complexes of the rare-earth elements scandium and yttrium: $[Ln(CH_2SiMe_3)_3(THF)_2]$ (**1.1**) and $[Ln(Np)_3(THF)_2]$ (**1.2**) (Np – neopentyl).[4] The ionic nature of lanthanide compounds is demonstrated in the synthesis of these *tris*(alkyl) complexes. The reaction between $LnCl_3$ and $LiCH_2SiMe_3$ is a salt metathesis

driven by the high lattice formation enthalpy of LiCl. The crystal structure of **1.1** was reported by Schumann *et. al.* in 2002.[5] Due to the low steric demand of the $-CH_2SiMe_3$ ligand the coordination geometry differs substantially across the 4f row. The Sm analogue has a distorted octahedral geometry with two CH_2SiMe_3 ligands and two *cis*- THF ligands. However, the Er, Yb and Lu analogues have a trigonal bipyramidal geometry with all the CH_2SiMe_3 ligands occupying the equatorial plane (see Figure 1.1). Compound **1.1** is thermally sensitive and prone to decomposition. The thermally stable ^{t}Bubipy adduct (^{t}Bu$_2$bipy)Lu(CH_2SiMe_3)$_3$ (**1.3**) was synthesised by Kiplinger et. al., but the reactivity was hampered by the fact that the bipy fragment remained bound to lutetium in the products which may not be desirable.[6]

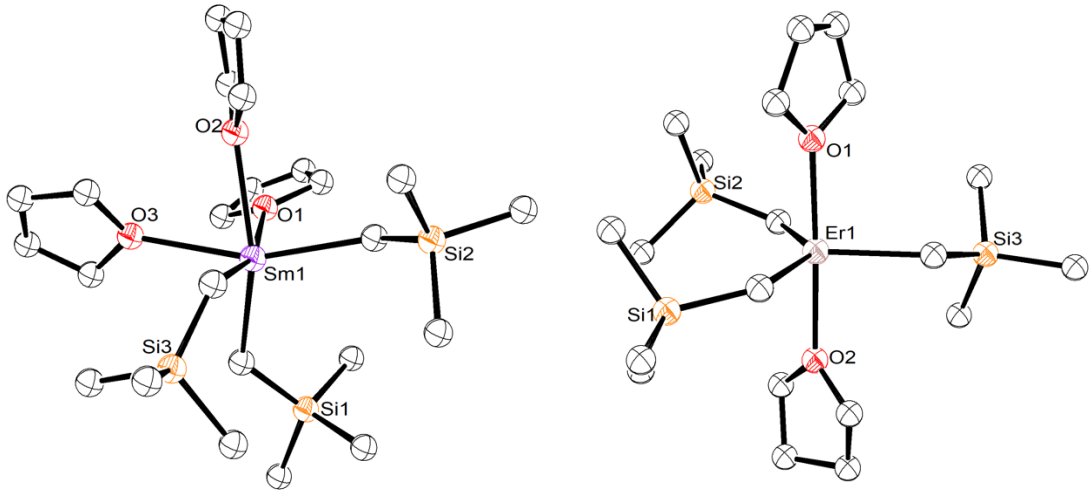

Figure 1.1. Molecular structures of [Sm(CH_2SiMe_3)$_3$(THF)$_3$] (left) and [Er(CH_2SiMe_3)$_3$(THF)$_3$] (right) highlighting differences in coordination geometry with decreasing Ln^{3+} ionic radius.[5]

Organolanthanide complexes often acts as Brønsted bases, reacting with an acidic E—H substrate and releasing a protonated ligand and forming a new Ln—E bond. Compound **1.1** has been used in a wide variety of deprotonation chemistry to make heteroleptic mono- or di-alkyl complexes of the formula $R_nLn(CH_2SiMe_3)_{n-1}$. Compound **1.1** is a good starting material because it is not prone to β-H elimination. In 2008, Kiplinger *et. al.* reported the first lanthanide phosphinidene complex: [{(2-^{i}Pr$_2$P-4-MePh)$_2$N}Lu=PMes] (**1.4**), synthesised

by reacting the PNP-pincer complex [{(2-^{i}Pr$_2$P-4-MePh)$_2$N}Lu(CH$_2$SiMe$_3$)$_2$] (**1.5**) with one equivalent of MesPH$_2$.[7] Compound **1.5** deprotonates MesPH$_2$ twice, releasing tetramethylsilane, to afford the phosphinidene in 52 % yield (Scheme 1.2).

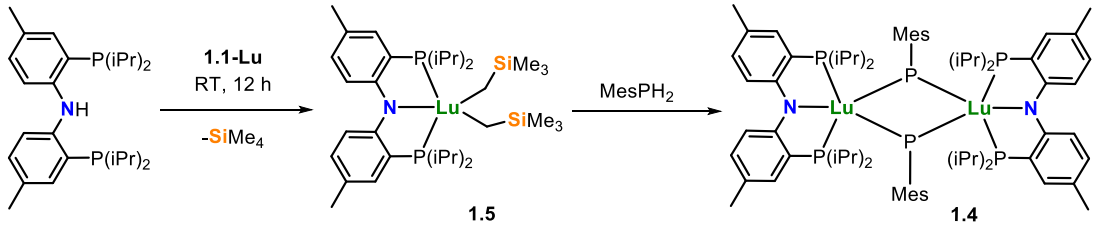

Scheme 1.2. Synthesis of the lutetium phosphinidine complex **1.4** using *tris*(alkyl) precursor.[7]

Another form of reactivity often seen in rare-earth alkyl complexes is insertion of unsaturated E=E substrates into the M—C bond (E = C=C, C=N etc). The 4f orbitals are radially contracted and interaction of C=C and C=E substrates with rare-earth metals are mostly electrostatic, so there is no orbital overlap with C=E π-orbitals. As a result, the reactivity is predominantly ligand based. C=C and C=N bonds are more polarisable than C-C and C-N single bonds and are thus more susceptible to nucleophilic attack when coordinated to a hard Lewis acidic metal centre. An example of such reactivity is that of **1.1-Lu** in the dearomatisation of N-heterocycles including terpyridines and pyrimidines. Kiplinger *et. al.* showed that by reacting one equivalent of **1.1-Lu** with terpyridine or 4,4',4''-tri-tertbutyl-2,2':6'-2''-terpyridine (^{t}Bu$_3$terpy) in toluene resulted in the formation of the 1,3-alkyl migration product **1.6** (Scheme 1.3).[8]

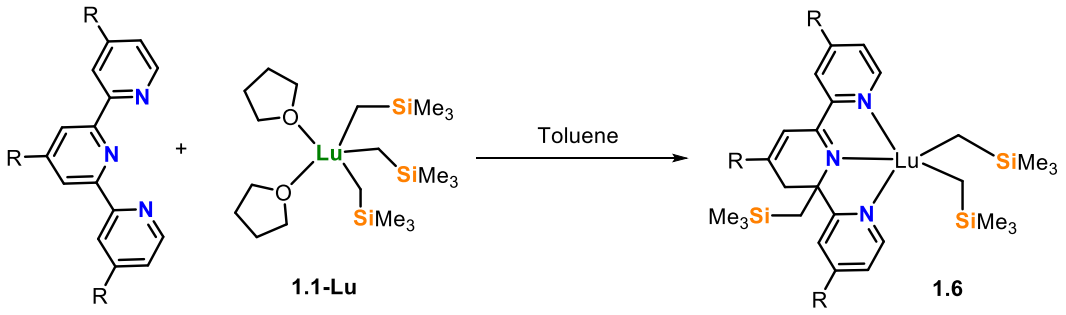

Scheme 1.3. Dearomatisation of terpyridines (R = H – terpy; R = tBu – tBu_3terpy) using **1.1-Lu**. R = H, ^{t}Bu.[8]

The central pyridine ring is dearomatised with the C=N bond being reduced to a single C—N bond with the $–CH_2SiMe_3$ group bound to the C α to the N atom. In the process electrons in the C=N π-bond move onto the N, forming an anionic amide ligand. To test the scope of this reactivity, ^{t}Bu_3tpy and tpy were reacted with $Cp^*Lu(CH_2SiMe_3)_2(THF)$. Upon stirring in hexanes at RT followed by work up XRD and NMR spectroscopy showed the reaction had quantitatively formed the 1,3-alkyl migration product in each case. Density functional theory (DFT) studies on the unsubstituted alkyl-terpy product and the target compound (^{t}Bu_3terpy)$Cp^*Lu(CH_2SiMe_3)_2$ show that the 1,3-migration product is more stable by 23.5 kcal mol^{-1} which is a significant energy change. An explanation for this is that there would be considerable relief of steric pressure after 1,3-alkyl migration takes place as the lutetium coordination number is reduced from 8 to 7.

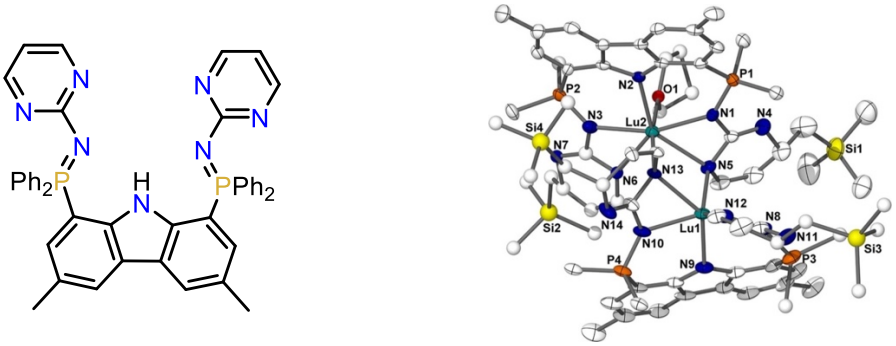

Figure 1.2. (Left) The bis(phosphinimine)carbazole (bpicbz-H) ligand. (Right) Molecular structure of **1.7**. Lu2 has pentagonal bipyramidal coordination geometry. Figure taken from reference 9.[9]

Hayes *et. al*. reported on the reactivity of **1.1-Lu** with pyrimidines in 2013 although the ligands used differ somewhat from the Kiplinger study.[9] The ligand used here was a bis(phosphinimine)carbazole (bpicbz-H) synthesised from 2-azidopyrimidine and 1,8-diphenylphosphino-3,6-dimethylcarbazole. Bpicbz-H and **1.1-Lu** were reacted in toluene-d_8 at -78°C and the reaction was followed *in situ* by multinuclear NMR spectroscopy at -10°C which showed formation of the carbazolyl-Lu complex [(bpicbz)Lu(CH_2SiMe_3)$_2$]. This was not isolated, however a reaction in 2:1 toluene-THF mixture over 18 hrs at room temperature (RT) gave a double alkyl insertion (migration) product **1.7** (Figure 1.2). As with the terpyridine reaction reported previously, the C=N bonds in the pyrimidine rings were dearomatised to C—N single bonds with the alkyl group bonded to the C α to one of the pyrimidine nitrogen atoms. The electrons in the heterocycle then shift onto the other nitrogen atom forming an amide ligand. Despite the steric encumbrance of the cbz ligand the alkyl migration product forms a dimer with the pyrimidine amide nitrogen atoms bridging between 2 lutetium ions. Interestingly, one of the lutetium ions has a coordinated THF and is 7 coordinate while the other is 6 coordinate. The 7 coordinate Lu^{3+} ion in **1.7** is approaching D_{5h} symmetry which is considered a favourable coordination geometry for single molecule magnet (SMM) behaviour in Dy^{3+} ions.[10-12]

1.1.2 Mono(cyclopentadienyl) Rare-Earth Alkyl Complexes

Complexes of the formula [Cp^RLn-R'$_2$(X)] (where R = Cp substituent(s), R' = alkyl and X = donor solvent) have displayed a range of reactivity including C—H activation, insertion and protonolysis to form cationic complexes, the latter having applications in catalysis.[13] Also referred to as 'half-sandwich' complexes, mono(cyclopentadienyl) rare-earth alkyls are typically synthesised from tris(alkyl) precursors with cyclopentadienes. One example is the lutetium complex [Cp*Lu(CH_2SiMe_3)$_2$(THF)] (**1.8**) reported by Scott *et. al.* in 2004.[14] Compound **1.8** is synthesised by reacting one equivalent of Cp*H with **1.1-Lu** in THF, the

THF can be displaced by DME or 2,2'-bipyridine (bipy). [Cp*Lu(CH_2SiMe_3)$_2$(bipy)] (**1.9**) deprotonates 2 equivalents of the bulky aniline Dipp-NH_2 to form the corresponding amide, [Cp*Lu(N(H)Dipp)$_2$(bipy)]. Compound **1.9** reacts with two equivalents of phenylacetylene to give the unexpected butatriendiyl bridged complex [{Cp*Lu(CCPh)(bipy)}$_2$(μ-η_2:η_2-PhC_4Ph)] (**1.10**) with one acetylide ligand and another acetylide couples to form a C_4 bridging moiety. Due to the lack of solubility of **1.10** in non-coordinating solvents, ^{1}H NMR spectroscopy was carried out in d_8-THF. The spectrum acquired did not correspond to **1.10** and addition of pyridine to the THF solution afforded crystals of the acetylide complex [Cp*Lu(CCPh)$_2$(py)]. Addition of a coordinating solvent breaks up the dimer to form the expected bis(acetylide) complex.

Mono(cyclopentadienyl) alkyls of lutetium also undergo C-H activation and insertion reaction with small molecules.[15] Compound **1.9** reacts with CO in benzene to form an alkoxide complex that has been C—H activated on one of the bipy rings *ortho*- to the N atom. The reaction is proposed to proceed via CO insertion into the Lu—C bond to form an acyl ligand. This acyl group then activates the C—H bond on the bipy ligand to form the alkoxide. A second equivalent of CO then inserts into the Lu—CH_2SiMe_3 bond which then tautomerises to form an enolate. Compound **1.8** reacts with one equivalent of Dipp-NH_2 to form the amide [Cp*Lu(N(H)Dipp)(CH_2SiMe_3)(bipy)] (**1.11**). When **1.11** is reacted with CO the bipy C-H activation product is formed but no further reaction occurs, neatly demonstrated the reactivity of Lu—C bonds with respect to harder Lu—N bonds.

Hou *et. al.* demonstrated that lanthanide imides can be synthesised from nitriles and lanthanide hydrides of the formula [{Cp^RLn(μ-H)$_2$}$_4$(THF)] (R = $C_5Me_4SiMe_3$) (**1.12**).[16] Benzonitrile reacts with **1.12** to from the imido complex [{Cp^RLn(μ_3-NCH_2Ph)$_2$}$_4$] (**1.13**) by addition of a hydride across the C≡N bond. Compound **1.13** reacts with four equivalents of benzonitrile to form an amidinate bridged complex. The reaction of **1.13** with an excess of

benzonitrile leads to the tetramerisation of benzonitrile. The trimer could also be formed catalytically by adding 0.25 mol% of **1.13** to benzonitrile.

1.1.3 Bis(cyclopentadienyl) Rare-Earth Alkyl Complexes

In 1983 Watson reported on the reactivity of the metallocene-alkyl complex [Cp*$_2$Lu(CH$_3$)] (**1.14-Lu**) (summarised in Scheme 1.4).[17] The study showed that not only can this highly reactive species activate sp^2 C—H bonds but also sp^3 C—H bonds in tetramethylsilane. Reacting **1.14-Lu** with H_2 in pentane at RT yields the hydride complex [Cp*$_2$LuH] (**1.15-Lu**) which is noted as monomeric by Watson, but crystallographic characterisation of the yttrium analogue reveals a dimeric structure in the solid state.[18] This hydride complex is also highly reactive and can activate sp^2 C—H bonds in benzene to form the phenyl complex [Cp*$_2$Lu(C$_6$H$_5$)] (**1.16**). Interestingly, this reaction is reversible due to the formation of hydrogen being thermodynamically unfavourable and the hydride is reformed upon exposure of **1.16** to hydrogen. The complex **1.14-Lu** also reacts with benzene but the reaction is slower than with the hydride complex. Compound **1.14-Lu** deprotonates pyridine in the 2- position to form the 2-pyridyl complex [Cp*$_2$Lu(C$_5$H$_4$N)] which has been confirmed by ^{1}H NMR spectroscopy. The ylide CH_2PPh_3 reacts with **1.14-Lu** to give a metallacyclic product by deprotonation of one of the phenyl rings in the *ortho*- position; Ln—H bonds are often the active species in many catalytic transformations.

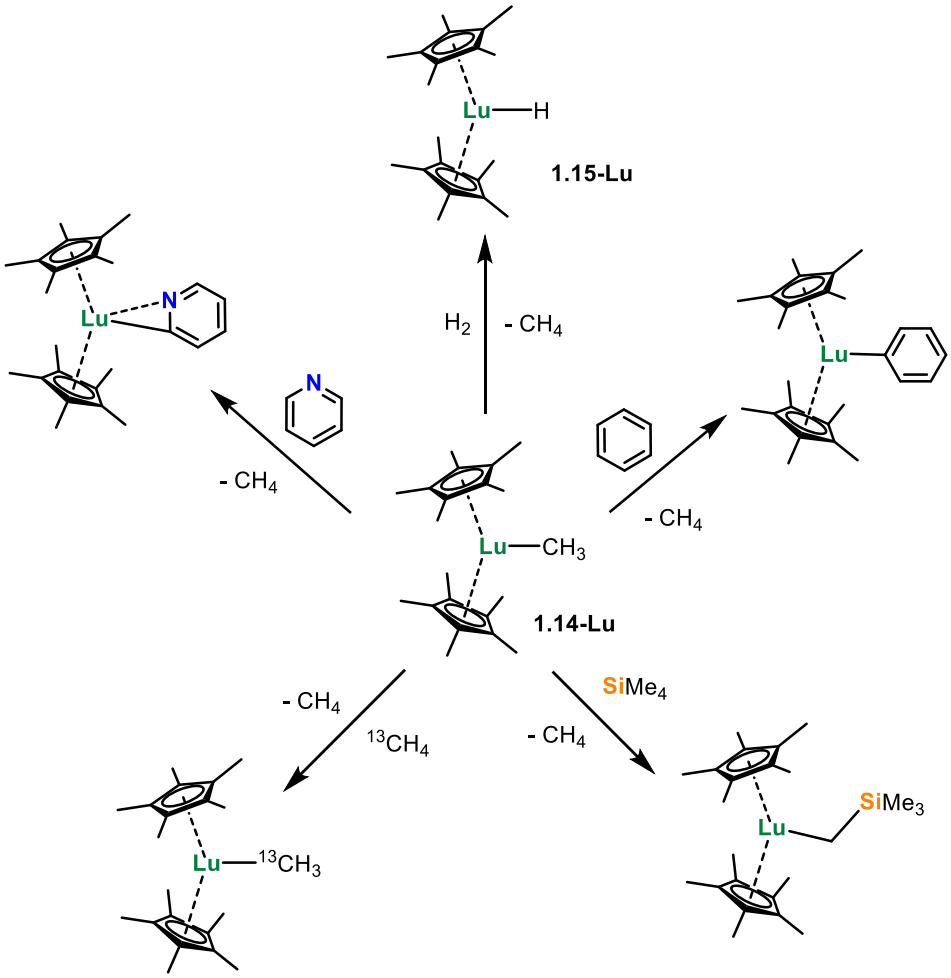

Scheme 1.4. Reactivity of **1.14-Lu** towards a variety of substrates.[17, 19]

In the same year Watson also reported on the reactivity of **1.14-Lu** with methane.[19] Methane is inert due to strong C—H covalent bonds (BDE = 337.2 kJ mol^{-1}). However, it was shown that the Lu—CH_3 bond reacts with $^{13}CH_4$ via a σ-bond metathesis mechanism to form the corresponding Lu—$^{13}CH_3$ complex and methane. The reaction was carried out in cyclohexane-d_{12} at 70°C and monitored by ^1H and ^{13}C NMR spectroscopy. The reaction is 50 % complete after 3.7 hours and kinetic study shows a linear relationship between the first order rate constant, *k* and methane concentration in solution.

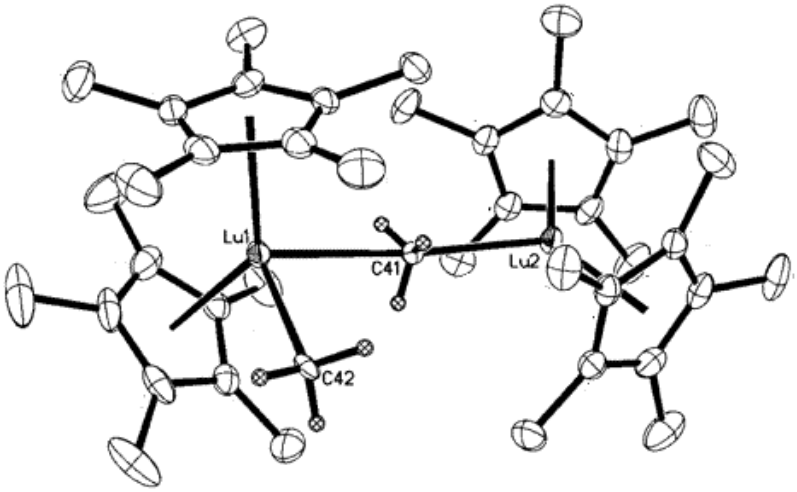

Figure 1.3. Molecular structure of **1.14-Lu.** The steric hindrance of the Cp* ligands prevents both methyl groups bridging. Figure reproduced from reference 20.[20]

Compound **1.14-Lu** also reacts with ethane and propane but the products were more prone to decomposition at RT due to β-H elimination. The $\{Cp^*_2Lu\}$ fragment is sterically crowded and partially prevents the formation of bridging dimers in solution. The molecular structure of **1.14-Lu**, reported in 2005, shows the formula to be $[Cp^*_2Lu(\mu\text{-}CH_3)Lu(CH_3)Cp^*_2]$ (Figure 1.13) where only one methyl group can bridge between two Lu^{3+} centres due to the bulky Cp* ligands.[20] The metal centre is highly Lewis acidic and the facile monomer-dimer exchange in solution allows for coordination of hydrocarbon substrates (in this case methane), as the monomer is coordinatively unsaturated.

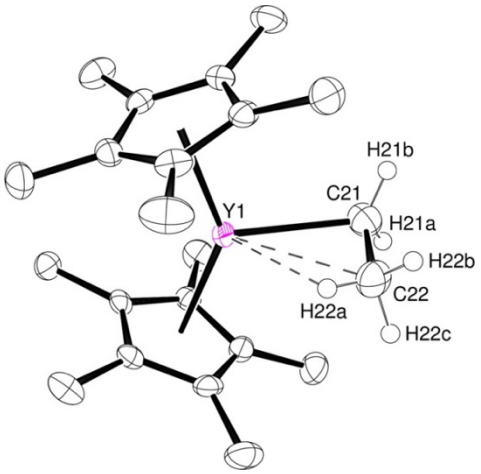

Figure 1.4. Molecular structure of **1.17** highlighting β-H agostic interaction with yttrium.[21]

In 2015 Evans *et. al.* reported the first crystallographically characterised rare-earth ethyl complex, [Cp*$_2$Y(CH_2CH_3)] (**1.17**) (Figure 1.4).[21] Alkyl complexes of rare-earth metals with β-hydrogen atoms pose more of a challenge to isolate than methyl complexes due to the possibility of decomposition via β-H elimination. **1.17** was synthesised by reacting [Cp*$_2$Y][BPh_4] with solid EtLi in pentane at -15^{o}C over 12 hours, producing a light yellow powder. Initial attempts at synthesising **1.17** resulted in a red-orange material being formed after stirring at RT for several hours. This was shown by ^{1}H NMR spectroscopy to be a tuck-over complex where one of the methyl groups on a Cp* ligand had been deprotonated to form a dianionic ligand: $(CH_2CpMe_4)^{2-}$. The term tuck-over describes the methylene group as bridging to another metal center, as opposed to being coordinated to the same metal center as the η^5-Cp ring ("tuck-in"). The other bridging ligand is a hydride. Carrying out the reaction at -35^{o}C over 2 days in methylcyclohexane-d_{14} gave the desired product according to ^{1}H NMR spectroscopy after filtration. Unusually, the signals corresponding to both CH_3 and CH_2 protons arise overlapping at 0.19 ppm, whereas previous reports of lanthanide ethyl complexes show a separation of 1.6 ppm between the two resonances. This suggested a potential Y---H_3C agostic interaction based on a prior study into the scandium analogue by Bercaw et.al. in 1987.[22] This was confirmed by XRD

analysis after single crystals of **1.17** were grown from a slow evaporation of a pentane solution at -78°C.

Compound **1.17** exhibits a range of reactivity typical of lanthanide alkyl complexes, including insertion of unsaturated substrates into the Y—C_{Et} bond, small molecule activation and β-hydrogen elimination. A sample of **1.17** was dissolved in methylcyclohexane-d_{14} and kept at 0°C to determine the decomposition pathway by NMR spectroscopy. No H_2 or ethylene was observed during decomposition which would be indicative of β-H elimination, however $[Cp^*_2YH]_2$ was observed as a decomposition product along with other, unidentified species. Taking a solid sample and heating it to 60°C under vacuum gave a dark red-orange solid as observed previously, the volatiles produced were collected in a liquid nitrogen cooled trap and subsequently vacuum transferred into an NMR tube containing C_6D_6. The ^{1}H NMR spectrum of this sample showed only ethylene and ethane. The presence of ethylene is proof that β-H elimination is involved in the decomposition of **1.17**, but a detailed mechanism is still elusive.

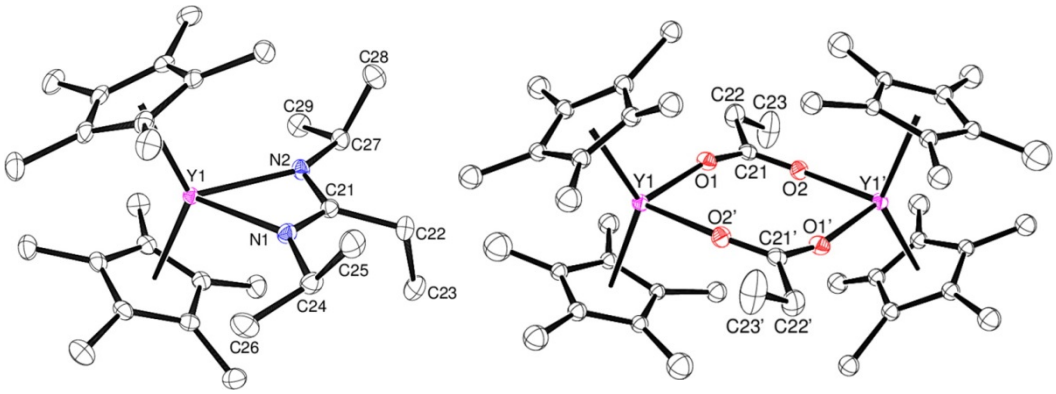

Figure 1.5. Structures of the ethyl-insertion products obtained from reactions of **1.17** with carbodiimide and CO_2.[21]

Compound **1.17** also reacts with the carbodiimide, ^{i}PrN=C=N^{i}Pr, and CO_2 to form the ethyl amidinate and ethyl carboxylate complexes via insertion of the unsaturated substrate into the Y—C bond (Figure 1.5). The most impressive aspect of the reactivity is the activation of

methane. Compound **1.17** reacts with 1 atmosphere (atm) of $^{13}CH_4$ at RT to give ethane and [Cp*$_2$Y($^{13}CH_4$)] which are observed alongside the by-products observed in the thermal decomposition of **1.16**.

The synthesis and structure of the allyl rare-earth metallocene complex Cp*$_2$Sm(C_3H_5) (**1.18-Sm**) was reported by Evans *et. al.* in 1990 (Scheme 1.5).[23] As samarium has a more accessible +2 oxidation state **1.18-Sm** could be synthesised from the divalent precursor Cp*$_2$Sm or the trivalent **1.15-Sm**. In each case, exposure of a solution of either precursor to an atmosphere of propene affords the allyl complex **1.18-Sm.**

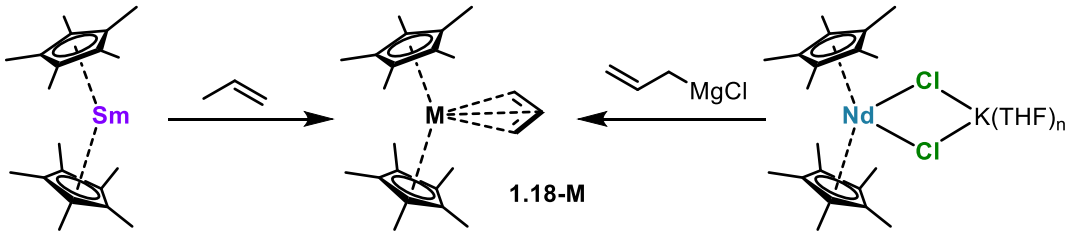

Scheme 1.5. Synthesis of the allyl complex **1.18-M** reported by Evans *et. al.* from divalent and trivalent precursors.[23]

The synthesis of the yttrium version was reported in 2005 using [Cp*$_2$Y(μ-Cl)$_2$K(THF)$_n$] (n = 0-2) as the precursor.[24] It was discovered that bis(cyclopentadienyl) rare-earth halides react rapidly with the Grignard reagent allylmagnesium chloride (C_3H_5MgCl) in aromatic solvents to form the corresponding rare-earth allyl complex. Compound **1.18** forms a monomer as opposed to a dimer or trimer due to the allyl ligand binding preferentially in a η^3 manner making a formally 9 coordinate complex.

The reactivity of **1.18** has been explored extensively since its discovery. The reaction of **1.18-Y** with 9-borabicyclo[3.3.1]nonane (9-BBN) leads to two products that co-crystallise in one unit cell.[25] Compound 9-BBN adds on to the allyl ligand in **1.18-Y** to form a C—B bond in the allylborate complex [$Cp^*_2Y(CH_2C(H)CHBC_8H_{14})$]. The second product formed is the borohydride complex [$Cp^*_2Y(\mu\text{-}H)_2BC_8H_{14}$] which can also be synthesised from **1.15-Y** and 9-BBN.

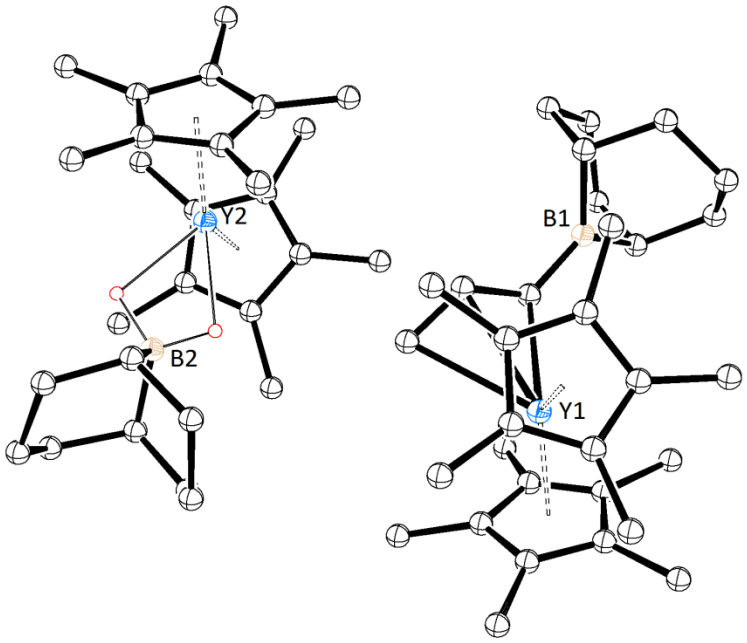

Figure 1.6. Structure of the two co-crystallised products of the reaction between **1.18-Y** and 9-BBN. The hydride ions are highlighted as red circles.[25]

The photolytic reactivity of **1.18-Y** was examined towards elemental sulfur and dinitrogen. It had been found previously that the structurally related [$Cp^*_2MCp^{Me4}$] (M = Y, Dy, Lu; Cp^{Me4} = C_5Me_4H) complexes form the dinitrogen bridged complexes [{Cp^*_2M}$_2$(μ-η^2:η^2-N_2)] when subjected to irradiation with UV light (450 W mercury lamp). **1.18-Y** also reduces dinitrogen to form the $(N=N)^{2-}$ bridged complex after irradiation with UV light for 24 hrs with a conversion of 50%. When two equivalents of **1.18-Y** were mixed with 0.125 equivalents of S_8 in toluene and subjected to UV irradiation for 4 hrs, the sulfide bridged complex [{Cp^*_2Y}$_2$(μ-S_2)] was formed. The structurally similar allyl complex [$(Cp^{Me4})_2Sc(C_3H_5)$] (**1.19**) has been shown to undergo σ-bond metathesis reactions with

dichalcogenides of the formula PhE-EPh (E = S, Se, Te).[26] Compound **1.19** reacts with PhS-SPh in toluene to form the dimeric, sulfide-bridged complex $[(Cp^{Me4})_2Sc(\mu\text{-}SPh)]_2$ with C_3H_5-SPh formed as the by-product. When the larger chalcogenides are reacted with **1.19** the monomeric complexes $[(Cp^{Me4})_2Sc(EPh)]$ (E = Se, Te) are formed, this is due in part to the increasing steric bulk of the chalcogen atom.

Compound **1.18** is an important precursor to rare-earth metallocene complexes with weakly-coordinating anions.[27] Evans *et. al.* reported on the synthesis of rare-earth tetraphenylborate complexes $[Cp^*_2M(\mu\text{-}Ph)_2BPh_2]$ or $[Cp^*_2M][BPh_4]$ (**1.20**) in 1998. Compound **1.20-Sm** was synthesised from Cp^*_2Sm and the oxidising agent $AgBPh_4$ affording the product and silver metal. The neodymium version **1.20-Nd** was synthesised by a protonolysis reaction of **1.18-Nd** with $[HNEt_3][BPh_4]$. The crystal structure shows the $[BPh_4]^-$ ion is coordinated in an η^2 fashion through two phenyl rings. Oddly, in contrast to related complexes, the tetraphenylborate complexes (**1.20-M**) are insoluble in toluene at RT but are soluble in benzene. **1.20-M** can be crystallised from hot toluene.

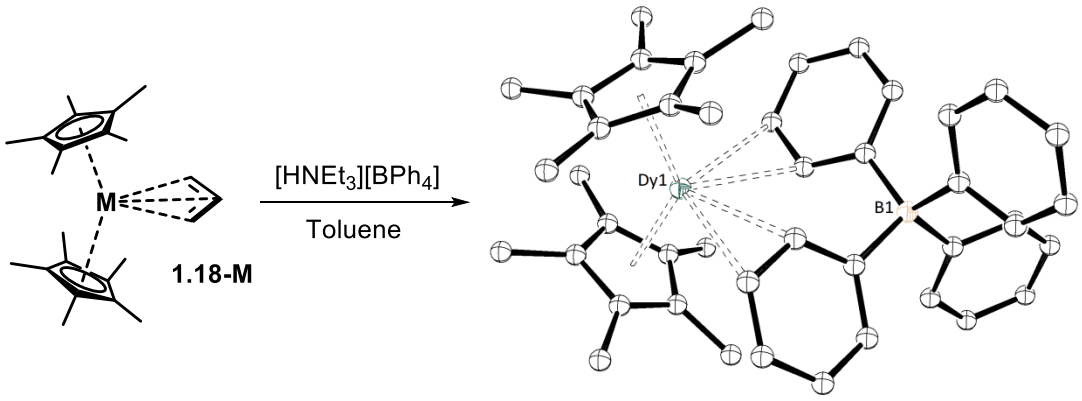

Scheme 1.6. Synthesis of unsolvated lanthanide metallocene cations $[Cp^*_2M(\mu\text{-}Ph)_2BPh_2]$ (**1.20**), the crystal structure shown is for Ln = Dy.[27]

1.2 Lanthanide Metallocene Alkyl Compexes in Catalysis

Complexes containing Ln—C bonds have been used in a variety of catalytic transformations and often in the strictest definition act as pre-catalysts for the true catalytic species. Such examples include hydroamination/phosphination, dehydrocoupling of a variety of substrates to form E—E bonds, olefin polymerisation and dearomatization of heterocycles.[28]

Lanthanide alkyl complexes were first considered as a viable replacement for zirconium and hafnium alkyl complexes for Ziegler-Natta olefin polymerisation catalysts by Pearce *et. al.* in 1978.[29] Cationic alkyl complexes of the heavier group 4 metals often required an alkylaluminoxane co-catalyst that was poorly defined (i.e. formula is an approximation). The TM-containing species was well defined, however. Complexes of the formula $[C_5R_nH_{5-n2}MCH_3]_2$ (R = Me, $SiMe_3$, Me_4Et; M = Er, Y) were found to be highly active homogeneous ethylene polymerisation catalysts. Firstly, increasing the steric bulk of the Cp ligand from Cp < Cp^{Me} < Cp' resulted in an increase in catalyst activity from 10.3 to 82.3 g $mmol^{-1}$ atm^{-1} hr^{-1}. Secondly, the molecular weight of the resulting polymer decreased, presumably due to a third trend which was a decrease in the lifetime of the catalyst. The proposed intermediate was determined to be a bridged, dimeric structure based on ^1H NMR spectra, but no crystallographic study was carried out. $[Cp^*_2LuMe]_2$ also catalyses the polymerisation of ethylene.

Interestingly, **1.14-Lu** only oligomerises propene.[30, 31] One of the most important factors to the stability and reactivity of lanthanide organometallic complexes is the steric bulk of the ligands bound to it. Propene reacts with **1.14-Lu** to form the isobutyl complex $[Cp^*_2Lu(CH_2CH(CH_3)_2)]$ which is sterically bulkier than the propyl complex generated on insertion of ethylene, which inhibits the reaction with a second equivalent of propene. As a result, the chain propagation step of the reaction is relatively slow compared to the chain

transfer and/or termination reactions. Chain transfer can occur via either β-H elimination or a β-CH_3 elimination from the isobutyl group to form either **1.15-Lu** or **1.14-Lu** respectively, but these reactions are reversible.[32] The termination step is through a C—H activation of propene to give the η^3-allyl complex [Cp*$_2$Lu($CH_2C(CH_3)CH_2$)] and alkane.

In 1987, Teuben *et. al.* first reported on the yttrium alkyl complexes **1.14-Y** and **1.15-Y** which were analogous to the known lutetium complexes.[33] Compound **1.14-Y** displayed similar reactivity to that of **1.14-Lu** with ethylene and propene. **1.15-Y** was also examined for its ability to polymerise various small olefins, as yttrium is much less expensive than lutetium and would pose a significant economic advantage if it displays similar reactivity.[34] Yttrium has a slightly larger ionic radius than lutetium, so it is possible that yttrium may be able to accommodate more sterically bulky alkenes and therefore polymerise propene. However, the study revealed that propene and branched alkenes such as isobutylene also impede the polymerisation. The reaction between the propene insertion product (after one-two insertions) and propene forms the η^3-allyl complex [Cp*$_2$Y($CH_2C(CH_3)CH_2$)]. When **1.15-Y** is reacted with an excess of 1-hexene higher oligomers are formed due to the termination reaction being slow as well as the propagation step. Study of the kinetics of ethylene polymerisation by **1.15-Y** has shown that the insertion of ethylene into the Ln—C bond follows a second order rate law at -80^{o}C by ^{1}H NMR spectroscopy.[34]

In a study by Marks *et. al.* it was shown that **1.15-La** and **1.15-Nd** do react with propene very rapidly but the products formed are the allyl complex, [Cp*$_2$La($CH_2C(CH_3)CH_2$)] and propane.[35] Therefore, the order of reactivity towards ethylene can be described as La > Nd > Y/Lu. Although **1.15-Nd** cannot polymerise propene it can take part in copolymerisation of 1-hexene with ethylene by stirring a solution of **1.15-Nd** in 1-hexene under an atmosphere of ethylene.

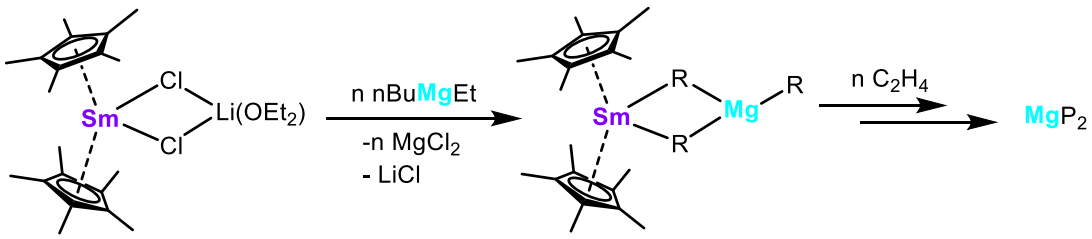

Scheme 1.7. Mechanism of olefin polymerisation by combining $[Cp^*_2Sm(\mu\text{-}Cl)_2Li(OEt_2)]$ with dialkylmagnesium.[36]

In 1996, Montreux *et. al.* reported on a different approach to ethylene polymerisation using Ln—alkyls.[36] By taking one equivalent of $[Cp^*_2SmCl_2Li(OEt_2)_2]$ (**1.21**) and a varying excess of a dialkylmagnesium (in this case ^{n}BuMgEt) in pentane or hexane and introducing an ethylene atmosphere, compounds of the formula ^{n}Bu—$(CH_2—CH_2)_n$—Mg—$(CH_2—CH_2)_n$—Et are formed. The value of n depends on the ratio of samarium to magnesium in solution. R—Mg—R' reacts with **1.21** to form a dinuclear alkyl bridged complex with samarium and magnesium which undergoes insertion chemistry with olefins to form polymers as magnesium salts. The polymer can then be isolated by hydrolysis of the P—Mg—P moiety to give $Mg(OH)_2$ and polyethylene. The polymers produced using this method have a very low polydispersity of the molecular weight.

In polymers the orientation, or relative position, of substituents with respect to each other, known as the tacticity, can have drastic impacts on the physical properties of the polymer. Research into ansa-metallocene complexes has shown that the steric impact of the ligands can influence how monomers insert into the Ln—C bond and the stereochemistry of the resulting chain. As the two Cp rings in ansa-metallocene are tethered by an R_2Si— group,

the positions of substituents on the Cp rings can infer a certain tacticity on polymers formed.[32]

The first ansa-metallocene complexes of lanthanides were reported by Marks *et. al*. in 1985 and the complex $[Me_2Si(2\text{-}SiMe_3\text{-}4\text{-}^tBuC_5H_2)_2LnH]_2$ (**1.22**) (Ln = Nd, Sm, Lu) was found to be an active catalyst for propene oligomerisation. The yttrium complex **1.22-Y** gave highly isotactic poly-α-olefins (>97 % mmmm – meaning identically *meso*-oriented stereochemical units). The only disadvantage is low molecular weight polymers were obtained (< 600 g mol^{-1}). However, when the Me_2Si— unit was replaced with a binapthoxysilyl unit high MW, isotactic polypentene was obtained. Which highlights that the subtle tuning of coordination geometry and steric environment can greatly alter the catalytic properties. The thulium tris-alkyl complex $[(^iPr\text{-}trisox)Tm(CH_2SiMe_3)_3]$ was also found to polymerise longer chain terminal alkenes with high tacticity. 1-hexene, 1-heptene and 1-octene were all successfully polymerised by $[(^iPr\text{-}trisox)Tm(CH_2SiMe_3)_3]$ in chlorobenzene with an isotacticity of 83 % or higher.[37] The catalyst was activated *in situ* by reacting with two equivalents of $[Ph_3C][B(C_6F_5)_4]$ to generate, presumably, a dicationic mono-alkyl complex of the formula $[(^iPr\text{-}trisox)Tm(ClC_6H_5)_n][B(C_6F_5)_4]_2$ although no structural analysis was carried out on this catalytically active species.

In 2012, Hou et. al. reported on the structural relationship of lanthanide metallocene allyl complexes with their propensity to catalyse the polymerisation of styrene.[38] Bis-allyl complexes of scandium, yttrium and lutetium were synthesised with bidentate *o*-aminophenyl-Cp and pyridyl-Cp ligands that have different bite angles around the metal center. The complexes $[(C_5Me_4\text{-}C_6H_4\text{-}o\text{NMe}_2)Ln(C_3H_5)_2]$ (**1.23**) exhibit a Cp_{cent}-Ln-N (bite) angle of 95.4° (Ln = Y) and 96.7° (Ln = Lu) resulting in a sterically crowded molecule. By comparison the pyridyl-Cp complexes $[(C_5Me_4\text{-}C_6H_4N)Ln(C_3H_5)_2]$ (**1.24**) have bite angles of 82.7 ° (Ln = Y), 86.6 ° (Ln = Sc) and 84.1 ° (Ln = Lu) (see Figure 1.7).

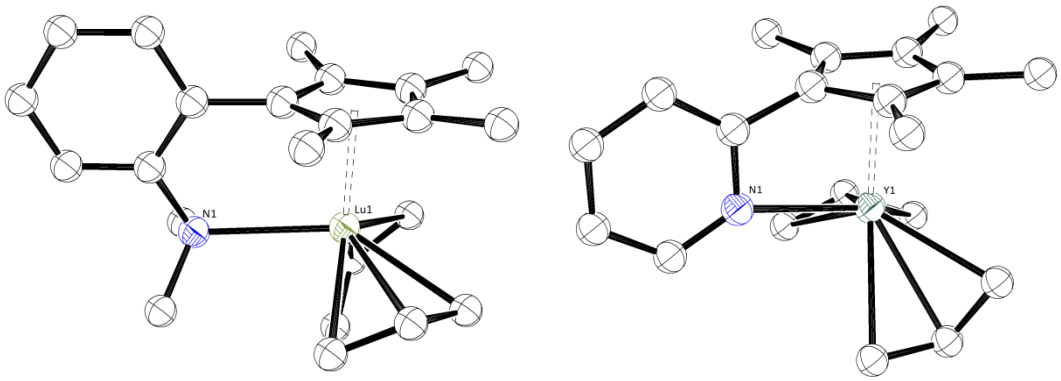

Figure 1.7. (Left) structure of **1.23-Lu** highlighting the shallower Cp_{cent}—Ln—N angle with respect to **1.24-Y** (right).[38]

The shallower angle between the Cp and pendant donor group in **1.24-M**, with respect to **1.23-M**, results in a greater area around the metal center available for substrate binding. The results reflect this structural observation as **1.23-Y** and **1.23-Lu** did not catalyse the polymerisation of styrene upon activation with $[Ph_3C][B(C_6F_5)_4]$ in the presence or absence of Al^iBu_3. It was proposed that the bulky Cp ligand inhibited the coordination of styrene. Also, the dimethylamino group is electron donating, thus making the metal center less Lewis acidic. All these factors inhibit alkene coordination and thus render the Ln complex catalytically inert. However, study on the pyridyl-Cp complexes show that **1.24-Y/Sc/Lu** do catalyse the polymerisation of styrene to highly syndiotactic PS (sPS). **1.24-Y** has a relatively low activity but gives 88 % sPS after 50 mins in toluene, the conversion from monomer to sPS, however, is only 20 %. The activity is improved and conversion is complete when performing the reaction in chlorobenzene, however the polymer produced is atactic (0 % sPS). Compounds **1.24-Sc** and **1.24-Lu** give complete conversion to > 99 % sPS in just 1 minute. This increase in reactivity with respect to **1.24-Y** is most likely due to the greater Lewis acidity of scandium and lutetium.

Addition of H—E bonds across unsaturated C=C substrates can be effectively catalysed by Ln-alkyl complexes. In 1992, Marks *et. al.* proposed a mechanism for the hydroboration of olefins using the complex [Cp*$_2$Ln(CH(SiMe$_3$)$_2$)] (**1.25**) (where Ln = La or Sm).[39] It proceeds via an initial reaction with catecholborane to form **1.15-La** and catB(CH(SiMe$_3$)$_2$). Compound **1.15-La** then reacts with an olefin to form the corresponding alkyl insertion product, this then undergoes a σ-bond metathesis with catBH to reform the Ln-H and the alkylborane. The scope of olefins includes primary, aryl, secondary and cyclic compounds. Quenching of the reaction with hydrogen peroxide and NaOH gives the alcohol. In many cases of hydro-elementations of unsaturated carbon substrates, it is often the case that the alkyl lanthanide complex in question will serve as a pre-catalyst with the hydride being the active species.

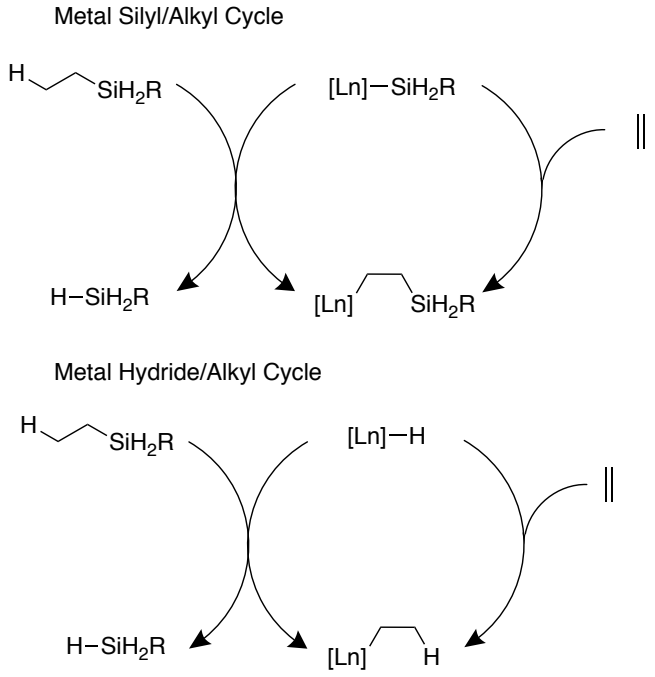

Scheme 1.8. Two proposed pathways for Ln-mediated olefin hydrosilylation, metal hydride/alkyl cycle has also been proposed for hydroboration.[39]

Olefin hydrosilylation works in a similar manner as the polarity of the B/Si—H bond is the opposite to that of C/N/P—H bond and the catalytic species is often formed via hydride transfer as opposed to deprotonation. In a 1995 study, $PhSiH_3$ was added to a variety of olefins using **1.25-La** as a catalyst.[40] The proposed mechanism follows one of two pathways as shown in Scheme 1.8. Firstly, formation of the Ln—H complex and $R_3Si—CH(SiMe_3)_2$ followed by insertion of the olefin into the Ln—H bond to form the Ln—alkyl. As with boranes, this reacts with another equivalent of silane to reform the hydride and the alkylsilane. A second mechanism was proposed involving deprotonation of $PhSiH_3$ to form the silyl-lanthanide complex, but this was not consistent with observations by ^1H NMR spectroscopy. The catalyst successfully converts a range of terminal mono and di-substituted alkenes to the corresponding silanes at low catalyst loading (0.5 mol%). It was also found that the ansa-metallocene complex $Me_2SiCp^{Me4}{}_2Sm—CH_2(SiMe_3)_2$ also promoted regioselectivity, in excess of 99 %, for a variety of aryl-substituted olefins. Adding a chiral substituent onto the Cp rings can also infer stereoselectivity in the product alkylsilane.

In 2013, Marks *et. al.* reported on the synthesis of organotin reagents by carbostannolysis of alkenes and alkynes using a catalytic amount (5 mol%) of **1.25-La**.[41] When **1.25-La** reacts with 2-(trimethylstannyl)pyridine (**1.26**) the 2-pyridyl lanthanum complex $[Cp^*{}_2La(2\text{-}C_6H_4N)]$ is formed which then undergoes an insertion reaction with ethylene to form the 2-ethylpyridyl complex. This reacts with a further equivalent of **1.26** by cleaving the C—Sn bond to reform $[Cp^*{}_2La(2\text{-}C_6H_4N)]$ and 2-Me_3Sn(ethyl)pyridine (Scheme 1.9).

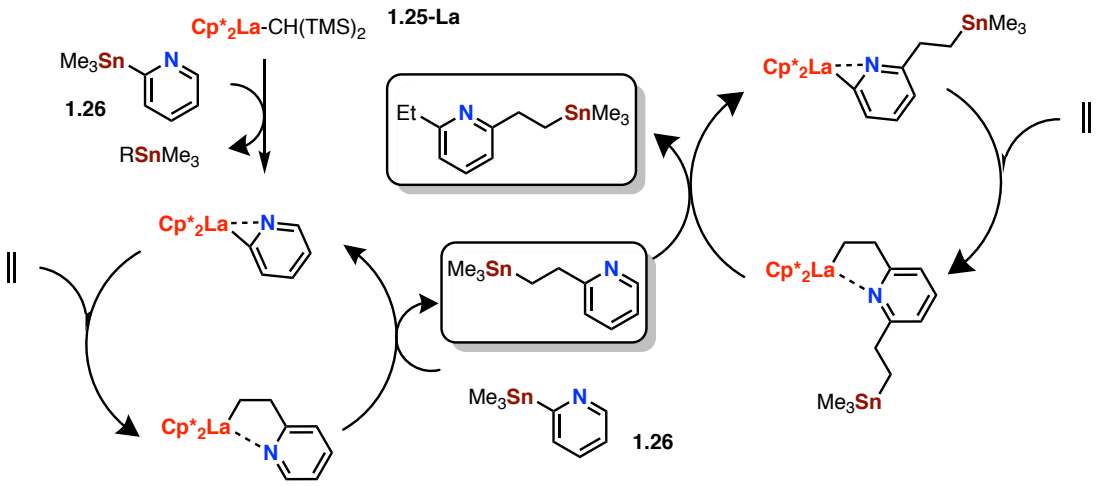

Scheme 1.9. Reaction mechanism reported by Marks *et. al.*, for the catalytic formation of C—Sn bonds.[41]

Complex **1.25-La** also catalyses the reaction between terminal alkynes and 2-Me_3Sn(pyridine) according to scheme 1.13. The active species is generated by deprotonation of the alkyne to give a {La—C≡C—R} complex. This reacts with **1.26** to give Me_3Sn—C≡C—R which inserts into the La—C≡C bond to form a *cis*-Me_3Sn-enyne which is protonated by another equivalent of alkyne to reform the {La—C≡C—R} complex. As the alkyne is mono-substituted, the side of the C≡C bond with the R group points away from the metal center, resulting in the formation of an (E)-stannyl-enyne in a 60:1 E:Z ratio of stereoisomers.

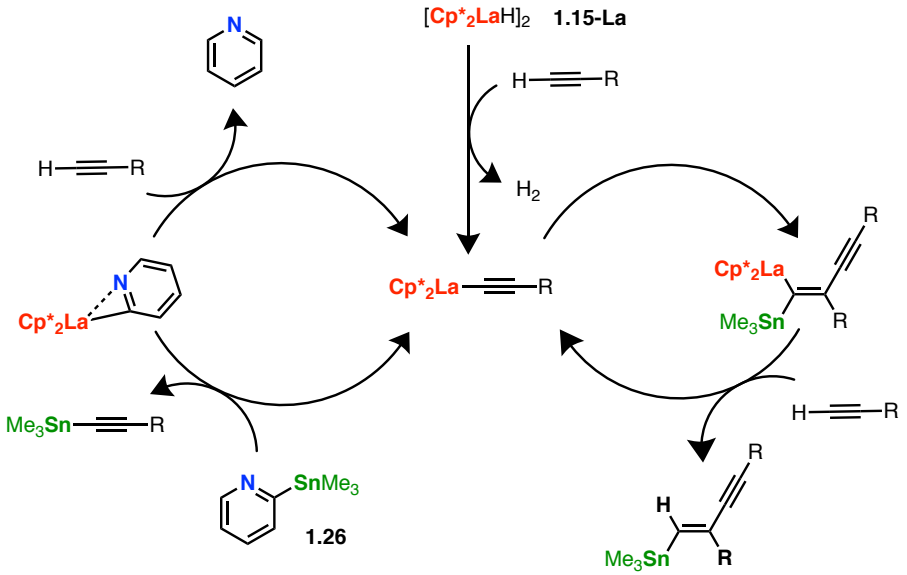

Scheme 1.10. Reaction mechanism for the formation of stannyl-enynes from **1.26** and terminal alkynes catalysed by **1.15-La**.[41]

Complex **1.15-La** can also catalyse the dearomatization of pyridines. 1,2-dihydropyridines are an important class of precursors to a range of natural products and pharmaceutical compounds. 1,2-hydroboration of a range of substituted pyridines with HBPin can be affected by 1 mol% of **1.15-La** under mild reaction conditions (C_6D_{12} or C_6D_6, 35°C). The substrate scope includes a range of 3- and 4- substituted pyridines with electron withdrawing (CF_3, I, H etc.) and donating (OMe, Me, Ph) groups although reactions times are typically longer with the latter.

^{1}H NMR and DFT studies show that the mechanism proceeds via initial coordination of up to 2 pyridine molecules breaking up the $[Cp^*_2La(\mu\text{-}H)]_2$ dimer. Insertion of the C=N bond into La—H bond then forms the 1,2-dearomatised amide. The substrate HBPin coordinates to the metal center where subsequent σ-bond metathesis between N—La---H and H—B---N forms the B—N hydroboration product and **1.15-La**.

1.3 Single Molecule Magnetism of Lanthanide Metallocene Complexes

F-block coordination complexes have attracted considerable interest since 2003 for their magnetic properties due to a phenomenon called magnetic anisotropy. In systems where all electrons are paired the electron density around a nucleus is isotropic in the ground state (no magnetic moment). However, complexes with unpaired electrons are anisotropic because there are partially filled orbitals. Lanthanide ions with an electron configuration of $4f^n$ where n is greater than 7 are well suited to the application of single molecule magnets (SMMs) as they possess the largest magnetic moments. The field of lanthanide organometallics first contributed to f-block single molecule magnetism in 2010 with the report of the first organometallic SMM (i.e. containing M—C bonds) $[Cp_2Dy(\mu\text{-bta})]_2$ which has a modest energy barrier to spin inversion, U_{eff}, of 33 cm^{-1}.[42]

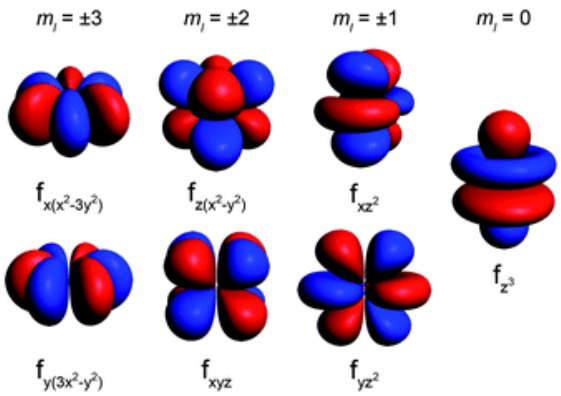

Figure 1.8. The shapes of the seven f-orbitals (general set) arising from the 2l + 1 projections of the 4f wavefunction.[43]

Lanthanides and actinides have the greatest propensity for magnetic anisotropy due to the number of orbitals available. For each value of orbital angular momentum quantum number, *l* (*l* = n-1, for lanthanides *l* = 3) there are 2*l* + 1 values of magnetic quantum number, m_l. For the 4f row there are thus seven degenerate orbitals. This means that there is a potential for up to seven unpaired electrons in the ground state, more than any d-block element. Dy^{3+} has the second largest single ion magnetic moment in the periodic table (μ_{eff}

= 10.6 μ_B) due to the five unpaired electrons in the $^{H}6_{15/2}$ ground state. Most SMMs are based on Dy^{3+} because although Ho^{3+} has a larger magnetic moment Dy^{3+} is a Kramers ion. Meaning that the ground state will exhibit bistability regardless of the symmetry around the Dy^{3+} ion.

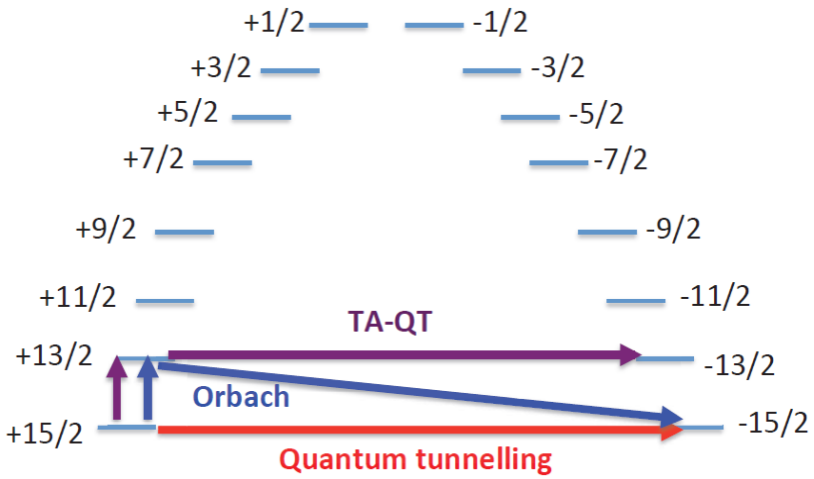

Figure 1.9. Some magnetisation relaxation mechanisms typically observed in Dy^{3+} complexes with a well-defined m_J = ±15/2 ground state (TA-QT – thermally-assisted quantum tunnelling).

Single-molecule magnetism arises from a molecular domain as opposed to the bulk material and exploits this intrinsic property of magnetic anisotropy.[44] Each molecule in a single molecule magnet (SMM) will respond independently to external magnetic fields and as such exhibit a phenomenon known as slow relaxation of magnetisation. For such a phenomenon to occur the ion in question must have magnetic bistability, i.e. a doubly degenerate ground state.[45] When placed in an oscillating (AC) magnetic field the magnetic susceptibility (χ) of a sample will lag behind the external AC field. This delay in response is measured on a superconducting quantum interface device (SQUID) magnetometer using in-phase (χ') and out-of- phase (χ'') components of magnetic susceptibility. An SMM will exhibit a peak in a plot of χ' or χ'' against ac field frequency at a range of temperatures.

There are two main quantifiers of how well an SMM performs: energy barrier to spin inversion (U_{eff}), and the blocking temperature (T_B). The coercivity (H_c) or remanence of the sample in a static field can also be an important property for potential applications in information storage. U_{eff} is expressed in either K or cm^{-1} and describes the energy required to convert a magnetised sample in the *+J* state to the corresponding *–J* state. The U_{eff} barrier can be bypassed by quantum tunnelling of magnetisation (QTM) whereby a spin will interchange directly ($+ m_J \rightarrow - m_J$), bypassing excited states. One aim of studies into SMMs is to supress the QTM relaxation mechanism, which occurs predominantly at low temperatures (up to 5 K) as it is not a thermally driven process. Magnetic hysteresis, also known as magnetic blocking, occurs when the relaxation time is so long that spin reversal is said to be blocked. It is measured by plotting magnetisation against dc field, M(H). The blocking temperature (T_B) can be defined as the temperature at which spin relaxation is 100 s.[46] Hysteresis is measured by placing a sample in a dc field and sweeping the magnetic field to saturation in one direction, then reversing the field and sweeping to negative saturation and back to zero field. The coercivity of the sample is the value of the field (H) at zero magnetisation (M).

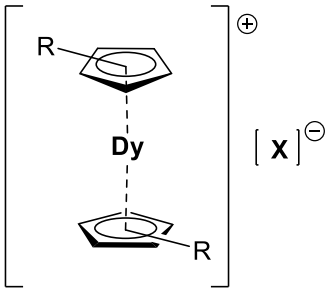

Figure 1.10. Ideal structure to maximise axiality in $\{Cp_2Dy\}$ complexes, a linear arrangement of Cp ligands about Dy^{3+} with a weakly or non-coordinating anion (X).

In recent years, magneto-structural correlations have been proposed and realised for a variety of Dy^{3+} SMMs. The m_J = ±15/2 state for Dy^{3+} has an oblate shape, meaning the orbital angular momentum for that state is projected further in the equatorial plane than it is in the axial plane.[43] As such the ligand field can be designed to minimise impact on that state and enhance its stability, leading to greater energy barriers to spin inversion i.e. U_{eff}. To this end, much focus has been on the $\{Cp^R_2Dy\}^+$ ligand scaffold as the cyclopentadienyl ligands create a strong axial ligand field. The ideal parameters are a Cp_{cent}—Dy—Cp_{cent} angle of 180° which would impart the greatest possible axiality and Dy—$E_{equatorial}$ bond lengths as long as possible to minimise the destabilising effect of the equatorial ligands on the m_J = ± 15/2 wavefunction (see Figure 1.10). To achieve these targets the use of ligands with soft donor atoms has been employed to substantial effect.

1.3.1 Lanthanide Metallocene SMMs with Soft Donor Atom Ligands

The vast majority of lanthanide chemistry is with complexes incorporating hard donor atoms such as O or N. Almost all coordination complexes are based around N- or O-donor atom ligands such as bipy and acac. In recent years there has been a surge in activity surrounding the synthesis and magnetic properties of organolanthanides with soft heteroatom donors.

In 2012, Layfield *et. al.* reported the first sulfur-bridged dysprosium SMM, $Cp^{Me}_2Dy(\mu\text{-}SSiPh_3)$ (**1.27**) (see Figure 1.11).[47] The gadolinium analogue, **1.27-Gd**, was also prepared. Compounds **1.27** were synthesised by reacting one equivalent of the tris-cyclopentadienyl precursor Cp^{Me}_3Ln with one equivalent of the lithium thiolate Ph_3SiSLi in toluene. The by-product $LiCp^{Me}$ makes a good leaving group due to its insolubility in aromatic and aliphatic solvents. Single crystal XRD analysis on **1.27-Dy** shows Dy—S bond lengths of 2.75(15) and 2.77(16) Å to the two bridging S atoms.

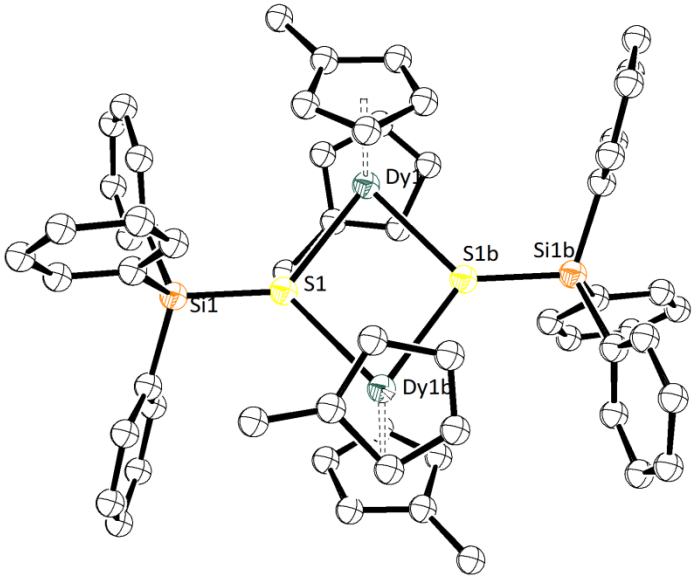

Figure 1.11. Molecular structure of the first S- bridged SMM **1.27**.[47]

The Cp_{cent}—Dy—Cp_{cent} angle is 127.3° which deviates substantially from the ideal 180°. Nonetheless, **1.27-Dy** is an SMM which shows peak maxima in the χ''(T) plot up to 30 K at 1.2 kHz oscillating field. Magnetic hysteresis was also observed on **1.27-Dy** at 1.8 K which indicates some suppression of QTM. The energy barrier to spin inversion was calculated to be U_{eff} = 133 cm^{-1}, which is calculated from the fitting of the Arrhenius law: $\tau = \tau_0 e(U_{eff}/k_BT)$ to a plot of $\ln(\tau)/T^{-1}$ which is linear in the temperature range that is dominated by thermal relaxation processes. Experimental data is very often combined with *ab initio* computational analysis to determine calculated energy gaps between ground and excited states, or Kramers doublets (KDs). The orientation of the main anisotropy axis around a Dy^{3+} ion can also be calculated and the degree of anisotropy can be quantified by the g-tensors. In a perfectly axial system g_z has a value of 20 (Ising limit) and $g_x = g_y = 0$. An *Ab initio* study on **1.27-Dy** reveals a calculated energy difference between the ground and 1st excited KD of 113 cm^{-1} which agrees well with the experimental value for U_{eff}, suggesting relaxation occurs via the first excited state. The orientation of the main anisotropy axis (the g_z tensor) in the ground KD was calculated to be almost perpendicular to the plane of the

Dy_2S_2 core. Synthesis of the Gd analogue allowed for determination of the exchange coupling between metal centres. As the ground state of Gd^{3+} is isotropic, the exchange coupling constant, J can be calculated from the spin-only contribution to the magnetic moment. For **1.27-Gd** the coupling constant is J = -0.105 cm^{-1} (-2J formalism) which implies that the coupling between Gd^{3+} centres is weak and antiferromagnetic.

In 2015, study into heavy p-block bridging ligands was extended to phosphorus with the aim of increasing the U_{eff} barrier and magnetic blocking capabilities of lanthanide metallocenes.[48] Phosphorus opens up a wider range of potential coordination chemistry with lanthanides such as accessing phosphide and phosphinidene, i.e. R_2P^- and RP^{2-} bridging ligands with greater than -1 charge. One equivalent of $MesPH_2$ reacts with $Cp^{Me}{}_3Dy$ in toluene to produce a 1:1 adduct $[Cp^{Me}{}_3Dy(PH_2Mes)]$ (**1.28-Dy**). Deprotonation of **1.28-Dy** with one equivalent of ^{n}BuLi in toluene affords the trimeric, phosphide-bridged dysprosium complex $[Cp^{Me}{}_2Dy(\mu\text{-}P(H)Mes)]_3$ (**1.29-Dy**). Subsequent deprotonation of **1.29-Dy** with another equivalent of ^{n}BuLi affords the lanthanide phosphinidene complex $[(Cp^{Me}{}_2Dy)_3(\mu\text{-}PMes)_3Li][Li(THF)_4]_2$ (**1.30**). The yttrium analogues of **1.28**-**1.30** were also synthesised.

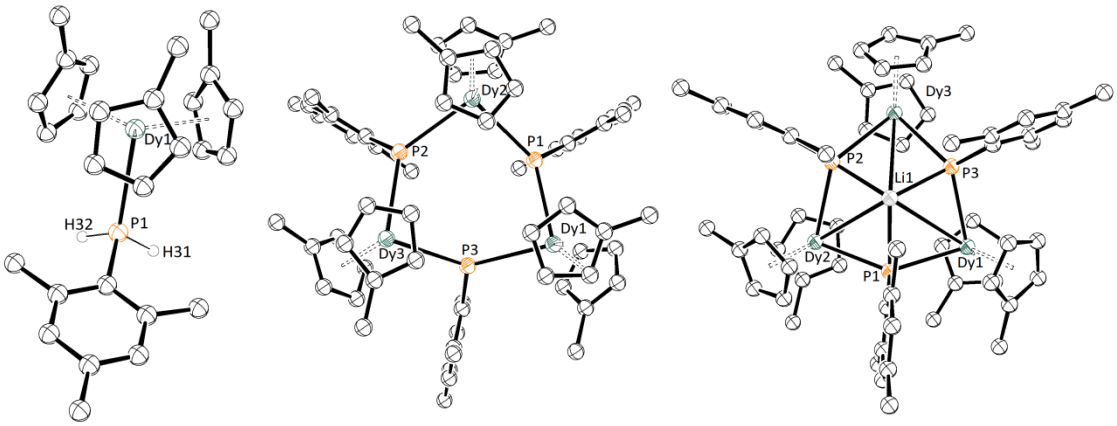

Figure 1.12. (From left to right) Molecular structures of **1.28-Dy**, **1.29-Dy**, and **1.30-Dy**, thermal ellipsoids drawn at 50% probability.[48]

AC magnetic susceptibility measurements on **1.29-Dy** reveal slow magnetic relaxation up to 31 K (1.2 kHz ac field) (χ''(ν) plot shown in Figure 1.13) which increases to 32 K upon doping of **1.29-Dy** into a diamagnetic matrix of **1.29-Y**. This practice of combining a small amount of Dy precursor (1-10%) with the isostructural yttrium precursor allows for the synthesis of 'magnetically diluted' samples. This process of magnetic dilution can eliminate intermolecular Dy---Dy interactions which can aid magnetic relaxation. It is often accompanied by an increase in U_{eff} and/or an opening of the hysteresis loop if magnetic hysteresis is observed in the neat Dy complex. Complex **1.29-Dy** has a U_{eff} barrier of 210 cm^{-1} which is substantially larger than that of **1.27-Dy** and increases to 256 cm^{-1} upon dilution of 5% Dy into **1.29-Y**. This essentially gives a mixture of DyY_2P_3 and Y_3P_3 (**1.29-Dy@Y**). The most pronounced effect of magnetic dilution in this case is seen in the M(H) plots. **1.29-Dy** shows very slight coercive field at 1.8 K however, the diluted sample shows open hysteresis loops up to 4.4 K and a much larger H_c at 1.8 K.

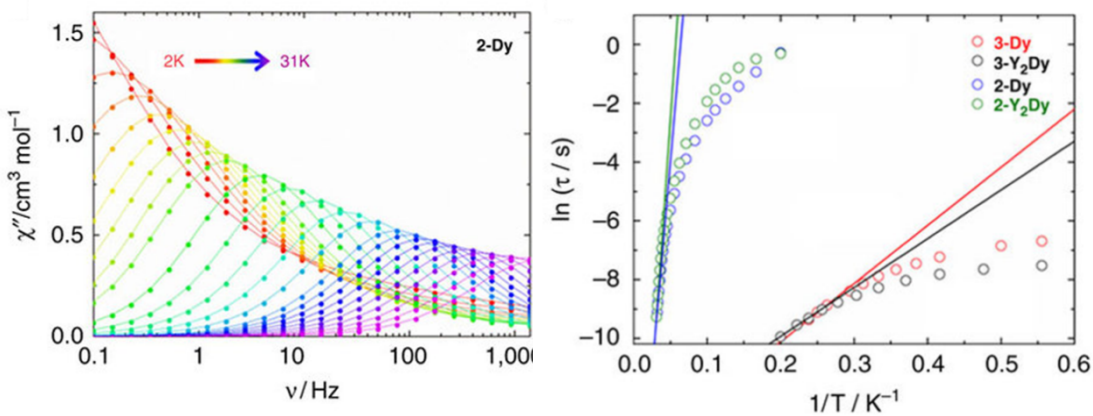

Figure 1.13. (Left) χ''(ν) plot for **1.29-Dy**; (right) Arrhenius plot.[48]

Complex **1.29-Dy** has a U_{eff} barrier 77 cm^{-1} larger than the S-bridged complex **1.27-Dy** with the same $\{Cp'_2Dy\}$ ancillary ligand framework. Despite the R- substituent on the sulfide being different to the phosphide complex, i.e. $SiPh_3$ vs. Mes, some structural comparisons can be drawn to explain the differences in the U_{eff} barrier and the temperatures up to which slow relaxation is observed. While the Cp_{cent}—Dy—Cp_{cent} angles, in the range of 126-126.45°, are comparable to the sulfide complex the Dy—P bonds fall in the range of

2.926(6)-2.951(6) Å, which are considerably longer than the longest Dy—S bond (2.77(16) Å) in **1.27-Dy**. As the phosphide ligand is further away from Dy^{3+} than the sulfide ligand the interaction is reduced in the equatorial plane, affording greater stability of the m_J = 15/2 ground state. *Ab initio* calculations suggest that the thermal relaxation proceeds predominantly through the second excited KD in the higher temperature regime. The Arrhenius plot shows deviation from linearity below 20 K suggesting QTM is becoming the dominant relaxation mechanism.

On extending the study to arsenic donor ligands it was found that the chemistry of $LnCp^{Me}_3$ (Ln = Y, Dy) with $MesAsH_2$ proceeds in the same manner as the phosphine chemistry.[49] Formation of a mesitylarsine adduct $[Cp^{Me}_3Ln(AsH_2Mes)]$ followed by subsequent deprotonations with ^nBuLi afforded the arsenide $[Cp^{Me}_2Ln(\mu\text{-}As(H)Mes)]_3$ (**1.31**) and the arsinidene $[(Cp^{Me}_2Ln)_3(\mu\text{-}AsMes)_3Li][Li(THF)_4]_2$ (**1.32**). The selenide bridged complexes $[Cp^{Me}_2Ln(\mu\text{-}SeMes)]_3$ (Ln = Dy, Y) (**1.33**) were also synthesised.[50] The synthesis of **1.33** differs from that of the phosphide and arsenide complexes in that no adduct is formed between $LnCp^{Me}_3$ and mesitylselenol. MesSeH is acidic enough to be deprotonated directly by $LnCp^{Me}_3$ and form the selenide. All Ln_3E_3 complexes (where E = P, As and Se) are essentially isostructural, with expected variations in bond lengths and angles.

Magnetic measurements on **1.31-Dy** and **1.33-Dy** reveal an increase in U_{eff} with respect to the P and S-bridged complexes described previously. Dy_3As_3 shows peaks in $\chi''(\nu)$ isotherms up to 39 K, which is 8 K higher than the neat dysprosium phosphide. The diluted **1.31-Dy@Y** complex also shows an increase in the observed temperature range of slow relaxation to 40 K, mirroring the effect of diluting the phosphide. The neat and diluted arsenide samples have U_{eff} barriers of 256 cm^{-1} and 301 cm^{-1} respectively which matches well with the increase in U_{eff} between neat and diluted phosphide complexes. This implies that the magnetic relaxation mechanisms are very similar if not identical to **1.29-Dy** which

is expected based on the structural similarity. The Dy—As bond lengths lie in the range of 2.984(18)-3.012(18) Å which is approximately 0.5 Å longer on average than the Dy—P bonds in **1.29-Dy** (*cf.* Dy—P: 2.926(6)-2.951(6) Å).

The reaction of mesitylstibine ($MesSbH_2$) with one equivalent of $^{n}BuLi$ and $Cp^{Me}{}_3Dy$ in toluene at low temperature affords the stibide complex $[Cp^{Me}{}_2Dy(\mu\text{-}Sb(H)Mes)]_3$ (**1.33**), which adopts the same structural conformation as the phosphide and arsenide complexes, **1.29-Dy** and **1.31-Dy**.[51] However, if the reaction is stirred for longer and warmed to RT, or the $Cp^{Me}{}_3Dy$, $^{n}BuLi$ and $MesSbH_2$ are added in a ratio of 3:3:4 the Zintl-like $[(Cp^{Me}{}_2Dy)_3\{\mu\text{-}(SbMes)_3Sb\}]$ (**1.34**) is formed (Figure 1.14). Reactivity studies using ^{1}H NMR spectroscopy showed that stibine dehydrocoupling occurs at RT with a catalytic amount of $Cp^{Me}{}_3Y$ (10 mol%) to form a mixture of Mes(H)Sb—Sb(H)Mes and $(MesSb{=}SbMes)_2$

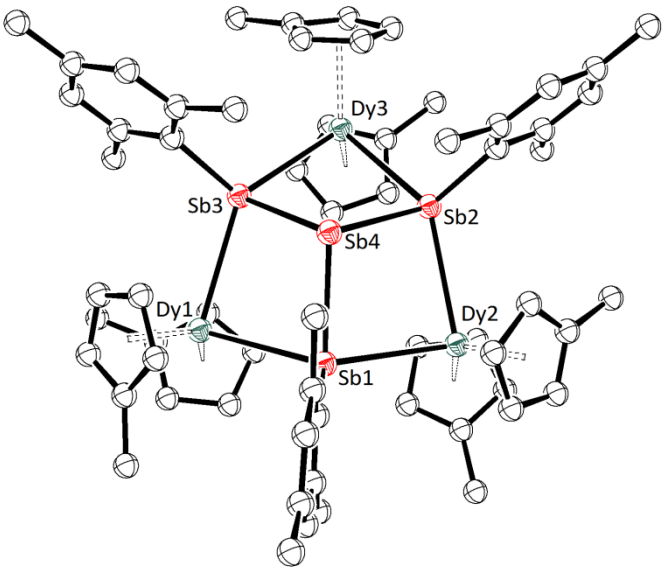

Figure 1.14. Structure of **1.34** highlighting the Zintl-like Dy_3Sb_4 unit.[51]

The AC magnetic susceptibility studies showed frequency dependence of χ'' up to 37 K for **1.33** and 35 K for **1.34**. Despite not observing an increase in the temperature of observed peak maxima from 0.1-1400 Hz AC field, the U_{eff} barrier of 345 cm^{-1} for **1.33** is much larger than the neat arsenide. This is observed with a concomitant increase in the Dy—E bond lengths, the Dy—Sb bonds range from 3.092(3)-3.212(3) Å and 3.119(1)-3.138(1) Å in **1.33**

and **1.34** respectively. The Zintl-like **1.34** has a U_{eff} barrier of 272 cm^{-1} which implies that the central Sb^{3-} ion decreases the axiality of the m_J = 15/2 ground state of the Dy^{3+} ions with respect tto the Dy_3Sb_3 system. Magnetic dilution of **1.33** and **1.34** has a negligible effect on the U_{eff} barrier with the energy barriers to spin inversion of Dy@Y_3Sb_3 and Dy@Y_3Sb_4 being 345 cm^{-1} and 270 cm^{-1} respectively. This implies that magnetic relaxation is not influenced by intramolecular Dy---Dy exchange interactions.

To date the field of dysprosium metallocene SMMs containing p-block soft-donor atom bridging ligands is limited to research conducted by the Layfield group. Due to the limits of the periodic table the trend of moving to softer bridging atoms can only yield a certain degree of increase in U_{eff} for multinuclear lanthanide SMMs. So it is necessary to employ other bridging ligands that generate a weak crystal field. In 2016, Layfield *et. al.* recognised that metal carbonyls are a good alternative due to the low energy lone-pair of electrons on the O atom of the C≡O ligands.[52] There are examples of metal carbonyls bonding to RE metals through the O atom to give a RE—O≡C:—M type motif, but under certain conditions metal-metal bonds between rare-earths and TMs can form.[53]

The rare-earth precursor [Cp*$_2$Ln(BPh_4)] (Ln = Dy, Y) was reacted with one equivalent of K[CpFe$(CO)_2$] in THF to give the isocarbonyl-ligated [Cp*$_2$Ln((μ-$OC)_2$FeCp)] (**1.35**) in 73% and 77% yield for Ln = Y and Ln = Dy respectively. XRD reveals that each metal centre is related by symmetry and bound to two isocarbonyl oxygen atoms in the equatorial plane from the [CpFe$(CO)_2]^-$ ligands. Using the sterically bulkier Cp* ligands results in a much more obtuse Cp_{cent}—Dy—Cp_{cent} angle of 141.5° with respect to that of the [Cp'$_2$Dy(μ-E(H)Mes)]$_3$ complexes. The Dy—O bond distances are 2.292(9) and 2.287(12) Å which are much smaller than the Dy—E distances observed in {Cp'$_2$Dy} complexes bridged by P, As and Se ligands.

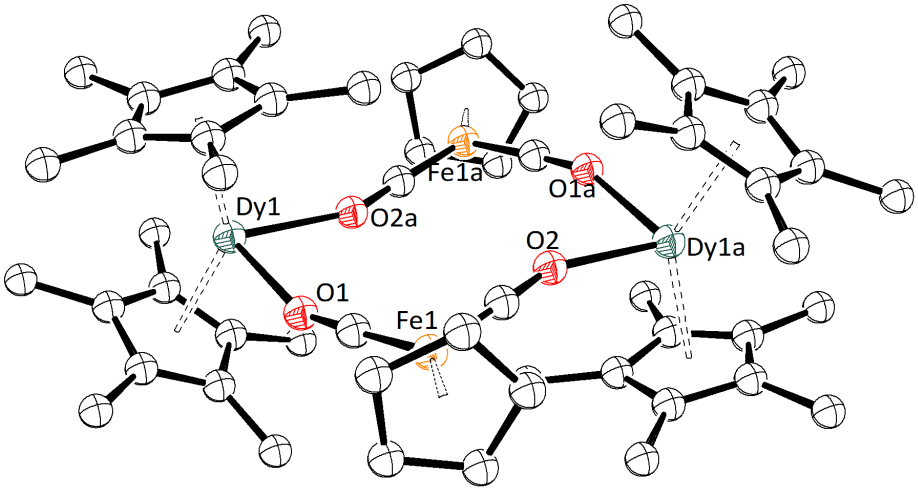

Figure 1.15. Molecular structure of the isocarbonyl ligated **1.35-Dy**.[52]

Despite the short Dy—O bonds in the equatorial plane **1.35-Dy** has very strong SMM character, displaying peak maxima in χ''(ν) isotherms up to 56 K at 1.4 kHz ac field. All the more impressive is that it shows SMMs becoming functional towards liquid nitrogen temperature (77 K). Using the Cole-Cole plot of χ'(χ'') the relaxation times (τ) can be extracted and used to plot τ^{-1}/ln(T) (or ln(τ)/T^{-1}) which is another way of expressing the temperature dependence of relaxation time. The energy barrier in this case was determined by fitting the whole curve in the Arrhenius plot as opposed to just the linear section. This can be done using the following equation:

$$\tau^{-1} = \tau_0^{-1} e^{-U_{eff}/k_B T} + CT^n + \tau_{QTM}^{-1} \quad (1.1)$$

which includes Raman and QTM parameters. The U_{eff} barrier for **1.35-Dy** was found to be 662 cm^{-1} which is the third largest energy barrier reported to date of any type of SMM. M(H) plots show butterfly hysteresis loops (also termed waist-restricted hysteresis) up to 6.2 K. The sharp drop in magnetisation on approaching zero field is due to QTM. *Ab initio* calculations on **1.35-Dy** reveal that the main magnetic axis of the ground KD runs parallel to the Cp*—Dy—Cp* bonds, which compliments the magnetostructural correlations found in previous examples of dysprosium metallocene SMMs. Interestingly, while the majority of

studies into spin relaxation pathways in dysprosium SMMs suggest relaxation primarily via a first or second excited KD, calculations of the energy separation between excited KDs in **1.35-Dy** suggest Orbach type relaxation occurs via at least the 4th, 5th or 6th excited states (calculated to be 639 cm^{-1}).

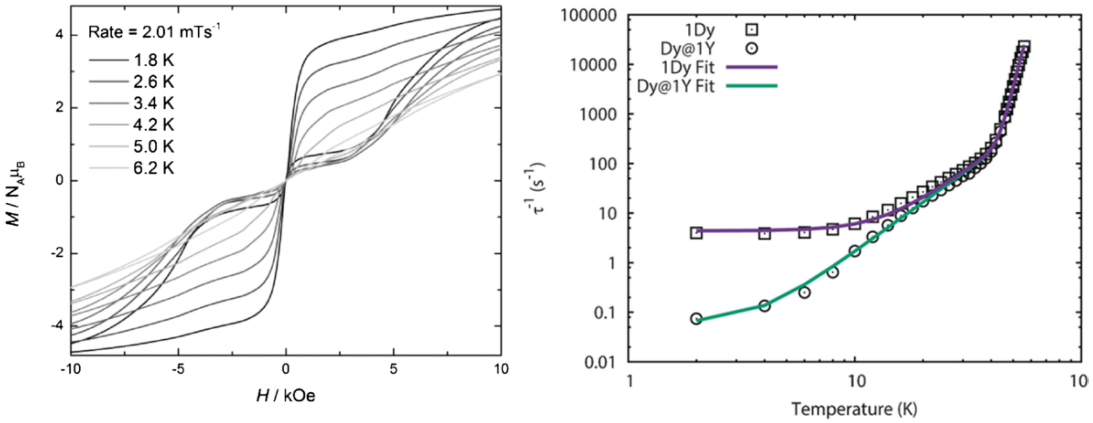

Figure 1.16. (Left) M(H) plot for **1.35-Dy** showing waist-restricted hysteresis. (Right) Arrhenius plot showing fit to the whole curve.[52]

1.3.2 Lanthanide Metallocene SMMs with Radical-bridging Ligands

Despite U_{eff} values climbing ever higher in lanthanide SMMs the blocking temperature has still been consistently below 10 K and the phenomenon of magnetic remanence at higher temperatures remains a formidable challenge. Stabilising the ground m_J state of Dy^{3+} is becoming easier to accomplish building on the principles of creating a strong axial ligand field and a weak equatorial field. However, regardless of how high the energy barrier to spin inversion is it can still be bypassed by QTM. In the last 5 years some impressive advances have been made to supress QTM using bridging ligands containing radicals.

A persistent problem in achieving high blocking temperatures has been the lack of strong exchange coupling between Ln^{3+} centres in multinuclear SMMs. In most SMMs the value for the exchange coupling constant, J, is on the order of a few wavenumbers. The reason for this is that Ln^{3+} ions have radially contracted 4f orbitals that to a first approximation don't overlap with orbitals of bridging ligands. One way to overcome this is to synthesise a bridging unit containing a radical. To that end some complexes have been reported by Long *et. al.* that contain N-heterocyclic ligands such as bipyrimidine (bpym) and 2,3,5,6-tetra-2-(pyridyl)pyrazine (tppz) that can be easily reduced to form radical anions.[54, 55]

In 2012, the complexes $[(Cp^*_2Ln)_2(\mu\text{-bpym})^{\cdot}][BPh_4]$ (Ln = Gd, Dy, Tb) (**1.36**) were synthesised from $Cp^*_2Ln(BPh_4)$ and bipyrimidine in THF followed by reduction with one equivalent of KC_8. Elimination of $KBPh_4$ afforded the monoanionic, radical-bridged complexes.[54]

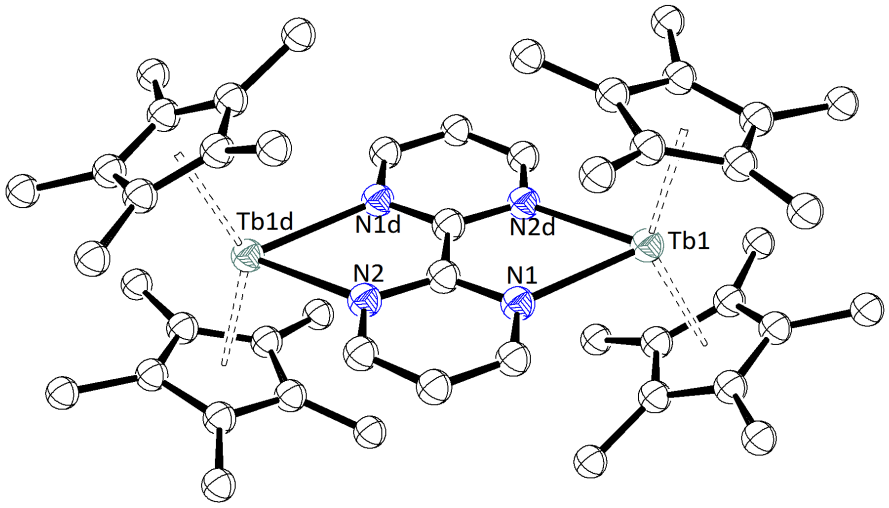

Figure 1.17. Molecular structure of **1.36-Tb**.[54]

The SMM characteristics are defined by the response of the sample to an AC magnetic field, however, in this case there is also an unusual response in DC field magnetic susceptibility measurements. $\chi_M T(T)$ plots for most Ln SMMs show a plateau or a small decline from RT down to around 50 K, below which the decline starts to become more pronounced at low temperatures. In (**1.36-Dy**) however the $\chi_M T$ value begins to increase below 100 K. **1.36-Tb** shows a steeper increase down to 25 K followed by a drop between 25 K and 1.8 K. **1.36-Dy** shows a similar increase up to 25 K followed by a very steep drop at 7 K which is indicative of magnetic blocking. To determine the exchange coupling the $\chi_M T(T)$ curve for **1.36-Gd** (Figure 1.18 – green triangles) was fitted to a spin only Hamiltonian, giving an exchange coupling constant of J = -10 cm^{-1} (-2J formalism). This value is an order of magnitude larger than most dinuclear Ln-SMMs indicating much stronger exchange coupling between Gd centres. The M(H) plot of **1.36-Dy** shows open hysteresis loops up to 6.5 K with a fairly large coercive field of H_c = 0.6 T at 3 K. This open hysteresis as opposed to waist restricted hysteresis is indicative of suppression of QTM in zero field.

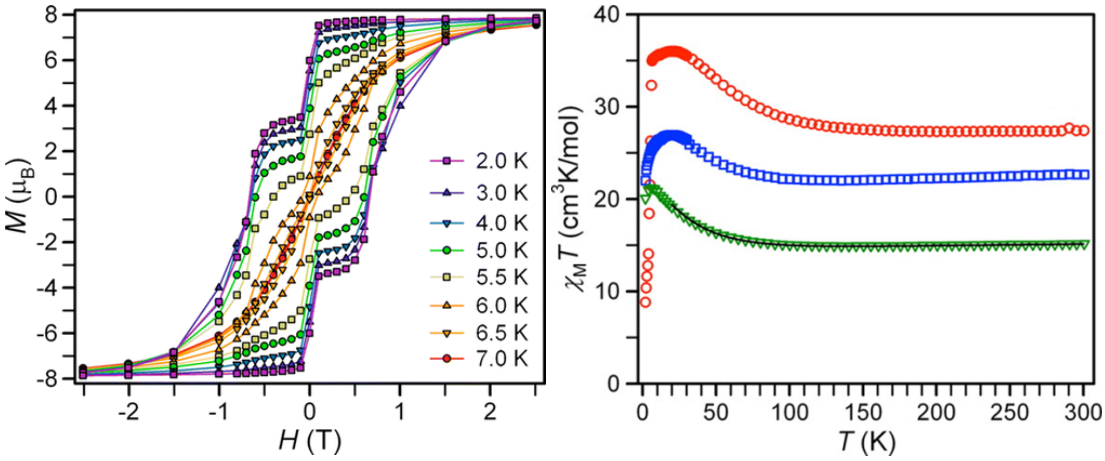

Figure 1.18. (Left) M(H) plot for **1.36-Dy** showing open hysteresis up to 6.5 K; (right) χ_MT(T) plot: red circles - **1.36-Dy,** blue squares - **1.36-Tb** and green triangles - **1.36-Gd**.[54]

AC magnetic susceptibility measurements on **1.36-Dy** reveal a relatively small spin reversal energy barrier, U_{eff} = 87 cm^{-1} which is likely due to the destabilising effect of hard N-donor atoms in the equatorial plane. The Dy—N bond lengths are 2.412(1) and 2.427(1) Å which are short with respect to other Dy—E bonds found in complexes with softer ligands.

In 2014, two sets of radical bridged, dinuclear lanthanide complexes of the multi-electron accepting tetra-2-pyridylpyrazine (tppz) ligand were reported.[55] In a similar manner to **1.36-Ln** the tppz-bridged complexes were synthesised by addition of neutral tppz to two equivalents of $Cp^*_2Ln(BPh_4)$ in THF followed by addition of one equivalent of KC_8. Work up afforded the complexes $[(Cp^*_2Ln)_2(tppz)^{\cdot}][BPh_4]$ (Ln = Gd, Dy, Tb) (**1.37**) upon crystallisation from THF.

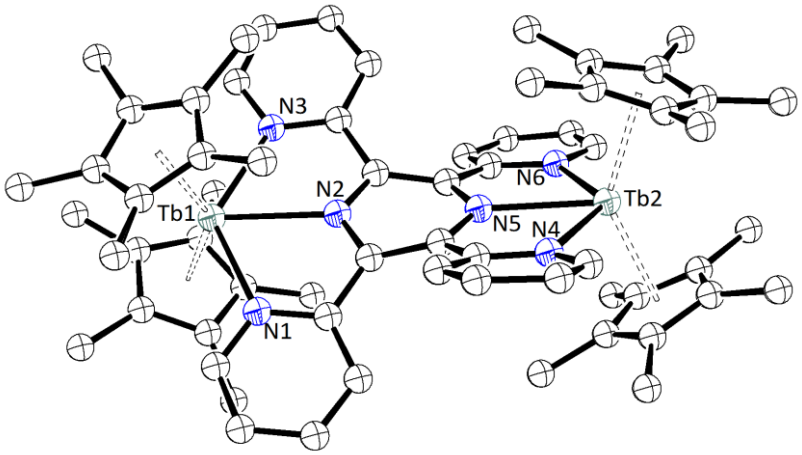

Figure 1.19. Molecular structure of **1.37-Tb** highlighting the substantial twist in the $tppz^{\bullet-}$ ligand. [55]

The radical anions could also be synthesised by reducing the $tppz^{\bullet-}$ unit to the radical trianion $tppz^{3-}$ to form $[K(2.2.2\text{-crypt})][(Cp^*_2Ln)_2(\mu\text{-}tppz^{\bullet})]$ (**1.37**). The anionic complexes containing the radical trianion tppz ligand show no response to an AC magnetic field. However, the cationic complexes **1.37-Tb** and **1.37-Dy** do show an energy barrier to spin reversal of U_{eff} = 5.1 cm^{-1} and 35.9 cm^{-1} respectively. DC magnetic measurements on **1.37-Dy** show open hysteresis loops in the M(H) plot up to 2.5 K, whereas further increases in temperature lead to a waist restricted hysteresis up to 3.5 K.

1.4 Divalent Lanthanide Chemistry

Whilst the chemistry of the lanthanide metals is dominated by the +3 oxidation state, there are exceptions to this trend across the period. Eu^{2+} and Yb^{2+} have half-filled ($4f^7$) and filled ($4f^{14}$) electron configurations respectively, so there is an inherent stabilising factor for these particular divalent ions. The highest 3rd ionisation energy of all the lanthanides is for europium. Samarium also adopts the +2 oxidation state in the solid state and in solution,

along with Eu^{2+}, Tm^{2+} and Yb^{2+} these ions have become known as the "classical" divalent lanthanides.[56, 57]

Divalent states of samarium, europium and ytterbium have been known since the 1920s, but they were usually synthesised in solution and examined by UV spectroscopy to assign the oxidation state.[58, 59] In 1980, Kagan synthesised SmI_2 (**1.38**) in THF solution and used it in a variety of organic reduction reactions (e.g. coupling of aldehydes and ketones to diols).[60-63] YbI_2 was synthesised in an identical manner. Despite its widespread use in organic synthesis the crystal structure of **1.38** was not reported for some 15 years until Evans reported the structures of the THF and DME solvates of **1.38** in 1995 (Scheme 1.11).[64] It was shown that it crystallises as $SmI_2(THF)_5$ (**1.39**) with two iodine ions in a *trans* configuration about the Sm ion and five THF molecules coordinated around the equatorial plane. The coordination geometry of **1.38** is pentagonal bipyramidal (D_{5h} symmetry).

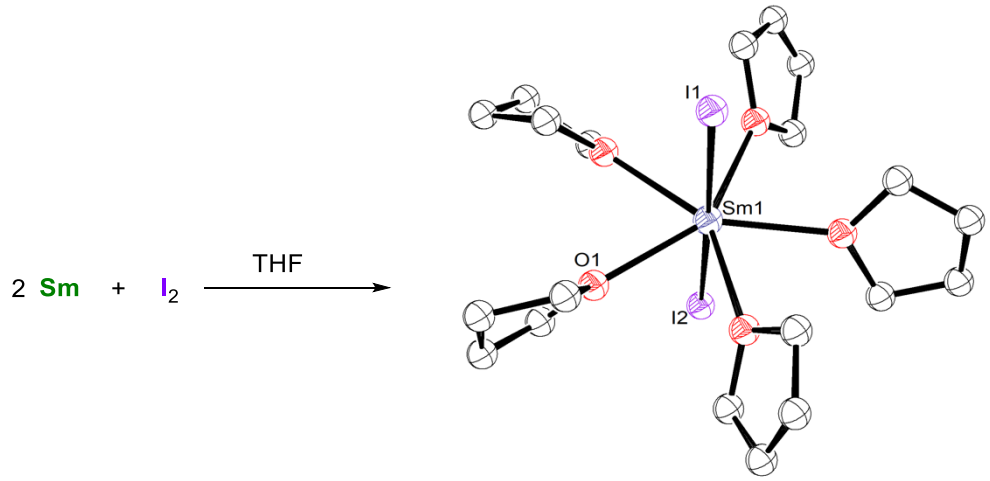

Scheme 1.11. Synthesis and molecular structure (ball and stick representation) of $SmI_2(THF)_5$.[64]

Until 1997 it was thought that non-classical Ln^{2+} ions (Ln^{2+} ≠ Sm, Eu, Tm, Yb) would be too strongly reducing to be synthesised and isolated. The reduction potential ($4f^n \rightarrow 4f^{n+1}$) in aqueous medium with respect to the normal hydrogen electrode (NHE) is -1.55 V for Sm^{2+}, but -2.3 V for Tm^{2+}, and Sm^{2+} is considered a strong one-electron reducing agent! However,

work by Bochkarev showed that it is indeed possible to synthesise and isolate divalent thulium as: $TmI_2(DME)_3$ (**1.40**).[65] The synthesis is more elaborate than that of the samarium and ytterbium diiodies, which are simply made from 1,2-diiodoethane and the metal filings in THF (Scheme 1.1). An excess of thulium metal and iodine are stirred in DME at room temperature for two days to give TmI_3 and unreacted thulium. The solution is decanted to remove excess iodine, more DME is added to the solids and the solution is heated to 80°C, producing a green solution. As the thulium metal and TmI_3 are heated together in solution, the thulium metal reduces the Tm^{3+} to the divalent, dark green Tm^{2+}. Compound **1.40** is very sensitive to light and air but can be isolated in moderate crystalline yields of 54% on a 5-10 gram scale. The structure of **1.40** was elucidated by X-ray crystallography and exhibits two iodine ions occupying the axial sites (at a I—Tm—I angle of 173.8° – Figure 1.20) with five O-donor atoms from DME ligands occupying the equatorial plane. The coordination geometry in **1.40** is very similar to that seen for $SmI_2(DME)_2(THF)$.

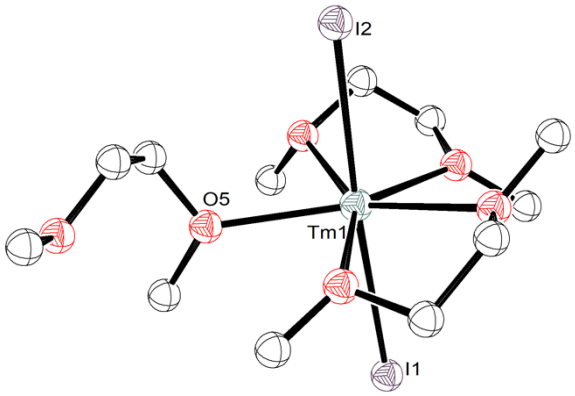

Figure 1.20. Molecular structure of $TmI_2(DME)_3$ with thermal ellipsoids drawn at 50% probability.[65]

The next lanthanide ions with the lowest reducing potential in the lanthanide series are Dy^{2+} and Nd^{2+}. In 1999, the first molecular complexes of Dy^{2+} and Nd^{2+} were synthesised: $LnI_2(DME)_3$ (**1.41** – Dy; **1.42** - Nd).[66] Despite establishing the procedure to synthesise **1.41** and **1.42**, Bochkarev *et. al.*, were not able to grow crystals suitable for X-ray diffraction study at the time, but **1.42** crystallographically characterised in a later study.[67] A magnetic

moment of 2.83 μ_B was observed for **1.42** which differs markedly from the value for Nd^{3+} (3.68 μ_B). UV spectroscopy and magnetic moment measurements suggested the presence of Ln^{2+}. IR spectra of **1.41** and **1.42** also matched previously recorded spectra for NdI_2 and DyI_2 in THF solutions, so the evidence for Dy^{2+} and Nd^{2+} was compelling.

The crystal structure of **1.42** was reported by Evans in 2000 and found to be isostructural to the Tm analogue (**1.40**).[68] Compound **1.42** is a powerful reductant, even more so than the thulium version. With a reduction potential of -2.5 V (aqueous solution vs. NHE) both complexes **1.41** and **1.42** are very unstable in DME or THF, but can be kept as solids over prolonged periods under an inert atmosphere of argon. A test of this reductive power was to mediate the reaction between an alkyl chloride and a ketone, to give a secondary alcohol after hydrolysis. The reaction proceeds at 0°C over one hour using $TmI_2(THF)_n$ but using $DyI_2(THF)_n$ the reaction is instantaneous at -45°C. $TmI_2(THF)_n$ is also able to reduce naphthalene and diphenylacetylene to afford dihydronapthalene upon hydrolysis and *cis*-stilbene, respectively.

To date, the only ligand environment that can stabilise divalent lanthanides, besides iodide, are cyclic aromatic ligands such as arenes and cyclopentadienyls. There is also one example of a molecular Sc^{2+} complex containing $[N(SiMe_3)_2]^-$ ligands.[69] By the early 2000s it became clear that there were two main strategies to synthesising more complex divalent lanthanide species. One being reduction of trivalent precursors and the other being transmetallations using pre-formed divalent precursors. In 2002, Nief *et. al.*, used the recently discovered TmI_2 to synthesise organometallic complexes of Tm^{2+} with phospholide and arsolide ligands according to Scheme 1.12.[70] Transmetallation reactions with two equivalents of [K(Dsp)] or [K(Dsas)] (Dsp = $C_4P(CH_3)_2(SiMe_3)_2$; Dsas = $C_4As(CH_3)_2(SiMe_3)_2$) with $TmI_2(THF)_3$ in Et_2O gave the corresponding TMS-substituted phospholide and arsolide complexes $[Tm(Dsp)_2(THF)]$ (**1.43**) and $[Tm(Dsas)_2(THF)]$ (**1.44**) in yields of 71% and 56%

respectively. The tert-butyl substituted analogues of **1.43** and **1.44** were also synthesised in a similar manner.

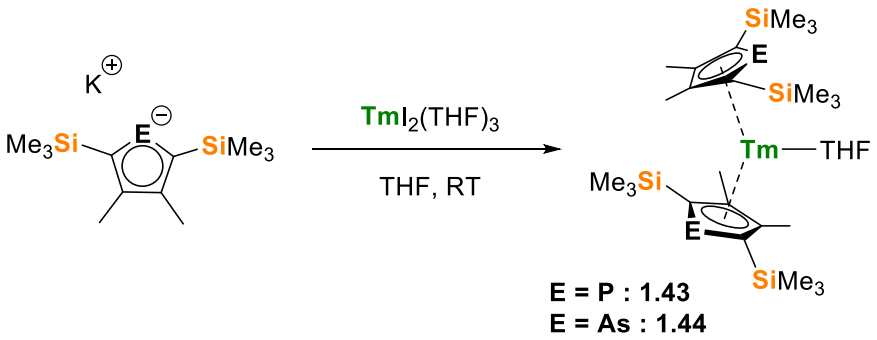

Scheme 1.12. Synthesis of Tm^{2+} complexes with P and As ligands.[70]

Tm^{2+} complexes with bulky cyclopentadienyl ligands have also been synthesised from TmI_3 and KCp^{ttt} followed by reduction with KC_8 to give $[Cp^{ttt}_2Tm(THF)]$ (**1.45**) in moderate yield of 47%. Whereas reacting TmI_2 with 2 equivalents of KCp^{ttt} affords compound **1.45** in a yield of just 32%.[71] This difference in yield is likely due to the propensity for Tm^{2+} to be oxidised to Tm^{3+} forming other by-products.

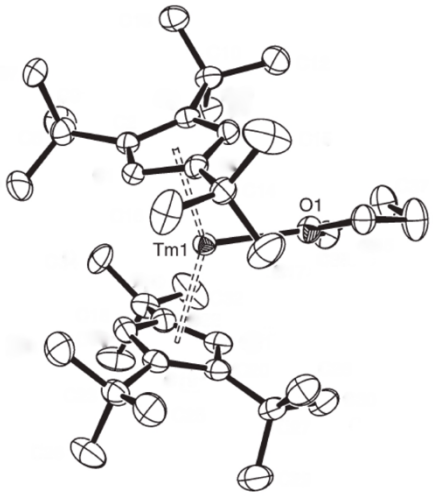

Figure 1.21. Molecular structure of the Tm^{2+} complex **1.45**.[71]

In the late 1990s there was a flurry of discoveries involving 'non-classical' divalent lanthanide ions, that were previously thought to be inaccessible, supported by Cp ligands.

In 1998, Lappert *et. al.* reported the first La^{2+} complex, containing a bridging benzene ligand [K([18]crown-6)-(η^2-C_6H_6)$_2$][(LaCp$^{tt}_2$)$_2$(μ-η^6:η^6-C_6H_6)]· 2 C_6H_6 (**1.46**) (Cp^{tt} = $C_5H_3{}^tBu_2$).[72] There is no significant bending of the C_6H_6 ligand, suggesting that it is singly-reduced (Figure 1.22). Previous attempts at reducing Cp''$_3$La (Cp'' = ($C_5H_3(SiMe_3)_2$)) gave a La^{3+} –ate complex with a doubly-reduced benzene ligand [K(18-c-6)][Cp''$_2$La(C_6H_6)] (**1.47**).[73] Heating a dark red solution of **1.47** in benzene to 70°C afforded a green solution from which no crystalline material could be obtained. However, EPR, ^{1}H NMR and UV-vis spectroscopy on this green solution suggested the presence of La^{2+}. Considering these results, attention switched from the silyl-substituted Cp'' ligand to the all-carbon equivalent Cp^{tt} ligand. Despite the different electrochemistry of LaCp$^{tt}_3$ ($E_{1/2}$ = 3.1 V) and LaCp''$_3$ ($E_{1/2}$ = 2.8 V), in THF, the reaction of LaCp$^{tt}_3$ with potassium metal in benzene still proceeds in a similar manner giving a dark red solution which slowly turned green. After storage at 4°C for one week, dark-green crystals of **1.46** were deposited and the structure was characterised by X-ray diffraction. This was a significant step towards accessing low-valent states of all the rare-earth metals.

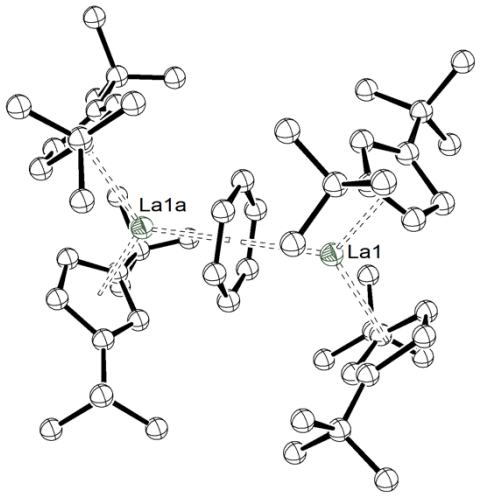

Figure 1.22. Molecular structure of the anion of **1.46** highlighting planar $(C_6H_6)^-$ bridging ligand, thermal ellipsoids drawn at 50% probability.[72]

In 2008, Lappert *et. al.* expanded the library of La^{2+} compounds by isolating the first monometallic species of La^{2+}.[74] Taking the trivalent precursor, [LaCp''$_3$], and reacting it with

one equivalent of potassium in the presence of the chelating agent 2.2.2-cryptand afforded the divalent complex [K(2.2.2-crypt)][LaCp''$_3$] (**1.48** – Figure 1.23). More than this they were able to put to rest any underlying doubt about the ability of lanthanum to form stable, divalent compounds. The di-nuclear complex reported 10 years earlier prompted some scepticism as there was potentially 3 different scenarios for the charges on the lanthanum ions and the benzene ligand; 1) $La^{2+}/La^{2+}/[C_6H_6]^-$; 2) $La^{2+}/La^{3+}/ [C_6H_6]^{2-}$ or 3) $La^{3+}/La^{3+}/ [C_6H_6]^{3-}$. SQUID measurements on **1.48** show that the compound is paramagnetic with a calculated magnetic moment of 1.4 μ_B.

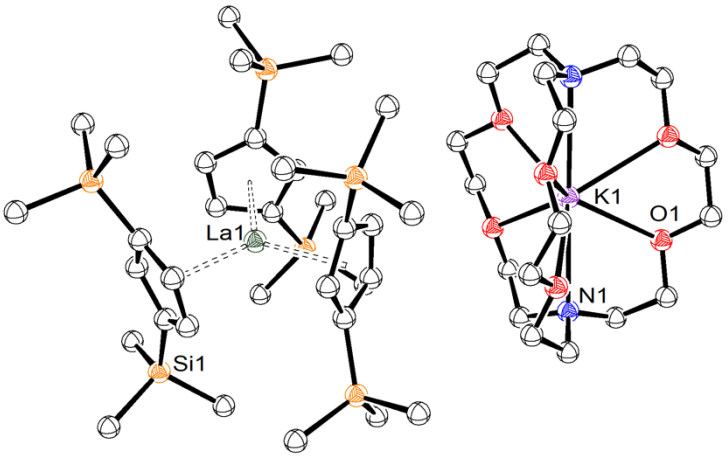

Figure 1.23. Molecular structure of **1.48**, the first monometallic La^{2+} complex.[74]

With Lappert's discoveries 10 years apart confirming that lanthanum can form an isolable divalent complex, the aim was then to fill in the gaps in the rare earth-lanthanide series.

Evans *et. al.* were able to synthesise the first molecular Y^{2+} complex in 2011.[75] Previous work had shown evidence for the formation of Y^{2+}, using EPR spectroscopy to study the reaction between [Y(N(SiMe$_3$)$_2$)$_3$] and potassium in an atmosphere of N_2 (see Figure 1.24).[76] As yttrium has a smaller atomic radius than lanthanum, the $(Cp')^-$ ligand was used instead of the more sterically hindering $(Cp'')^-$ ligand used by Lappert. Reacting Cp'$_3$Y with KC_8 in the presence of 18-crown-6 at -45°C afforded the Y^{2+} complex [K(18-c-6)][Cp'$_3$Y] (**1.49-Y**). **1.49-Y** is stable at low temperatures but decomposes from dark purple to an orange

solution in 30 minutes at RT. A contributing factor to this instability is thought to be the close proximity of the K counterion to the Cp' ring bound to yttrium which may have a high lattice enthalpy.

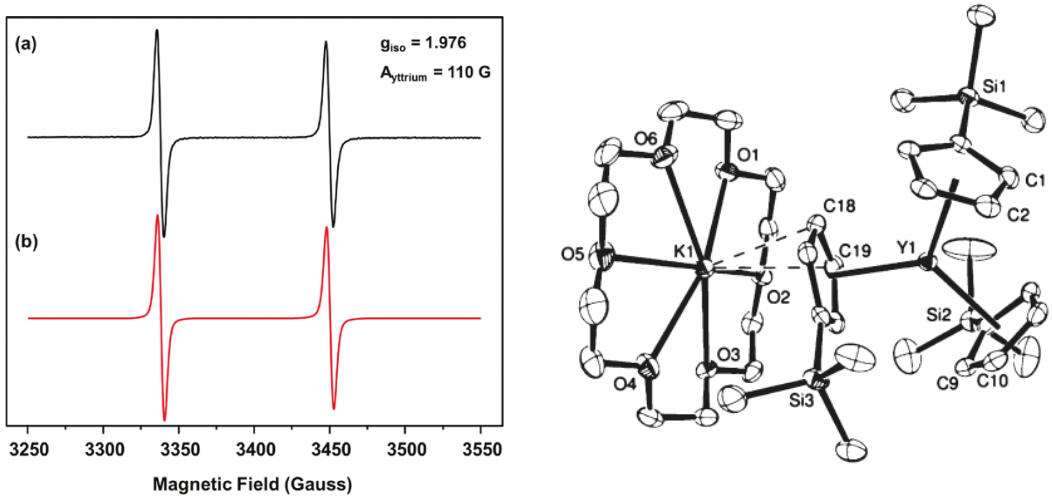

Figure 1.24. (Left) EPR spectrum of YN''_3/KC_8 in THF (black) and simulated spectrum (red). Doublet is consistent with electron spin coupling to I=1/2 ^{89}Y nucleus, the large coupling constant is consistent with Y^{2+}. (Right) Crystal structure of the first molecular Y^{2+} complex (**1.49-Y**).[75]

Molecular complexes of holmium and erbium in the +2 oxidation state were discovered in 2012 using the same tris-cyclopentadienyl ligand framework as used for **1.49-Y**.[77] The synthetic method was the same as that used for **1.49-Y** with the exception of having each component of the reaction pre-chilled to -35°C. X-ray diffraction revealed **1.49-Ho** and **1.49-Er** to be isostructural with **1.49-Y**. Comparing the Cp_{cent}—M bond distances to those of Cp'_3Ln showed that **1.49-Ho/Er/Y** have a $4f^n5d^1$ electron configuration (n = 10 – Ho; 11 – Er; 0 – Y). DFT calculations show the d_{z2} orbital is much lower in energy for the Ln^{2+} ions relative to the Ln^{3+} ions.

Four more previously inaccessible Ln^{2+} ions were reported with the synthesis of molecular complexes of Pr^{2+}, Gd^{2+}, Tb^{2+} and Lu^{2+} of the formula: [K(2.2.2-crypt)][Cp'_3Ln] (**1.50-Ln**) in

2013. The Y, Ho and Er complexes were also synthesised with the cryptand ligand according to Scheme 1.13.[78]

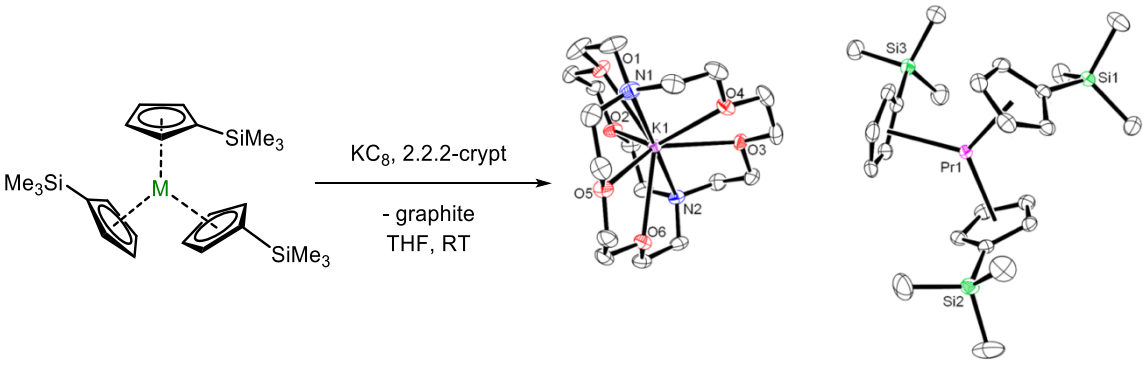

Scheme 1.13. Synthesis of the Ln^{2+} complexes where M = Y and all the lanthanide metals (except radioactive Pm). Molecular structure of **1.50-Pr** shown as a representative example of the isostructural series.[78]

2.2.2-cryptand was used as a co-ligand for K^+ when it was found that the reaction using the scheme outlined above with 18-crown-6 and Cp'_3Tb gave an unusual product, with an inverted sandwich cation, $\{[K(18\text{-}c\text{-}6)_2](\mu\text{-}Cp')\}\{Cp'_3Tb\}$ (**1.51**). The synthesis and characterisation of **1.51** was the first crystallographic evidence of decomposition of complexes of this type to KCp' fragments due to the fact the K^+ ion had picked up a [K(18-c-6)Cp'] unit. In the structures of **1.49-Ln** the proximity of the K^+ counterion can explain the low stability of the products, perhaps due to the dissociation of a Cp' ligand from the Ln ion, and the need to perform the reaction at -35°C, **1.50-Ln** also demonstrates that the $[Cp'_3Ln]^-$ anion is stable when not coordinated to any counterion. By using 2.2.2-cryptand, the K^+ ion is now completely sequestered and the resulting complexes have increased stability with respect to their 18-crown-6 analogues. The reaction proceeds quickly in THF at room temperature and gives crystalline products that are stable at RT. Compound **1.50-Y** has been used to reduce biphenyl and naphthalene.[79]

In order to accurately assess the differences between the +2 and +3 oxidation states in the $[LnCp'_3]^n$ (n = 0, -1) framework, it was necessary to synthesise **1.50-Ln** complexes (Ln = La,

Ce, Nd, Sm, Eu, Dy, Tm, Yb), including the traditional four divalent lanthanides, using 2.2.2-cryptand in place of 18-c-6.[1] Direct structural comparisons between $LnCp'_3$ and [K(2.2.2-crypt)][Cp'_3Ln] showed that all the non-classical Ln^{2+} complexes (**1.50-Ln**; Ln ≠ Sm, Eu, Tm, Yb) have Ln-Cp_{cent} bond lengths in the range of 0.02-0.032 A (<1 %) longer than their $LnCp'_3$ counterparts. This is in line with these compounds having a $4f^n5d^1$ electron configuration. The traditional Ln^{2+} ions (Ln = Sm, Eu, Tm, Yb) have Ln-Cp_{cent} distances 0.123-0.156 A (≈ 6 %) longer than that of their Ln^{3+} analogues. The 'classical' Ln^{2+} ions have a $4f^{n+1}$ configuration, the larger difference in bond lengths to the ligands is due to an extra electron residing in the radially contracted 4f orbital.

UV-vis spectroscopy on **1.50-Ln** (Ln = Y, La and all lanthanides except Pm) also suggests that all but the classical Ln^{2+} ions have a $4f^n5d^1$ configuration. The spectra all have similar features (including high molar extinction coefficients – see Figure 1.25) to the spectra obtained on **1.50-Y** and **1.50-Lu** which must have electron configurations of $4d^1$ and $5d^1$ respectively (Y^{3+} - $4d^0$; Lu^{3+} - $4f^{14}$). Whereas, the spectra for **1.50-Sm/Eu/Tm/Yb** show much smaller extinction coefficients and transitions that are Laporte-allowed 4f→5d.

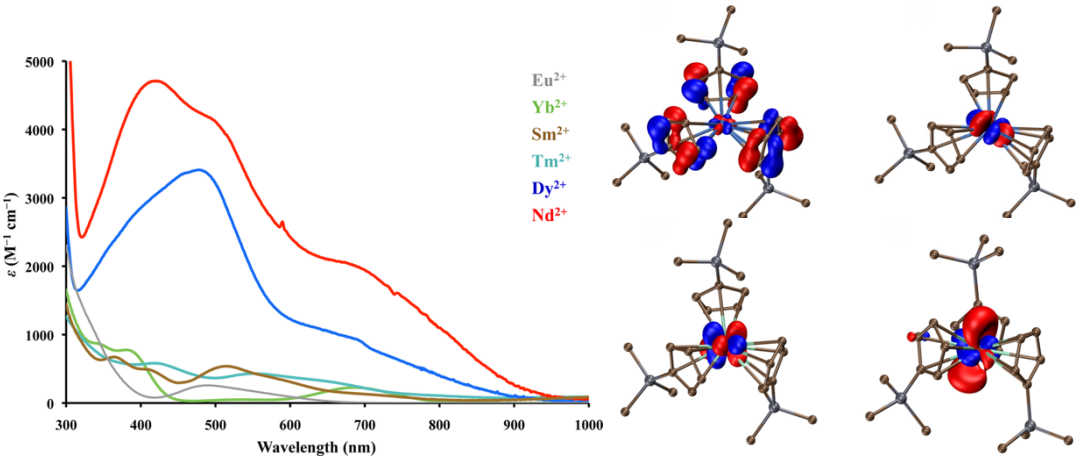

Figure 1.25. (Left) UV-vis spectra of some **1.50-Ln** compounds. (Right) DFT calculations of the MO plots for Cp'_3Dy (top left), Cp'_3Nd (bottom left), **1.50-Dy** (top right) and **1.50-Nd** (bottom right).[1]

Density Functional Theory (DFT) calculations however, cast doubt on the case of neodymium and dysprosium. The LUMO of Cp'_3Nd shows mostly f-character whereas the HOMO of **1.50-Nd** shows considerable d_{z2} character. Of the 90% contribution from the metal center, 29 % has d- and 60 % has f-character. Despite this finding, all the experimental evidence suggests $5d^1$ configuration for **1.50-Nd**. For Dy, the calculations suggest that the LUMO of Cp'_3Dy and the HOMO of **1.50-Dy** are both f-orbitals, despite all the experimental results suggesting otherwise.

In summary, many of the advancements made in lanthanide organometallic chemistry in the last 20-30 years have been based around complexes containing cyclopentadienyl ligands. Bis(cyclopentadienyl) lanthanide alkyl complexes have been synthesised and studied for their reactivity. Much progress has been made in olefin polymerisation catalysis to synthesise industrially relevant compounds such as polyethylene and polystyrene. Lanthanide metallocene complexes have also transformed the field of single molecule magnetism. Complexes of the formula $[Cp^{Me}_2Dy(\mu\text{-}E(H)R]_n$ (where E = P, As, S, Se, Sb) with

soft donor atom ligands have been show to lead to concomitant increase in U_{eff} with increasing atomic radius of the bridging atom, E. Lanthanide metallocenes bridged by radical ligands have been shown to promote magnetic blocking (or hysteresis).

The divalent state is now known for all lanthanide metals. Evans *et. al.* have shown that the complexes of the formula: $[K(2.2.2\text{-crypt})][LnCp'_3]$ (Ln = Y and all lanthanides except Pm) can be synthesised and isolated. Ln^{2+}ions can be categorised as 'classical' (with an electron configuration of $4f^{n+1}$) or 'non-classical' ($4f^n5d^1$). Spectroscopic and DFT studies revealed all the newly discovered Ln^{2+} ions belong to the latter category. DFT calculations cast some ambiguity of the electron configuration of Nd^{2+} and Dy^{2+}.

1.5 Aims of the PhD

The project set out in this thesis has two main aims. The first aim is to synthesise rare-earth metallocene ^{n}butyl complexes of the formula $[Cp^R_2Ln^nBu]$ (R = H or Me; Ln = Dy and Y) and study the reactivity towards a variety of C—H acidic substrates such as ferrocene and N-heterocyclic carbenes (NHCs), as well as elemental chalcogens. These substrates were chosen as their reactivity towards ^{n}BuLi is well known and a rare-earth ^{n}butyl complex may provide bespoke reactivity. In principle, such rare-earth ^{n}butyl complexes should be accessible from salt metathesis reactions of rare-earth halide ($[Cp_2LnCl]_2$) or cyclopentadienyl precursors (Cp_3Ln) with ^{n}BuLi. Yttrium will be used as it is a diamagnetic analogue of mid-to-late lanthanides (ionic radius of Y^{3+} is very similar to that of Dy^{3+}) so reactivity can be studied by multinuclear NMR spectroscopy. Dysprosium will be used because it has a large magnetic moment and is conducive to making single molecule magnets (SMMs) with large energy barriers to spin inversion, U_{eff}.

The second aim of the project is to study the magnetic properties of Dy^{3+} complexes. Little is known about the magnetic properties of multinuclear dysprosium complexes bridged by

carbon donor-atom ligands, so all dysprosium versions of complexes synthesised will be analysed by SQUID magnetometry to determine if they are SMMs.

Previous work in the Layfield group has been based on the tritopic ligand hexaazatrinaphthalene (HAN). In principle, a tri-metallic lanthanide complex of HAN could show good magnetic blocking properties. A side aim of this project is to synthesise the first lanthanide-HAN complex with a suitable Dy^{3+} precursor and examine its dynamic magnetic properties.

Chapter 2

Results & Discussion: Synthesis, Reactivity & Magnetism of Rare-Earth ^{n}Butyl Complexes

2 Results & Discussion: Synthesis, Reactivity & Magnetism of Rare-Earth ^{n}Butyl Complexes

2.1 Introduction

Rare-earth alkyl complexes contain highly reactive Ln—C bonds, as such they are prone to decomposition in air, moisture and are often thermally sensitive. Alkyl complexes of rare-earth metals are typically based on $–CH_3$, $–CH_2SiMe_3$ or benzyl groups. These ligands lack a β-H atom which rules out the possibility of decomposition via β-H elimination. The most readily available, and often cheapest, alkylating reagent is n-butyllithium (^{n}BuLi). To date there is just one complex of a rare-earth bearing an n-butyl ligand that has been isolated and crystallographically characterised. In 2003, Okuda *et. al.* reported the ^{n}Bu-bridged yttrium complex $[Y(\eta^5{:}\eta^1\text{-}C_5Me_4SiMe_2NCMe_3)(\mu\text{-}CH_2CH_2Et)]_2$ supported by an amine-tethered cyclopentadienyl ligand (see Figure 2.1).[80] Variable-temperature ^{1}H NMR spectroscopy showed there is a fluxional process involving agostic interactions of β-CH_2 groups to the yttrium centre. The α-CH_2 resonance is a triplet at RT but on cooling to -80^{o}C it becomes a doublet of triplets centred at δ -0.20 ppm which implies coupling to β-CH_2 protons, split by coupling to an I = ½ ^{89}Y nucleus.

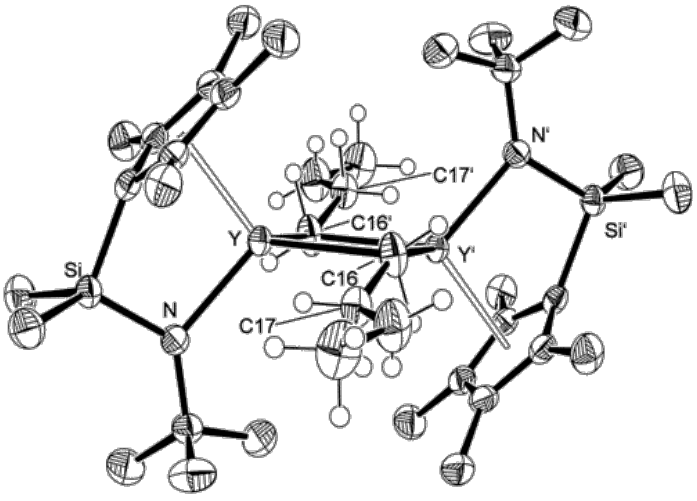

Figure 2.1. Molecular structure of an ^{n}butyl ligated yttrium complex, reported by Okuda *et.al*. The thermal ellipsoids are drawn at 50% probability level.[80]

Rare-earth ^{n}butyl complexes have been proposed as intermediate species in olefin polymerisation as transient species by ^{1}H NMR spectroscopy and formed *in situ* as precursors to elemental chalcogen insertion reactions.[34, 81]

Previous work, by Schumann *et. al.*, into alkylation of the tris-Cp lanthanides Cp_3Ln (Ln = Nd, Lu) with *n*-, *sec*- and *tert*-BuLi showed that *sec*-BuLi reacts with Cp_3Nd to form a product that decomposes at -30°C to give butene and Cp_2NdH.[82] Decomposition of what is presumably $Cp_2Ln(sec\text{-}C_4H_9)$ is also observed in the reaction with Cp_3Lu at 0°C to give the analogous lutetium complex Cp_2LuH and butene. No reaction occurred between ^{n}BuLi and Cp_3Ln (Ln = Nd, Lu), however, $PrCp_3$ does react with ^{n}BuLi to give the –ate complex $[Li][Cp_3Pr(^{n}Bu)]^{-}$. Alkylation of $NdCp_3$ with ^{t}BuLi in THF at -78°C gave the alkyl lanthanide complex $Cp_2Nd(^{t}Bu)$ upon work up. $Cp_2Nd(^{t}Bu)$ reacts with H_2 in toluene to form isobutene and Cp_2NdH. The enhanced stability of the *tert*-butyl complex over the *sec*-butyl complexes is likely due to increased agostic interactions between the metal centre and the $–CH_3$ protons.

Bis(cyclopentadienyl) rare-earth complexes are an important class of compounds that have been applied in catalysis and single molecule magnetism. The main routes into organolanthanide compounds of interest are via salt metathesis reactions which can produce –ate complexes, often require heating and long reaction times to ensure completion.

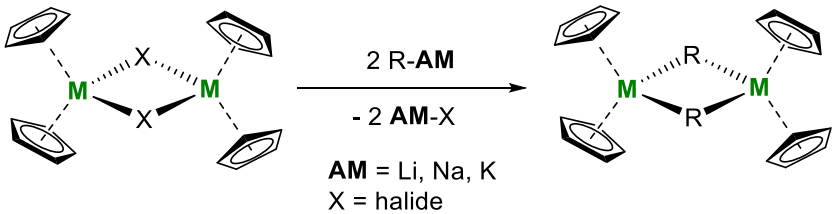

Scheme 2.1. Generic reaction scheme of salt-metathesis reactivity of rare-earth metallocenes (R = aryl, alkyl).

An alternative route into novel organolanthanide complexes is via deprotonation of acidic E—H substrates with Ln—alkyl complexes. These reactions tend to be cleaner, faster and produce either gaseous or inert liquid by-products.

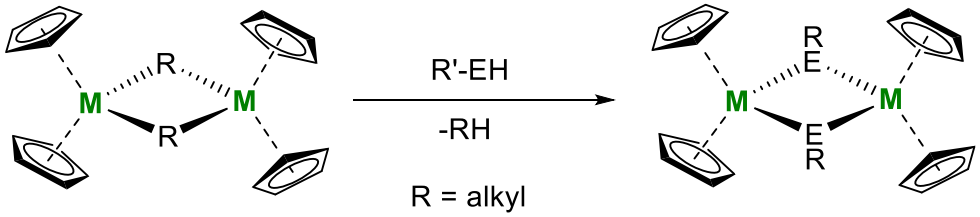

Scheme 2.2. Generic reaction scheme showing the reactivity of rare-earth alkyls with acidic E—H substrates (E = C, N, O, S, P, As, Se etc; R = alkyl, aryl).

In order to develop bespoke reagents for deprotonation chemistry, the aim of the work set out in this chapter is to synthesise rare-earth ^{n}butyl complexes, using ^{n}BuLi as an alkylating reagent. Study of the reactivity of rare-earth ^{n}butyl complexes towards the C—H acidic substrates ferrocene and N-Heterocyclic carbenes (NHCs) will be carried out with a view to developing functionalised ferrocenes and NHCs.

2.2 Synthesis & Characterisation of Rare-Earth ^{n}Butyl Complexes $[Cp^{Me}_2M(\mu\text{-}^{n}Bu)]_2$

Addition of a methyl group to a cyclopentadiene ring can greatly enhance the solubility of cyclopentadienyl rare-earth complexes. Cp_3Y is insoluble in aliphatic and aromatic solvents and is only sparingly soluble in coordinating solvents such as THF and Et_2O, which is due to the polymeric nature of Cp_3Y in the solid state.[83] However, Cp^{Me}_3Y (where $Cp^{Me} = C_5H_4CH_3$) has high solubility in toluene, benzene and has partial solubility in pentane. Making Cp^{Me}_3Y much more amenable to further chemistry.

An initial study into the reactivity between the unsubstituted Cp_3Y and ^{n}BuLi revealed that the reaction only went to approximately a third completion by ^{1}H NMR, as the yield of products was very low with prolonged reaction times. Heating of the reaction was initially avoided due to the thermal instability of rare-earth alkyl complexes. Applying heat to the

reaction and adding an excess of ^{n}BuLi gave almost no isolable product on work up. No crystalline product could be obtained. This is consistent with the findings of Schumann *et. al.* as they report no reaction at all with Cp_3Nd.

In contrast, Cp^{Me}_3M (where M = Dy, Y) does react with ^{n}BuLi in toluene to form the dinuclear, C-bridged alkyl complex $[Cp^{Me}_2M(\mu\text{-}^{n}Bu)]_2$ (**2.1**) according to scheme 2.1. ^{n}BuLi solution in hexanes was added to a solution of Cp^{Me}_3M gradually at -78^{o}C and once addition is complete, the reaction mixture is then allowed to warm gradually to RT. As the reaction mixture heats up, the transmetallation occurs within five minutes which can be observed as the colour of the reaction mixture changes from pale yellow to colourless. Formation of $LiCp^{Me}$ aids the reaction because in the absence of coordinating solvent it forms a 1D polymeric chain which is insoluble and thus easy to separate from the product. After 1 hr of stirring at RT the solution was then filtered and crystals can be grown from a supersaturated solution. Toluene or benzene can be used for crystallisation of **2.1** and slow evaporation of solutions in either solvent produced X-ray quality crystals. The crystalline yields from toluene are 58% (**2.1-Y**) and 62% (**2.1-Dy**), this is partly due to the high solubility of **2.1** in toluene.

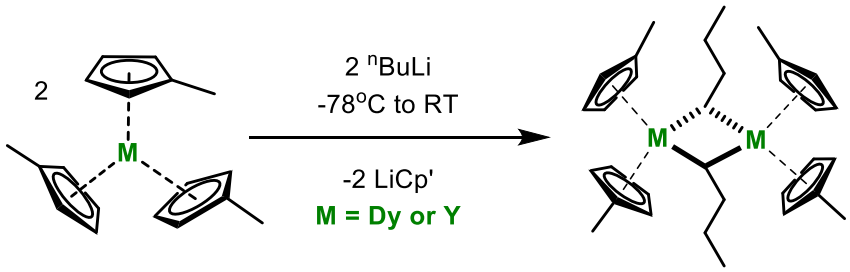

Scheme 2.3. Synthesis of $[Cp^{Me}_2M(\mu\text{-}^{n}Bu)]_2$.

Surprisingly, **2.1** is stable enough at RT to allow synthesis on a two to three-gram scale, which is a requirement for a reagent to be used as a convenient starting material. When toluene is switched for hexane, the filtration becomes much quicker because LiCp' forms a gel as it precipitates from toluene. In hexane, $LiCp^{Me}$ forms as a powder which greatly

reduces the time taken to isolate the product. The isolated yield also increases to 72% for **2.1-Y** and 78% for **2.1-Dy**. The most remarkable aspect of **2.1** is its thermal stability. Despite containing β-H atoms **2.1** is stable in the solid state for at least 24 hrs at RT and can be stored for several months at -40°C. Other [$Cp_2M—C_nH_{2n+1}$] systems decompose rapidly above 0°C so the thermal stability of **2.1** is rare amongst materials of its kind.[21]

Single crystal XRD on **2.1** revealed an incommensurate diffraction pattern. In most cases the unit cell can be assigned a space group which can be repeated indefinitely in three dimensions to reproduce the whole crystal. When a crystal is incommensurate there is some long range order but also other features that repeat in a way that is aperiodical. As such it makes structure solution difficult without invoking higher dimensional space. The space group has been determined as $P2_12_12$ for **2.1-Y** (structure shown in Figure 2.2), but the {Cp^{Me}_2Y} fragments are disordered over two positions making detailed structural analysis of bond lengths and angles difficult. Nonetheless, the structure can be solved and refined to reveal a dimeric, ^{n}butyl bridged complex with the n-butyl chains twisting slightly relative to the Y_2C_2 core. The structure refinement of **2.1-Dy** is unstable and of poor quality.

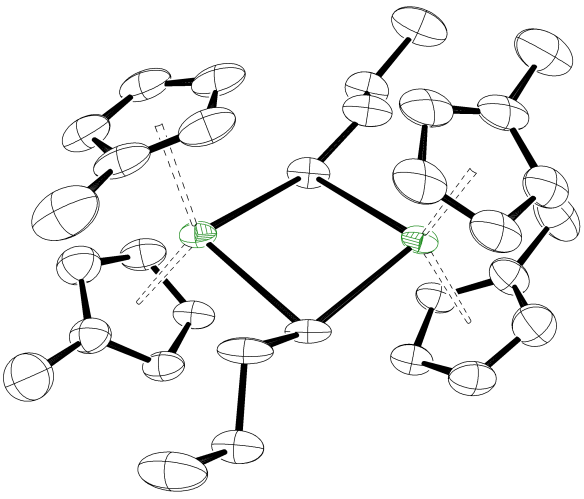

Figure 2.2. ORTEP representation of **2.1-Y** with thermal ellipsoids set at 50% probability. H-atoms omitted for clarity. Green – yttrium; carbon – black. Bond distances: Y—Cp_{cent} – 2.379(5)-2.383(6) Å; Y—$C_{equatorial}$ – 2.551(8)-2.567(8) Å. Cp_{cent} Y—Cp_{cent} angle: 125.7(2)°.

The ^{1}H NMR spectrum of **2.1-Y** (Figure 2.3) shows the characteristic signals expected for two Cp^{Me} rings, two triplets at δ 5.97 and 5.86 ppm corresponding to the two magnetically inequivalent (Cp)C—*H* environments and a singlet at δ 2.09 ppm arising from the methyl protons. The four resonances attributed to the $-CH_2CH_2CH_2CH_3$ groups appear between δ 1.33 and -0.44 ppm.

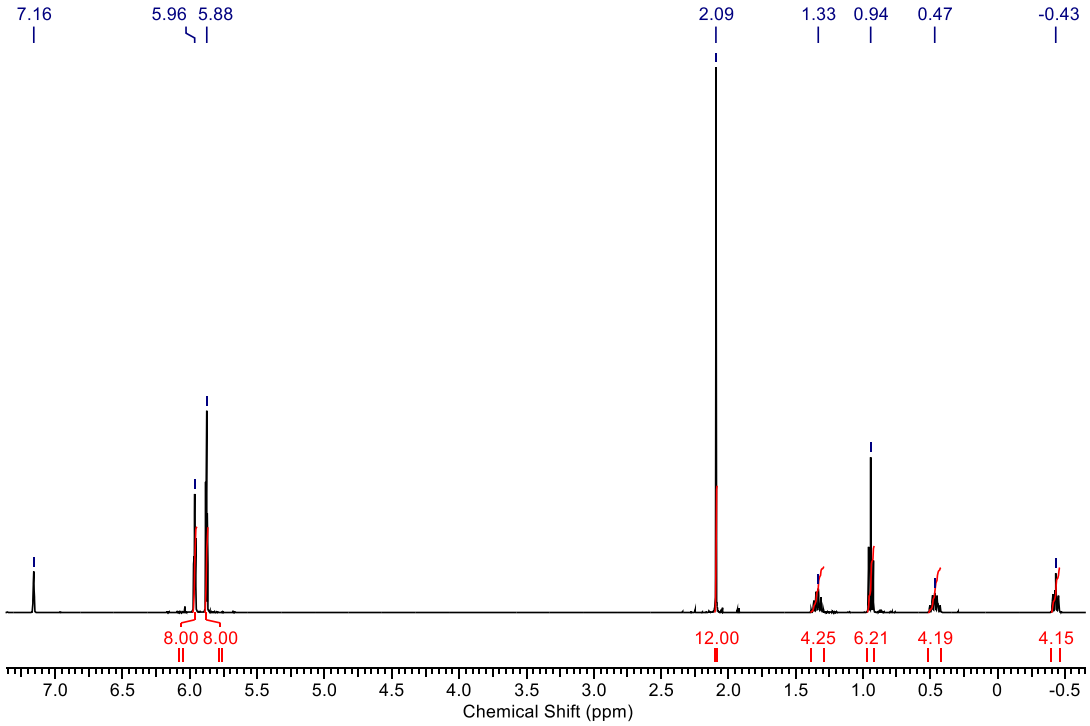

Figure 2.3. ^{1}H NMR spectrum of compound **2.1-Y** in C_6D_6.

The chemical shift of the C_α—*H* protons (δ -0.44 ppm) is typical for yttrium alkyl complexes, the peak is a triplet of triplets which is explained by coupling to two protons on the adjacent carbon atom split by coupling to two spin-½ ^{89}Y nuclei.[84] The ^{2}J ^{89}Y-^{1}H coupling constant is 1.5 Hz which is in the range of a 2-bond ^{89}Y-^{1}H coupling constant. This suggests that **2.1** retain a dimeric structure in solution. The close proximity of the Cα bound protons in **2.1-Y** to a highly electropositive metal center results in increased shielding of those nuclei from an external magnetic field. Oddly, the triplet resonance arising from the protons on the δ-C appear further upfield than the sextet from the γ-C protons. One would

expect the further a proton is from the metal centre through bonds in an aliphatic chain, the further upfield the resonance would appear. A possible explanation for this could be an NOE type interaction with the Y nucleus as the n-butyl chains would have some degree of flexibility in solution, however this is unlikely based on steric congestion. ^{13}C NMR and HSQC 2D experiments were also used to confirm the structure in solution, which provided information on the coupling of ^{1}H and ^{13}C resonances, thus allowing the resonances for the ^{n}Bu protons to be assigned accurately. IR spectra on **2.1** feature strong absorption bands in the region between 400-1000 cm^{-1} that can be attributed to C-H bending mode in the Cp rings. Weaker absorption bands at 1300-1500 cm^{-1} and 2750-2900 cm^{-1} are attributed to the ^{n}Bu C-H bend and stretch vibrational modes respectively.

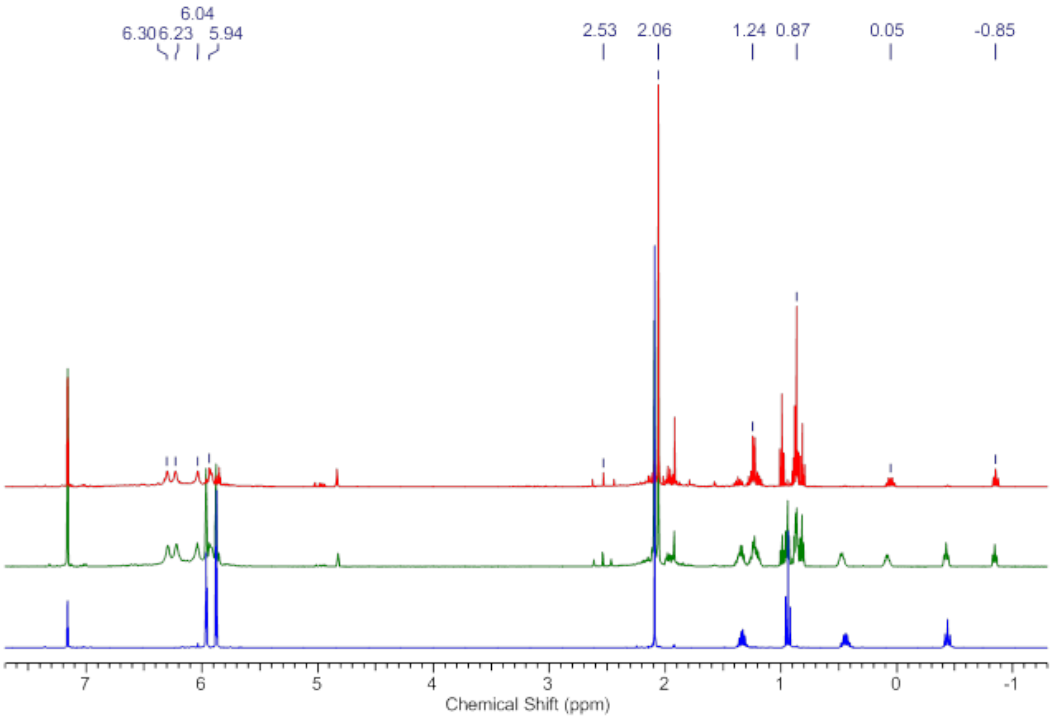

Figure 2.4. Overlay of ^{1}H NMR spectra showing the decomposition of **2.1-Y** in C_6D_6 at 25°C. Spectra taken after 0.25 hours (blue), seven days (green) and 11 days (red). Peaks correspond to the red spectrum.

The stability of **2.1-Y** in C_6D_6 was monitored by ^{1}H NMR spectroscopy in C_6D_6 over the course of several days at RT. An initially colourless solution slowly turns yellow over the course of two to three days and becomes progressively darker. After seven days at RT (green spectrum – Figure 2.4) **2.1-Y** shows signs of decomposition with several new peaks growing into the ^{1}H NMR spectrum. There are signs of β-H elimination occurring with a number of signals in the range of δ 4.81-5.04 ppm consistent with the presence of an alkene, however no signal between 3.50-4 ppm is observed which is typical of Cp_2Y—H complexes.[85, 86] The Cp*C*—H resonances also begin to diminish and four new poorly resolved signals begin to emerge, which could be indicative of one new {Cp^{Me}_2Y} species forming. The decomposition of **2.1-Y** is almost complete after 11 d as the resonances attributed to **2.1-Y** have essentially disappeared. Attempts to crystallise the product of decomposition were unsuccessful, a yellow oily substance remains after complete removal of benzene.

2.3 Reactivity of Rare-Earth ^{n}Butyl Complexes Towards Ferrocene: Synthesis & Characterisation of Ferrocenyl Rare-Earth Complexes

Ferrocene was chosen as a reagent to test the reactivity of **2.1** with respect to ^{n}BuLi. ^{n}BuLi reacts with ferrocene to form a mixture of two products regardless of the stoichiometry used, i.e. $[(C_5H_4Li)_2Fe]$ or $[(C_5H_5)Fe(C_5H_4Li)]$.[87]

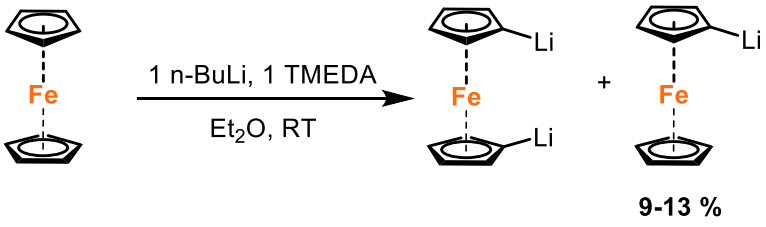

Scheme 2.4. Reactivity of ^{n}BuLi with ferrocene.[87]

Initially, the reaction was carried out on a 100 mg scale, **2.1-Y** and two equivalents of ferrocene being stirred at RT and then concentrated, which gave an insoluble orange powder. A study of the reactivity by ^{1}H NMR spectroscopy in C_6D_6 showed that almost no reaction occurs after 1 hr at RT. However, if the reaction mixture is left to stand over several days the solution gradually turns from yellow to dark orange, and spectra taken after five days reveal reaction on the ferrocene Cp rings, with the appearance of a new signal at δ 3.84 ppm. Two complex multiplets at 0.86 and 1.23 ppm also appear and are attributed to butane. After seven to ten days dark orange-red crystals formed in the NMR tube.

XRD analysis on the crystals showed the product to be the ferrocenyl-bridged, dinuclear complex $[Cp^{Me}{}_2Y(\mu\text{-}\eta^1\text{:}\eta^5\text{-}C_5H_4FeCp)]_2$ (**2.2-Y**, Figure 2.6). There are only three other known examples of ferrocenyl rare-earth complexes, in each case they were synthesised by salt metathesis reactions with $LnCl_3$ and 2-Me_2NCH_2FcLi.[88-90] Compound **2.2** is the first example of a complex containing a ferrocenyl anion bridging two rare-earth ions. Previous examples of ferrocenyl rare-earths are –ate complexes where the amidoferrocenyl ligand is either ancillary or bridging to a Li counterion (Figure 2.5).[88-90]

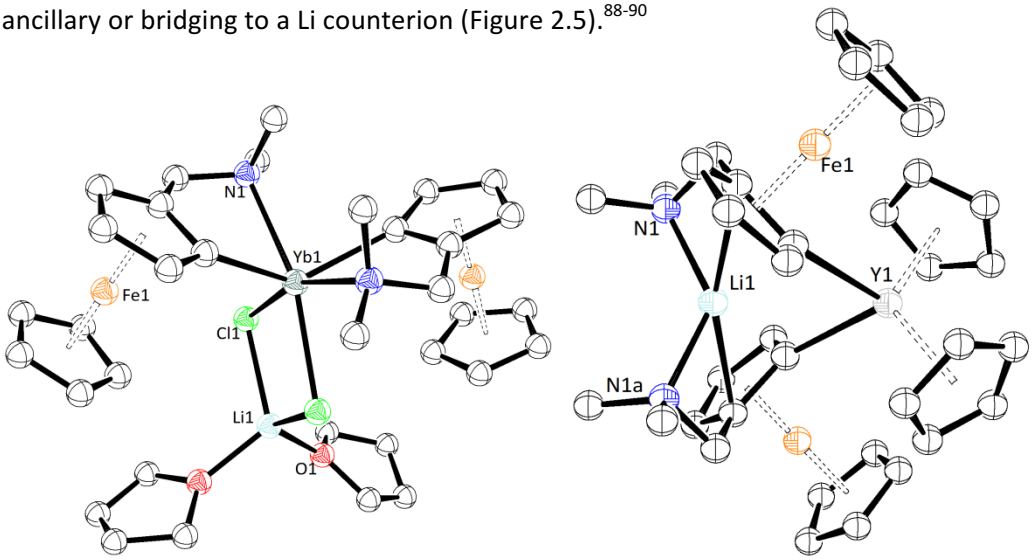

Figure 2.5. (Left) Structure of (2-$Me_2NCH_2Fc)_2Yb(\mu\text{-}Cl)_2Li(THF)_2$.[88] (Right) structure of the bis(cyclopentadienyl)yttrium ferrocenyl complex, $Cp_2Y(\mu\text{-}2\text{-}Me_2NCH_2Fc)_2Li$.[89]

Compound **2.1-Y** deprotonates one of the Cp rings of ferrocene to release two equivalents of butane and form a dimer, according to scheme 2.5, which bridges via an η^5 interaction of the deprotonated Cp ring with the second yttrium ion. Compound **2.2-Y** is completely insoluble in aromatic solvents and does not go back into hot toluene once crystallised. Crystallisation of **2.2-Y** tends to occur over two to seven days depending on the concentration of the reaction mixture, the product slowly forms as large dark orange-red blocks in modest yield (50% **2.2-Y**; 54% **2.2-Dy**).

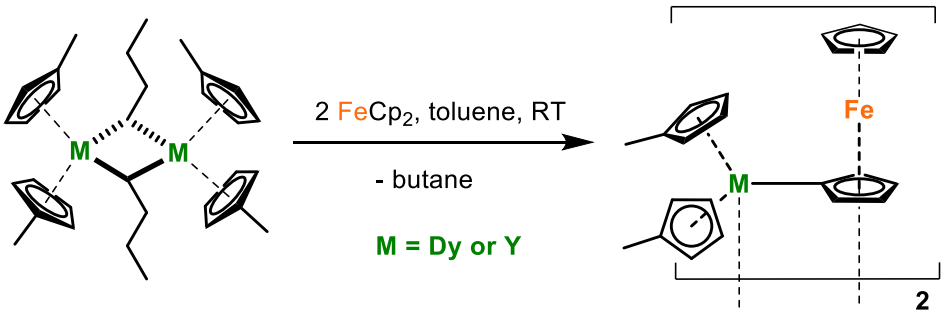

Scheme 2.5. Synthesis of $[Cp^{Me}_2M(\mu\text{-}\eta^1\text{:}\eta^5\text{-}C_5H_4FeCp)]_2$ (compound **2.2**).

Due to the lack of solubility in toluene or benzene, ^{1}H NMR spectroscopic study on the product was carried out in THF-d_8. The ^{1}H NMR spectrum of **2.2-Y** reveals only one resonance arising from the Cp^{Me} protons, which usually feature as two sets of triplets in aromatic solvents arising from the two inequivalent ring C—H protons coupling to each other. The C_5H_5—Fe signal occurs at δ 3.97 ppm and the signals arising from the deprotonated ferrocene ring resonate at 3.96 and 4.11 ppm and integrate as expected for two protons in two distinct chemical and magnetic environments. There are only two signals arising from THF which correspond to uncoordinated THF. There is no THF bound to yttrium and an oligomer persists in solution, the resonances arising from free and bound THF would be shifted with respect to each other if this were the case.

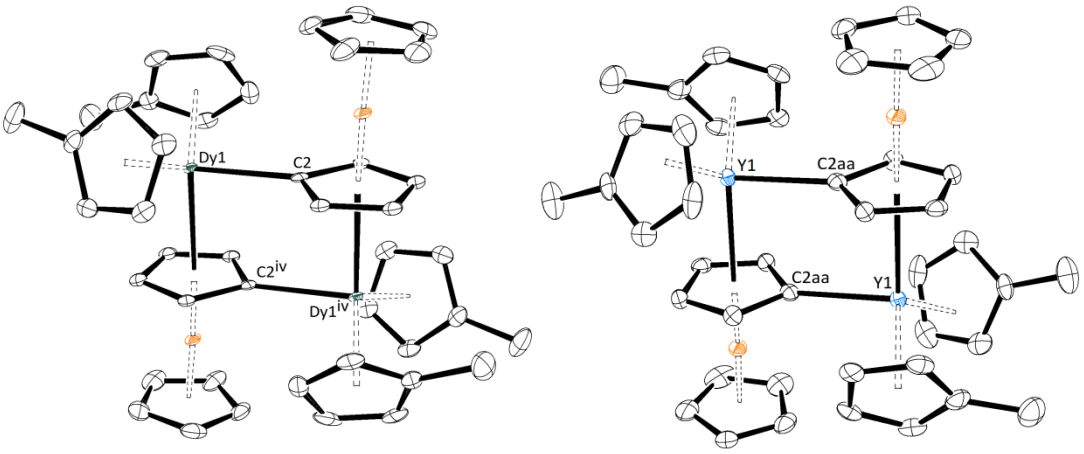

Figure 2.6. ORTEP representations of **2.2-Dy** (left) and **2.2-Y** (right) with thermal ellipsoids set at 50% probability. H-atoms omitted for clarity.

The isostructural dysprosium complex $[Cp^{Me}{}_2Dy(\mu\text{-}\eta^1\text{:}\eta^5\text{-}C_5H_4FeCp)]_2$ (**2.2-Dy**) also forms from the reaction of two equivalents of ferrocene and **2.1-Dy** in toluene. An XRD study on a single crystal revealed the Dy—C2 bond length is 2.461(4) Å which is relatively short compared to Dy—E bonds where E is a softer donor atom such as phosphorus or sulfur. The Dy—$Cp^{Me}{}_{cent}$ distances are 2.42(10) Å and 2.43(6) Å. The Dy—(Fe)Cp_{cent} distance is 2.601(2) Å which is much longer than the distance between the Dy^{3+} ion and the η^1-bound $(C_5H_4)^{2-}$ ligand. Each Dy^{3+} ion is formally 10-coordinate and the coordination environment around each metal center resembles that of the rare-earth analogue Cp_3Y, which forms a polymeric chain in the solid state with each Y^{3+} ion coordinated η^5 to three Cp rings and to one carbon atom of a neighbouring Cp_3Y unit. IR spectroscopy reveals a very similar spectrum to that of **2.1** as only aromatic C-C and C-H bonds are present in the compound.

Table 2.1. Summary of important bond lengths and angles of compounds **2.1** and **2.2**.

	2.1-Y	2.2-Dy	2.2-Y
M-Cp_{cent}/ Å	2.379(5)- 2.383(6)	2.421(2)- 2.430(2)	2.421(2)- 2.428(2)
M-C_{donor}/ Å	2.551(8)- 2.567(8)	2.461(4)	2.468(4)
Cp_{cent}-M-Cp_{cent}/ ^{o}	125.7(2)	121.43(7)	121.32(7)

It is important to understand the reactivity of **2.1** with respect to its precursor Cp^{Me}_3M as well as ^{n}BuLi. A control experiment was carried out on the NMR scale between Cp^{Me}_3Y and ferrocene in a 1:1 stoichiometry. No reaction was found to occur at RT or at 80^{o}C, which shows that the $(Cp^{Me})^{-}$ ligand is less Brønsted basic than the $(^{n}Bu)^{-}$ ligand, which is expected as $(Cp^{Me})^{-}$ is a stable 6 π-electron, aromatic ligand. The synthesis and isolation of **2.1** and **2.2** are important results because it has been demonstrated here that ferrocene can be deprotonated once using the relatively stable rare-earth ^{n}butyl complexes (**2.1**). Deprotonation of ferrocene with **2.1** forms the mono-deprotonated **2.2** exclusively whereas ^{n}BuLi gives a mixture of mono- and di-lithiated ferrocenes. Mono-lithiation of ferrocene with is currently achievable using ^{t}BuLi which is pyrophoric, using **2.2** could be a safer alternative to reliably mono-substitute ferrocenes upon quenching with electrophiles.

Mulvey *et. al.* reported on the reactivity of mixed metal bases with ferrocene. The lithium aluminate base [(TMP)Li(μ-TMP)(μ-^{i}Bu)Al^{i}Bu$_2$] doubly deprotonates ferrocene.[91] The sodium magnesiate base [NaMg{N^{i}Pr$_2$}$_3$] can deprotonate ferrocene four times.[92]

2.4 Reactivity of Rare-Earth ^{n}butyl Complexes Towards N-Heterocyclic Carbenes

2.4.1 Introduction

N-Heterocyclic Carbenes (NHCs) are compounds that contain a divalent, 6-electron C-atom bonded to two N atoms in an n-membered ring. They are good σ-donors and the vast majority of NHC reactivity involves coordination to metal centres via the C2 carbon atom.

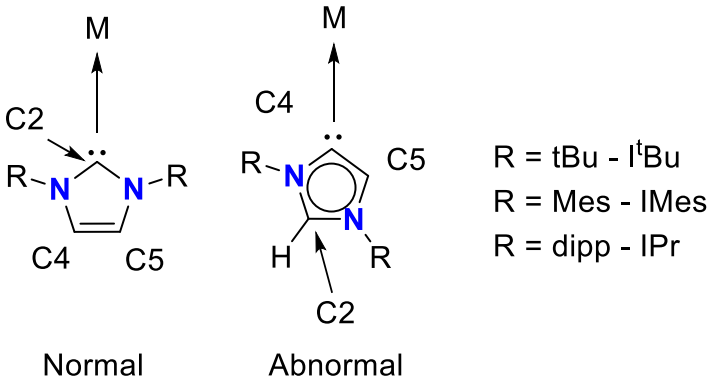

Figure 2.7. Schematic diagram of an NHC with conventional atom labelling.

This is especially important in catalysis as coordination of NHCs can affect the electronic structure of the metal centre. The most commonly used NHCs have an unsaturated C=C backbone meaning the protons bonded to the C4 and C5 positions are mildly acidic (pK_a of C—H bond in imidazolium cations ranges from 21-25). Rare-earth NHC complexes are also less explored than the TM-NHC counterparts, this due in large part to the hard Lewis acidity of rare-earth metals and the lack of available oxidation states limit metal-based reactivity. Typically rare-earth NHC complexes are NHC adducts of rare-earth halides or bis(cyclopentadienyl) complexes.[93] A variety of tethered-NHC ligands are also known with scandium, yttrium and the lanthanides. Cui *et. al.* recently reported alkoxy-NHC ligated rare-earth complexes that polymerise isoprene, amido-NHC complexes of rare-earth metals are also known.[94] Whilst many rare-earth NHC complexes contain tethered carbenes there are examples of non-tethered NHC complexes with the $\{Cp_2M\}$ motif.

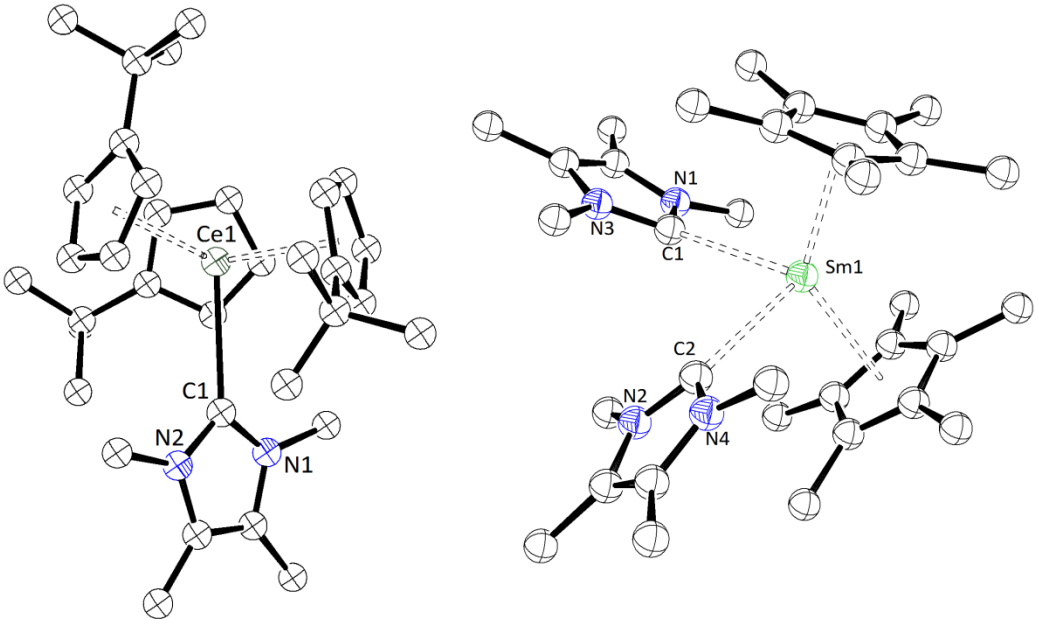

Figure 2.8. Molecular structures of $[Cp^{t}_{3}Ce(IMe_4)]$ (left) and $[Cp^{*}_{2}Sm(IMe_4)_2]$. Ellipsoids at 50 % probability.[95]

Arduengo *et. al*. reported a series of carbene adducts of $Cp^{*}_{2}Sm$ in 1994.[95] Two equivalents of the low molecular weight NHC IMe_4 (1,3,4,5-tetramethylimidazol-2-ylidene) can coordinate to $Cp^{*}_{2}Sm$ affording the complex $[Cp^{*}_{2}Sm(IMe_4)_2]$ upon work up. The analogous ytterbium complexes have also been reported by Schumann *et. al.* Samarocene-NHC adducts are also known with bulkier carbenes as there is space to accommodate the steric bulk of larger R groups in the equatorial plane. Ephritikhine *et. al.* have also reported NHC adducts of various cyclopentadienyl cerium complexes.[96] IMe_4 forms adducts with $Cp^{t}_{3}Ce$ (Cp^{t} = C_5H_4tBu) and $Cp^{*}_{2}CeI$ to form $[Cp^{t}_{3}Ce(IMe_4)]$ and $[Cp^{*}_{2}CeI(IMe_4)]$ respectively. To date there are no known normal NHC adducts of dysprosium or yttrium and as of 2009 no NHC complexes of gadolinium or terbium had been reported.[97]

Arnold *et.al.* have shown that tethered rare-earth NHC complexes can react with azides to form insertion products,[98] functionalise silyl chlorides[99] and activate small molecules such as CO and CO_2.[100]

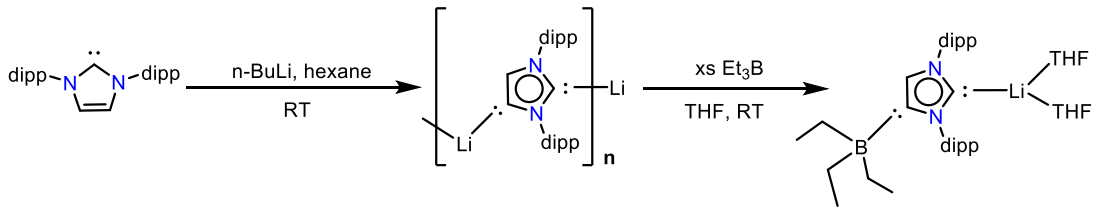

Scheme 2.6. Lithiation of NHC with ^{n}BuLi reported by Robinson *et.al.*[101]

In 2010, Robinson *et.al.* reported the first anionic di-carbene (ADC) complex, [:C{[N(2,6-$iPr_2C_6H_3$)]$_2$CHCLi}]$_n$ (**2.3**) which was synthesised by reacting IPr with ^{n}BuLi in hexane.[101] The C(4)—H bond is deprotonated affording a polymeric compound in which the Li^+ cation is coordinated to the C4 carbon and the C2 carbenic carbon of a neighbouring IPr molecule. The THF solvate is formed up on addition of THF but the complex is still forms a coordination polymer as only one THF coordinates to the Li^+ ion. The same structure results when IPr is reacted with lithium metal in THF. In order to ascertain the anionic, di-carbene character of **2.3** Lewis acids Et_3B and Me_3Al were added which resulted in the formation of an adduct **2.3**·BEt_3. This proved the presence of an electron pair on the C4 carbon and that it was indeed anionic.

Subsequently, it has been found that many different organometallic bases react with NHCs to form ADCs. Goicoechea *et.al.* have shown that reacting [M(Mes)$_2$] (where M = Fe, Mn) with IPr leads to the formation of an adduct [(IPr)M(Mes)$_2$].[102, 103] Upon reduction with KC_8 the anionic (bis)di-carbene complex: K[(Mes)M^{2+}(IPr)$_2$] forms, where each IPr ligand has been deprotonated in the C4 position to form an anion. Addition of a Lewis acid (Et_3Al) forms the adduct with coordination at the C2 atom showing the dicarbene nature of the ligands (see Figure 2.9).

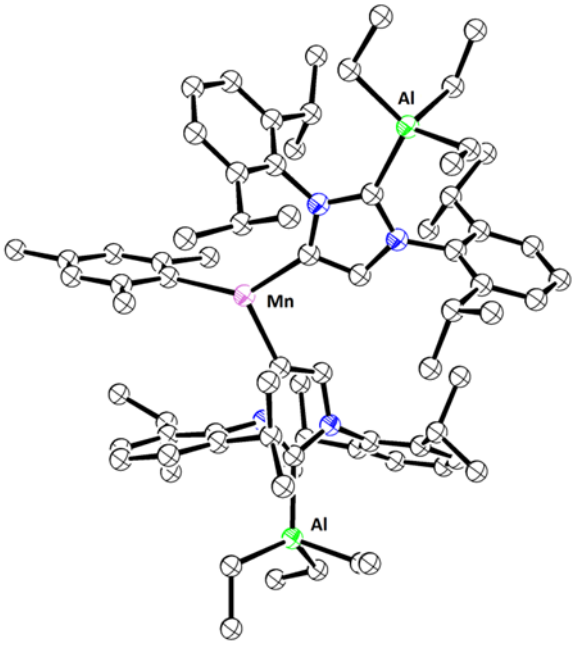

Figure 2.9. Structure of the Mn-ADC complex K[(mes)M^{2+}(IPr^{-}· $Et_3Al)_2$].[102] Ellipsoids at 50 % probability.

Mixed metal bases bearing ^{n}butyl and ^{t}butyl ligands have also been deployed in non-classical NHC reactivity to great effect. A study by Hevia *et.al.* showed the sodium zincate base [Na(TMEDA)][(TMP)Zn(^{t}Bu)$_2$] (**2.4**), when reacted with IPr, forms the mono-zincated NHC complex [Na(THF)$_3$][:C{[N(2,6-iPr2C$_6$H$_3$)]$_2$CHCZn(tBu)$_2$}].[104] Deprotonation again occurs at the C4 position. A di-zincated NHC forms upon reaction of **2.4** with the Zn-normal NHC adduct [(IPr)Zn(^{t}Bu)$_2$] according to Scheme 2.7. Interestingly, neutral dialkylzinc reagents do not deprotonate IPr.

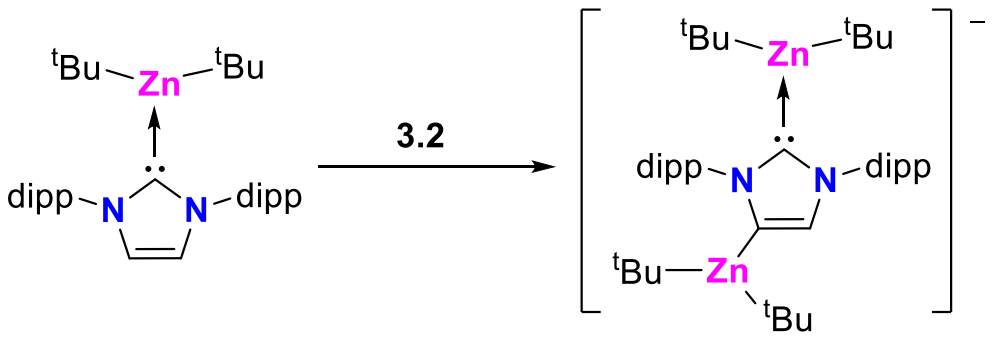

Scheme 2.7. Formation of an ADC by deprotonation of a normal NHC adduct.[104]

Sodium and potassium magnesiate bases also react with IPr to form a variety of C4 functionalised anionic di-carbenes.[105] The K-Mg pre-inverse crown base $[\{KMg(TMP)_2(^nBu)\}_6]$ (TMP = tetramethylpiperidide) reacts with IPr in a methylcyclohexane/THF mixture (scheme 2.8) to give the ADC complex $[\{KMg(IPr^-)_2(^nBu)(THF)\}_n]$ where the Mg anion has one $(^nBu)^-$ substituent and the K counterion is coordinated in an η^3 manner to one of the arene rings of the carbene.

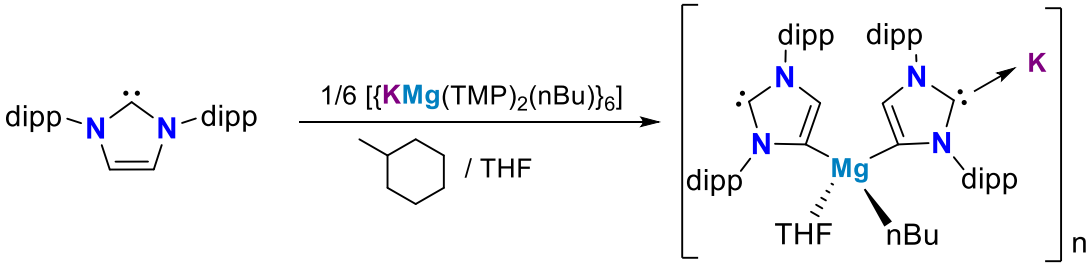

Scheme 2.8. Reactivity of a mixed metal inverse crown complex towards IPr.[105]

However, the sodium magnesiate base $[Na(TMEDA)][Mg(TMP)_2(^nBu)]$ affords the magnesium-ate complex $[(THF)_3Na(IPr^-)Mg(THF)(IPr^-)_2]$ when reacted with three equivalents of IPr. The solvated sodium counterion is coordinated to one of the IPr anions at the C2 position. Perhaps the most unusual reactivity is observed when the Na-Mg pre-inverse crown complex $[Na_4Mg_2(TMP)_6(^nBu)_2]$ is reacted with one equivalent of IPr. Not only is the C4 position deprotonated but also the *para*- position of the dipp- arene ring.

The work set out in this chapter explores the reactivity of **2.1** with NHCs to establish reactivity with respect to ^{n}BuLi and other ^{n}butyl alkali metal bases described above.

2.4.2 Reactivity of $[Cp^{Me}_2M(\mu\text{-}^{n}Bu)]_2$ Towards I^{t}Bu & IPr

I^{t}Bu and IPr were chosen for initial reactivity study of **2.1** with NHCs as I^{t}Bu is a low MW carbene with a relatively low steric demand and the diisopropylphenyl-substituted IPr is much larger and more sterically cumbersome. The R substituent on the NHC can also affect the σ donor- π acceptor capability. There are two main modes of reactivity expected to occur between **2.1** and NHCs. Firstly, deprotonation of the acidic C—H bonds on the unsaturated backbone and secondly, formation of an M—NHC complex with the carbene coordinating to the metal center via the C2 carbon. NHCs are good σ-donors, hence could break up the dimer of **2.1-Y** in solution and form a monomeric complex.

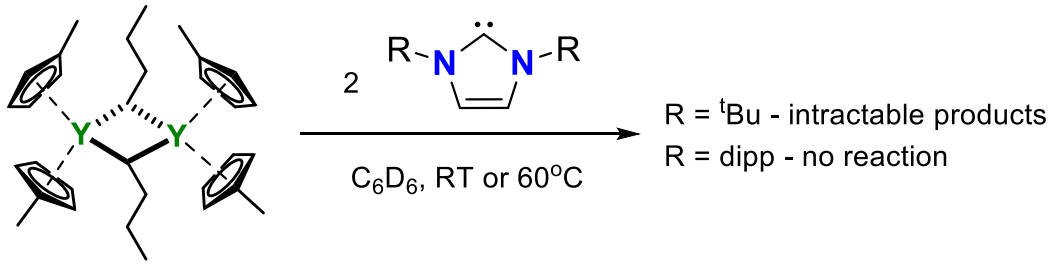

Scheme 2.9. Reactions of **2.1-Y** with I^{t}Bu and IPr.

The reactions were carried out in a 1:1 stoichiometry according to scheme 2.9. The reaction with I^{t}Bu produced an insoluble white precipitate after two days but no crystalline material could be obtained. The ^{1}H NMR spectrum of the reaction mixture shows mostly starting materials however, some new signals do appear (Figure 2.10). Attempts to carry out the reaction on a 100 mg scale yielded a brown oil and no crystalline product.

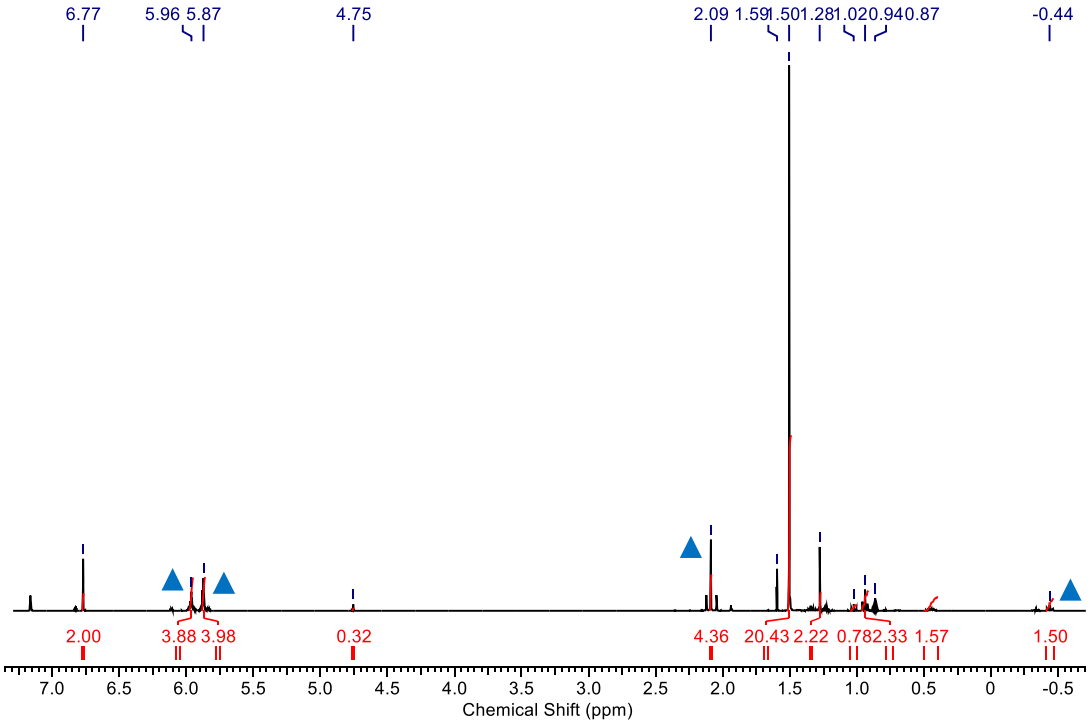

Figure 2.10. ^{1}H NMR spectrum of the reaction mixture of **2.1-Y** and I^{t}Bu taken after 2 days at RT. Peaks marked with blue triangles correspond to **2.1-Y**.

IPr does not react with **2.1-Y** at RT or 60^{o}C. ^{1}H NMR spectra show only the presence of starting materials after 4 hrs at RT. Heating the reaction mixture to 60^{o}C overnight gives the decomposition products of **2.1-Y** and unreacted IPr. This is unexpected as although the IPr ligand is sterically bulky, the backbone C—H protons should still be accessible for reactivity to occur as the dipp substituents would be facing away from the metal center.

2.4.3 Reactivity Towards IMes: Synthesis & Characterisation of [Cp^{Me}_2M(IMes')]

The reactivity of **2.1** with IMes differs markedly from I^{t}Bu and IPr. When combined in a 1:1 stoichiometry the product formed is somewhat unexpected. Instead of the expected deprotonation of the acidic C—H bonds on the backbone, one of the *ortho*-methyl groups on the mesityl substituent was deprotonated.

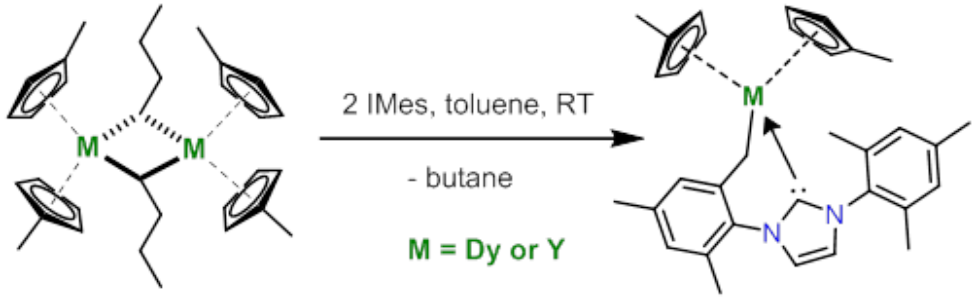

Scheme 2.10. Synthesis of **2.5**.

Upon addition of IMes in benzene to a solution of **2.1** in benzene at RT there is an immediate colour change from colourless to bright yellow. Evaporation of the solvent leaves a yellow powder that is the analytically pure benzyl- tethered NHC complex: [Cp^{Me}_2M(IMes')] (**2.5**) (where M = Y, Dy; IMes' = *o*-Me deprotonated IMes ligand) in high yields (85% and 86% for **2.5-Y** and **2.5-Dy** respectively) according to scheme 2.10. Compound **2.1** deprotonates IMes once in the *ortho*-methyl position of one of the mesityl groups. The carbonic carbon atom then coordinates to the metal centre. Compounds **2.5-Y** and **2.5-Dy** crystallise as large blocks by slowly evaporation of a toluene solution or as thin plates from a cooled, supersaturated Et_2O solution. Compounds **2.5-Y** and **2.5-Dy** have low solubility in hexane. When the reaction was followed by ^{1}H NMR spectroscopy it was found that the benzyl-NHC complexes form quantitatively with no other side products observed.

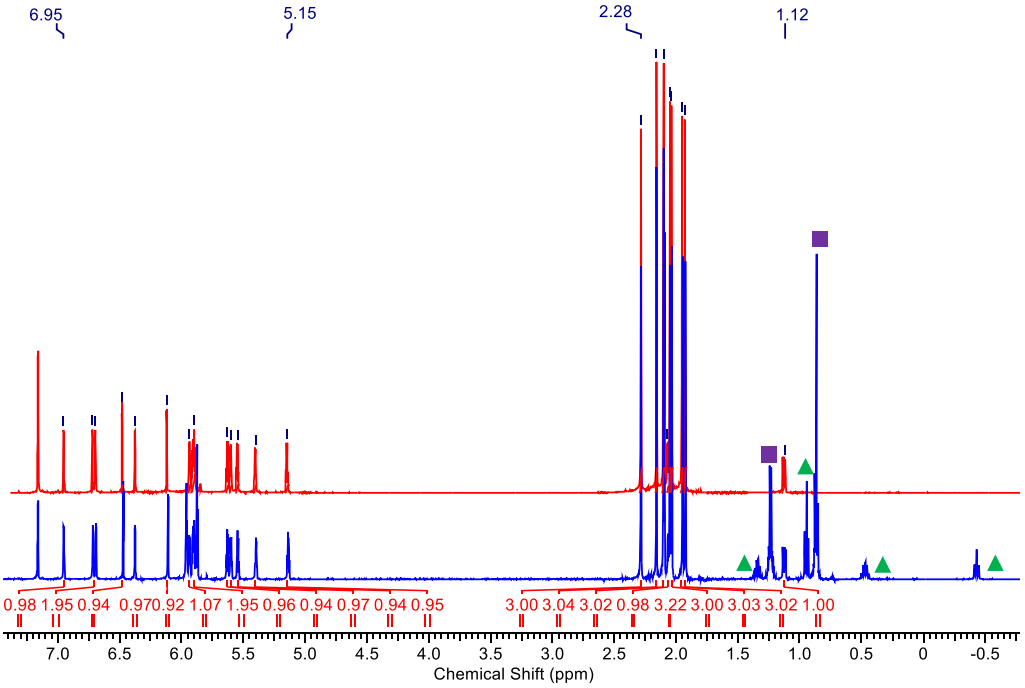

Figure 2.11. Overlay of ^{1}H NMR spectra for the reaction mixture initially containing **2.1-Y** and IMes (blue spectrum) and the spectrum of compound **2.5-Y** after isolation (red spectrum). Resonances marked with green triangles are ^{n}butyl protons in unreacted **2.1-Y** and purple squares correspond to butane.

An XRD study shows **2.5-Y** and **2.5-Dy** to be isostructural and both compounds crystallise in the monoclinic $P2_1/c$ space group. In each case there are two molecules in the asymmetric unit that exhibit very slight differences in M—C bond lengths in the equatorial plane. In **2.5-Y**, the Y1—C1 bond lengths are 2.538(9) Å and 2.542(9) Å, which are longer than the Y1—C10 bonds at 2.455(9) Å and 2.473(10) Å. The Cp_{cent}—Y—Cp_{cent} angles are 128.29(16)° and 128.53(19)° which are much more obtuse than the corresponding angles found in **2.2-Y** at 121.3(8)° and **2.2-Dy** at 121.41(2)°. This implies the ligand field is more axial than trigonal in **2.5-Y**.

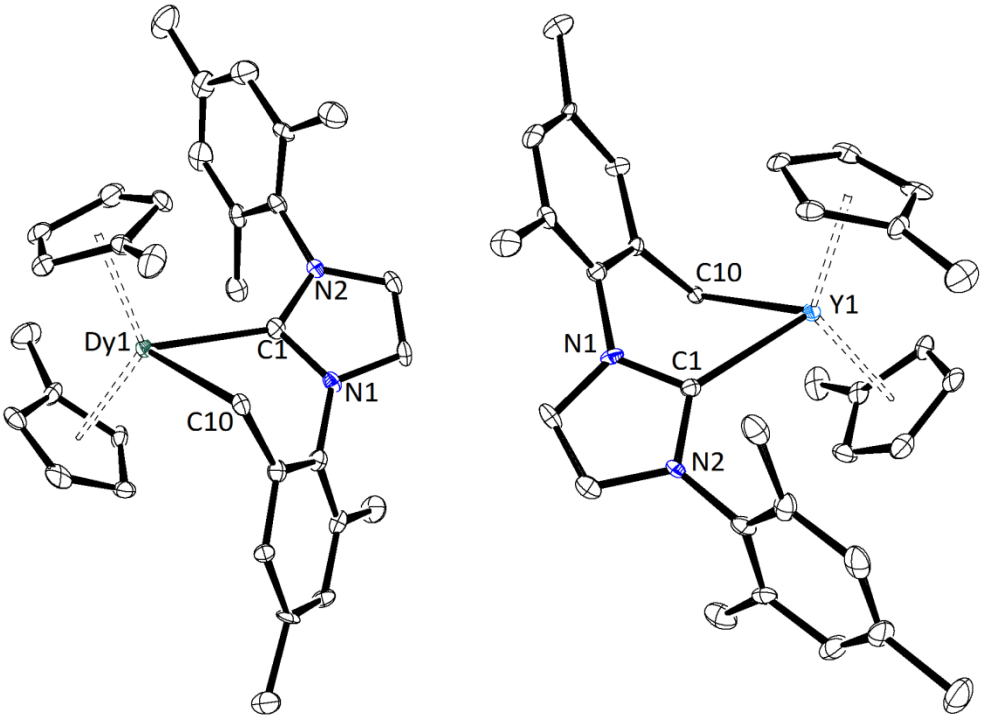

Figure 2.12. ORTEP representation of the molecular structure of **2.5-Dy** (left) and **2.5-Y** (right) with thermal ellipsoids set at 50% probability. One of two molecules present in the asymmetric unit displayed in each case. H-atoms omitted for clarity.

The Dy1—C10 bond lengths in **2.5-Dy** are 2.448(10) Å and 2.451(9) Å for each of the two molecules in the asymmetric unit. The Dy1—C1 bond lengths are 2.534(9) Å and 2.531(9) Å, which are comparable to other Y-NHC complexes reported in the literature.[94, 106] Despite the NHC being a strong σ-donor the bond lengths to the 4f ion are approximately 0.1 Å longer than the interaction between the anionic carbon and the 4f ion. This highlights the radially contracted nature of 4f orbitals and the little overlap with the C1 σ-bonding orbital on the carbene. The interaction is electrostatic in nature. The Cp_{cent}—Dy—Cp_{cent} angles are 128.55(15)° and 128.71(15)° for the two molecules in the asymmetric unit.

^{1}H NMR spectroscopy on **2.5-Y** shows that there is a high degree of magnetic and chemical inequivalence in proton environments as there are 14 peaks in the vinylic/aromatic region

of the spectrum (δ 5.1 – 7.0 ppm) and there are 14 aromatic or C(sp^2)—H protons in the molecule. The aromatic C—H protons on the deprotonated mesityl substituent of the carbene are chemically inequivalent, due to the asymmetric nature of the IMes' ligand. The same can be said for the protons bonded to the NHC backbone. Similar reactivity with IMes has been observed before by Okuda *et. al.* with [Ln(CH_2SiMe_3)$_3$(THF)$_3$] (Ln = Y, Lu).[107, 108] When [Ln(CH_2SiMe_3)$_3$(THF)$_3$] is reacted with IPr and IMes the corresponding adducts form. [(IPr)Ln(CH_2SiMe_3)$_3$] does not react any further but addition of IMes to **1.16-Y** in THF results in the C—H activated IMes product [(IMes')Y(CH_2SiMe_3)$_2$(THF)$_2$] with one equivalent of $SiMe_4$ generated as the by-product. There are also inequivalent aromatic proton environments however the signals are reported to be broad singlets, **2.5-Y** shows more well resolved multiplicity of the peaks in the aromatic region allowing for a reliable assignment of each signal.

This type of IMes cyclometallation reactivity has also been observed with transition metals.[109, 110] Reduction of [(IMes)$_2$CoCl] with sodium-mercury amalgam resulted in the Co^{2+} complex [Co(IMes')$_2$] presumably via a transient Co^0 species (presumably [Co(IMes)$_2$]) followed by dehydrogenation of the IMes ligands to form the product. An intermediate Co^{1+} hydride species is proposed by Deng *et. al.* The same mode of reactivity is observed with iron. Thermolysis of an IMes-osmium cluster in benzene also results in IMes being deprotonated in the *ortho* position.[111] When IMes is added to [(COD)$PtMe_2$] initially an adduct forms [(IMes)$_2$$PtMe_2$] with the IMes ligands cis- to each other in a square planar Pt^{2+} complex that can be crystallised.[112] If the reaction time is extended, the unusual complex [(IMes')(IMes)PtMe] is formed. It was proposed to go via an oxidative addition of one of the IMes C—H bonds to Pt forming an intermediate Pt^{4+} complex followed by reductive elimination of one equivalent of methane.

Compounds **2.1** differ somewhat in their reactivity to carbenes with respect to ^{n}BuLi, unlike the observations made by Robinson *et. al.* **2.1** do not show any reactivity at all towards IPr, possibly due to the steric hindrance imparted by the dipp substituents. However, **2.1** does react with IMes instantaneously to form the benzylic, tethered NHC complexes **2.5** as the exclusive product.

2.4.4 Control Experiment with Cp^{Me}_3M and IMes

Building on the result with IMes and the ^{n}butyl complex **2.1** the control experiment with Cp^{Me}_3M was carried out according to scheme 2.11 to establish reactivity with respect to the precursor. In this case the benzyl tethered-carbene complexes **2.5** were not the expected products, due to the lower basicity of Cp^{Me}_3M. It was anticipated in this case that a M—NHC adduct would form due to the strong σ-donating property of the carbene.

On mixing Cp^{Me}_3M (M = Dy, Y) and IMes in a 1:1 stoichiometry in benzene at RT the abnormal NHC (aNHC) adducts $[Cp^{Me}_3M(aIMes)]\cdot C_6H_6$ (**2.6**) formed as large colourless block crystals in good to high yields (81% M = Y; 68% M = Dy).

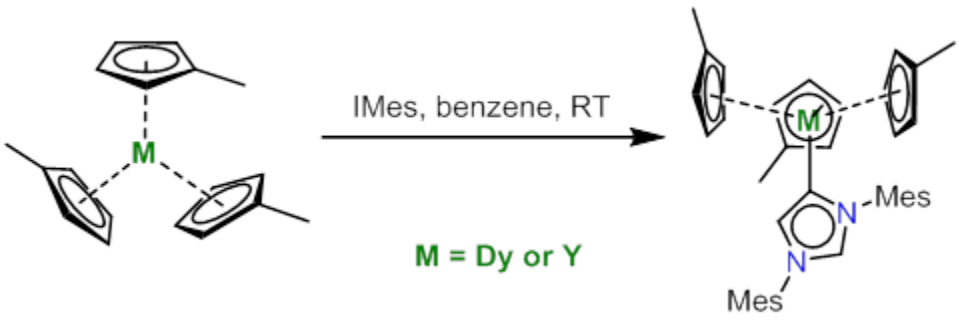

Scheme 2.11. Reaction of tris(cyclopentadienyl) precursors with IMes.

The structures of **2.6** were confirmed by XRD (see Figure 2.13). Both **2.6-Y** and **2.6-Dy** are isostructural and show two molecules in the unit cell along with two benzene molecules from solvent in the crystal lattice. There is a C—H---π hydrogen bonding interaction

between the C2—H proton and the plane of a Cp ring bound to a Dy^{3+} of a neighbouring molecule (see Figure 2.14). The H—Cp_{cent} distance in **2.6-Dy** is just 2.337(5) Å which is much smaller than comparable bonds in other metal complexes.[113] This could explain why **2.6** are highly insoluble in aliphatic and aromatic solvents and won't re-dissolve in benzene or hot toluene once crystallised. They are also insoluble in THF.

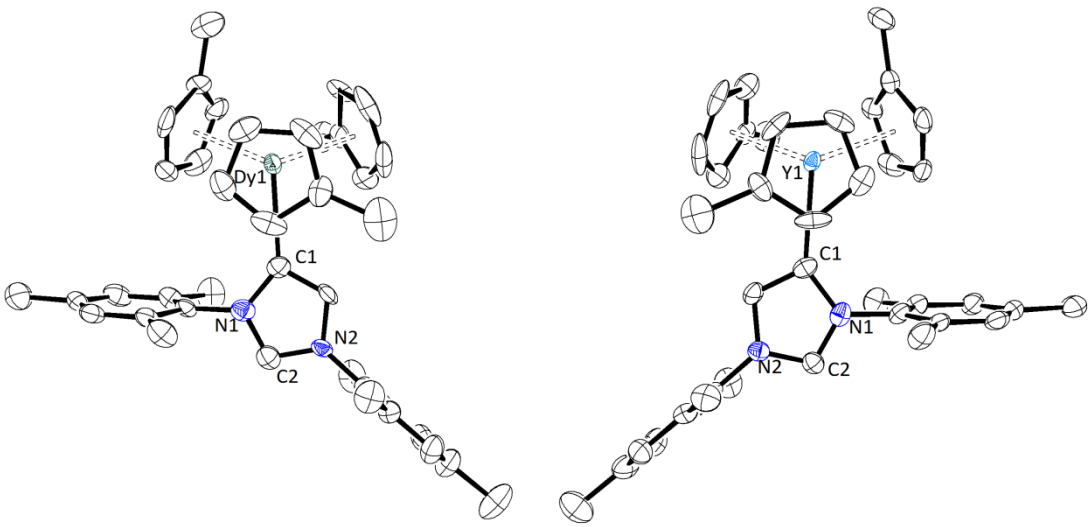

Figure 2.13. ORTEP representations of (left) **2.6-Dy** and (right) **2.6-Y**. Thermal ellipsoids are set at 50% probability, H-atoms omitted for clarity.

The Dy1—C1 bond length in **2.6-Dy** is 2.588(9) Å and the Dy—Cp_{cent} distances which range from 2.481(5)-2.501(5) Å. Due to the trigonal planar geometry about the N atoms in IMes it can be seen that the mesityl substituents point in the same direction resulting in a considerable steric demand on one side of the molecule. Coordinating in an abnormal way via the C1 atom would greatly relieve steric pressure with respect to coordination via the C2 atom as a normal NHC, the tris(cyclopentadienyl) ligand field already fills a great deal of the coordination sphere around the dysprosium ion.

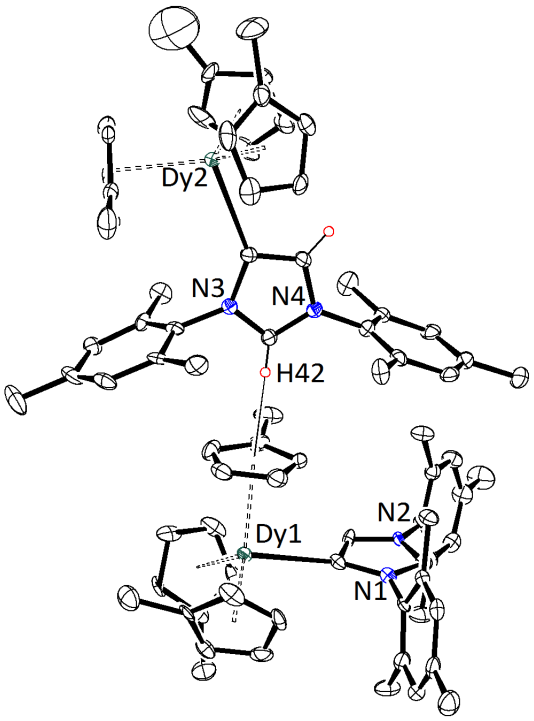

Figure 2.14. Extended molecular structure of **2.6-Dy** highlighting the short C—H---π interaction with an adjacent Cp^{Me} ring. Thermal ellipsoids are set at 50% probability.

2.4.5 Abnormal Carbene Rearrangement in [Cp^{Me}_3Y(aIMes)] – An NMR Study

Due to the lack of solubility of **2.6** in aromatic solvents and THF no suitable NMR data could be acquired on the isolated yttrium complex **2.6-Y**. The reaction between Cp^{Me}_3Y and IMes was carried out on the NMR scale in order to ascertain the solution structure of **2.6-Y** and also gain insight into the mechanism of its formation. The only other example of a rare-earth aNHC complex is obtained via a reduction of an amido-tethered NHC complex [N''$_2$YL] with $KC_{10}H_8$ in THF.[114] The C2 carbon atom coordinates to the K counterion and the carbene coordinated to yttrium through the C4 carbon.

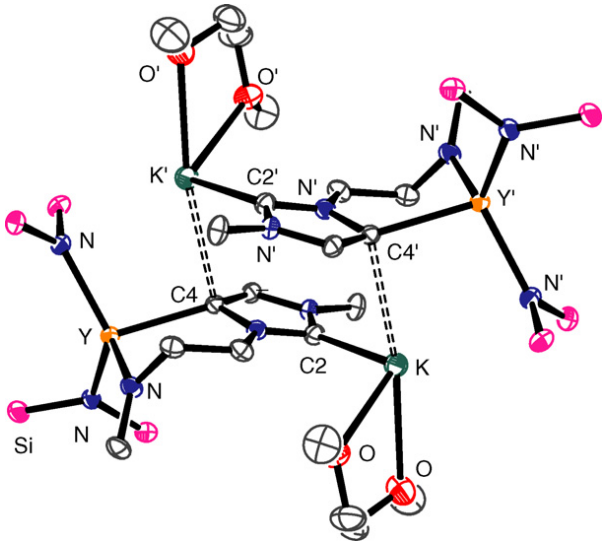

Figure 2.15. Molecular structure of the yttrium aNHC complex reported by Arnold *et. al.*[114]

Upon dissolution of Cp^{Me}_3Y and IMes, **2.6-Y** gradually crystallises out of solution on standing at RT. This is unusual as most abnormal NHC complexes usually require some heating of a pre-formed normal NHC complex. Layfield *et. al.* reported the normal to abnormal rearrangement of a 3 coordinate iron complex [(IPr)Fe(N(SiMe$_3$)$_2$)$_2$](**2.7**).[115] The normal carbene adduct **2.7** rearranges to form the aNHC complex [(aIPr)Fe(N(SiMe$_3$)$_2$)$_2$] (**2.8**) when a solution of **2.7** is heated in toluene.

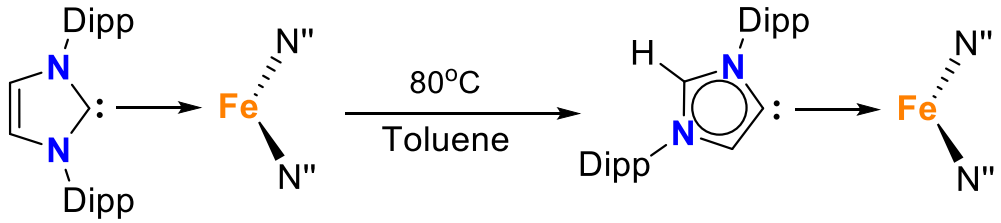

Scheme 2.12. Carbene rearrangement observed in 3 coordinate iron complexes, reported by Layfield *et. al.*[115]

Hevia *et. al*. have also demonstrated similar reactivity with the gallium complex [(IPr)Ga(CH_2SiMe_3)$_3$] (**2.9**).[116] When **2.9** is heated in benzene at 100°C, it is converted to the abnormal NHC complex [(aIPr)Ga(CH_2SiMe_3)$_3$] in 10 hrs. The same reaction in THF results in full conversion after 1 hr. The solvent medium has also been demonstrated to have an effect on the normal to abnormal rearrangement of NHC complexes of aluminium, gallium and indium.[117] The complexes [(I^tBu)MMe_3] (M = Al, Ga, In) are crystallised from pentane but rearrange to form the corresponding abnormal NHC complexes when dissolved in THF.

The reaction shown in scheme 2.11 was initially carried out on a scale of 0.495 g of starting materials in a combined volume of 6 mL of benzene (c ≈ 260 mM). Under these conditions at RT **2.6-Y** crystallises out of solution upon standing over 5 days, with crystals beginning to form after 2 days at RT. When the reaction was scaled down to an NMR tube (c =120 mM) no material crystallised out of solution but a darkening of the solution was observed over several days. This showed that there may be a concentration dependency on the rate of normal to abnormal conversion. In order to confirm the concentration dependence of the rate of aNHC formation a series of experiments were prepared with a concentration of precurors between 80-160 mM.

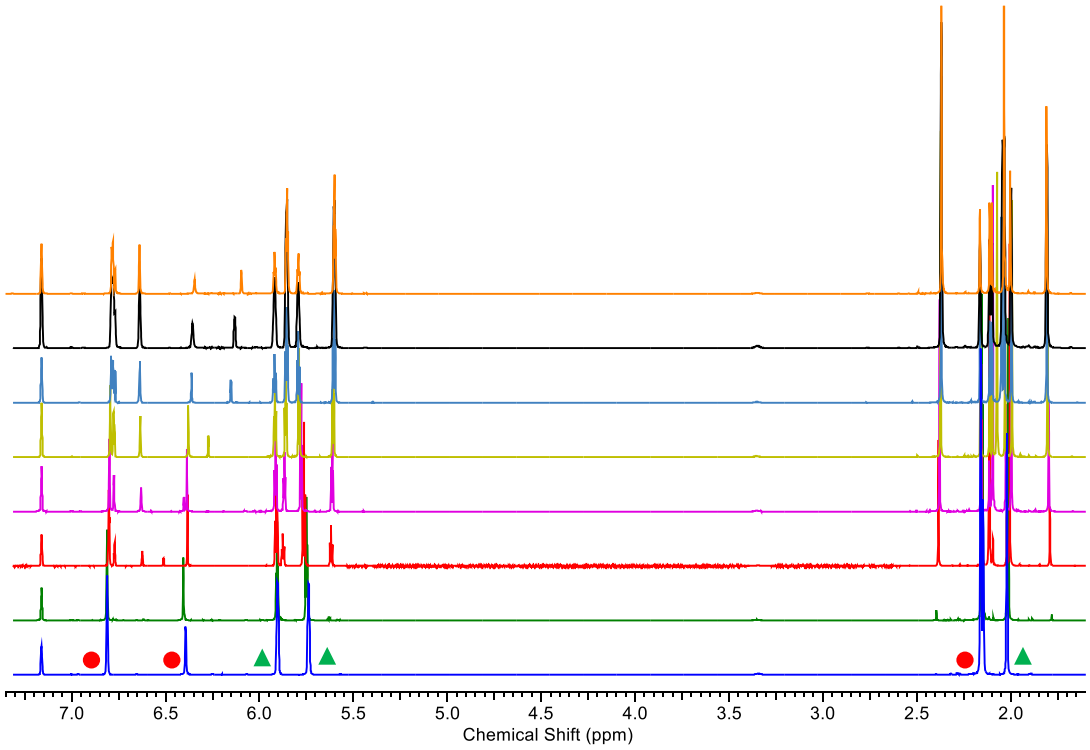

Figure 2.16. Overlay of ^{1}H NMR spectra of the reaction of $Cp^{Me}_{3}Y$ and IMes in C_6D_6 at RT (c = 120 mM). Blue – t = 0.25 h; green – t = 6 hr; red – t = 24 h; purple – t = 72 h; yellow – t = 96 h; light blue – t = 192 h; black – t = 240 h; orange – t = 576 h. Peaks labelled with red circles (from downfield to upfield) are assigned to the aryl C-H, backbone C=C-H and CH_3 groups on IMes. The peaks labelled with green triangles correspond to the (Cp)C-H and CH_3 resonances in $Cp^{Me}_{3}Y$.

The concentration of reagents in the initial NMR experiment was 120 mM. At RT no crystals form over the course of 3-4 weeks. After two days some reactivity is evident from the appearance of new resonances at δ 5.88 and 5.62 ppm which correspond to a new $\{Cp^{Me}_{2}Y\}$ species forming in solution. New signals also emerge in the region of 1.80-2.40 ppm as the symmetry of the IMes ligand is broken and the –C*H*$_3$ environments become inequivalent. Typically C2—*H* resonances in aNHC complexes occur in the range of 8-9.50 ppm due to being in between two electron withdrawing N atoms, thus creating a substantial deshielding effect. No resonance is observed in any spectra at any concentration downfield of the benzene solvent signal at 7.16 ppm corresponding to a C2—H resonance. A signal is

observed that can be assigned to the C5—*H* signal which shifts upfield over time. After two days at RT a doublet appears at 6.51 ppm which shifts to 6.10 ppm over the course of 24 days, the coupling constant is 1.26 Hz which is typical of ^{89}Y-^{1}H ^{2}J-coupling. The signal integrates to 1 proton with respect to all the other assigned resonances which gives strong evidence for the formation of **2.6-Y** in solution. It is worthy of note that no evidence is seen of any formation of a normal C2 bound NHC complex in solution, i.e. [Cp$^{Me}_{3}$Y←IMes].

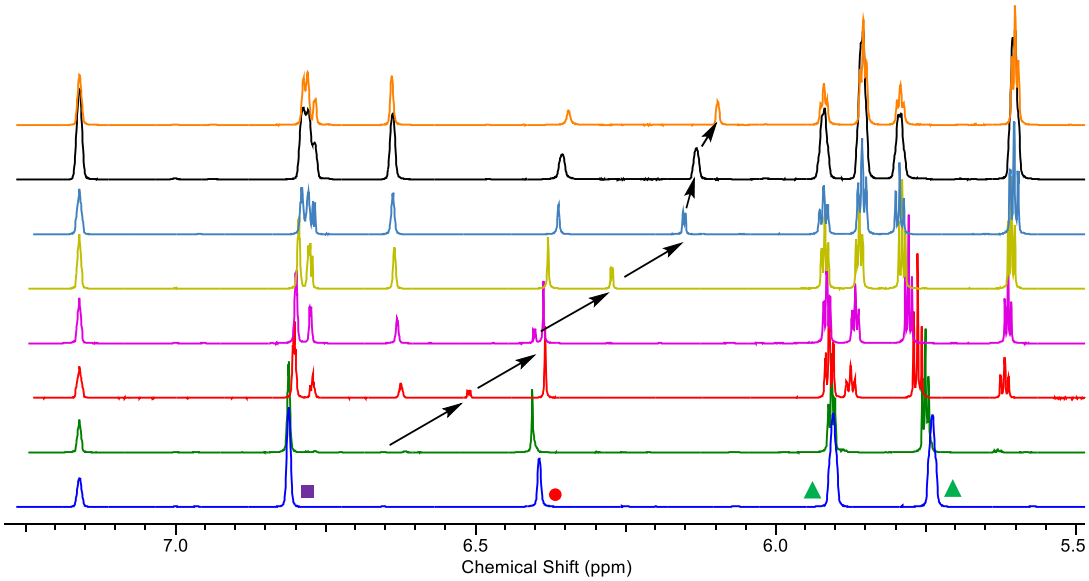

Figure 2.17. Aromatic region of the ^{1}H NMR spectra taken of the reaction between Cp$^{Me}_{3}$Y and IMes in C_6D_6 at RT (c = 120 mM). Blue – t = 0.25 h; green – t = 6 hr; red – t = 48 h; purple – t = 72 h; yellow – t = 96 h; light blue – t = 192 h; black – t = 240 h; orange – t = 576 h. Green triangles – (Cp)C-H; red circle – backbone C=C-H; purple square – aryl C-H. Arrows highlight shift of peak appearing after 6 hours at δ 6.65 ppm.

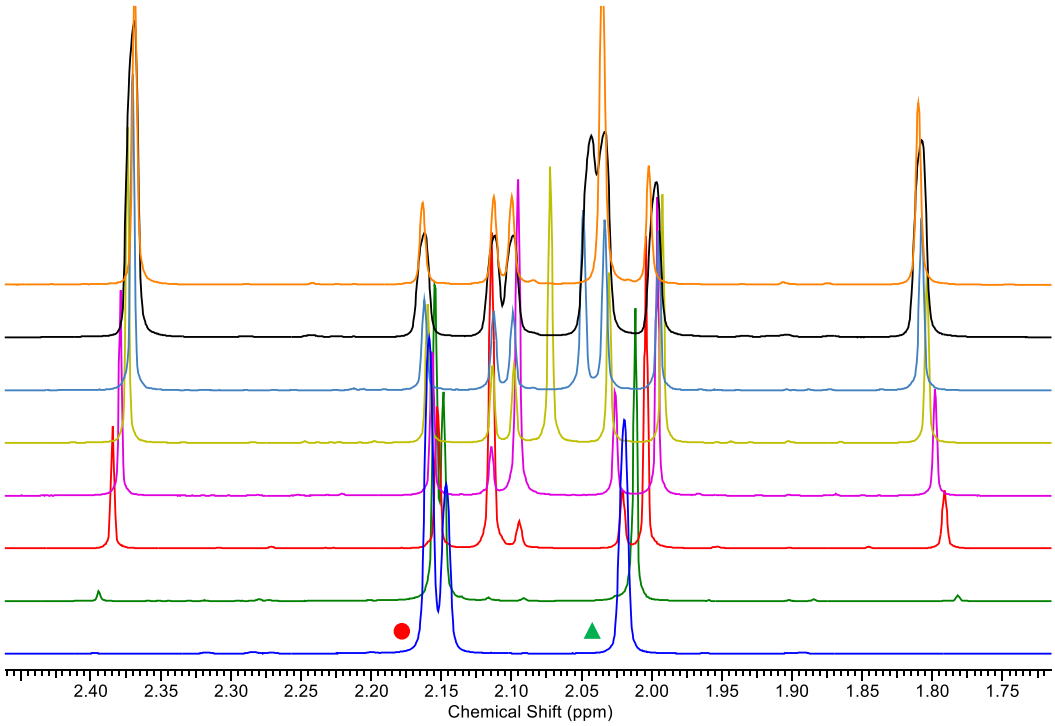

Figure 2.18. Alkyl region of the ^{1}H NMR spectra taken of the reaction between $Cp^{Me}_{3}Y$ and IMes in C_6D_6 at RT (c = 120 mM). Blue – t = 0.25 h; green – t = 6 hr; red – t = 48 h; purple – t = 72 h; yellow – t = 96 h; light blue – t = 192 h; black – t = 240 h; orange – t = 576 h.

As **2.6-Y** did not crystallise out of solution at a reactant concentration of 120 mM it was necessary to prepare more concentrated samples to observe if crystals of **2.6-Y** form to match observations made with the scaled-up synthesis. Over the course of the reaction between $Cp^{Me}_{3}Y$ and IMes at a concentration of 140 mM, a similar rate of conversion to **2.6-Y** was observed to the 120 mM reaction over the first 4 days. However, the rate of the conversion began to increase with respect to the 120 mM experiment after 5 days and large, colourless crystals of **2.6-Y** formed after 7 days. Compound **2.6-Y** crystallised after 5 days at 160 mM. From t = 0 to 4 days the rate of conversion was also found to be higher at 160 mM than at lower concentrations. Reactions between $Cp^{Me}_{3}Y$ and IMes were also

carried out at lower concentrations of 100 mM and 80 mM to confirm the concentration dependent formation of **3.4-Y**. As expected a slower conversion to the product is observed as the concentration of reagents is reduced.

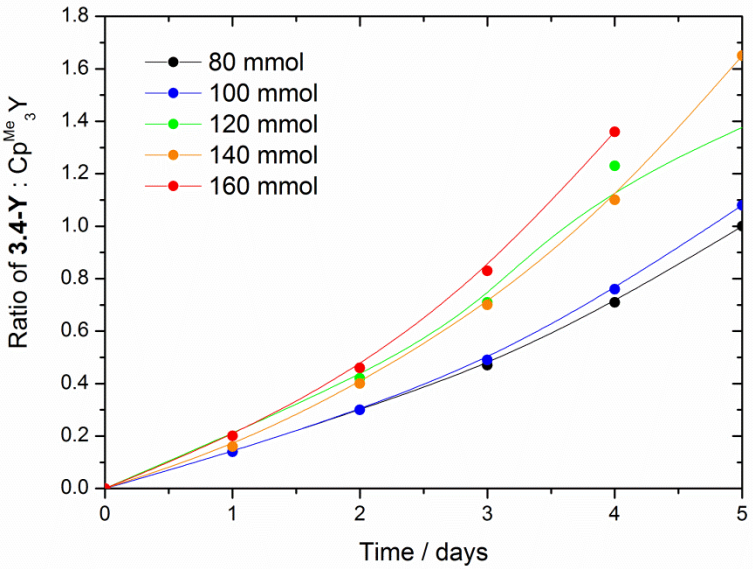

Figure 2.19. Plot of the ratio of **2.6-Y** and Cp^{Me}_3Y in solution during the first 5 days at a range of concentrations at RT. The ratios were calculated using the integrals of the peaks arising from the (Cp)C—*H* signals of Cp^{Me}_3Y and **2.6-Y**.

It has been demonstrated by previous studies that heating a pre-formed M—NHC complex can affect an isomerisation to the corresponding aNHC complex.[115] When a 120 mM solution of Cp^{Me}_3Y and IMes in benzene-d_6 is heated to 60°C, the formation of **2.6-Y** proceeds faster than at RT. The ratio of **2.6-Y** to reactants in solution after 3 hrs is approximately equal to that of the RT reaction after 24 hrs.

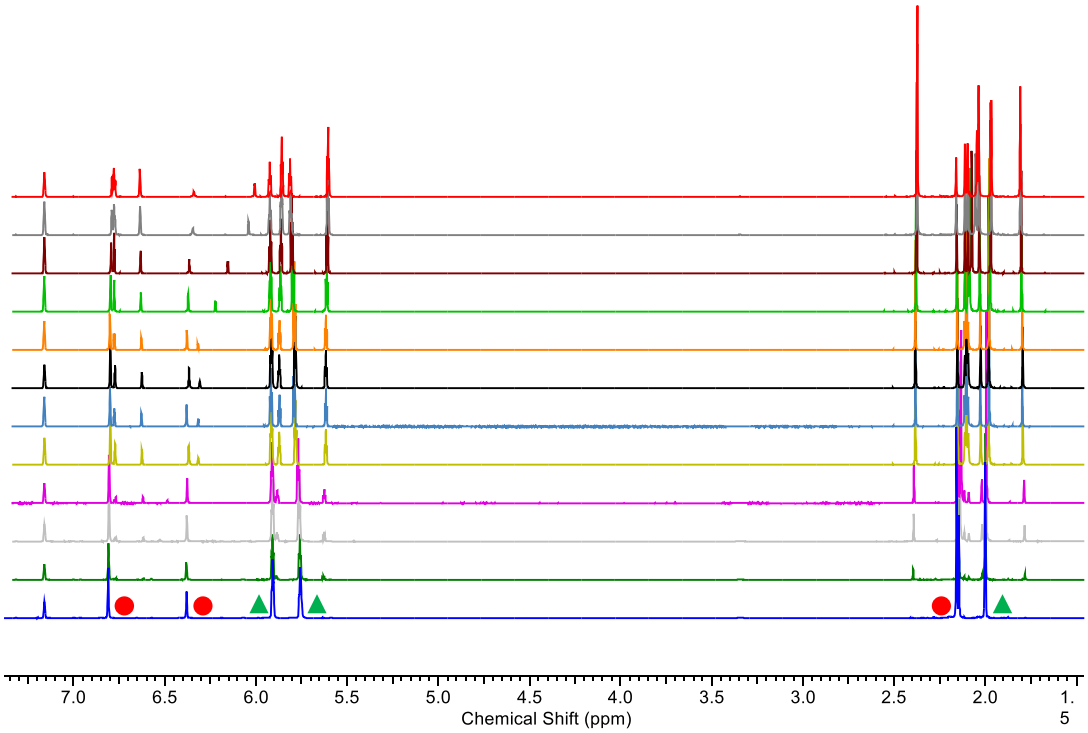

Figure 2.20. ^{1}H NMR spectra taken of the reaction between $Cp^{Me}_{3}Y$ and IMes in C_6D_6 at 60°C for 6 days (blue to orange spectra) followed by cooling to RT and leaving to stand at RT further 9 days (green to sky blue spectra) (c = 120 mM). Blue – t = 0.25 h; green – t = 1 hr; red – t = 2 hrs; purple – t = 3 hrs; yellow – t = 24 hrs; light blue – t = 48 h; black – t = 120 h; orange – t = 144 h; light green – t = 168 h; brown – t = 216 h; grey – t = 288 h; sky blue – t = 360 h. (Red circles – IMes; green tringles – $Cp^{Me}_{3}Y$).

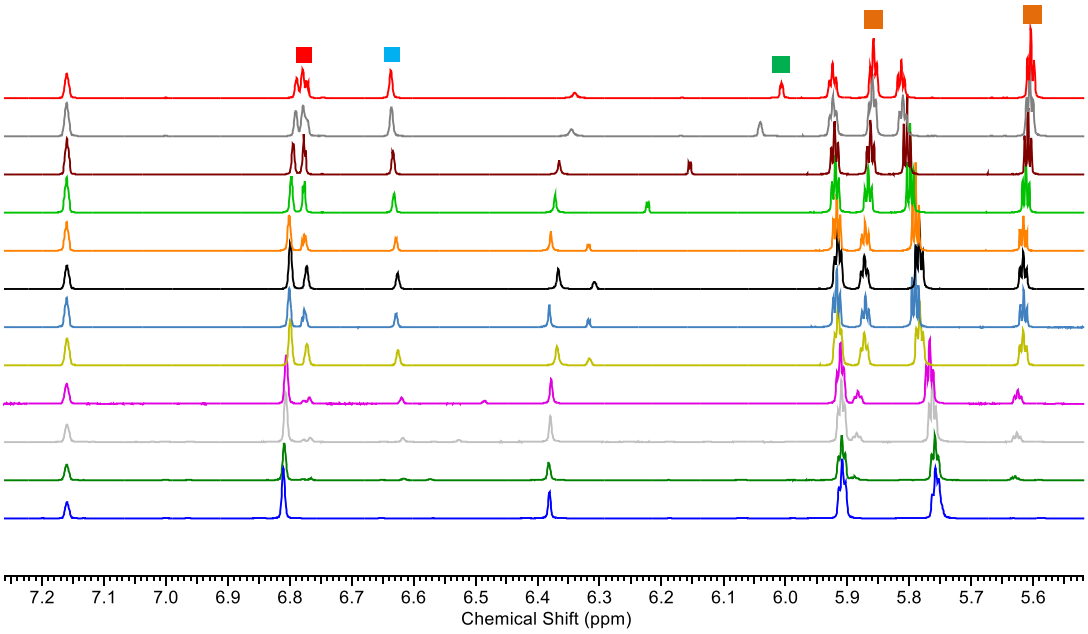

Figure 2.21. Aromatic region of the ^{1}H NMR spectra taken of the reaction between $Cp^{Me}{}_{3}Y$ and IMes in C_6D_6 at 60°C for 6 days (blue to orange spectra) followed by cooling to RT and leaving to stand at RT further 9 days (green to sky blue spectra) (c = 120 mM). Blue – t = 0.25 h; green – t = 1 hr; red – t = 2 hrs; purple – t = 3 hrs; yellow – t = 24 hrs; light blue – t = 48 h; black – t = 120 h; orange – t = 144 h; light green – t = 168 h; brown – t = 216 h; grey – t = 288 h; sky blue – t = 360 h. (Squares assigned to **2.6-Y**).

Between 24 hrs and 6 days heating at 60°C the reaction appears to stop altogether, the sample was then allowed to cool to RT and spectra were collected over the following 9 days which show the reaction rate begins to increase once again. This implies that the reaction is in a dynamic equilibrium between the aNHC complex and the starting materials. Initial formation of **2.6-Y** is relatively fast with respect to the RT experiment at the same concentration, however the rate of formation of the product falls to zero after 24 hrs at 60°C. The thermal energy in the system must be large enough to overcome the Gibbs free energy barrier to reform the starting materials. At RT the equilibrium is shifted towards the product **2.6-Y.**

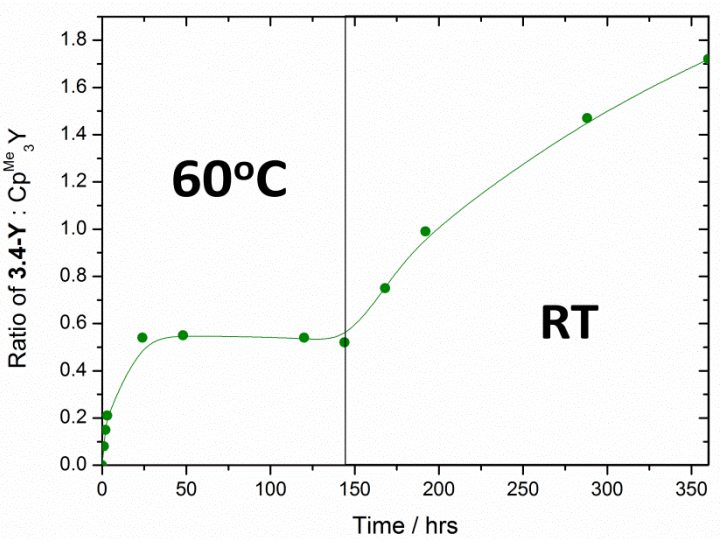

Figure 2.22. Ratio of Cp^{Me}_3Y and **2.6-Y** in solution over time with initial heating followed by cooling back to RT (c = 120 mM). Solid line is a guide for the eye.

There is limited study in the literature into the mechanism of carbene rearrangement in M-NHC complexes. Dagorne *et. al.* reported on the mechanism of carbene rearrangement in the aluminium complex $[(I^tBu)AlMe_3]$.[117] They also did not observe any intermediate species being formed by ^1H NMR spectroscopy, however DFT study implied that I^tBu is displaced by THF when an excess of THF is added to a DCM-d_2 solution. The presence of a coordinating solvent appears to promote isomerisation to the abnormal adduct $[(al^tBu)AlMe_3]$. A 5 coordinate transition state is proposed followed by dissociation of the carbene, which then isomerises and expels THF.

In the case of **2.6-Y,** no coordinating solvent was used. Attempts to acquire NMR data on an isolated, crystalline sample of **2.6-Y** in THF-d_8 were unsuccessful as the crystals are insoluble. However, after several days at RT a pale yellow solution forms presumably due to THF preferentially binding to Y resulting in the formation of $[Cp^{Me}_3Y(THF)]$ and IMes. A potential mechanism for the formation of **2.6-Y** is shown in scheme 2.13. Due to the hard Lewis acidity of Y^{3+} there may be some initial weak interaction between IMes and Cp^{Me}_3Y, as

the electron configuration of Y^{3+} is d^0 there is no possibility of back-donation to the carbene. This would result in electron density being pulled onto the electron withdrawing N atoms in the ring making the backbone protons more acidic relative to free IMes. An equivalent of IMes could then deprotonate the backbone of the pseudo-coordinated IMes forming an ion pair with an anionic IMes deprotonated at the C4 position and an IMes-H cation. The anionic species would then rearrange to coordinate to Y through the anionic C4 carbon and the C2 carbon would then deprotonate $[IMes\text{-}H]^+$ reforming IMes and **2.6-Y**.

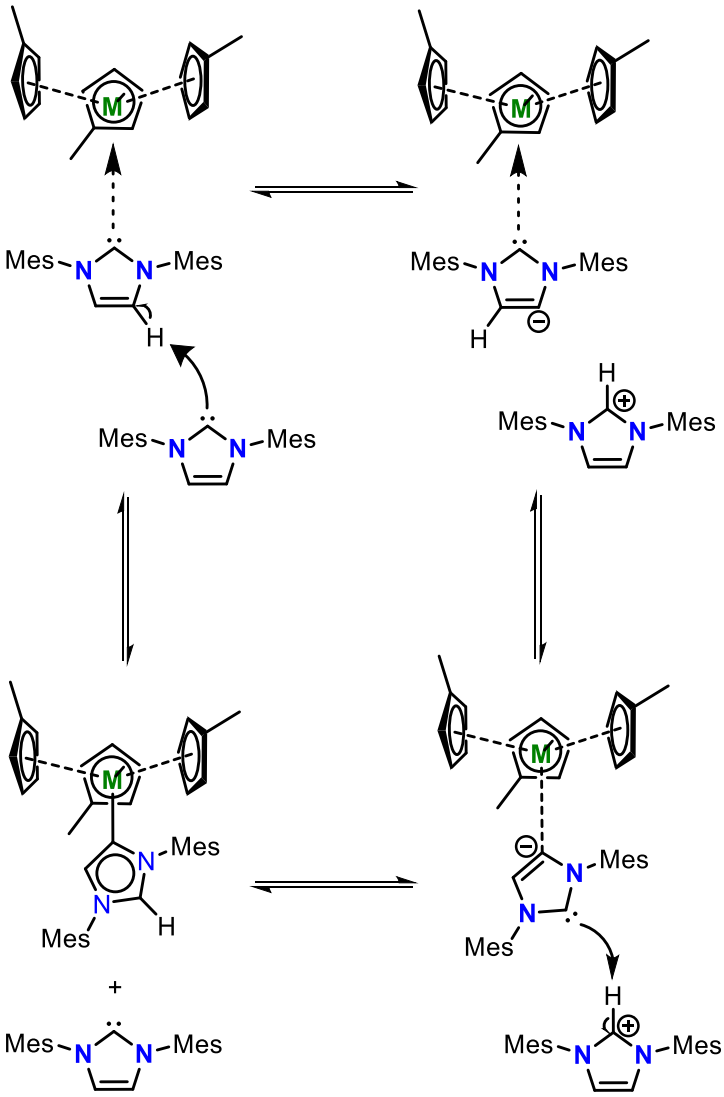

Scheme 2.13. Proposed mechanism for the formation of **2.6-Y** from IMes and Cp^{Me}_3Y.

Each step in the mechanism proposed above is reversible as there is evidence for the carbene rearrangement being a dynamic equilibrium.[117] Increasing the concentration has been shown to accelerate the forward reaction toward the aNHC complex **2.6-Y,** as crystals form after a shorter time period at higher concentrations. DFT calculations will be required in order to fully understand the mechanism of carbene rearrangement at Cp^{Me}_3Y. Computational analysis will be able determine the transition states and the energies of any intermediates formed.

In summary, it has been found that rare-earth ^{n}butyl complexes, **2.1**, react with IMes to form benzyl tethered carbene complexes **2.5**. Compounds **2.5** are formed exclusively with no reactivity observed between **2.1** and the backbone C—H protons as initially expected. A control experiment between Cp^{Me}_3M (M = Y, Dy) and IMes afforded the abnormal NHC complexes **2.6** which crystallise out of solution upon standing at RT. A ^{1}H NMR spectroscopic study of the reaction between Cp^{Me}_3Y and IMes revealed a concentration dependence for the rate of formation of **2.6-Y**. There is evidence for the reaction being reversible as prolonged heating results in a halting of the forward reaction.

2.5 Magnetic Susceptibility Study of Dysprosium Complexes

The magnetic properties of **2.1-Dy** and **2.2-Dy** were examined using SQUID magnetometry in alternating current (AC) and direct current (DC) magnetic fields to elucidate the presence or absence of slow magnetic relaxation. AC current generates an oscillating magnetic field, hence when a sample is placed in an oscillating field there will be a frequency dependent response of the magnetic susceptibility if the sample behaves as an SMM.[44]

Whilst the $\{Cp^{Me}_2Dy\}$ moiety imposes a strong axial ligand field the ground state is not well defined, due to a strong equatorial field generated by relatively hard, carbanion donors, and is likely not the $m_J = \pm 15/2$ KD. The $Cp^{Me}_{cent}—Dy—Cp^{Me}_{cent}$ angle in **2.2-Dy** is 121.41(2)^o

which is a significant deviation from 180°. The plane perpendicular to the {Cp^{Me}_2Dy} axis is occupied by an η^5 interaction to the bridging ferrocenyl ligand and a relatively short Dy—C2 bond. It has been demonstrated that soft interactions in the equatorial plane are required to give rise to SMM behaviour. In this case the $(C_5H_4)^{2-}$ ligand is a hard σ-donor and thus has a destabilising effect on the ground KD.

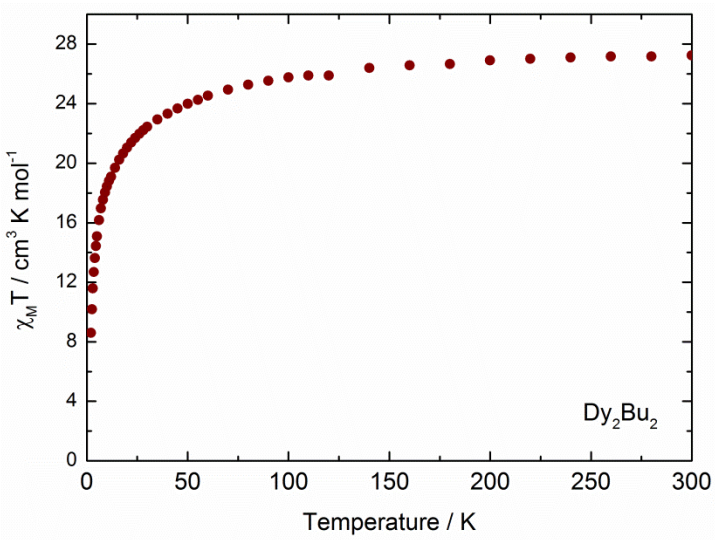

Figure 2.23. Plot of $\chi_M T(T)$ for compound **2.1-Dy** measured from 1.8-300 K at 1 T DC field.

DC magnetic susceptibility measurements were carried out on **2.1-Dy**. In the $\chi_M T/T$ plot (Figure 2.23) the $\chi_M T$ value is 27.24 cm^3 K mol^{-1} at 300 K, which is in good agreement with the calculated value of 28.3 cm^3 K mol^{-1} for two non-interacting Dy^{3+} ions (g_j = 4/3; $^6H_{15/2}$). As the sample is cooled, the $\chi_M T$ product begins to decrease below 150 K, the value of $\chi_M T$ declines more rapidly below 50 K to a value of 6.59 cm^3 K mol^{-1} at 2 K. There is no sharp increase in the $\chi_M T$ value at any point on cooling which suggests the Dy^{3+} ions are weakly antiferromagnetically coupled. It can also signify thermal depopulation of excited m_J states as the sample is cooled towards liquid helium temperatures.

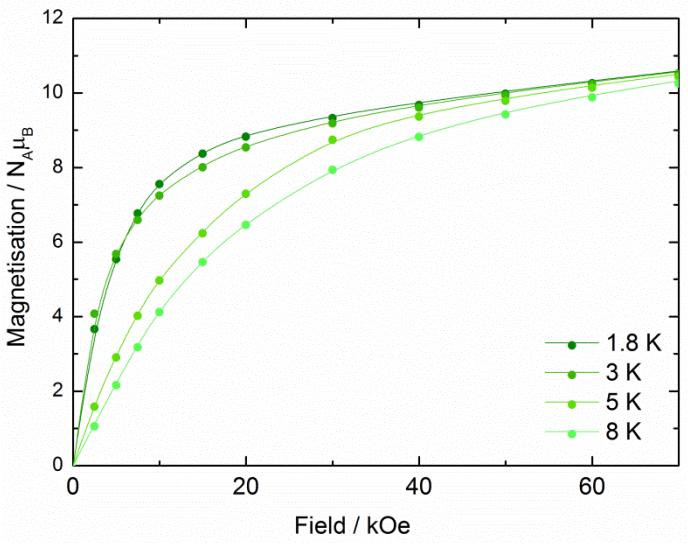

Figure 2.24. Plot of M(H) for compound **2.1-Dy**.

The M(H) plot shows a sharp increase in magnetisation with increasing field strength at 1.8 K up to 10 kOe, upon increasing the magnetic field further the magnetisation increases more steadily as the sample approaches saturation at 70 kOe. The value for the magnetisation is 10.58 μ_B which is in good agreement with the expected value of two non-interacting Dy^{3+} ions (10.7 μ_B) at 7 T. The slope of the curve shows the magnetisation is still increasing at 70 kOe it is likely that this field strength is too low to achieve saturation of the magnetisation in this sample. On heating to 8 K the slope of the curve becomes shallower, the value of M decreases to 10.32 μ_B at 70 kOe as thermal energy of the system inhibits alignment of spins throughout the system.

The DC magnetic susceptibility of **2.2-Dy** also shows weak antiferromagnetic coupling between Dy centers (Figure 2.25). The plot of $\chi_M T(T)$ (figure 2.5) shows the value of $\chi_M T$ to be 28.06 cm^3 K mol^{-1} at 300 K which is in line with the predicted value of 28.3 cm^3 K mol^{-1} based on two non-interacting Dy^{3+} ions. This decreases in a similar manner to **2.1-Dy** on cooling, with a sharp decline below 30 K. The sample also has a higher than predicted magnetisation value of 11.31 μ_B under a field of 70 kOe at 1.8 K which may be due to a small energy gap between ground and excited KDs. The rate of increase in magnetisation also decreases as the temperature increases. Both **2.1-Dy** and **2.2-Dy** show no response to a small AC field at 1.8 K and hence do not behave as SMMs.

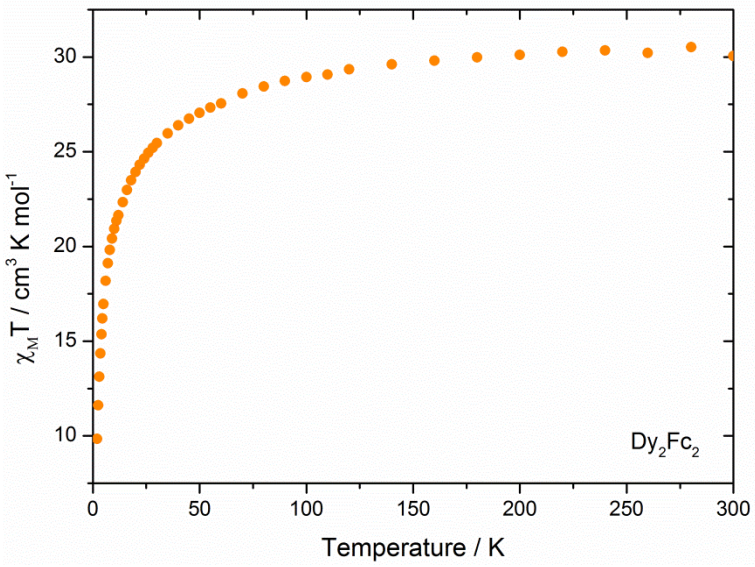

Figure 2.25. Plot of $\chi_M T(T)$ for compound **2.2-Dy** measured from 1.8-300 K at 1 T DC field.

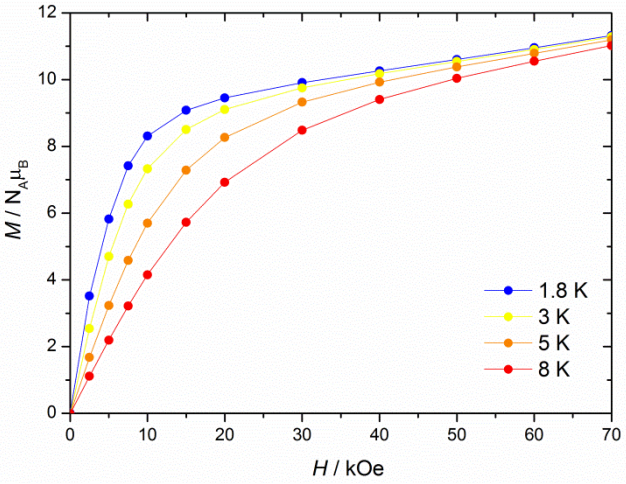

Figure 2.26. Plot of M(H) for compound **2.2-Dy**.

The measurements of **2.1-Dy** and **2.2-Dy** show a lack of response to oscillating magnetic field in zero DC field. These compounds are not SMMs because they don't fulfil the magneto-structural requirements for stabilising the oblate mJ = ±15/2 ground state for Dy^{3+} (Figure 2.27).

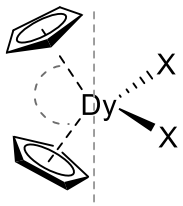

Figure 2.27. Direction of the anisotropy axes typically observed in {Cp_2Dy} complexes. The softer the interaction of the X ligands with Dy^{3+}, the more favourable for SMM properties to be observed.

A ligand field with low axiality in **2.2-Dy** coupled with short Dy—C bonds in the equatorial plane explain the lack of a well-defined ground KD in these systems. It can also be seen that

carbanion bridging ligands are relatively hard with respect to heavier p-block donor-atom ligands.

Magnetic susceptibility measurements were carried out on **2.5-Dy** to ascertain the presence or absence of single molecule magnet behaviour. DC magnetic susceptibility measurements were also carried out, the molar magnetic susceptibility of **2.5-Dy** at 300 K was found to be 13.01 cm^3 K mol^{-1} which is lower than the expected value of 14.17 cm^3 K mol^{-1} per free Dy^{3+} ion. Low values for $\chi_M T$ have been observed recently in 7 coordinate Dy^{3+} SMMs and has been attributed to strong crystal field splitting and large energy separation between ground and excited KDs. Upon cooling the $\chi_M T$ product decreases gradually down to 100 K below which the value begins to decline more steeply. There is a sharp drop below 25 K which is due to thermal depopulation of excited states.

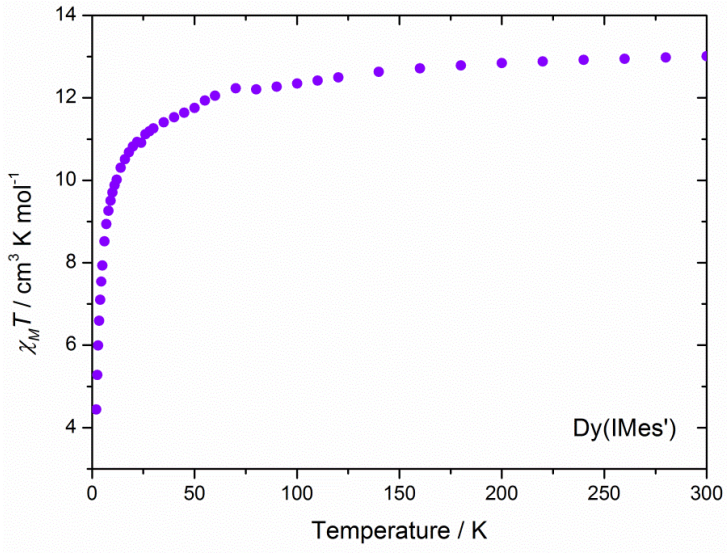

Figure 2.28. The plot of the product of molar magnetic susceptibility and temperature ($\chi_M T$) against temperature for **2.5-Dy**.

The magnetisation of **2.5-Dy** was measured from 1.8–8 K in a sweeping DC field up to 7 T. At 1.8 K the magnetisation rises steeply to 4.04 μ_B at 1 T followed by a steadier rise towards

saturation at 7 T, however, it can be seen from the plot of M(H) that the curve has not plateaued at 7 T so the sample may not have reached full saturation. The value of M is 5.33 μ_B which is expected for a mono-nuclear Dy^{3+} species. On increasing the temperature the increase in magnetisation is shallower which is indicative of magnetic anisotropy. No AC response was detected, ruling out the presence of any frequency dependant magnetic relaxation.

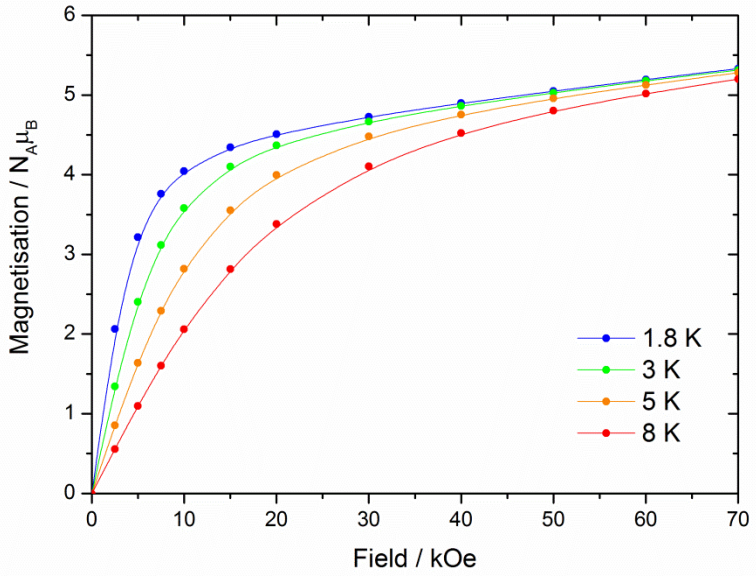

Figure 2.29. Plot of M(H) for **2.5-Dy**.

The magnetic properties of **2.6-Dy** were measured. Due to the structural similarities between **2.6-Dy** and the previously measured ferrocenyl compound **2.2-Dy** it is unlikely to provide a stabilising effect on the ground KD of Dy^{3+}. As expected, **2.6-Dy** shows no response to an AC magnetic field and is therefore not an SMM. The $\chi_M T(T)$ plot follows the same trend on cooling as **2.5-Dy**, the value for $\chi_M T$ at 280 K is 13.89 cm^3 K mol^{-1} which corresponds to the expected free ion value (14.17 cm^3 K mol^{-1}) for Dy^{3+}. The precipitous drop in $\chi_M T$ occurs below 30 K to reach a value of 4.71 cm^3 K mol^{-1} at 2 K.

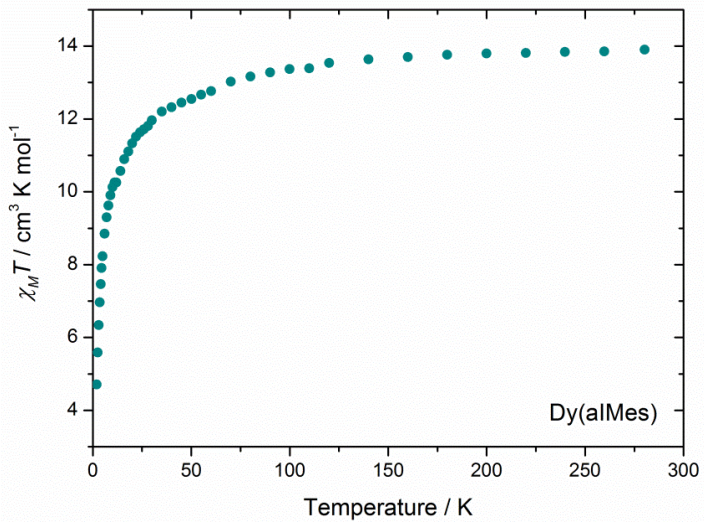

Figure 2.30. The plot of the product of molar magnetic susceptibility and temperature ($\chi_M T$) against temperature for **2.6-Dy**.

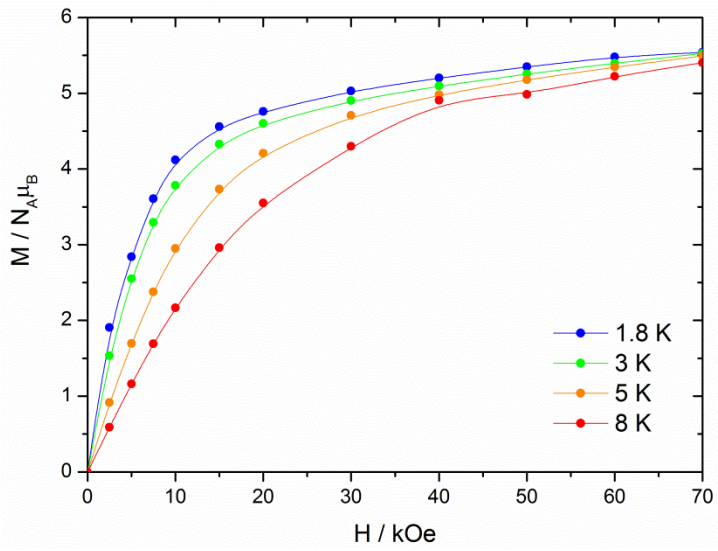

Figure 2.31. Plot of M(H) for **2.6-Dy**.

The magnetisation of **2.6-Dy** was measured from 1.8-8 K between 0 and 7 T. The value of the magnetisation at 1.8 K is 5.54 μ_B at 7 T which is in line with the expected value of a free ($^6H_{15/2}$; g_J = 4/3) Dy^{3+} ion (5.35 μ_B).

2.6 Conclusions

In summary, it has been shown that rare-earth metallocene ^{n}butyl complexes can be synthesised and isolated on a three-gram scale. Furthermore, **2.1** is stable at RT for at least 24 hours and can be stored at -40^{o}C indefinitely. Solution ^{1}H NMR spectroscopic study revealed that **2.1-Y** is oligomeric in solution, most likely a dimer. Compound **2.1** reacts with two equivalents of ferrocene to form the ferrocenyl-bridged dimer, $[Cp^{Me}_{2}M(\mu\text{-}\eta^{1}\text{:}\eta^{5}\text{-}C_{5}H_{4}FeCp)]_{2}$ (M = Dy, Y) (**2.2**). The mono-deprotonated product is the only crystalline product isolated which contrasts with the reactivity of ^{n}BuLi with ferrocene, where a mixture of mono- and di-deprotonated products are isolated regardless of the stoichiometry used. Compound **2.1** deprotonates IMes on one of the methyl-groups of a mesityl group to form the tethered-benzyl carbene complex $[Cp^{Me}_{2}M(IMes')]$ (M – Dy, Y; **2.5**). A study of the reaction by ^{1}H NMR spectroscopy revealed that compound **2.5** is the exclusive product.

A control experiment between $Cp^{Me}_{3}M$ and IMes resulted in the formation of the first f-block abnormal carbene complex $[Cp^{Me}_{3}M(aIMes)]$ (M = Dy, Y; **2.6**). The reaction between $Cp^{Me}_{3}Y$ and IMes was studied by ^{1}H NMR spectroscopy at a range of concentrations. It was found that the higher the concentration, the faster the rate of formation of the product, **2.6-Y**. Heating the reaction mixture initially led to a faster conversion to product, however the reaction ceases to continue to a point and only proceeds upon cooling the reaction mixture to RT. This suggests the formation of **2.6-Y** is in equilibrium with the starting reagents.

Compounds **2.1-Dy**, **2.2-Dy**, **2.5-Dy** and **2.6-Dy** were analysed by SQUID magnetometry to determine their dynamic and static magnetic properties. None of the compounds showed a response to an AC magnetic field and hence are not SMMs.

Chapter 3

Results and Discussion; Reactivity of Rare-Earth ^{n}Butyl Complexes with Elemental Chalcogens: Synthesis of Rare-Earth Chalcogenide Clusters

3 Results and Discussion; Reactivity of Rare-Earth ^{n}butyl Complexes with Elemental Chalcogens: Synthesis of Rare-Earth Chalcogenide Clusters

3.1 Introduction

Rare-earth chalcogenide complexes of low and higher nuclearity are usually synthesised by either oxidation of metal powders with dichalcogenide compounds of the formula RE—ER, or by reacting well defined complexes containing Ln—E bonds (E = S, Se, Te) with elemental chalcogens.[118] In 1994, Evans *et. al.* were able to synthesise a hexanuclear samarium sulfide cluster by reduction of elemental sulfur with decamethylsamarocene (Cp^*_2Sm).[119]

One key aspect of rare-earth chemistry with chalcogens and dichalcogenides is that the nature of the isolated products is dependent on reaction times and conditions. The samarium cluster $[\{Cp^*Sm\}_6Se_{11}]$ (**3.1**) is formed when $[\{Cp^*_2Sm\}_2(\mu\text{-}\eta^1\text{:}\eta^3\text{-}S_3)(THF)]$ (**3.2**)[120] is dissolved in toluene-d_8. **3.1** crystallises out of solution 3-7 days after **3.2** is dissolved, this was shown to happen reproducibly.

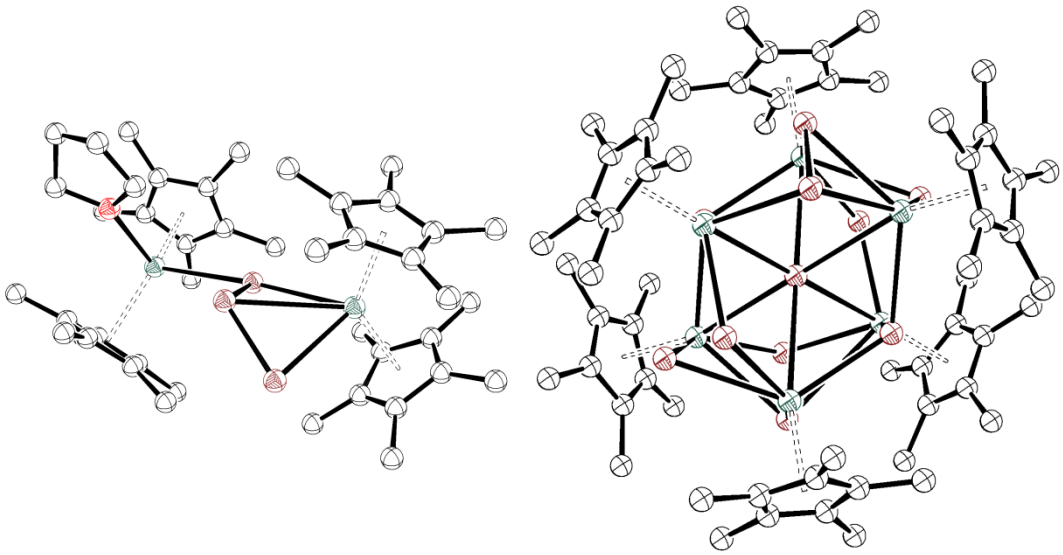

Figure 3.1. (Left) Molecular structure of **3.2**. (Right) Crystal structure of the samarium-selenium cluster **3.1.** Green – samarium; dark red – selenium; black – carbon.[119]

Interestingly, no crystals were obtained from a solution of **3.1** in benzene which illustrates the sensitivity of **3.2** to the solvent medium. Compound **3.2** was a unique structure at the time because 10 of the 11 selenium atoms are diselenide $(Se—Se)^{2-}$ fragments but the eleventh is an Se^{2-} anion that sits in a central cavity coordinated to all six Sm^{3+} ions.

Octanuclear lanthanide-sulfur clusters were synthesised utilising the reductive chemistry of zero-valent lanthanide metals. Brennan *et. al.* showed that complexes of the formula "$Ln(SPh)_3$" can be synthesised *in situ* from the metal powder and PhS—SPh in the presence of mercury in THF.[121] After stirring for 1 day a substoichiometric amount (0.75 eq) of sulfur was added to the reaction mixture and after work up the crystalline material found to be $[Ln_8S_6(SPh)_{12}(THF)_8]\cdot$ 2.9 THF (Ln = Pr, Nd and Gd) was isolated. This chemistry shows that sulfur can insert into Ln—S bonds to form higher nuclearity clusters over prolonged reaction times. Mercury can also become incorporated into rare-earth chalcogen clusters in reactions with a Sm/Hg amalgam.[122] When combined with PhSe—SePh in THF followed by addition of elemental selenium the octanuclear cluster $[Sm_8Se_6(SePh)_{12}(THF)_8]$ forms, however in DME when sulfur is added to the reaction mixture in place of selenium, the unusual ion pair cluster $[Sm_7S_7(SePh)_6(DME)_7][Hg_3(SePh)_7]$ is formed. This work exhibits the range of potential products that can form in reactions with elemental chalcogens and the drastic effects of solvent and reaction conditions.

Rare-earth-chalcogen clusters can also form upon decomposition of well-defined mononuclear complexes also demonstrated by Arnold *et. al.*[123]

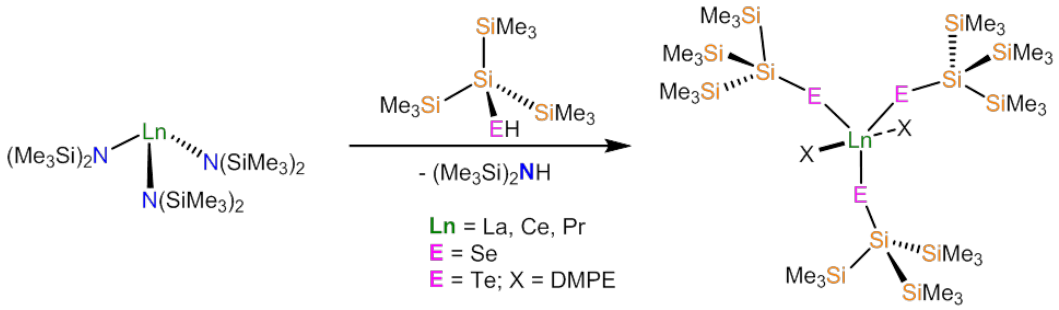

Scheme 3.1. Formation of well-defined lanthanum selenide and tellurides reported by Arnold *et. al*. The telluride is a precursor to a pentanuclear La-Te cluster.[123]

Protonolysis of $[La(N(SiMe_3)_2)_3]$ with the bulky selenol and tellurol compounds HE—$Si(SiMe_3)_3$ resulted in the formation of the lanthanum selenide and telluride complexes; $[La(ESi(SiMe_3)_3)_3]$ (where E = Se, Te). Addition of DMPE to $[La(TeSi(SiMe_3)_3)_3]$ gave the isolable complex $[(DMPE)_2La(TeSi(SiMe_3)_3)_3]$ (Scheme 3.1). In the absence of DMPE the tellurium complex $[La(TeSi(SiMe_3)_3)_3]$ decomposes upon stirring at RT. Removal of the solvent and extraction of the residues into hexanes and subsequent crystallisation afforded the pentanuclear lanthanide clusters $Ln_5Te_3[TeSi(SiMe_3)_3]_9$ (Ln = La, Ce, Y).

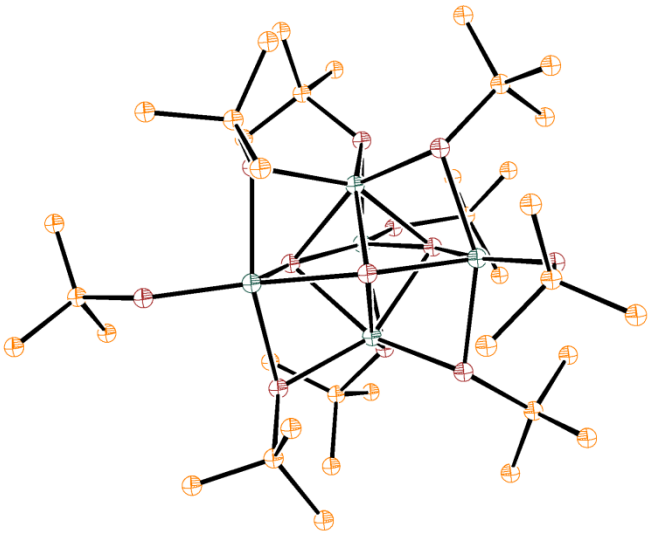

Figure 3.2. Molecular structure of the cerium telluride cluster $Ce_5Te_3[TeSi(SiMe_3)_3]_9$ which forms upon decomposition of $[(DMPE)_2Ce(TeSi(SiMe_3)_3)_3]$. Methyl groups omitted for clarity. Orange – silicon; brown – tellurium; dark green – cerium.[123]

In 2005 Weng *et. al.* reported on the insertion of sulfur into Y—C bonds for the first time.[81] Bis(cyclopentadienyl)yttrium alkyls were prepared from $[Cp_2Y(\mu\text{-}Cl)]_2$ and MeLi and ^{n}BuLi in toluene at -30°C to form $[Cp_2Y(\mu\text{-}CH_3)]_2$ (**3.3**) and $[Cp_2Y(\mu\text{-}^{n}Bu)]_2$ (**3.4**) respectively *in situ*. There was strong evidence for formation of the *n*-butyl complex **3.4** *in situ*, but no characterisation was made. Sulfur was successfully inserted into the Y—C bond in each case to form $[Cp_2Y(\mu\text{-}SR)]_2$ (R = Me (**3.5**), ^{n}Bu (**3.6**)). The reaction between **3.3** formed *in situ* and two equivalents equivalents of sulfur (0.25 equivalents of S_8) was carried out at RT in toluene and forms **3.5** in 65% yield. Following the same synthetic procedure, **3.4** reacts in a different way towards sulfur. After stirring at RT for 12 hrs, subsequent work up in THF/hexane afforded the tetranuclear μ_3-sulfide complex $[\{Cp_2Y\}_2(\mu_3\text{-}S)(THF)]_2$ (**3.7**). Compound **3.7** is proposed to have formed due to competing reactivity of **3.6** with elemental sulfur at a higher temperature. The by-products were identified as $(^{n}Bu)_2S$ and ^{n}BuS—S^{n}Bu by GC/MS.

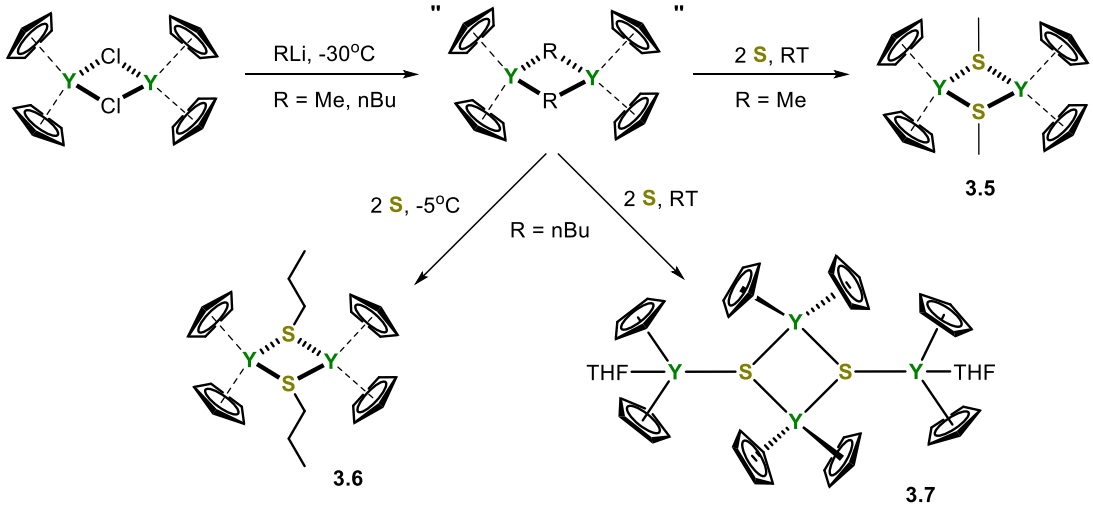

Scheme 3.2. Reactivity of putative Cp_2Y-alkyl complexes (marked in quotations as no characterisation is provided on these complexes) with sulfur under various reaction conditions.[81]

When the reaction between **3.4** formed *in situ* and sulfur is warmed to -5°C and stirred for 5 hrs subsequent work up affords compound **3.6**. The instability of rare-earth complexes of the formula $[Cp_2M(\mu\text{-}SR)]_2$ in the presence of sulfur was demonstrated by reacting $[Cp_2Yb(\mu\text{-}SEt)]_2$ with sulfur in THF at RT. Sulfur is reduced by the ethylsulfide ligand to form **3.7-Yb** and the disulfide bridged complex $[\{Cp_2Yb(THF)\}_2(\mu\text{-}\eta^2\text{:}\eta^2\text{-}S_2)]$.

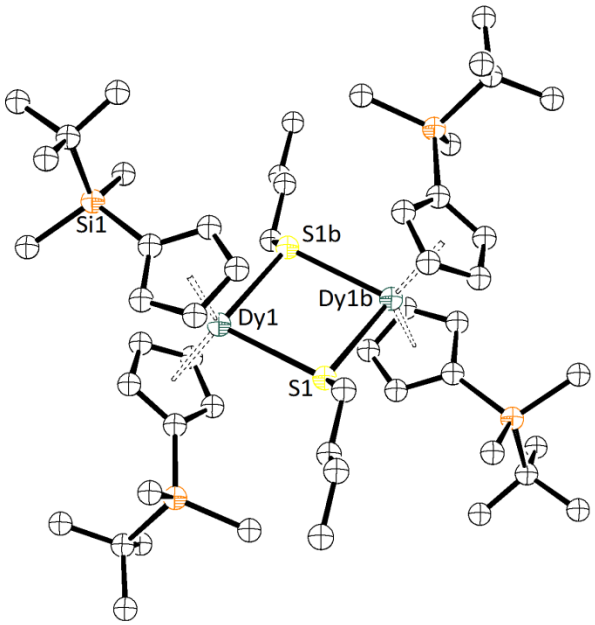

Figure 3.3. Molecular structure of $[^{TBDMS}Cp_2M(\mu\text{-}S^nBu)]_2$. Thermal ellipsoids shown at 50% probability.[124]

The steric bulk of the ancillary Cp ligands has a marked effect on the reactivity of $\{Cp_2M\}$ complexes with elemental sulfur. In 2007, the Weng *et. al.* synthesised $[^{TBDMS}Cp_2M(\mu\text{-}Cl)]_2$ (M = Y, Dy, Er, Yb) with the much bulkier *t*-butyl(dimethyl)silyl substituted Cp ligands.[124] The methyl- and n-butyl bridged complexes $[^{TBDMS}Cp_2M(\mu\text{-}R)]_2$ (R = Me, *n*-Bu) were synthesised *in situ* and reacted with sulfur. When the reactions are carried out at RT, both the methyl and ^{n}butyl complexes insert sulfur into the M—C bond to form solely $[^{TBDMS}Cp_2M(\mu\text{-}SR)]_2$ (R = Me, ^{n}Bu). The greater steric bulk of the ancillary ligands imparts a greater kinetic stability to the product, with respect to the unsubstituted Cp complex, meaning that further reactivity with sulfur does not occur.

The steric bulk of the thiol ligand can also have a profound effect on the product formed.[125] Protonolysis reactions of $[M(N(SiMe_3)_2)_3(\mu\text{-}Cl)Li(THF)_3]$ (M = Pr, Sm) with ^tBuSH and EtSH afforded $[((Me_3Si)_2N)_2M(\mu\text{-}S^tBu)]_2$ and the tetranuclear cluster $[Li(THF)_4][\{(Me_3Si)_2N\}_4Pr_4(\mu_4\text{-}SEt)(\mu\text{-}SEt)_8]$ respectively.

A recent study by Edelmann *et. al.* has shown that bulky scorpionate (tris(pyrazolyl)borate) ligands can stabilise lanthanide complexes bearing polysulfide ligands.[126] Reacting the divalent precursors $[M(Tp^{iPr2})_2]$ (M = Sm , Yb) with one equivalent of sulfur led to the formation of two distinct polysulfide compounds depending on the conditions. In a toluene/THF mixture, $[Sm(Tp^{iPr2})_2]$ reacts with 1 equivalent of S_8 to give the monomeric, polysulfide complex $[(Tp^{iPr2})Sm^{3+}(iPr\text{-}pzH)(S_5)]$ with an $(S_5)^{2-}$ ligand. The ytterbium version reacted with one equivalent of sulfur in toluene leads to the dinuclear, polysulfide complex $[\{(Tp^{iPr2})(iPr_2pzH)(iPr_2pz)Yb\}_2(\mu\text{-}S_4)]$. In each case a Tp ligand is lost. A protonated pyrazole, and a pyrazolyl anion are coordinated to each metal centre.

Interestingly, Zhou *et. al.* have recently reported that rare-earth pentasulfides can be synthesised in a stepwise manner from thiolate to sulfide to disulfide starting from an yttrium alkyl complex $[Tp^*Y(CH_2Ph)_2(THF)]$ (**3.8**).[127] This is achieved by controlling the stoichiometry of sulfur atoms to precursor. As such, 0.25 equivalents of S_8 reacts with **3.8** to form a tetranuclear cluster $[\{Tp^*_2Y\}_4(\mu\text{-}SCH_2Ph)_6\text{-}(\mu_4\text{-}S)]$ (**3.9**) (shown in Figure 3.4) with benzylthiolate ligands bridging between {Tp*Y} moieties.

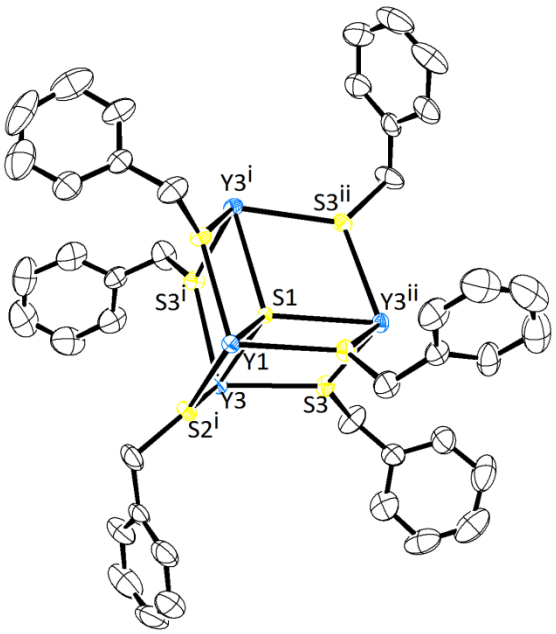

Figure 3.4. Molecular structure of **3.9**, thermal ellipsoids set at 30% probability. Tp* groups and H-atoms omitted for clarity.[127]

Reacting Y_4S_7 with 0.125 S_8 resulted in the loss of 2 equivalents of dibenzylsulfide and one equivalent of dibenzyl disulfide to form an Y_4S_4 cluster.[127] Y_4S_4 can be converted to the disulfide bridged complex: $[Tp^*Y(THF)(\mu\text{-}S_2)]_2$ (**3.10**) with 0.5 equivalents of S_8. The monomeric pentasulfide $[Tp^*Y(THF)(S_5)]$ is formed upon reacting **3.10** with 3/8 of S_8. This series of complexes shows that the synthesis of higher nuclearity sulfides can be undertaken in a controlled, rational way.

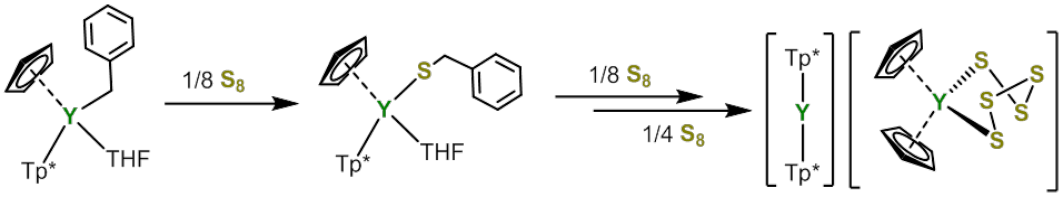

Scheme 3.3. Formation of yttrium pentasulfide complex from stepwise reduction/inserton of sulfur into Y—C bonds and Tp* ligand scrambling.[127]

A heteroleptic, mono-alkyl starting material [Tp*(Cp)Y(CH_2Ph)(THF)] also reacted with 0.125 equivalents of S_8 to form the corresponding thiolate complex [Tp*(Cp)Y(SCH_2Ph)(THF)] with an insertion of sulfur into the Y—C bond. Upon subsequent additions of 0.125 S_8 and 0.25 S_8, a ligand scrambling occurs, resulting in the formation of **3.10** and the ion pair [$(Tp^*)_2Y$][$Cp_2Y(S_5)$] respectively.

The work set out in this chapter aims to establish the reactivity of the *n*-butyl complexes [$Cp^{Me}{}_2M(\mu$-*n*Bu)]$_2$ towards elemental chalcogens with a view to synthesising rare-earth chalcogens bridged complexes and explore their SMM properties.

3.2 Results & Discussion: Synthesis & Characterisation of Rare-Earth Chalcogen Clusters: [$Cp^{Me}{}_{10}M_6(S_3)_2S_2$] (M = Dy, Y)

The reaction of **3.1** with 0.25 equivalents of S_8 in toluene at RT produced a small quantity of pale yellow crystals on standing for two days. Single crystal XRD analysis revealed the products to be the hexanuclear clusters [$Cp^{Me}{}_{10}M_6(S_3)_2S_2$] (**3.11**) (M = Dy, Y) according to Scheme 3.4, which crystallise in the monoclinic $P2_1/n$ space group. Increasing the stoichiometry to 0.5 equivalents of S_8 resulted in a yield of 53% based on sulfur as the limiting reagent.

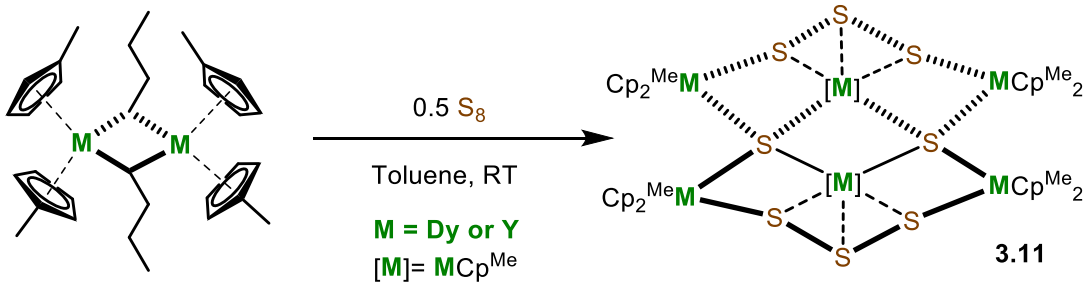

Scheme 3.4. Synthesis of **3.11**.

Based on the previous study of Zhou *et. al.* it has been found that Cp ligands bearing bulky substituents can kinetically stabilise the sulfur insertion product and prevent competing reactivity of the resulting ^{n}butylthiolate complex with unreacted sulfur.[124] At RT the putative unsubstituted Cp complex $[Cp_2Y(\mu\text{-}^{n}Bu)]_2$ made *in situ* from $[Cp_2Y(\mu\text{-}Cl)]_2$ and *n*-BuLi reacts with sulfur at RT to form a tetranuclear complex **3.7** with bridging $(S)^{2-}$ ligands.

Reacting the pre-isolated ^{n}butyl complex **2.1** with sulfur results in the formation of a larger cluster with two, distinct bridging sulfur moieties (asymmetric unit shown in Figure 3.5). The first is an $\mu^4\text{-}S^{2-}$ ligand that bridges between two $\{Cp^{Me}_2M\}$ units and the two central metal ions, the other is the unusual $\eta^3\text{-}(S_3)^{2-}$ ligand that coordinates to the central $\{Cp^{Me}M\}$ and to two $\{Cp^{Me}_2M\}$ units on opposite sides of the molecule. There are only two other crystallographically characterised examples of such a trisulfide ligand in the literature, which are $[(HMDS)_3M(\mu\text{-}S_3)(K\text{-}18\text{-}c\text{-}6)]$ where M = U,[128] Th.[129] A complex containing an $\eta^2\text{-}S_3$ ligand of the formula $[(Me_3Si)_2N]_2Y[\eta_2\text{-}S_3N(SiMe_3)_2](THF)$ is also formed as a by-product of the reduction of sulfur by the dinitrogen bridged complex $[\{(HMDS)_2Y(THF)\}_2(\mu\text{-}N_2)]$.[130]

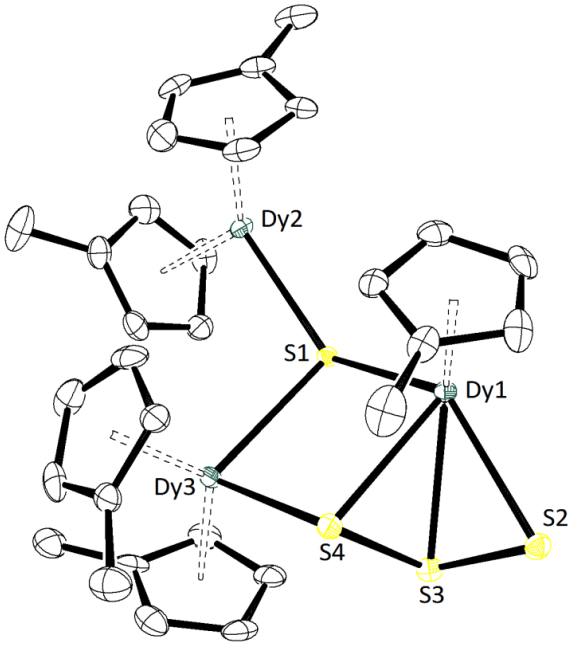

Figure 3.5. ORTEP representation of the asymmetric unit of **3.11-Dy** with H-atoms omitted for clarity. Thermal ellipsoids shown at 50% probability.

3.11-Dy also crystallises in the monoclinic $P2_1/n$ space group. The Dy2-S1 and Dy3-S1 bond lengths are 2.764(7) Å and 2.805(9) Å respectively which is similar to other Dy—S distances reported previously.[47, 131] The bonds from Dy1 to the $(S_3)^{2-}$ atoms are longer; Dy1—S2 – 2.795(8) Å, Dy1—S3 – 2.836(10) Å and Dy1—S4 – 2.778(9) Å which indicates a slightly weaker interaction as the negative charge is spread over three atoms. The Dy3—S4 and Dy2—S2 bond distances are 2.705(8) Å and 2.730(9) Å respectively and are the shortest of all the Dy-S interactions in the molecule. This suggests that the negative charge on the $(S_3)^{2-}$ ligand lies on the outer S atoms.

The Cp_{cent}—Dy—Cp_{cent} angles for the $\{Cp^{Me}{}_2Dy\}$ units are 127.03(18)° (Dy3) and 128.83(7)° (Dy2) which are in line with other $[Cp^{Me}{}_2Dy—R]_n$ complexes reported previously.[47]

The central Dy^{3+} ion (Dy1) has a less well-defined coordination geometry. It is coordinated to one η^5-Cp^{Me} ligand and five sulfur atoms. The axial field of each $\{Cp^{Me}{}_2Dy\}$ unit is defined by the Cp_{cent}—Dy—S3 axis with the sulfide ions coordinating in the plane perpendicular. The core of the Dy_6S_8 cluster (shown in figure 3.6) is in a chair type conformation, with a planar Dy_2S_2 unit in the centre and one trisulfide unit pointing up and the opposite pointing down.

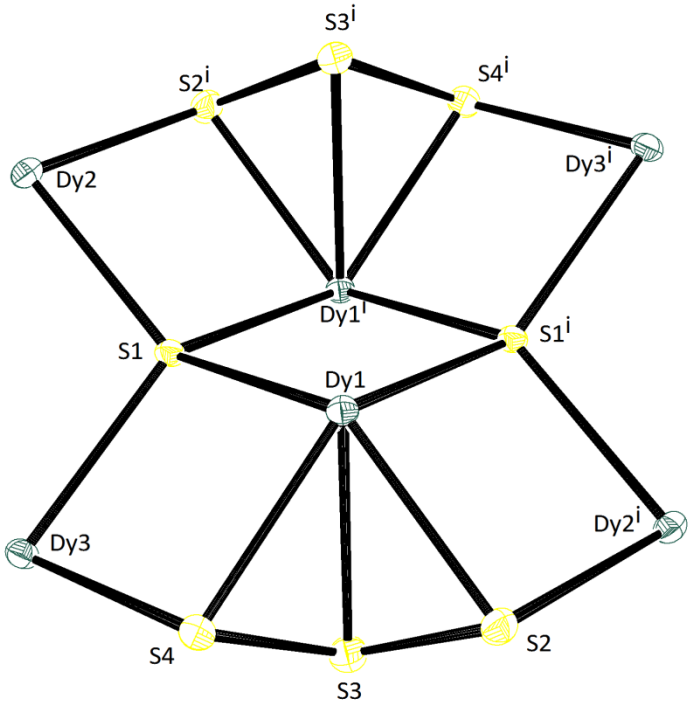

Figure 3.6. The Dy_6S_8 core of the compound **3.11-Dy** highlighting the puckered, chair shape.

The isostructural yttrium-sulfur cluster **3.11-Y** was characterised by ^{1}H NMR spectroscopy. As **3.11-Y** is insoluble in non-coordinating solvents such as hexane and benzene THF-d_8 was required to obtain a spectrum. When THF-d_8 is added to **3.11-Y** the crystals do not dissolve immediately but require repeated inversion of the NMR tube over several minutes. The spectrum shows just two singlets at δ 5.84 and 2.17 ppm which can be assigned to the Cp—C*H*$_3$ and CpC—*H* protons respectively. This is unusual as normally two triplet resonances would be expected from the CpC—*H* protons.

3.3 Magnetic Susceptibilty Study of $[Cp^{Me}_{10}Dy_6(S_3)_2S_2]$

The magnetic properties of compound **3.11-Dy** were measured on a SQUID magnetometer in DC and AC magnetic fields. To date there is only one previous study on the magnetism of a lanthanide-chalcogenide clusters reported by Layfield *et. al.* on the gadolinium, terbium and dysprosium clusters $[Li(THF)_4][Ln_4\{HMDS\}_4(\mu\text{-}SEt)_8(\mu_4\text{-}SEt)]$.[131] The dimer $[Cp^{Me}_2Dy(\mu\text{-}SSiPh_3)]_2$ has also been measured for it's SMM properties and exhibits a U_{eff} barrier of 133 cm^{-1}.[47]

The DC magnetic susceptibility measurements of **3.11-Dy** at H_{dc} = 1 T show the typical values and trends for a Dy^{3+} complex. The value of $\chi_M T$ at 300 K is 84.55 cm^3 K mol^{-1} which is in line with the calculated value of six non-interacting Dy^{3+} ions (85.02 cm^3 K mol^{-1} - $^6H_{15/2}$; g_J = 4/3). The $\chi_M T(T)$ plot shows a plateau from 300 K on cooling to 150 K at which point the $\chi_M T$ product begins to decrease. The decrease becomes sharper below 100 K before dropping precipitously to a value of 28.12 cm^3 K mol^{-1} at 2 K. This is indicative of weak antiferromagnetic exchange between Dy^{3+} ions and the sharp decrease can be explained by thermal depopulation of excited KDs within the spin-orbit coupled ground state.

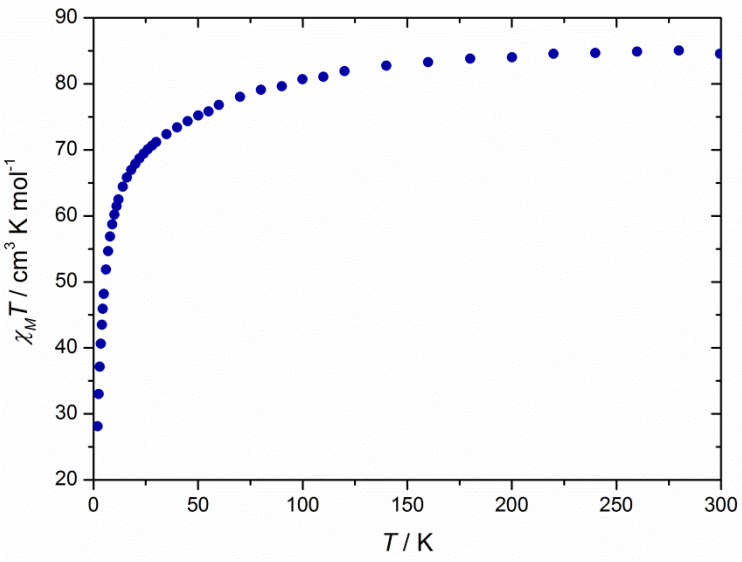

Figure 3.7. Plot of χ_MT(T) for compound **3.11-Dy**. H_{dc} = 1 T.

The magnetisation was measured from 0-7 T at 1.8 – 5 K. The M(H) plot follows a similar trend to previous complexes reported here. At 1.8 K the rise in magnetisation is steeper at lower fields, which demonstrates the presence of magnetic anisotropy. The value of magnetisation close to saturation at 1.8 K is 31.22 μ_B which is close to the calculated value of six non-interacting Dy^{3+} ions (6 x 5.35 μ_B – 32.1 μ_B).

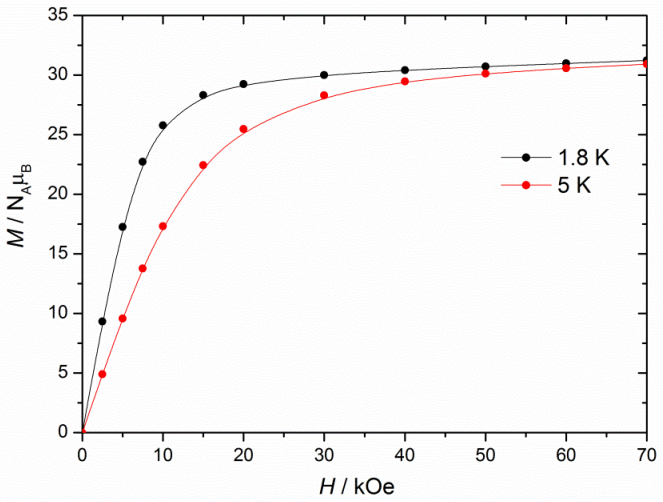

Figure 3.8. Plot of M(H) for compound **3.11-Dy**. Solid lines are a guide for the eye.

The dynamic magnetic susceptibility was measured in zero DC field using a small oscillating field (H_{ac} = 1.55 Oe – see Figure 3.9). Frequency dependent in- (χ') and out-of-phase (χ'') magnetic susceptibility is observed in the range of 2 - 18 K from 0.1 Hz – 1.4 kHz with peak maxima in the χ''(ν) isotherms up to 15 K. The peaks shift to higher frequency on increasing the temperature and the peak maxima from 16 to 18 K do not appear in the frequency range of the magnetometer. This implies that the ground KD is not well separated from the excited m_J states and that the relaxation time is decreasing rapidly on increasing the temperature.

In many cases QTM is observed at temperatures below 5 K where the thermal energy is too low to enable relaxation via excited m_J states. At 2 K the peak maxima for χ'' be observed at low or high frequencies. However, **3.11-Dy** shows a strong temperature independent process occurring below 4 K. The peak in the χ''(ν) isotherm at 2 K occurs at 564 Hz and the peak at 3 K comes at 169 Hz which does not coincide with the trend from 5-18 K in which a more linear increase in χ''(ν) peak maxima is observed. This indicates the relaxation of the magnetisation at low temperatures is strongly influenced by QTM. A similar phenomenon is observed in the undiluted dysprosium selenide complex $[\{Cp^{Me}_2Dy\}_3(\mu\text{-}SeMes)_3]$.[50]

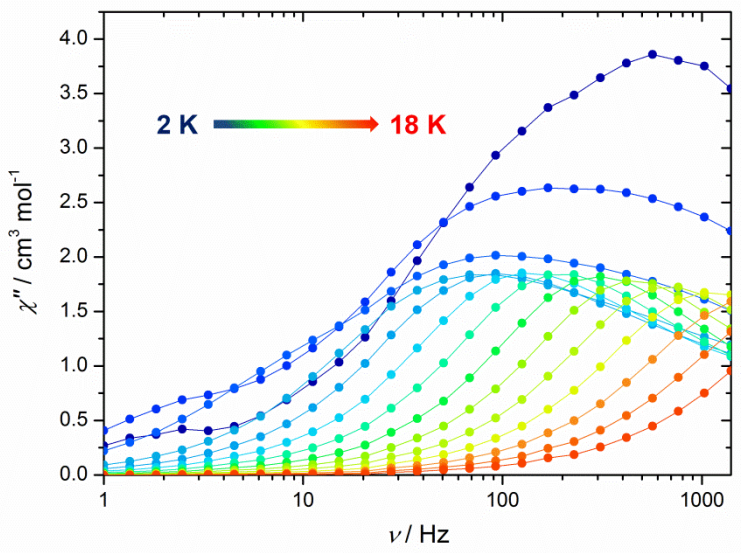

Figure 3.9. Plot of the out-of-phase component of the magnetic susceptibility against frequency, χ''(ν), measured with an AC field of 1.55 Oe, for compound **3.11-Dy**.

The in-phase magnetic susceptibility also reveals frequency dependence up to 18 K, as the temperature increases the traces become flatter indicating that the thermal energy in the system is causing the spins to relax much faster than the frequency of the oscillating field. At 18 K there is a very slight downturn in χ' above 1 kHz (Figure 3.10).

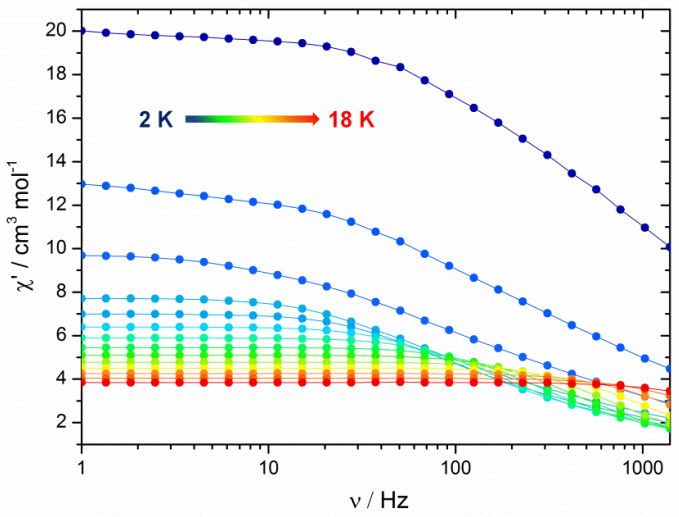

Figure 3.10. Plot of the in-phase component of the magnetic susceptibility against frequency, χ'(ν), measured with an AC field of 1.55 Oe, for compound **3.11-Dy**

The Cole-Cole or Argand $\chi''(\chi')$ plot reveals the distribution of relaxation times. The range of α parameters quantifies the range of relaxation times. At higher temperatures (> 5 K) the predominant relaxation mechanism is usually a thermally driven process, either an Orbach mechanism which occurs via an excited ± m_J state to the ground ∓ m_J state, or thermally-assisted QTM. A so-called 'double hump' feature in the Cole-Cole trace shows there are two relaxation process happening at a certain temperature. This is seen more commonly at low temperatures (< 5 K) where QTM is dominant but thermal relaxation processes can also be present.

The Cole-Cole plot for **3.11-Dy** can be fitted with just one relaxation mechanism although there is some evidence of a second relaxation mechanism present at low temperature (2-3 K). As the χ''(v) plot shows the relaxation in the lower temperature regime to be temperature independent it is likely that the small bump in the Cole-Cole is due to a small thermal contribution to the relaxation, with QTM being the dominant process.

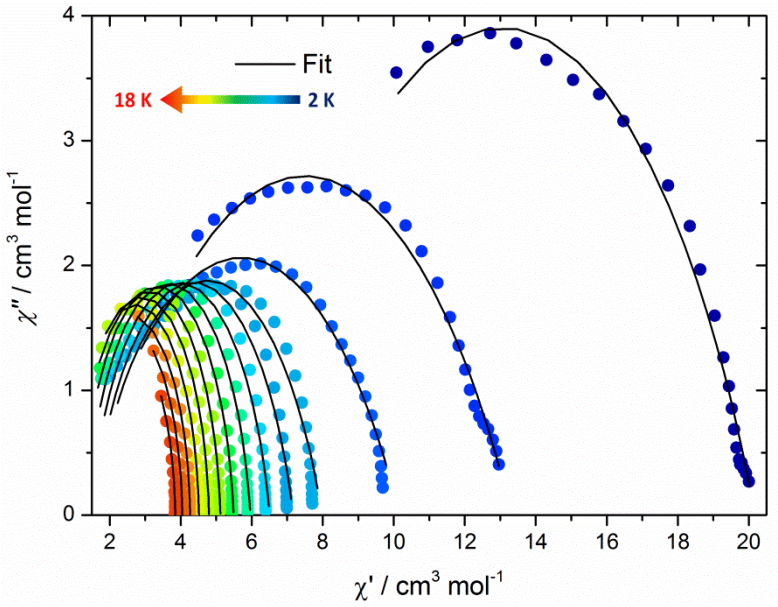

Figure 3.11. Cole-Cole plot of the out-of-phase against in-phase components of the magnetic susceptibility for compound **3.11-Dy**. Solid line represents a fit to the experimental data.

The energy barrier to spin reversal can be ascertained by fitting the Cole-Cole plot to a generalised Debye model to extract the relaxation time, τ, at the peak maxima for each temperature. The U_{eff} barrier can be calculated using the Arrhenius equation, $\tau = \tau_0 \, e(\frac{U_{eff}}{k_B T})$, from which the value was determined to be U_{eff} = 72.9 cm^{-1} (τ_0 = 1.33x10^{-7} s). Whilst this is a modest energy barrier to spin reversal it is comparable to the energy barrier reported for the Tb_4 and Dy_4 thiolate cage complexes (U_{eff} = 4.6 cm^{-1} and 46 cm^{-1} in zero field for Tb_4 and Dy_4, respectively) reported by Layfield *et. al.*[131]

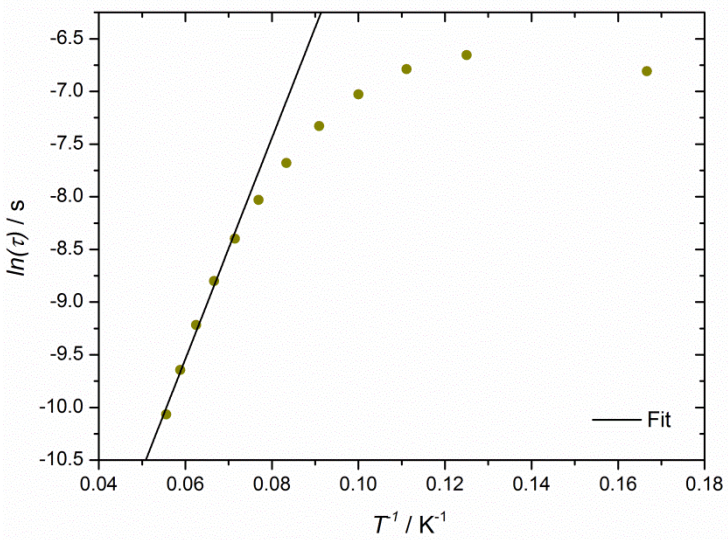

Figure 3.12. Arrhenius plot for compound **3.11-Dy** showing a linear fit of the higher temperature region from which a value of U_{eff} = 72.9 cm^{-1} can be extracted.

The higher temperature regime is linear which is indicative of a thermal relaxation process. Deviation from linearity in the Arrhenius plot implies the mechanism of magnetic relaxation is not thermally driven and QTM is becoming the dominant mechanism.

3.4 Reactivity of Rare-Earth ^{n}butyl Complexes Towards Elemental Selenium

Selenium occurs in two main allotropes, grey and red, which can be either amorphous Se or have the formula Se_8 akin to sulfur. For these studies, grey selenium powder was used to explore the reactivity with rare-earth ^{n}butyl complexes. Unlike sulfur, selenium is insoluble in common organic solvents and initial observations of a reaction between an excess of selenium (4 equivalents or 2:1 ratio of Se to M) and **2.1-Y** in C_6D_6 showed no colour change or any sign of selenium reacting at RT. On heating the reaction mixture to 80^{o}C a colour change to yellow was observed which is consistent with decomposition of **2.1-Y** as it decomposes at RT over several days in solution. However, continued heating for a period of 15 hrs resulted in the formation of dark orange-yellow crystals on top of a layer of unreacted selenium. XRD analysis of a single crystal showed the structure was the analogous selenium cluster: $[Cp^{Me}_{10}Y_6(Se_3)_2Se_2]$ (**3.12-Y**).

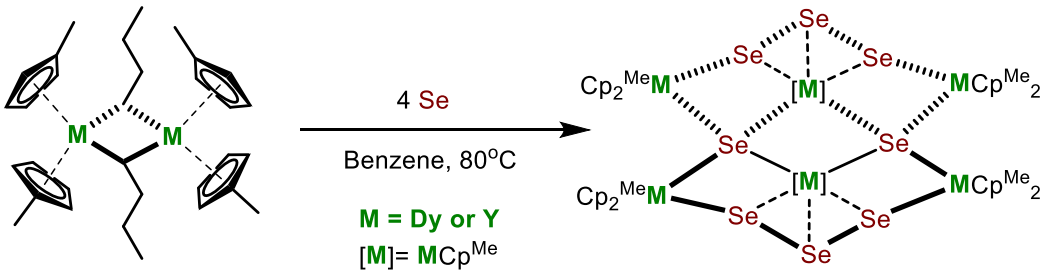

Scheme 3.5. Synthesis of the rare-earth selenium cluster complexes **3.12**.

Considering the different reactions conditions employed here when compared to the synthesis of **3.11** it is surprising that the same cluster is formed with selenium. It is unlikely that the *n*-butyl complex remains in solution for a long time at 80^{o}C as the solution turns a dark yellow colour within minutes on heating. It is most likely that an intermediate species is active in the reaction with selenium, possibly the hydride $[Cp^{Me}_2M(\mu\text{-}H)]_n$ forming as a

result of decomposition through β-H elimination. Interestingly, when **2.1** is reacts with two equivalents of Se (1:1 Se to M) under the same conditions, all the selenium is consumed generating a deep yellow solution from which no crystalline material could be isolated.

The crystal structure of **3.12-Dy**, which crystallises in the monoclinic space group C2/c, reveals some subtle differences in the bond lengths and angles with respect to **3.11-Dy.** The central Dy_2Se_2 unit is a square with the Dy3-Se1 bond lengths of 2.907(6) Å, whereas the central Dy_2S_2 core in **3.11-Dy** being slightly rhombus-shaped with two sets of bond lengths for the Dy—S bonds. The Cp_{cent}—Dy—Cp_{cent} angles are 130.08(3)° (Dy1) and 127.16(3)° (Dy2) which is a significant difference crystallographically. The Cp_{cent}—Dy—Cp_{cent} angle around Dy1 is more obtuse than many other $\{Cp^{Me}{}_2Dy\}$ complexes with soft donor ligands. The Dy—Se bond distances in the equatorial plane of each $\{Cp^{Me}{}_2Dy\}$ unit are; Dy1—Se1: 2.873(6) Å, Dy1—Se4: 2.842(7) Å, Dy2—Se1: and Dy2-Se2: respectively which is an increase in approximately 1.5 Å over the equivalent bonds in **3.11-Dy.** The bond distances from dysprosium to the $(Se_3)^{2-}$ unit are; Dy3—Se2 – 2.943(6) Å, Dy3—Se3 - 2.964(6) Å and Dy3—Se4 – 2.931(6) Å.

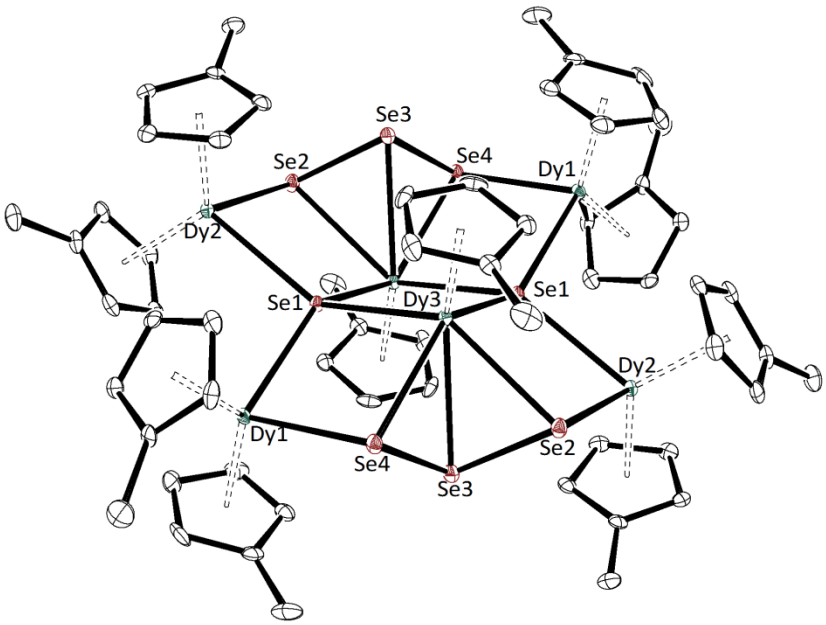

Figure 3.13. ORTEP representation of the crystal structure of **3.12-Dy**. H-atoms have been omitted for clarity. Thermal ellipsoids set at 50% probability.

3.12-Y is isostructural but an adequate structure refinement could not be obtained due to ambiguity of the space group. Whilst a solution can be made using the same C2/c space group as the isostructural **3.12-Dy** when all the atoms are refined anisotropically, most carbon atoms show as non-positive definites (NPDs). The Y_6Se_8 core of the structure can be refined in $P2_1/n$, which is the space group exhibited by the sulfur compounds **3.11**, however the Cp^{Me} rings cannot be refined. Unfortunately, further characterisation of **3.12** was not possible due to the insolubility of both **3.12** and the excess unreacted selenium. Attempts to wash the crystals away from the selenium powder were unsuccessful. **3.12** can be extracted from unreacted selenium with THF. However, it has been shown in previous study that the solvent can drastically effect the formation of rare-earth-chalcogen clusters especially in the presence of excess chalcogen. Benzene was decanted from the crystals of **3.12** and unreacted selenium, THF was then added and the mixture and left to stand at RT for 5 minutes. During this time the crystals of **3.12** dissolved leaving behind unreacted selenium. The THF solution was then decanted from the unreacted selenium. Two different compounds have been crystallised upon evaporation of the dark red THF solution. One is the ion pair cluster compound $[Cp^{Me}{}_2Y(THF)_3][\{Cp^{Me}Y(Se_2)\}_6Se]$ (**3.13-Y**) and the dinuclear complex $[\{Cp^{Me}{}_2Y(THF)\}_2(\mu\text{-}\eta^2\text{:}\eta^2\text{-}Se_2)]$ (**3.14-Y**).

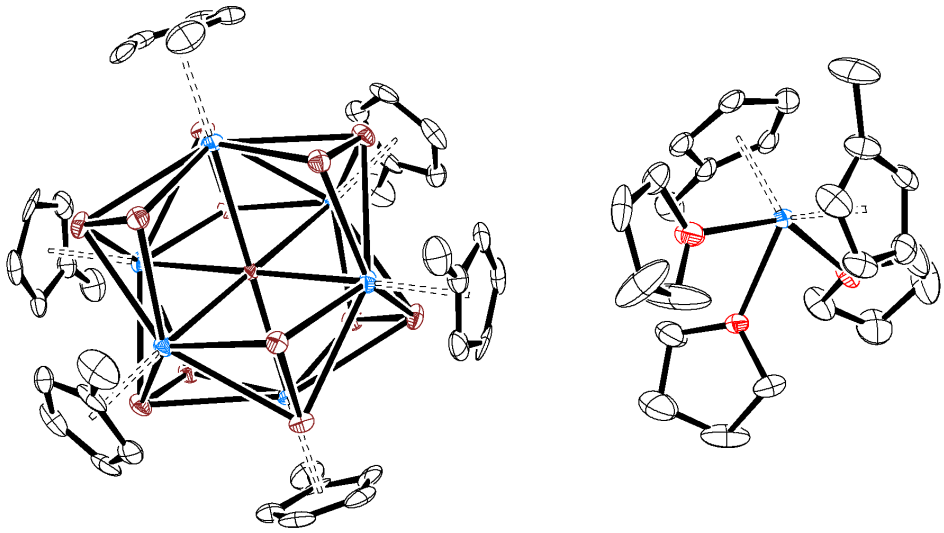

Figure 3.14. ORTEP representation of the crystal structure of **3.13-Y**, H-atoms omitted for clarity. Thermal ellipsoids set at 50% probability. Atoms are colour coded as follows: Y – light blue; Se – dark red; O – red; C – black.

Typically, upon concentration of the THF solution compound **3.13-Y** crystallises as orange blocks, however despite repeated attempts to grow crystals of **3.13-Y** reproducibly, an orange powder was obtained as opposed to single crystals. Compound **3.14-Y** forms as dark red crystals but the quality of the X-ray data is very low. It is evident that formation of these selenium clusters is governed by many different aspects as repeated attempts to crystallise either complex using identical reaction conditions only lead to formation of dark red crystals and an orange powder.

It's possible that as the reaction proceeds at either RT or elevated temperature that any initial product being formed is still reactive towards elemental sulfur or selenium. So there would be competing reactivity between any initial product formed and the starting material with unreacted elemental chalcogen. There's also the possibility of intermediate species reacting with rare-earth starting material, hence why it can be difficult to control or predict the outcomes from these types of reactions.

3.5 Conclusions

In summary, the rare-earth ^{n}butyl complexes **2.1** react with elemental sulfur and selenium at RT to produce the hexanuclear clusters $[Cp^{Me}_{10}M_6(S_3)_2S_2]$ which contain a seldom seen trisulfide $(S_3)^{2-}$ ligand. **3.11-Dy** was found to be an SMM in zero field albeit with a very small energy barrier of inversion of the magnetisation. The reactivity with selenium was hampered by the insolubility of both selenium and **3.12** in aromatic solvents. SQUID magnetometry was not possible on **3.12-Dy** due to inability to extract the crystals from unreacted selenium whilst also keeping the structure of the cluster intact. Compound **3.12** can be separated from selenium in THF, however once solubilised more selenium is consumed leading to a mixture of products which proved difficult to crystallise reproducibly.

Chapter 4

Magnetic Frustration in a Hexaazatrinapthalene-Bridged Trimetallic Dysprosium Single-Molecule Magnet

4 Magnetic Frustration in a Hexaazatrinapthalene-Bridged Trimetallic Dysprosium Single-Molecule Magnet

4.1 Preface

SMMs containing multiple, highly anisotropic lanthanide ions are commonplace with many examples incorporating a variety of, primarily, hard O- and N- donor ligands. Ln-phthalocyaninato (Pc) complexes have been shown to effectively stabilise the ground KD of Tb^{3+}, and a heteroleptic Tb-Pc complex [Tb(Pc)(Pc')] has one of the highest energy barriers to spin inversion to date (652 cm^{-1}).[132] This is in part due to the square anti-prismatic coordination geometry which can stabilise an oblate m_J state.[43] Tb^{3+} is a non-Kramers ion however, which means that the ligand field has to impart axial coordination geometry to the metal center to ensure the spin-orbit coupled ground state is bistable. Dy^{3+} is a Kramers ion so regardless of the coordination geometry the ground m_J state will be bistable, which increases the probability of observing SMM behaviour.

A new sub-group of SMMs was discovered in 2008 which contain multiple Ln^{3+} ions that have non-collinear arrangements of the main anisotropy axes (Figure 5.1), meaning they all lie in the plane of the Ln^{3+} ions.[133] These have been dubbed 'single-molecule toroics' or SMTs.

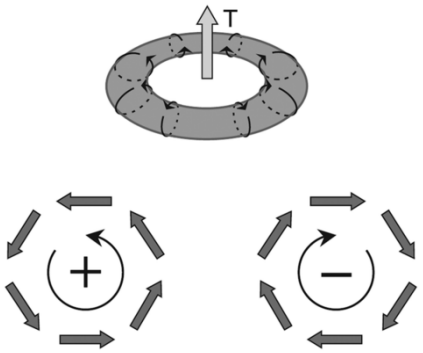

Figure 4.1. Diagrammatic representation of a toroidal magnetic moment comprised of individual spins in a molecule.[134]

This is becuase the main anisotropy axes in the molecule form a torus. Strong intra-molecular dipolar coupling between Ln^{3+} ions has been demonstrated to be the cause of toroidal magnetic moments of the ground states in all SMTs. There are 4 sub-categories of SMTs, the first is net toroidal moment SMTs.[134] These are compounds that contain a toroidal magnetic moment with no total magnetic moment in the ground state. An example of the net toroidal moment phenomenon is a Dy_6 wheel $[Dy(Htea)(NO_3)]_6 \cdot 8$ MeOH (Htea = triethanolamine), (**4.1**) reported by Murray *et. al.* which contains an S_6 symmetry axis.[135] High symmetry is a necessity for a net toroidal moment to occur because the magnetic moments of each Dy^{3+} ion cancel each other out completely resulting in a non-magnetic ground state.

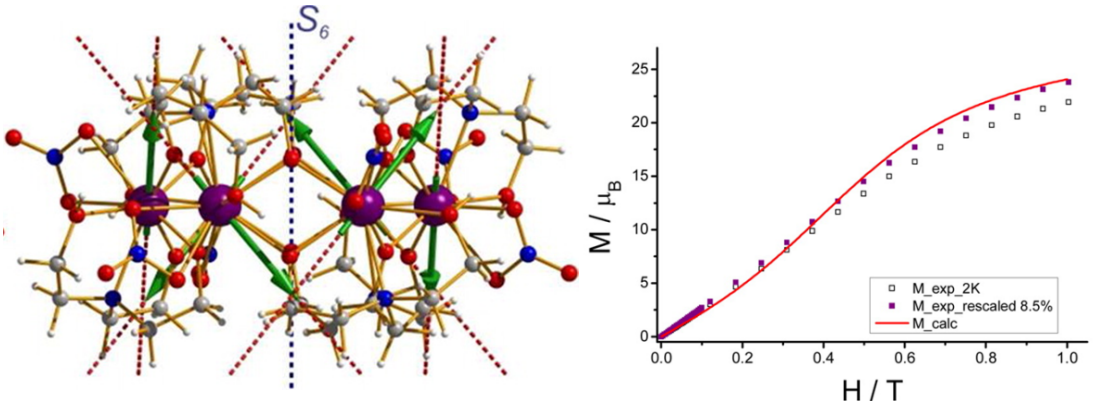

Figure 4.2. (Left) Green arrows represent the anisotropy axes for each ground state Dy^{3+} ion in **4.1**, the blue dotted line shows the S_6 symmetry axis. (Right) M(H) plot of **4.1** showing inflection at low field.[135]

In **4.1**, each anisotropy axis is at an angle of 43° with respect to the S_6 symmetry axis, as the direction of the anisotropy axis alternates around the ring (73° with respect to each other) the individual moments cancel. SMT behaviour can be seen in M(H) plots as an inflection at low temperature where the magnetisation rises more slowly at low field. Often single crystal μ-SQUID measurements are required to track the response to AC and DC fields at a defined orientation with respect to the magnetic field.[136]

Another example of a net toroidal moment SMT is the Dy_4 complex $[Dy_4(\mu_3\text{-}OH)_2(\mu\text{-}OH)_2(2,2\text{-bpt})4(NO_3)_4(EtOH)_2]$ (**4.2**) (bpt = 3,5-bis(pyridin-2-yl)-1,2,4-triazole) containing Dy^{3+} ions arranged in a square bridged by pyridyltriazole and hydroxide ligands.[137] *Ab initio* calculations revealed the structure has a toroidal non-magnetic ground state which is backed up by experimental evidence. The χ'T value drops to zero at approximately 2.5 K indicating the ground state is indeed non-magnetic and toroidal in nature.

The second type of SMT is a mixed moment SMT, these do have a magnetic ground state but with a toroidal moment also. These complexes have low symmetry, are typically Dy_3 triangles, and as such the individual magnetic moments on each of the Dy^{3+} ions in the molecule do not cancel out perfectly. The Dy_3 triangle complex $[Dy_3(\mu_3\text{-}OH)_2L_3Cl_2(H_2O)_4][Dy_3(\mu_3\text{-}OH)_2L_3Cl(H_2O)_5]Cl_5 \cdot 19\ H_2O$ (L = *o*-vanillin) (**4.3**) reported by Powell *et. al.* in 2006 was the first example of an SMM where the excited states showed typical slow magnetic relaxation behaviour whereas the ground state did not.[138]

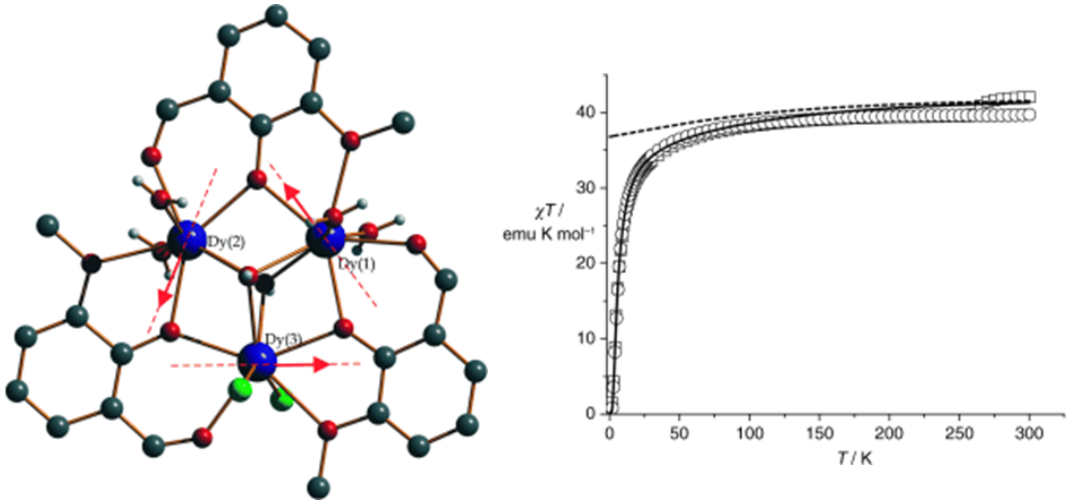

Figure 4.3. (Left) Structure of compound **4.3** the red arrows show the direction of the anisotropy axes in the ground state. (Right) Plot of $\chi_M T(T)$ for compound **4.3**.[133, 138]

Upon consideration of the DC magnetic susceptibility data, the $\chi_M T$ value drops to almost zero at 1.8 K upon cooling suggesting the ground state is diamagnetic. In the report the

$\chi_M T(T)$ plot cannot be fitted at low temperature even when allowing the crystal field parameters to vary freely. They propose "significant intratrimer antiferromagnetic interactions" as the potential cause of this sharp decrease in $\chi_M T$ below 30 K. High level *ab initio* methods were yet to be implemented on multimetallic 4f systems at the time and the concept of a toroidal magnetic moment is not mentioned here. The M(H) plot at 1.8 K also shows a slow increase in magnetisation at low field until approximately 0.7 T at which point the magnetisation begins to increase sharply. The AC data also reveals some unusual magnetic property as the out-of-phase component of the magnetic susceptibility (χ'') disappears upon cooling whereas in a normal SMM it would increase. At higher temperatures (7-10 K) Dy_3 obeys the Arrhenius law and shows a conventional slow magnetic relaxation.

In 2008 Chibotaru *et. al.* applied *ab initio* computational methods to the Dy_3 triangle complex reported by Powell.[133] Complete active-space self-consistent field (CASSCF) is a method which allows for calculation of orbitals with low lying excited states, ideal for magnetism of 4f complexes. In the context of SMMs CASSCF can be used to compute the energy difference between ground and excited KDs in Dy^{3+} complexes. The vector of the main anisotropy axis (or easy axis of magnetisation) can also be derived based on the crystal field. When **4.3** was calculated using these methods it was found that the anisotropy axes of each of the Dy^{3+} ions in the triangle pointed in the Dy_3 plane. In each case the vector of the anisotropy axes were tangential to the vertex of each side of the triangle, meaning the directions of the magnetic moments cancel out.

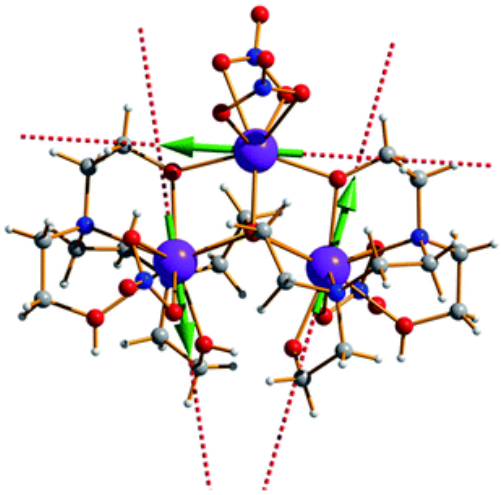

Figure 4.4. Ball-and-stick representation of the structure of compound **4.4**. Red dotted lines - computed anisotropy axes for the ground state, green arrows - highlighting the exchange interactions.[139]

Another trimetallic, mixed moment SMT $[Dy_3(HL)(H_2L)(NO_3)_4]$ (L = *N*, *N*, *N*, *N*-ethoxy-ethylenediamine) (**4.4**) displays slow magnetic relaxation below 30 K and a toroidal magnetic moment in the ground state evidenced by *ab initio* calculations and DC magnetisation data.[139] Interestingly, **4.4** shows a large coercive field (H_c = 0.5 T) at 0.04 K suggesting the ground state does have an overall magnetic moment. The reason for this is that the computed anisotropy axes in **4.4** form an isosceles triangle as opposed to an equilateral one, so the magnetic moments do not cancel out entirely. **4.4** also shows a paraelectric-ferroelectric transition when heated to 470 K and a hysteresis loop in the plot of polarisation against electric field.

The other subcategories of SMTs are zero-toroidal moment and enhanced toroidal moment SMTs, where neighbouring units of linked toroidal moments either have opposite signs and cancel out or align ferromagnetically and reinforce one another, respectively. One such example of a zero-toroidal moment SMT is the 1D coordination polymer$\{[Cu(Val)_2CH_3OH][L_3Ln_3(\mu_3\text{-}OH)_2(NO_3)_4]\}_n$ (val – D-valine) (**4.5**) based on the *o*-

vanillin ligand that contained Dy_3 triangles bridged by a Cu^{2+} moiety.[140] The synthesis of **4.5** is interesting in its own right because reacting *o*-vanillin with D- or L-valine produces a ligand that can bind both copper and dysprosium and different sites. The copper preferentially binds to the valine part of the ligand while the dysprosium ions bind to the *o*-vanillin unit. The result is a chain of Dy_3 triangles linked by {Cu(val)} units.

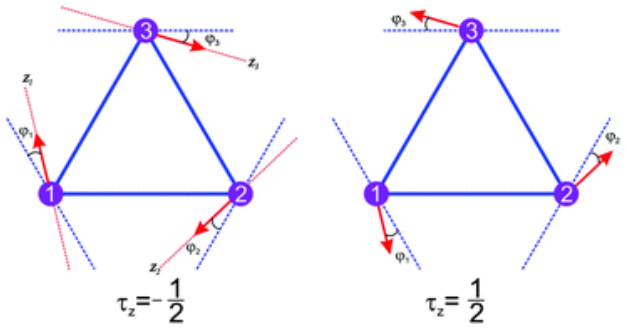

Figure 4.5. Schematic representation of the toroidal moments of alternating Dy_3 triangles in the 1D $CuDy_3$ chain (**4.5**). Purple circles represent Dy^{3+} ions and red arrows depict the computed ground state anisotropy axes with respect to the tangent of each triangle vertex (blue dotted line).[140]

DC magnetic susceptibility study on **4.5** at H = 0.1 T shows a precipitous drop in the $\chi_M T$ product against temperature below 25 K dropping to a value of 4.02 cm^3 K mol^{-1} at 2 K. The magnetisation data shows a shallower increase in magnetisation at lower field which is typical of SMTs. The AC susceptibility data also reveals a drop in χ' upon decreasing temperature but the value is above zero at 2 K indicating there is a magnetic ground state. When examined with computational methods it is found that alternating Dy_3 triangles along a chain contain toroidal magnetic moments with opposite signs, so the net toroidal moment is zero. Each magnetic moment is almost tangential to each triangle vertex and lies close to the plane of each Dy_3 triangle (θ = 0.1-10.2°). These toroidal moments interact with each other via an exchange coupling with the Cu^{2+} ions.

Enhanced toroidal moment SMTs are complexes which contain multiple toroidal moments that interact with each other ferromagnetically to produce an overall toroidal moment greater than the sum of the individual parts. Powell *et. al.* were able to couple two Dy_3 triangles together by adding 2-hydroxymethyl-6-methoxyphenol to a reaction mixture containing *o*-vanillin and $DyCl_3 \cdot x\ H_2O$.[141] The alcohol is deprotonated, presumably by either NEt_3 or furfurylamine in the reaction mixture, and the resulting alkoxide bridges between two Dy_3 units.

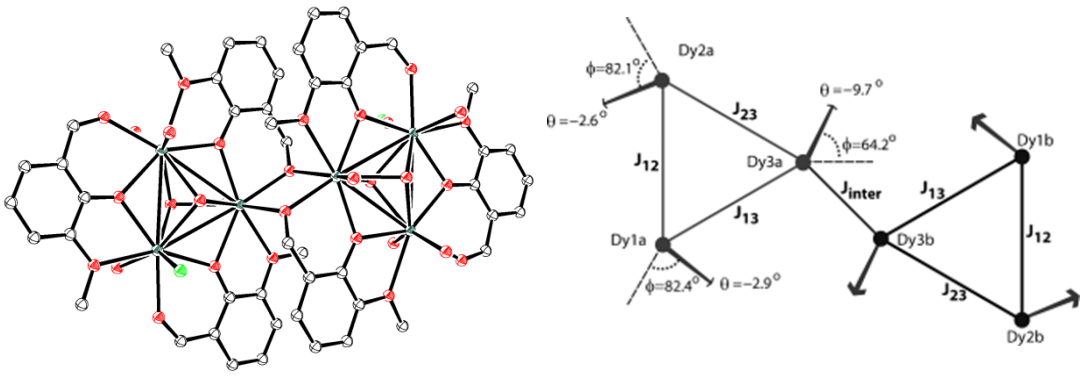

Figure 4.6. (Left) structure of compound **4.6** (atom colours: Dy - dark green, O – red, Cl – green, C – black). (Right) Schematic of the computed anisotropy axes of each Dy^{3+} ion of **4.6** in the ground state. The angle θ describes deviation of the anisotropy axis from the Dy_3 plane, ϕ represents angle of the axis with respect to the bisector of each point of the triangle.[141]

The Dy_6 cluster $[Dy_6(\mu_3\text{-}OH)_4L_4L'_2\text{-}(H_2O)_9Cl]Cl_5 \cdot 15\ H_2O$ (**4.6**) contains two Dy_3 triangles with calculated anisotropy axes all coplanar with the Dy_6 plane corroborating experimental evidence (DC magnetisation and AC susceptibility) of a non-magnetic ground state. The two Dy_3 triangles in **4.6** couple antiferromagnetically and the direction (or sign) of the toroidal moment in each triangle is the same which leads to an enhanced toroidal magnetic moment. Dy_3 triangles have also been coupled using a Schiff base ligand to create a hexanuclear compound showing similar magnetic properties.[142, 143]

The field of SMTs is currently dominated by the study of trinucelar Dy^{3+} complexes however recent study has also shown tetranuclear Dy_4 complexes can also display a range of SMT behaviour.

In 2016, Chandrasekhar *et. al.* reported on a Dy_4 complex $[Ln_4(LH)_2(\mu_2\text{-}\eta_1\text{:}\eta_1\text{Piv})(\eta_2\text{-Piv})(\mu_3\text{-OH})_2]\cdot 2\ H_2O\cdot 2$ MeOH (**4.7**) (L ligand shown in Figure 4.7; piv = $^{t}BuCOO^{-}$) that is best classified as a mixed moment SMT.[144] The M(H) data and the dynamic magnetic susceptibility data appear as an SMM. There is no prominent S-curve in the M(H) plot and the value of χ'' increases on decreasing temperature, implying the ground state is magnetic.

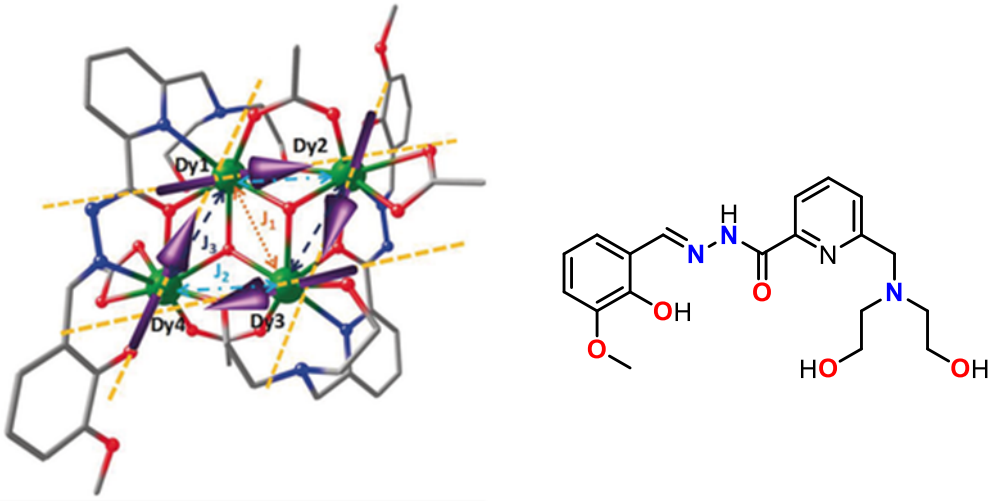

Figure 4.7. (Left) Structure of compound **4.7** with ground state anisotropy axes shown as purple arrows. (Right) the ligand LH_4 used in the synthesis of **4.7**.[144]

Ab initio calculations show that the anisotropy axes of the Dy^{3+} ions are all tangential to the parallelogram formed by the Dy_4 plane and the ground state does have a toroidal magnetic moment. The energy gap between the ground and first excited KD is calculated at just 4.68 cm^{-1} which is put forward as an explanation as to why the ground state appears to be magnetic. The energy gap is small enough that sufficient mixing of the energy levels is still observed even at temperatures as low as 2 K.

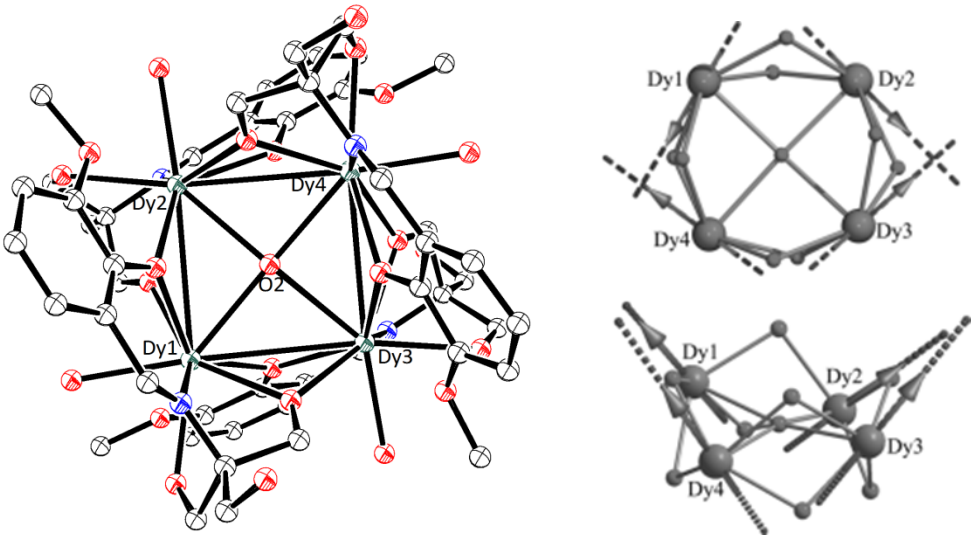

Figure 4.8. (Left) structure of the Dy_4 square compound **4.8** reported by Shanmugam. (Right) Computed anisotropy axes for each Dy^{3+} site in **4.8**, figure from reference 137.[145]

A pseudo-C_4 symmetric Dy_4 complex reported by Shanmugam was also discovered to behave as an SMT.[145] Despite being of high symmetry and potentially a net toroidal moment SMT it was found using SHAPE software that one of the Dy sites has more distorted coordination geometry than the other 3. *Ab initio* calculations also showed that one of the four anisotropy axes deviated from the Dy_4 plane by a greater degree (43°) than the other three (6.2-15.9°). As a result the ground state is magnetic but a small inflection can be observed in the M(H) plot.

4.2 Introduction to Hexaazatrinaphthalene (HAN) Bridged Complexes

Most SMTs reported to date are synthesised using multidentate ligands that do not necessarily guarantee a triangular arrangement of Dy^{3+} ions. One way to approach the synthesis of trimetallic systems in a rational way is to use a 3-fold symmetric ligand with well-defined binding sites. One such ligand that has garnered much interest in the Layfield group is hexaazatrinaphthalene (HAN), which has the potential to be oxidised or reduced, due to a large π-conjugated framework containing low-energy π* antibonding orbitals.[146]

HAN could facilitate strong exchange between coordinated metal centers. Complexes of HAN derivatives are known with copper and cobalt containing neutral hexaazatriphenylene (HAT) ligands.[147-149] One complex of a HAN dianion is also known.[150]

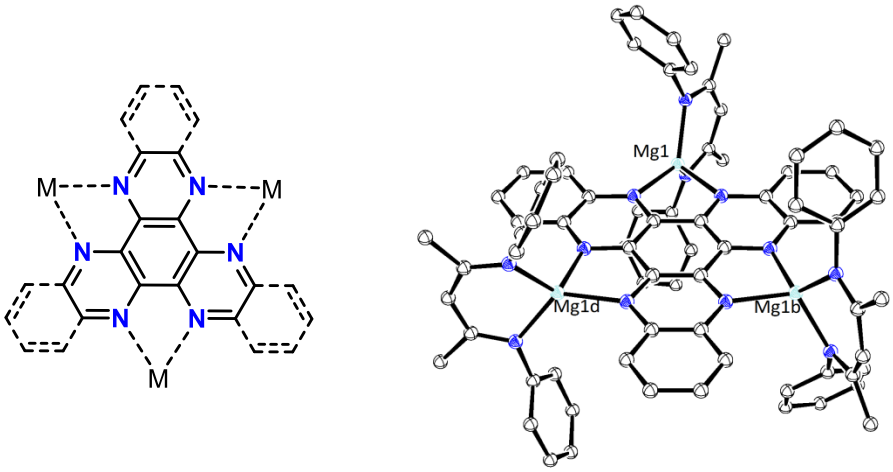

Figure 4.9. (Left) ChemDraw schematic diagram of HAT and the HAN derivative in dotted lines. M represents a metal ion coordinating to HAT(N) in a typical fashion. (Right) Structure of compound **4.9** which is the first example of a triply-reduced HAN ligand. iPr groups have been omitted for clarity.[151]

Previous study by Layfield *et. al.* has shown that HAN can be reduced not just once but three times to form the radical trianion $\{HAN\}^{3-\cdot}$.[151] Reacting 1.5 equivalents of the Mg^{1+} reagent $[(nacnac)Mg]_2$ with HAN in toluene afforded the magnesium complex $[(HAN)\{Mg(nacnac)\}_3] \cdot C_7H_8$ (**4.9**). X-band EPR spectroscopy on **4.9** shows a broad singlet at g = 2.003 which is indicative of a S = ½ spin system, this open-shell doublet character of the HAN ligand is also supported by DFT calculations.

It is also possible to generate anionic HAN complexes with transition metals. In 2016, it was discovered that the HAN ligand could be reduced to the monoanion by reacting it with K metal and 18-c-6 in toluene.[152] It is worth noting that HAN is highly insoluble in every common organic solvent with the exception of chloroform in which it is sparingly soluble. As a result, the potassium complex [HAN][K(18-c-6)] (**4.10**) could not be crystallised but was

obtained as a red powder in high yield. The EPR spectrum revealed extensive hyperfine structure as a result of the electron spin coupling to carbon and nitrogen.

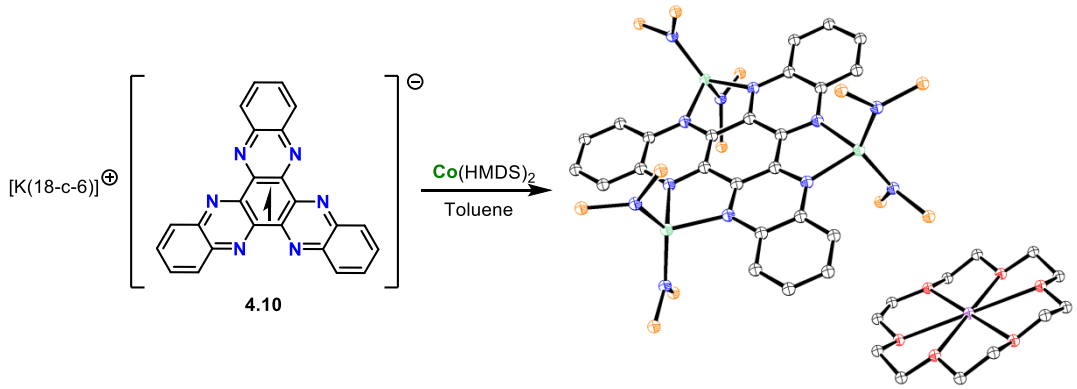

Scheme 4.1. Reaction of mono-reduced potassium salt of HAN with $Co(HMDS)_2$ to form compound **4.11**. Structure of **4.11** has the CH_3 groups removed for clarity (atom colours: Co – light green, N – blue, O – red, Si – orange, C – black, K –purple).[152]

The reaction between **4.10** and $[Co(HMDS)_2]$ (HMDS - $:N(SiMe_3)_2$) affords the cobalt complex $[(HAN)\{Co(HMDS)_2\}_3][K(18\text{-c-}6)]$ (**4.11**) which contains a mono-anionic HAN ligand. The DC magnetic susceptibility measurements show a pronounced increase in $\chi_M T$ on cooling which is due to strong antiferromagnetic interaction between Co^{2+} ions and the radical ligand. **4.11** was subjected to DFT study and it was found that the anisotropy axes of the Co^{2+} ions are nearly perpendicular to the HAN plane and are all collinear. The $\chi_M T(T)$ plot could be fitted adequately with values of $J_1 = -15\ cm^{-1}$ (Co---Co interactions) and $J_2 = -290\ cm^{-1}$ (Co---$HAN^{\cdot-}$ interaction). The J_2 value is very large which indicates a very strong exchange coupling between the Co ions and the spin on the HAN ligand.

Based on the previously reported work with s-block and d-block complexes of HAN there is a potential for the development of lanthanide SMMs by reacting HAN with dysprosium precursors. The work set out in this chapter details the synthesis and magnetic properties of the first reported complex of a lanthanide-HAN complex reported by Grindell *et. al*.[153]

4.3 Synthesis and Characterisation of a HAN-Bridged Trimetallic Dysprosium Complex

$Dy(thd)_3$ (thd = 2,2,6,6-tetramethyl-3,5-heptanedionato) was chosen as a precursor to a trimetallic Dy-HAN complex due to it being formally 6-coordinate and able to occupy at least two other atoms around the Dy^{3+} ion. The syntheses of the mono-metallic bipy[154] and 1,10-phenanthroline[155] adducts $[(thd)_3Dy(L)]$ (L = bipy, 1,10-phen) has been described previously which was promising as each binding site on HAN is analogous to bipy/phen.

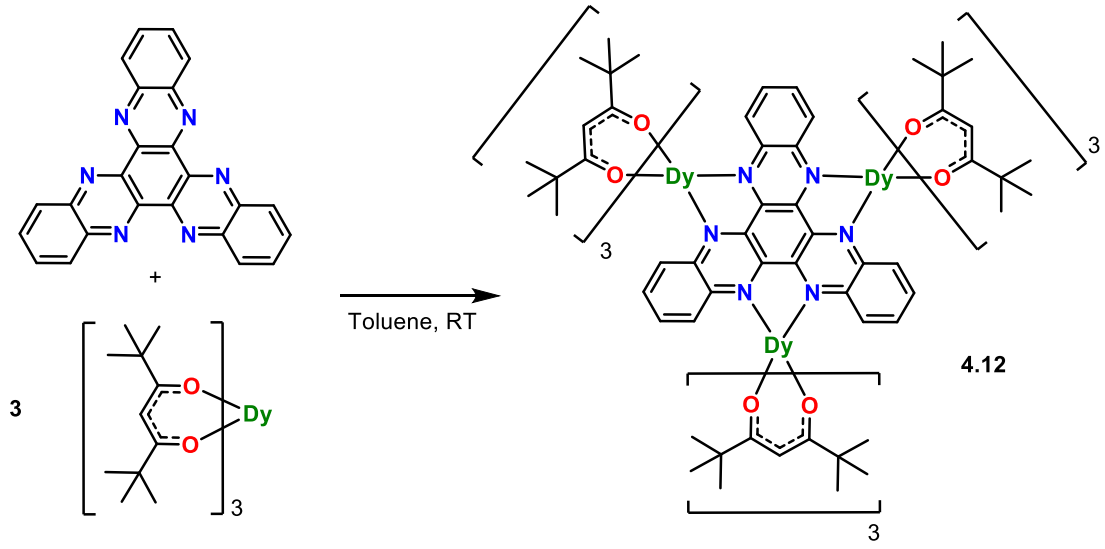

Scheme 4.2. Synthesis of compound **4.12**.

The reaction between three equivalents of $Dy(thd)_3$ and HAN at RT affords the trimetallic complex $[\{(thd)_3Dy\}_3HAN]\cdot 3\ C_7H_8$ (**4.12**) as deep red crystals in 86% yield according to scheme 4.2. XRD analysis shows **4.12** crystallises in a the monoclinic, $P2_1/c$ space group (structure shown below in figure 4.10). HAN is highly insoluble in toluene so a concentrated reaction mixture is required to ensure all the HAN is drawn into solution. Approximately 45 minutes of stirring at RT affords a dark red solution which was filtered, reduced in volume and stored at 2°C leading to formation of large, dark red needles.

Attempts to reduce **4.12** with KC_8 afforded a dark orange-brown solution after filtration away from a black powder which was presumably graphite. On workup however only a dark brown powder could be isolated from toluene or Et_2O.

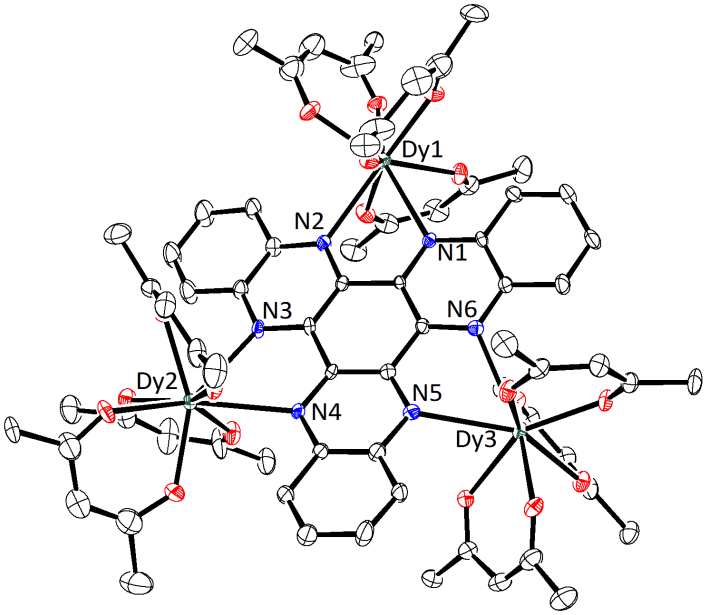

Figure 4.10. ORTEP representation of the crystal structure of compound **4.12** with thermal ellipsoids set at 50 % probability. CH_3 groups and H-atoms have been omitted for clarity.

The Dy^{3+} ions in **4.12** are 8 coordinate with a DyO_6N_2 coordination sphere. The aim was to synthesise a complex with D_{4d} symmetry as this has been shown to stabilise the ground m_J state of Dy^{3+} and Tb^{3+}. The Dy1—O bond lengths are in the range of 2.256(5) – 2.342(5) Å. The Dy2—O and Dy3—O bond lengths are 2.251(6) – 2.315(6) Å and 2.259(5) – 2.318(5) Å respectively. The Dy1—N bond lengths are 2.669(5) and 2.646(6) Å whereas the Dy2 and Dy3—N distances are 0.03-0.1 Å longer and lie in the range of 2.694(6) – 2.760(6) Å. Dy1 and Dy2 reside in the plane of the HAN ligand whereas Dy3 lies 1.044 Å out of the plane implying there are two distinct Dy^{3+} environments.

The coordination geometry for each Dy^{3+} ion in **4.12** was analysed using SHAPE software to determine deviations from a certain point group.[156] A numerical value is given representing the deviation of the coordination environment from each point group. The results show that the Dy ions are best described as having distorted D_{2d} symmetry (triangular dodecahedron) with the CShM values of Dy1, Dy2 and Dy3 being 0.84, 1.624 and 1.797 respectively. This confirms that there are two distinct Dy^{3+} environments in **4.12** which

could impact on the magnetic properties, possibly resulting in two magnetic relaxation mechanisms being present.

4.12 was also characterised by UV-vis and IR spectroscopy. Interestingly, it appears that the $Dy(thd)_3$ fragments are bound relatively weakly to the HAN ligand. In preparing a sample for UV-vis spectroscopy the toluene solution changes from dark red to colourless upon dilution to the low concentration ($x10^{-5}$ M) required and the UV-vis spectrum shows just two peaks in the UV region at 376 and 393 nm. The IR spectrum shows characteristic C-C absorptions in the fingerprint region and the absorption at around 1600 cm^{-1-} can be attributed to the C=N stretching mode. The absorption between 2750-3000 cm^{-1} is likely due to the aromatic C-H stretching mode.

4.4 Magnetic Susceptibility Study of [{(thd)$_3$Dy}$_3$HAN]

The molar magnetic susceptibility of compound **4.12** was measured in a static field (H_{dc} = 1 kOe) in the temperature range of 1.8 – 300 K (figure 4.11).

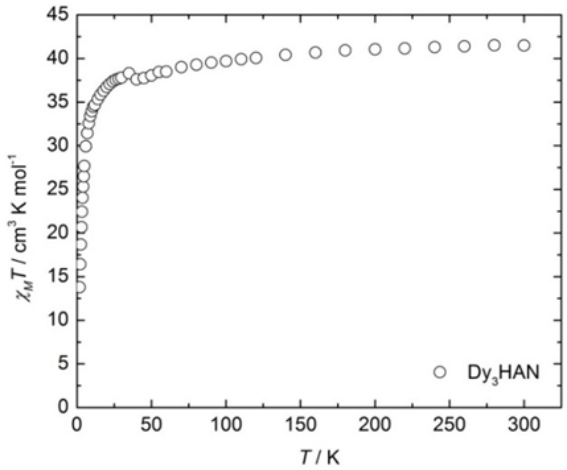

Figure 4.11. The $\chi_M T(T)$ plot for compound **4.12**.

The value of $\chi_M T$ at 300 K is 41.57 cm^3 K mol^{-1} which corresponds to the expected value for three non-interacting Dy^{3+} ions ($^6H_{15/2}$, g_J = 4/3; $\chi_M T$ = 42.51 cm^3 K mol^{-1}).The $\chi_M T$ decreases gradually down to 50 K at which point the drop becomes more pronounced to reach a

value of 16.42 cm^3 K mol^{-1} at 2 K. This relatively large value of $\chi_M T$ at 2 K suggests that the ground state has a magnetic moment (11.89 μ_B at 1 T). The precipitous drop in $\chi_M T$ is a consequence of thermal depopulation of low lying excited KDs within the Russel-Saunders coupled $^6H_{15/2}$ ground term.

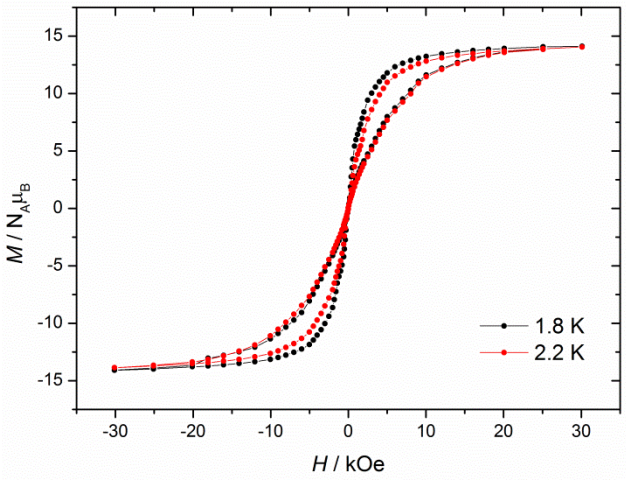

Figure 4.12. Magnetization (*M*) vs. field (*H*) hysteresis loops for **4.12** at 1.8 K and 2.2 K, using an average sweep rate of 1.93 mT s^{-1}. Solid lines are a guide for the eye.

The magnetisation of **4.12** was measured between 1.8 and 8 K in a field of 0-70 kOe. It is clear that significant anisotropy is present as the magnetisation curves are non-superimposable at increasing temperature. At 1.8 K the magnetisation increases sharply at low field before reaching close to saturation at 70 kOe with a value of *M* = 15.54 μ_B which agrees well with the expected value for 3 Dy^{3+} ions (15.75 μ_B). Compound **4.12** was also found to exhibit magnetic hysteresis up to 2.2 K which is waist-restricted (figure 4.12). This implies that QTM is prevalent at low fields.

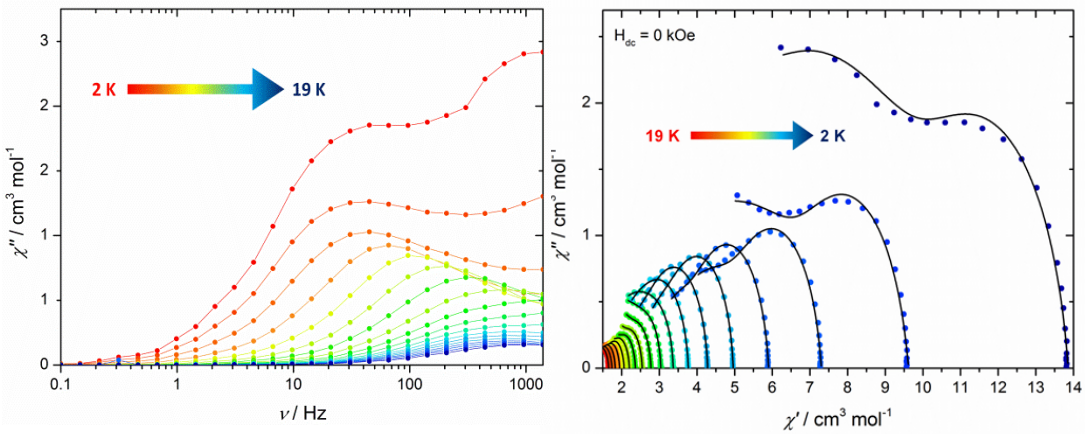

Figure 4.13. (Left) Frequency dependence of the out-of-phase (χ'') magnetic susceptibility for **4.12** using an oscillating field of H_{ac} = 1.55 Oe and zero applied field. (Right) Argand diagram for **4.12** in zero d.c. field.

The dynamic magnetic properties of **4.12** were measured in zero field (H_{dc} = 0 kOe) with a small oscillating field (H_{ac} = 1.55 Oe). There is a clear frequency dependence of the in-phase (χ') and out-of-phase (χ'') components of the magnetic susceptibility and peak maxima in the χ''(ν) plot are observed at 1 K intervals from 2-19 K. In the 2 K isotherm there are two peaks present that correspond to two different relaxation processes. The presence of two relaxation processes is confirmed in the Cole-Cole plot χ'(χ'') as two peaks can be seen at 2 K with inflections visible up to 5 K. The χ'(χ'') plot was fitted with α parameters in the range of 0.09-0.59 which is indicative of a wide range of relaxation times. As the temperature increases there is just one peak showing that the magnetic relaxation is dominated by a thermal process. Above 10 K the peaks occur past the frequency limit of the SQUID magnetometer as the relaxation time becomes shorter. This is consistent with the relaxation time increasing drastically upon increasing the temperature. This is consistent with the hypothesis that the two crystallographically distinct Dy sites may give rise to more than one relaxation process.

Despite all the peaks occurring on top of each other in the highest temperature region of the χ''(ν) plot it was possible to determine a U_{eff} barrier of 22 cm^{-1} (τ_0 = 8.21 x 10^{-6} s) from the Arrhenius plot.

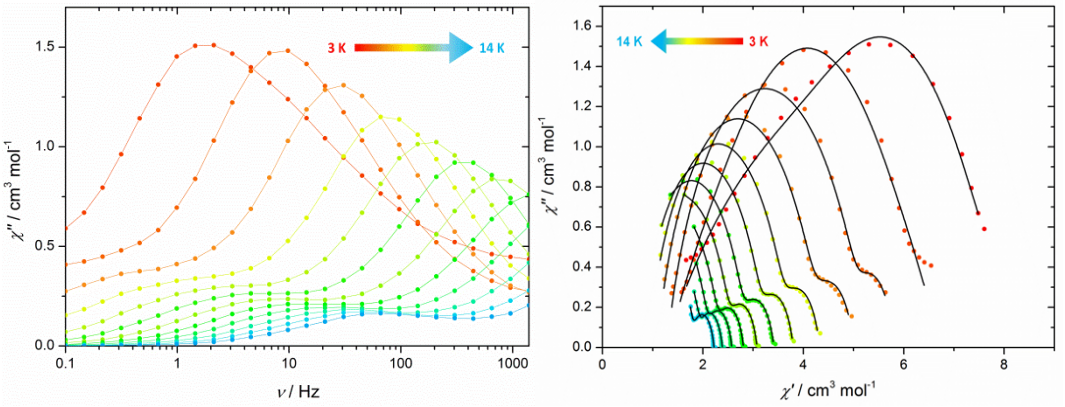

Figure 4.14. (Left) Frequency dependence of the out-of-phase (χ'') magnetic susceptibility for **4.12** using an oscillating field of H_{ac} = 1.55 Oe and an applied field of H_{dc} = 1 kOe. (Right) Argand diagram for **4.12** in 1 kOe d.c. field.

In an optimised field of 1 kOe the two relaxation processes are more visible from 3-14 K. Applying a field can alter the energy levels of the ground term KDs which can supress QTM. On increasing the temperature the peak observed at lower frequency diminishes and a higher temperature process can be seen to take over. This is clearer in the Argand plot, as the temperature increases a double-hump feature becomes more pronounced. At higher temperatures it is likely due to two separate thermal relaxation processes arising from different Dy sites as QTM is normally observed at low temperature (< 5 K).

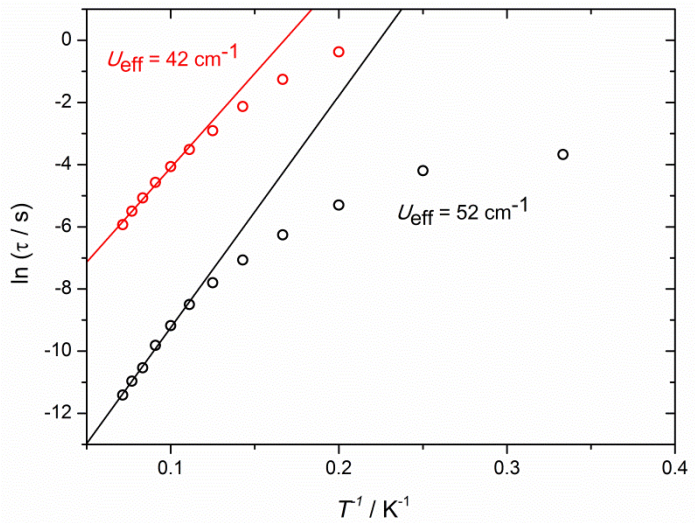

Figure 4.15. Arrhenius plot for **4.12** in an applied field of H_{dc} = 1 kOe.

Fitting the Cole-Cole plot affords two sets of relaxation times that can be used to extract two energy barriers from the Arrhenius plot. Fitting the linear region of each trace using the Arrhenius relationship ($\tau = \tau_0 \exp(-U_{eff}/k_BT)$ allows for the determination of two energy barriers of U_{eff} = 42 cm^{-1} (τ_0 = 3.8 x 10^{-6} s) and U_{eff} = 52 cm^{-1} (τ_0 = 5.6 x 10^{-6} s).

In order to gain more insight into the ground state electronic structure *ab initio* calculations of the CASSCF/RASSI type were performed on **4.12** using the MOLCAS 8.0 suite of software. Due to the extensive computing power required to simulate a system with multiple 4f centers (Dy^{3+} electron configuration is $4f^9$) **4.12** was calculated as three separate [{$(thd)_3$Dy}HAN] fragments.

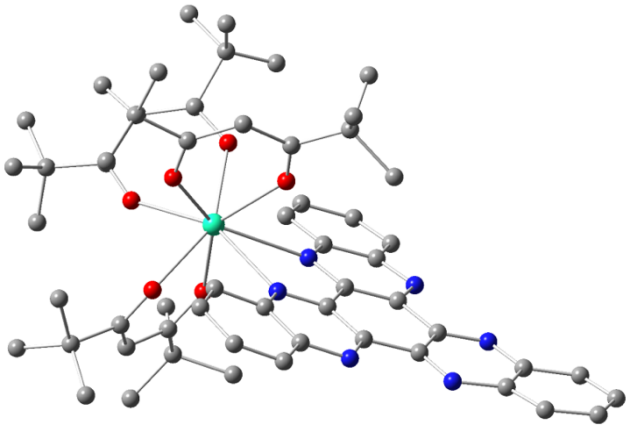

Figure 4.16. Structure of the [{(thd)$_3$Dy}HAN] fragment used for *ab initio* calculations. H-atoms are omitted.

The calculated energy separations of the lowest lying KDs are shown in table 4.1. The computed energy barriers are somewhat larger than those observed experimentally. This may mean the relaxation mechanism is not purely one type.

Table 4.1. Energies of the ground (KD = 1) and excited KDs for each Dy^{3+} ion in **4.12**. The g-tensors shown are shown for the ground KDs.

KD	Dy(1)	Dy(2)	Dy(3)
1	0	0	0
2	121	152	64
3	238	252	177
4	314	336	279
5	379	421	369
6	446	505	470
7	549	627	542
8	710	794	621
g_x	0.016	0.001	0.009
g_y	0.030	0.005	0.018
g_z	19.290	19.950	19.120

The g-tensors for each Dy ion approach the Ising limit of $g_z = 20$ showing that the Dy^{3+} ions are highly anisotropic in the ground state. The computed energies and g-tensors are also in

line with experimental observations of two distinct Dy environments that are not related by symmetry.

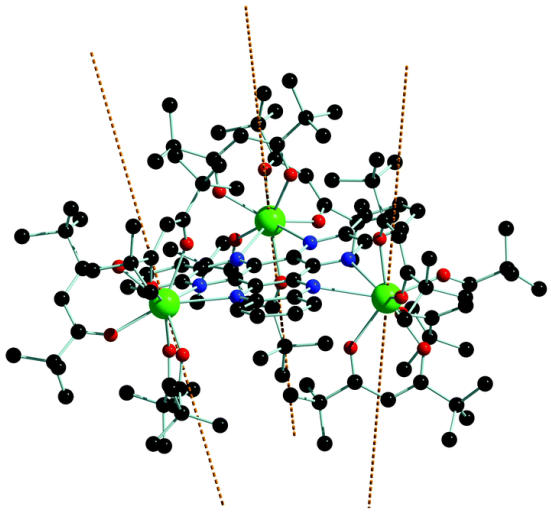

Figure 4.17. Calculated anisotropy axes for **4.12** shown as yellow dotted lines.

Calculation of the anisotropy axes reveal that compound **4.12** is not a single molecule toroic. The anisotropy axes are nearly perpendicular to the N_6 plane of the HAN ligand at angles of 82°, 71° and 68°. This corroborates experimental observations of a significant molar magnetic susceptibility at 2 K in zero field and with an applied field of 1 kOe.

$$\widehat{H} = -[\left(J_{12}^{dip} + J^{exch}\right)\hat{\tilde{s}}_{1,z1}\hat{\tilde{s}}_{2,z2} + \left(J_{13}^{dip} + J^{exch}\right)\hat{\tilde{s}}_{1,z1}\hat{\tilde{s}}_{3,z3} + \left(J_{23}^{dip} + J^{exch}\right)\hat{\tilde{s}}_{2,z2}\hat{\tilde{s}}_{3,z\,3} \quad (4.1)$$

The total magnetic interactions in **4.12** were also calculated using the Hamiltonian operator (Equation 4.1). The exchange coupling J_{exch} can be ascertained from the Lines parameters which are determined by fitting the experimental static magnetic data. This factors in the angles between the anisotropy axes of interacting Dy^{3+} ions. The values of the dipolar and exchange coupling for each Dy---Dy interaction are shown in Table 4.2.

Table 4.2. Values of the Ising exchange parameters in **4.12**.

	J_{ex} / cm^{-1}	J_{dip}/ cm^{-1}
Dy(1)-Dy(2)	–2.3	–0.29
Dy(1)-Dy(3)	–2.5	–0.29
Dy(2)-Dy(3)	–2.5	–0.28

They all have a negative sign which implies weak antiferromagnetic coupling between Dy^{3+} ions. **4.12** is an example of a ground state frustrated spin system due to the antiferromagnetic alignment of spins and the odd number of Dy^{3+} ions in the molecule. This phenomenon has been observed previously in trimetallic systems.[50, 157]

4.5 Conclusions

The first lanthanide complex of HAN has been synthesised in high crystalline yield and characterised by XRD. Magnetic property measurements revealed **4.12** displays magnetic hysteresis up to 2.2 K and is an SMM in zero field, with two distinct relaxation processes at low temperature. In an applied field of 1 kOe two magnetic relaxation processes were found to occur with energy barriers of U_{eff} = 42 cm^{-1} and 52 cm^{-1}. *Ab initio* computational analysis revealed that **4.12** is not an SMT, which is in line with the experimental evidence. The Dy^{3+} ions are weakly, antiferromagnetically coupled in the ground state and **4.12** is a frustrated spin system.

Chapter 5

Conclusions & Future Work

5.1 Conclusions & Future Work

The aims of the PhD have been met successfully. The first aim was to synthesise rare-earth ^{n}butyl complexes and study their reactivity. Not only was compound **2.1** synthesised successfully but was also found to be surprisingly stable under ambient conditions. This enabled **2.1-Y** and **2.1-Dy** to be scaled up and synthesised on a three-gram scale.

The reactivity of **2.1** was examined towards a variety of C-H acidic substrates as well as elemental sulfur and selenium. When **2.1** was reacted with ferrocene the resulting product was the mono-deprotonated rare-earth ferrocenyl complex **2.2**. This is an important result because by comparison, the reactivity of ^{n}BuLi with ferrocene is not as straightforward. Additives such as TMEDA are required to deprotonate ferrocene with ^{n}BuLi and there is little control over the products formed, which is usually a mixture of mono- and di-lithiated ferrocene.

Compound **2.1** was also reacted with NHCs. No reaction was observed between IPr and **2.1-Y** at RT and only decomposition of **2.1-Y** was observed at elevated temperature. Whilst by ^{1}H NMR spectroscopy there seemed to be a reaction between **2.1-Y** and I^{t}Bu, work up only afforded an intractable solid. The reaction between **2.1** and IMes was clean and complete almost instantaneously upon complete addition of the reagents. The *o*-Me deprotonated IMes' complex **2.5** was obtained in high yield. The reactivity was unexpected as it was postulated that the backbone C—H protons on IMes would be more acidic and hence more susceptible to deprotonation. This reactivity is observed between IPr and ^{n}BuLi. A control experiment between $Cp^{Me}_{3}M$ and IMes afforded crystalline [$Cp^{Me}_{3}M$(aIMes)] (M = Dy, Y; **2.6**). Whilst no intermediate species were observed in the ^{1}H NMR spectra of the reaction mixtures, the rate of formation of **2.6-Y** was found to be concentration and temperature dependant.

There is great potential for **2.1** to be commercialised as it can be synthesised on a multi-gram scale and stored as a solid indefinitely at -40°C. Compound **2.1** is also stable in the solid state for at least 24 hours. Compound **2.1** has shown a bespoke reactivity towards the substrates investigated here, with respect to ^{n}BuLi. There is potential for **2.2** to be used as a synthon to synthesise mono-substituted ferrocenes without using ^{t}BuLi, which is pyrophoric.

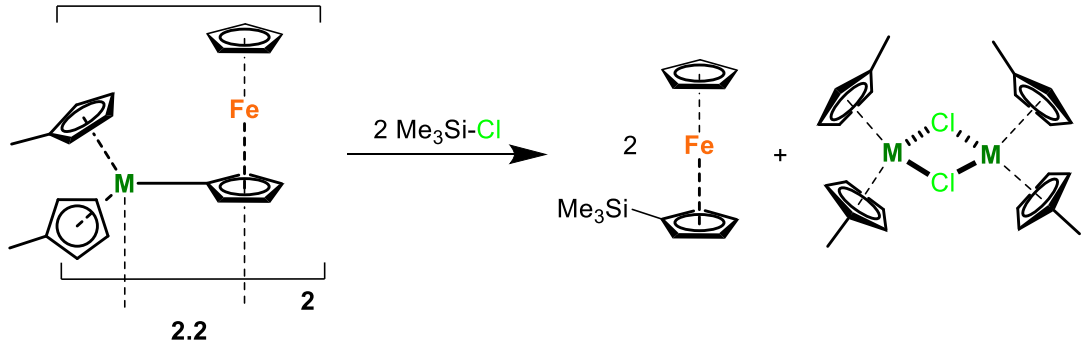

Scheme 5.1. Proposed functionalisation of ferrocenes with **2.2** (representative example).

The reaction between **2.1** and ferrocene leads to the mono-deprotonated ferrocenyl complex (**2.2**) exclusively. Future research will explore the possibility of quenching **2.2** with a variety of electrophiles to form mono-substituted ferrocenes with a range of functional groups. Using aryl or silyl halides could lead to C-C or C-Si bond formation with $[Cp^{Me}{}_2MCl]_2$ as a byproduct due to the Ln^{3+} ions high affinity for halides.

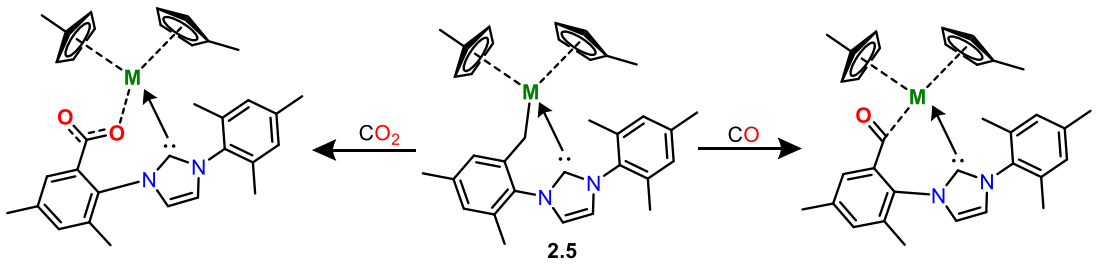

Scheme 5.2. Proposed small molecule activation reactivity of **2.5**.

Small molecule activation reactivity with **2.5** will be explored. When **2.5** is reacted with CO or CO_2 the corresponding acyl or carboxyl carbene complexes could form. Protonation of

these hypothetical complexes with a suitable acid would afford NHCs with pendant carboxylic acid or aldehyde functional groups.

Dynamic magnetic susceptibility studies on **2.1-Dy**, **2.2-Dy**, **2.5-Dy** and **2.6-Dy** revealed that carbon donor-atom bridging ligands are not conducive to SMM properties. None of the aforementioned complexes showed a response to an AC magnetic field. The reason for this is that all the ligands explored here create a hard equatorial field around the Dy^{3+} ion and destabilise the $m_J = \pm 15/2$ ground state. The state of the field of lanthanide SMMs has been transformed with the recent publication of a dysprosium metallocene complex $[Cp^{ttt}_2Dy][B(C_6F_5)_4]$.[158] This complex fulfils the ideal magneto-structural requirements for an SMM (Figure 1.10). The $[B(C_6F_5)_4]$ anion is completely non-coordinating and as such there is essentially no equatorial ligand field around Dy^{3+}. This gives rise to magnetic hysteresis observed at 60 K, which dwarfs all previous records including that of the terbium complex $[\{Tb(N(SiMe_3)_2)_2)(THF)\}_2(\mu\text{-}N_2)]^-$ which exhibits hysteresis up to 14 K.[159] This means that an upper limit has been reached on what molecular complexes can achieve. As such future work in this field will involve developing methods of incorporating SMMs into devices for quantum information storage and/or processing.

Compound **2.1** was also found to reduce the elemental chalcogens sulfur and selenium to form the hexanuclear cluster complexes: $[Cp^{Me}_{10}M_6(E_3)_2E_2]$ (M = Dy, Y; E = S (**3.11**), Se (**3.12**)). Compound **3.11-Dy** was found to be an SMM with a U_{eff} barrier of 73 cm^{-1}, no hysteresis was observed. Whilst the selenium version **3.12-Dy** could be synthesised, adequate separation of the crystals from unreacted selenium could not be achieved. Extraction of mixtures of **3.12** and selenium with THF did lead to crystalline products. However, different products were obtained on repeated attempts. Future work will involve exploring reaction conditions that favour formation of one product over the mixture that is normally observed.

A trimetallic complex of hexaazatrinaphthalene (HAN) is reported. Compound **4.12** was synthesised by combining 3 equivalents of $Dy(thd)_3$ with one equivalent of HAN. Compound **4.12** is an SMM in zero DC field however the two relaxation mechanisms observed are better resolved in an applied field of 1 kOe. The energy barriers for each of the relaxation processes are 42 and 52 cm^{-1}. Future work on **4.12** will explore the possibility of creating a radical bridging HAN ligand as radical bridging ligands have been shown to enhance the exchange coupling between metal centres in lanthanide SMMs. There are two possible routes to the target compound; one is to reduce **4.12** with KC_8 or cobaltocene, the other is to oxidise **4.12** with Ag^+ salts or ferrocenium salts to afford a radical cationic HAN ligand.

Chapter 6

Experimental Section

6.1 General Considerations

All manipulations reported herein were carried out under dry, oxygen-free argon on a Schlenk line or in an argon-filled glove box. Glassware was oven-dried and placed under vacuum whilst hot before use. Preparations of samples for analysis were carried out in the glove-box.

All solvents were dried by refluxing over either potassium or sodium-potassium alloy for at least 3 days prior to distillation. The solvents were then transferred onto 4 Å molecular sieves and degassed with three freeze-pump-thaw cycles. When reactions were carried out at -78^{o}C this was achieved with a cold bath of dry ice and acetone.

Anhydrous rare earth trichlorides (Strem Chemicals), dysprosium nitrate hexahydrate (Alfa), 2,2,6,6-tetramethylheptane-3,5-dione (Sigma) and ^{n}BuLi (1.6 M in hexanes, Acros Organics) were used as received. Di-methylcyclopentadiene (Alfa or Sigma) was cracked, at around 160^{o}C to afford the monomeric methylcyclopentadiene, and distilled under argon using a 20cm Vigreux column and concentrated to approximately a third of the volume prior to use. This ensures that any cyclopentadiene impurity is removed. The distillate was then added to a suspension of NaH in THF dropwise at RT. NaCp^{Me}, LnCp$^{Me}_{3}$,[160] IMes,[161] IPr,[161] I^{t}Bu[162] and hexaazatrinapthalene (HAN)[163] were prepared according to literature procedures. Ferrocene (Sigma) was sublimed under argon (50^{o}C / x10^{-2-} mbar) and stored in an argon filled glove box prior to use. Sulfur and selenium (Sigma) were dried *in vacuo* and stored in the glove box prior to use.

X-Ray diffraction data were obtained from an Oxford Instruments XCalibur2 diffractometer, an Agilent SuperNova using MoKα radiation (λ = 0.71073 Å) or a Bruker Prospector APEX-II using CuKα radiation (λ = 1.5418 Å). All crystal structures were solved using direct methods with the SHELXS or intrinsic phasing with the SHELXT structure solution programs. All non-

hydrogen atoms were refined anisotropically using the least squares method in the SHELXL structure refinement program.[164-166]

NMR spectra were recorded on either a Bruker Avance-III 400 MHz or a **Bruker Avance II+ 500 MHz** spectrometer. Benzene-d_6 and THF-d_8 were dried by heating under vacuum for 5-7 days over molten potassium, followed by vacuum transfer into an oven dried ampoule.

Elemental analyses were carried out at the elemental analysis service at London Metropolitan University, UK by Stephen Boyer.

IR spectra were recorded using solid samples on a Bruker Alpha Diamond ATR spectrometer.

Magnetic measurements were carried out on a Quantum Design MPMS XL SQUID magnetometer in the range of 1.8 – 300 K. Due to the air and moisture-sensitive nature of the samples they were either placed in a KelF capsule or flame sealed under vacuum in an NMR tube. The samples prepared in NMR tubes are restrained in solid eicosane to prevent torqueing.

Ab initio quantum chemical calculations were carried out using the MOLCAS 8.0 suite of software and were of the CASSCF/RASSI/SINGLE_ANISO type. The SINGLE_ANISO program computed the local magnetic properties.[167] Calculations were carried out in collaboration with Liviu Chibotaru and Veacheslav Vieru at KU Leuven.

6.2 Synthesis for Chapter 2

$[Cp^{Me}{}_2Y\{\mu\text{-}{}^nBu\}]_2$ (2.1-Y) ^{n}BuLi (5.74 mL, 1.6 M in hexanes) was added to a suspension of $Cp^{Me}{}_3Y$ (3 g, 9.19 mmol) in hexane (150 mL) at -78°C. Once the addition was complete the resulting thicker, pale yellow suspension was allowed to warm to room temperature. On warming the reaction mixture becomes clearer, then quickly loses it colour and a white

precipitate is formed. The white suspension was stirred at room temperature for 2 hours. The mixture was allowed to settle, filtered and the hexane removed *in vacuo*. The resulting white powder was washed with cold pentane (15 mL), dried under vacuum and isolated (2.001 g, 72%). Crystals suitable for X-ray diffraction were grown from a concentrated toluene solution stored at -30°C. **Elemental analysis**, found/% (calculated)/%; C, 62.86 (63.16); H, 7.63 (7.62). **^{1}H NMR** (C_6D_6, 298.15 K, *δ*/ppm): 5.96 (t, $^{3}J_{HH}$ = 2.69 Hz, 8 H, Cp C*H*); 5.87 (t, $^{3}J_{HH}$ = 2.69 Hz, 8H, Cp C*H*); 2.09 (s, 12 H, Cp CH_3); 1.33 (sextet, $^{3}J_{HH}$ = 7.18 Hz, 4H, γ-CH_2); 0.94 (t, $^{3}J_{HH}$ = 7.34 Hz, 6H, δ-CH_3); 0.44 (quintet, $^{3}J_{HH}$ = 8.56 Hz, 4H, β-CH_2); -0.44 (tt, $^{3}J_{HH}$ = 8.56 Hz, $^{2}J_{YH}$ = 1.47 Hz 4H, α-CH_2). **^{13}C NMR** (C_6D_6, 298.15 K, δ/ppm): 120.4 (Cp*C*-$(CH)_2$); 112.87 (Cp*C*H); 109.62 (Cp*C*H); 38.58 (α-*C*H_2); 32.53 (β-*C*H_2); 30.68 (γ-*C*H_2); 15.75 (*Me*Cp); 14.16 (δ-*C*H_3). **IR** (solid) ν_{max} (cm^{-1}): 2950 (w), 2923 (w), 2866 (w), 1454 (w), 1376 (w), 1046 (w), 1031 (m), 969 (w), 945 (w), 931 (w), 824 (m), 752 (s), 621 (m), 492 (m).

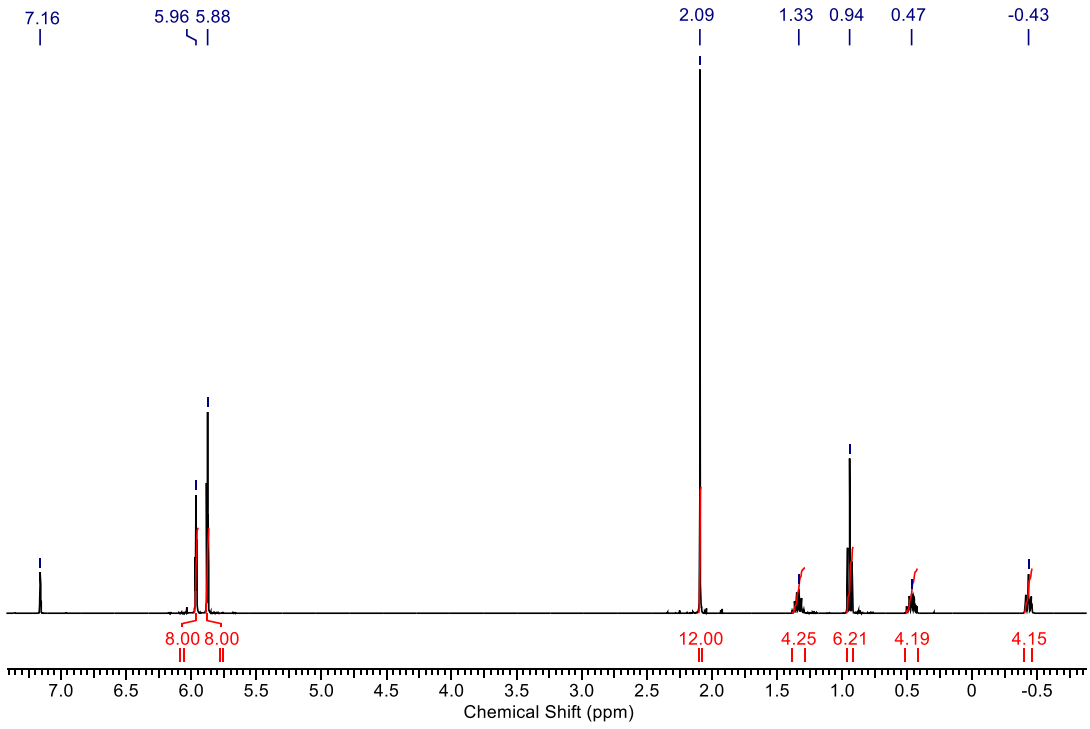

Figure 6.1. ^{1}H NMR spectrum of **2.1-Y**.

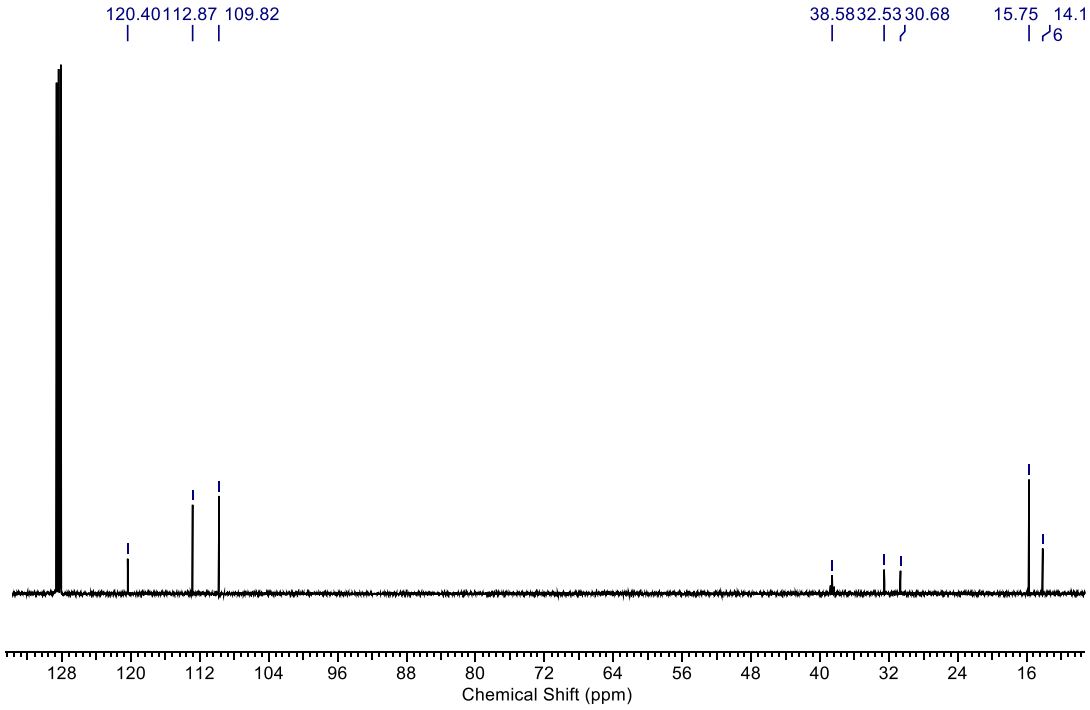

Figure 6.2. ^{13}C NMR spectrum of **2.1-Y**.

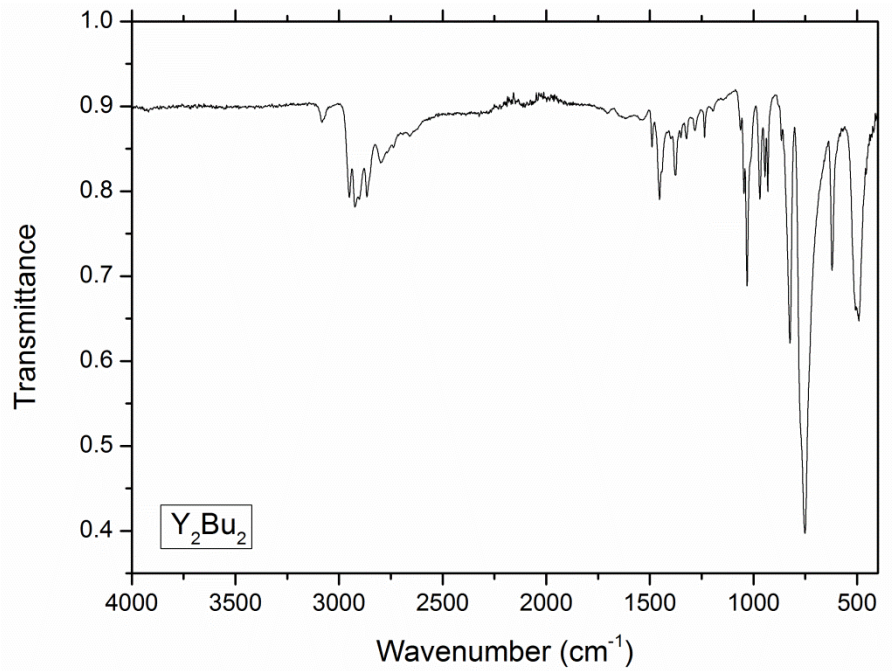

Figure 6.3. IR spectrum of **2.1-Y**.

[Cp$^{Me}_2$Dy{μ-^{n}Bu}]$_2$ (2.1-Dy) was synthesised in an identical manner to **2.1-Y** using Cp'$_3$Dy (3 g, 7.5 mmol) and ^{n}BuLi (4.7 mL, 1.6 M in hexanes). Yield (2.21 g, 78 %). Crystals suitable for X-ray diffraction were grown from a concentrated toluene solution stored at -30°C. **Elemental analysis**; found/% (calculated)/%; C, 50.67 (50.86); H, 6.02 (6.14). **IR** (solid) ν_{max} (cm^{-1}): 2950 (w), 2923 (w), 2866 (w), 1454 (w), 1046 (w), 1030 (m), 969 (w), 931 (w), 824 (m), 751 (s), 621 (m), 489 (m).

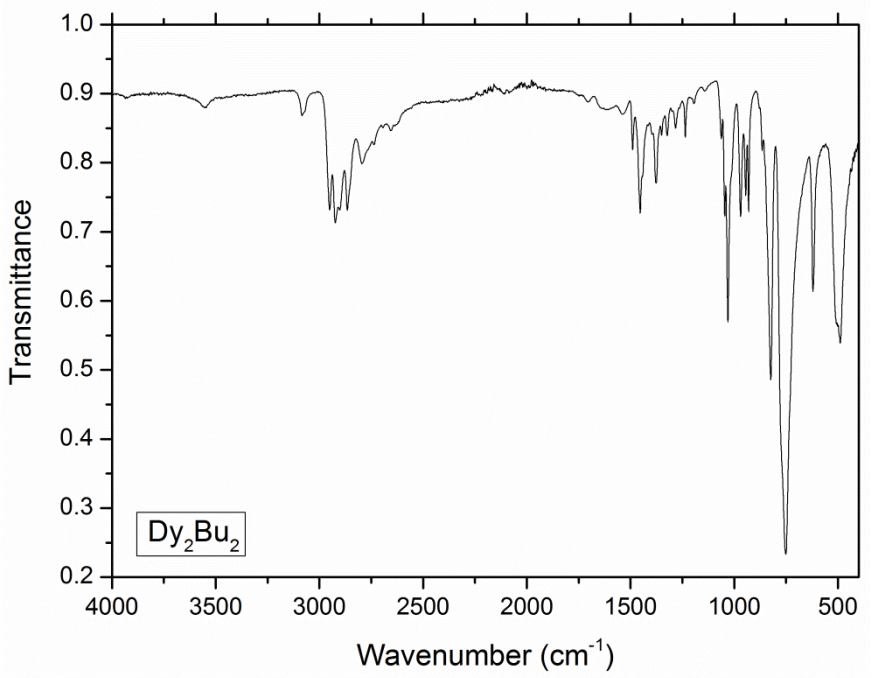

Figure 6.4. IR spectrum of **2.1-Dy**.

[Cp$^{Me}_2$Y{μ-(C$_5$H$_4$)FeCp}]$_2$ (2.2-Y) Toluene (11 mL) was added to **2.1-Y** (0.669 g, 1.1 mmol) and ferrocene (0.409 g, 2.2 mmol) at room temperature with stirring. Once all the solids were dissolved the mixture was left to stand at room temperature. Large, dark red crystals formed after 24 hrs and more crystals continued to form over the next 3 days. The solution was decanted and the crystals dried under reduced pressure and isolated (0.474 g, 50%). Elemental analysis; found/% (calculated)/%; C, 61.19 (61.14); H, 5.37 (5.36). **^{1}H NMR** (d$_8$-THF, 298.15 K, δ/ppm): 6.04 (s, 16 H, Cp^{Me}C-*H*); 4.01 (t, $^3J_{HH}$ = 1.35 Hz, 4H, FeC$_5$H$_4$-C*H*); 3.97

(s, 10H, FeCp*H*); 3.96 (t, $^{3}J_{HH}$ = 1.74 Hz, 4H, FeC_5H_4-C*H*); 2.18 (s, 12H, *Me*Cp). **^{13}C NMR** (d_8-THF, 298.15 K, δ/ppm): 129.72 (Y-C_5H_4-Fe); 122.29 ($Cp^{Me}C$-$(CH)_2$); 111.78 (Cp^{Me}*C*H); 110.42 (Cp^{Me}*C*H); 99.9 (Fe-C_5H_4); 99.27 (Fe-C_5H_4); 79.77 (Fe-C_5H_4); 70.37 (Fe-C_5H_4); 67.25 (Fe-C_5H_5); 15.24 ($Cp^{Me}CH_3$). **IR** (solid) ν_{max} (cm^{-1}): 3083 (w), 2961 (w), 2922 (w), 2895 (w), 2859 (w), 1410 (w), 1107 (w), 1084 (w), 1075 (w), 1050 (w), 1032 (w), 1010 (m), 931 (w), 831 (m), 747 (s), 623 (w), 503 (m), 478 (w).

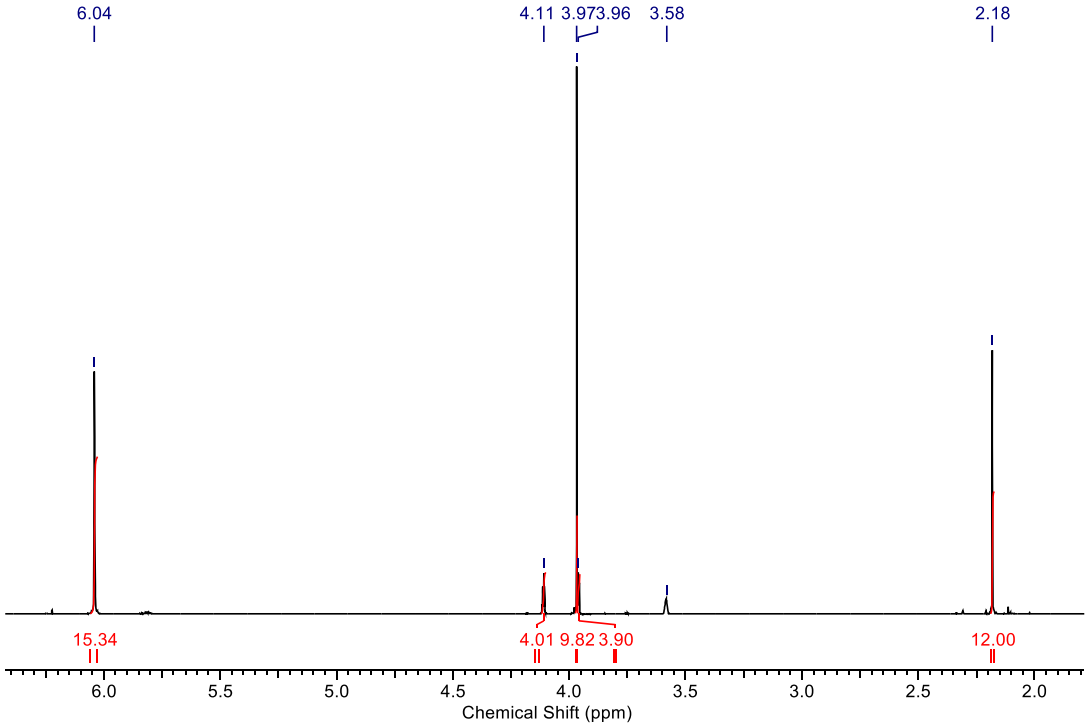

Figure 6.5. ^{1}H NMR spectrum of **2.2-Y**.

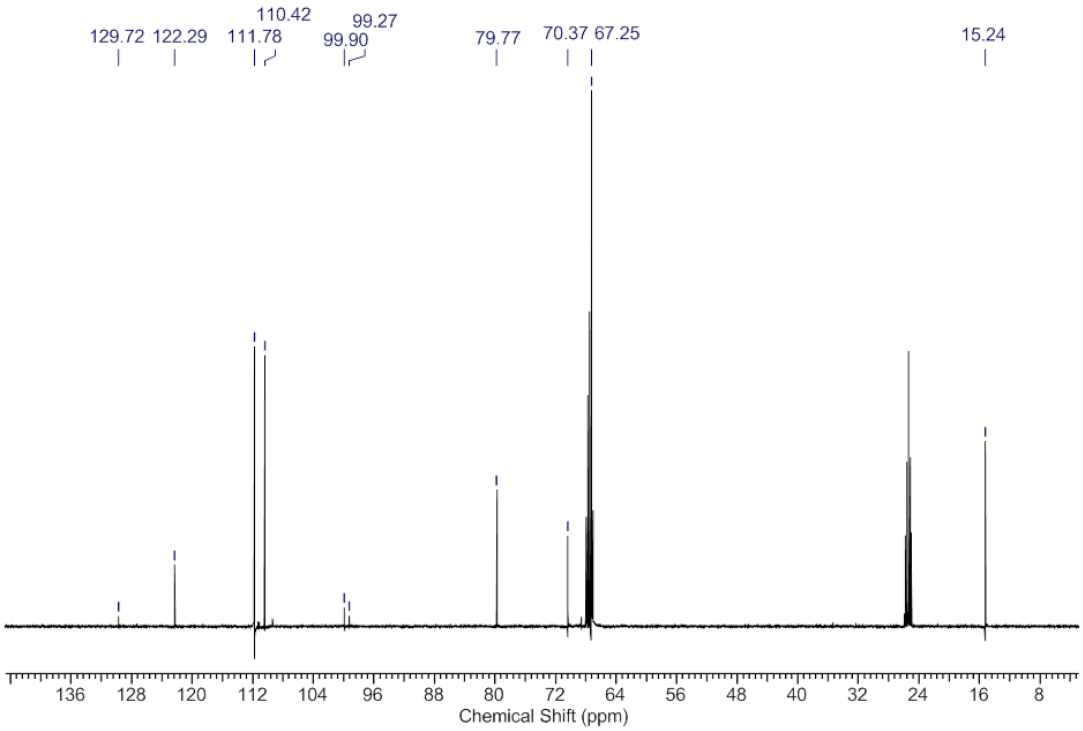

Figure 6.6. ^{13}C NMR spectrum of **2.2-Y**.

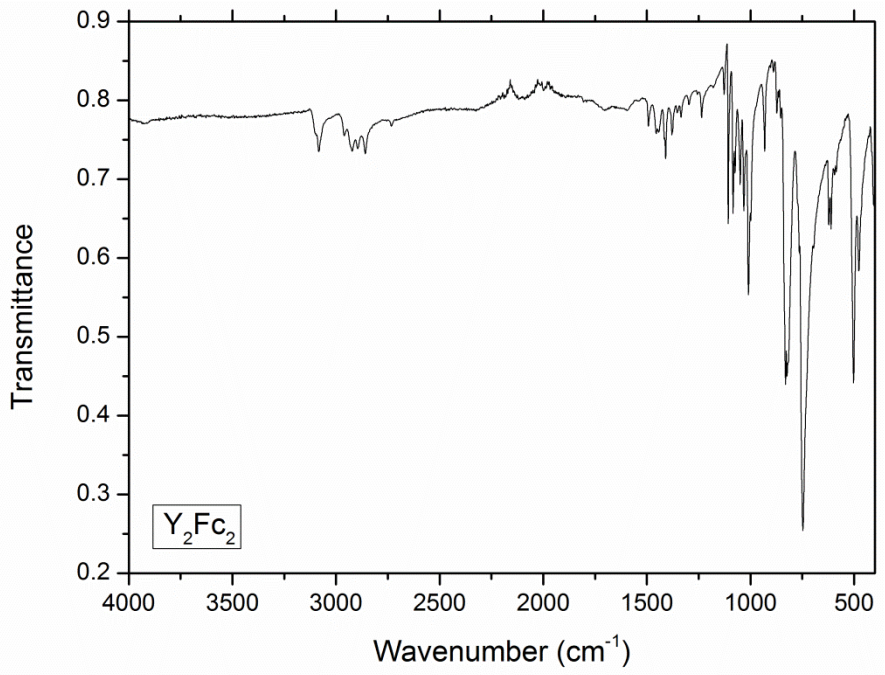

Figure 6.7. IR spectrum of **2.2-Y**.

[Cp^{Me}_2Dy{μ-(C_5H_4)FeCp}]$_2$ (2.2-Dy) was synthesised in a similar manner to **2-Y** using **2.1-Dy** (0.248 g, 0.328 mmol) and ferrocene (0.122 g, 0.657 mmol). Yield (0.18 g, 54 %). **Elemental analysis**; found/% (calculated)/%; C, 52.32 (52.24); H, 4.67 (4.58). **IR** (solid) ν_{max} (cm^{-1}): 3082 (w), 2961 (w), 2922 (w), 2895 (w), 2859 (w), 1455 (w), 1410 (w), 1380 (w), 1107 (w), 1084 (w), 1075 (w), 1049 (w), 1032 (w), 1010 (m), 931 (w), 831 (m), 747 (s), 622 (w), 503 (m), 478 (w).

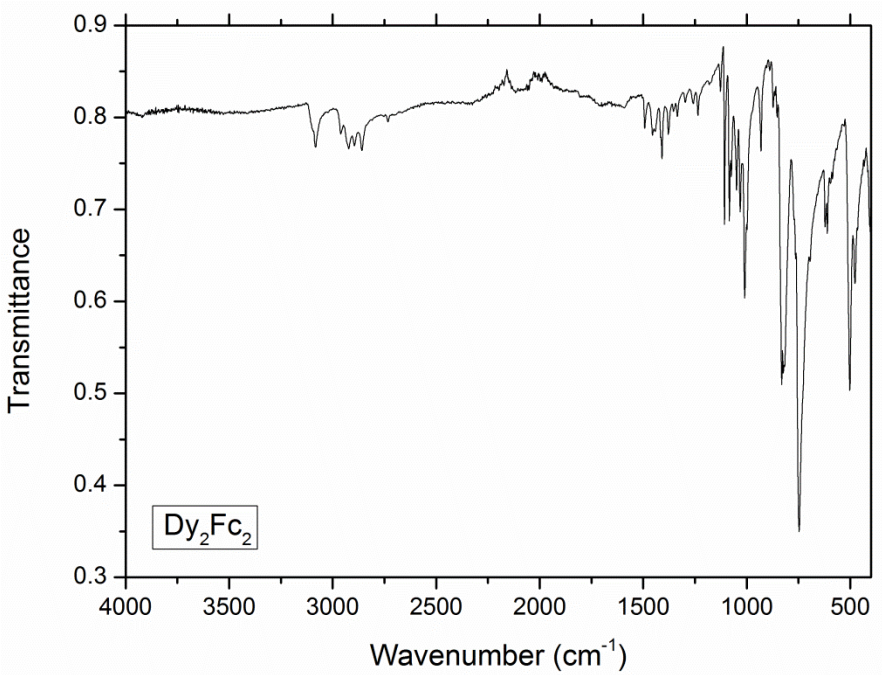

Figure 6.8. IR spectrum of **2.2-Dy**.

[Cp^{Me}_2Y(IMes')] (2.5-Y) A solution of IMes (0.1 g, 0.328 mmol) in toluene (3 mL) was added dropwise to a solution of **2.1-Y** (0.1 g, 0.164 mmol) in toluene (3 mL) at RT. Upon addition of IMes the reaction mixture there was an immediate colour change from colourless to bright yellow. The mixture was left to stand at RT for 1.5 hrs then the solution was evaporated to dryness, affording an analytically pure, yellow powder (0.154 g, 85 %). Crystals suitable for X-ray diffraction were grown from a concentrated toluene solution stored at -30°C. **Elemental analysis**, found/% (calculated)/%; C, 62.86 (63.16); H, 7.63

(7.62). **^{1}H NMR** (C_6D_6, 298.15 K, δ/ppm): 6.95 (s, 1 H, ArC-*H5*); 6.72 (s, 1 H, ArC-*H6*); 6.70 (s, 1 H, ArC-*H4*); 6.48 (d, $^{3}J_{HH}$ = 1.59 Hz, 1 H, C=C(N)-*H2*); 6.38 (s, 1 H, ArC-*H3*); 6.12 (d, $^{3}J_{HH}$ = 1.59 Hz, 1 H, C=C(N)-*H1*); 5.94 (q, $^{3}J_{HH}$ = 2.84 Hz, 1 H, CpC-*H14*); 5.90 (m, 2 H, CpC-*H12/11*); 5.63 (q, $^{3}J_{HH}$ = 2.81 Hz, 1 H, CpC-*H13*); 5.60 (q, $^{3}J_{HH}$ = 2.81 Hz, 1 H, CpC-*H10*); 5.55 (q, $^{3}J_{HH}$ = 2.81 Hz, 1 H, CpC-*H7*); 5.40 (q, $^{3}J_{HH}$ = 2.84 Hz, 1 H, CpC-*H8*); 5.15 (q, $^{3}J_{HH}$ = 2.84 Hz, 1 H, CpC-*H9*); 2.28 (s, 3 H, Ar-C$H_3$20); 2.16 (s, 3 H, Ar-C$H_3$19); 2.10 (s, 3 H, Ar-C$H_3$21); 2.07 (d, $^{3}J_{HH}$ = 2.84 Hz, 1 H, Y-C*H*); 2.05 (s, 3 H, Ar-C$H_3$17); 2.04 (s, 3 H, Ar-C$H_3$18); 1.95 (s, 3 H, Cp-C$H_3$15); 1.93 (s, 3 H, Cp-C$H_3$16); 1.12 (dd, $^{2}J_{HH}$ = 3.47 Hz, 1 H, Y-C*H*). **^{13}C NMR** (C_6D_6, 298.15 K, δ/ppm): 194.74 (N*C*N); 194.35 (C=*C*(N)-H); 184.46 (C=*C*(N)-H); 152.77 (Ar*C*-N); 139.3 (Ar*C*-N); 138.13 (Ar*C*-CH_2); 136.95 (Ar*C*-H); 135.05 (Ar*C*-H); 135.02 (Ar*C*-H); 130.31 (Ar*C*-H); 129.87 (Ar*C*-CH_3); 124.14 (Ar*C*-CH_3); 123.89 (Ar*C*-CH_3); 122.78 (Ar*C*-CH_3); 121.48 (Ar*C*-CH_3); 120.49 (Cp*C*-$(CH)_2$); 120.01 (Cp*C*-$(CH)_2$); 112.98 (Cp*C*H); 111.38 (Cp*C*H); 110.92 (Cp*C*H); 110.31 (Cp*C*H); 110.15 (Cp*C*H); 109.19 (Cp*C*H); 108.91 (Cp*C*H); 108.75 (Cp*C*H); 48.43 (Ar-*C*H_3); 48.3 (Ar-*C*H_3); 21.78 (Ar-*C*H_3); 21.21 (Ar-*C*H_3); 20.0 (Ar-*C*H_3); 18.79 (Y-*C*H_2); 15.58 (*Me*Cp); 15.05 (*Me*Cp). **IR** (solid) ν_{max} (cm^{-1}); 2957 (w), 2922 (w), 2896 (w), 2858 (w), 1586 (w), 1557 (w), 1487 (w), 1389 (w), 1266 (m), 1168 (w), 929 (w), 858 (m), 810 (s), 756 (s), 735 (s), 684 (w), 659 (w), 625 (w), 596 (w), 566 (m), 549 (w), 521 (w), 496 (w), 465 (w).

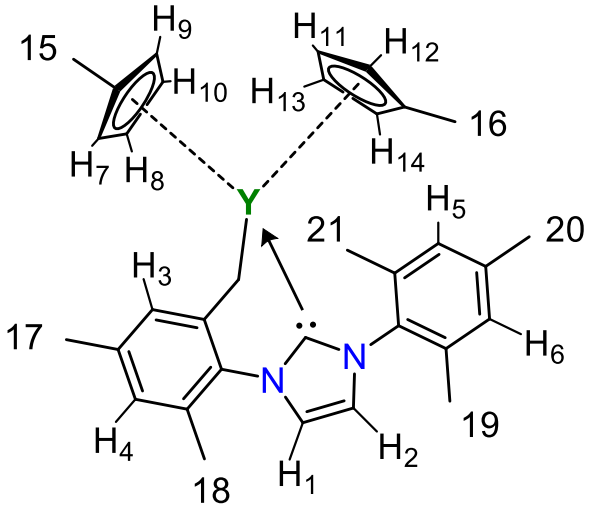

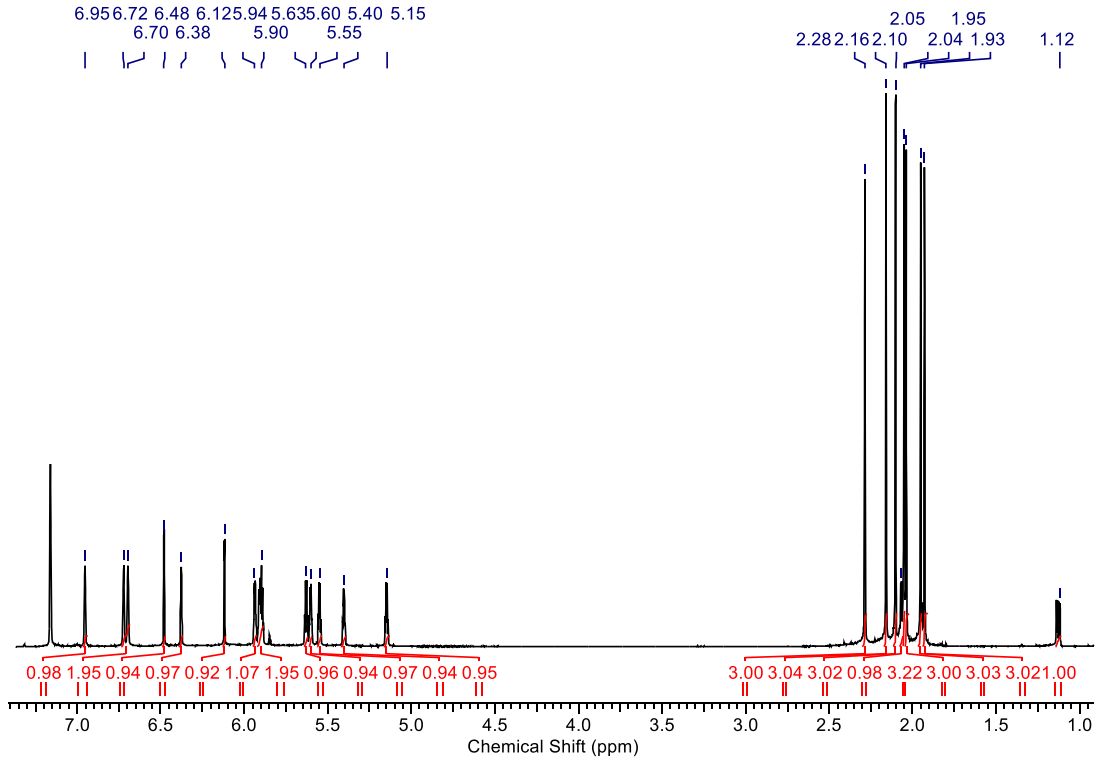

Figure 6.9. ^{1}H NMR spectrum of **2.5-Y**.

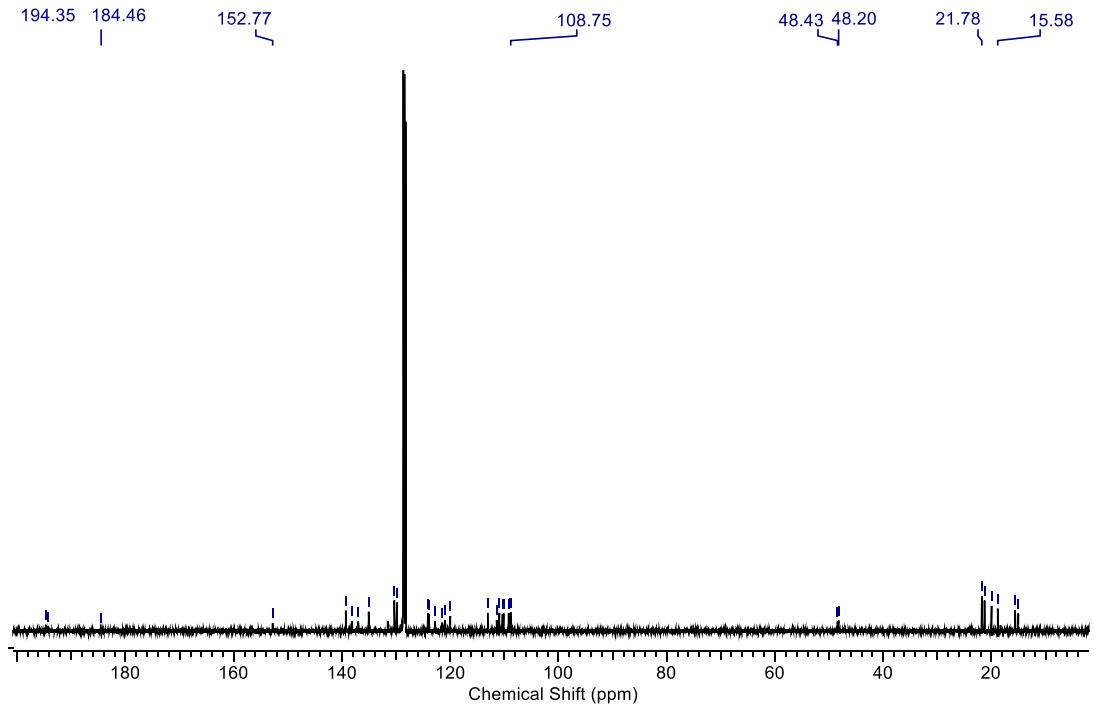

Figure 6.10. ^{13}C NMR spectrum of **2.5-Y**.

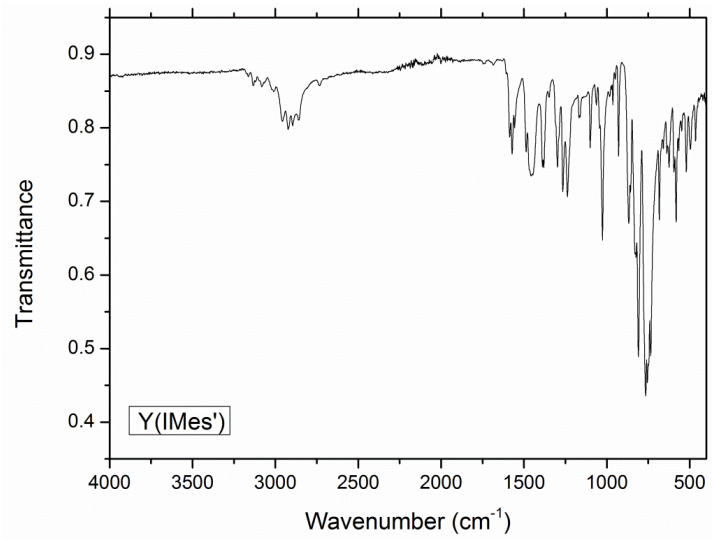

Figure 6.11. IR spectrum of **2.5-Y**.

[Cp^{Me}_2Dy(IMes')] (2.5-Dy) was synthesised in an identical manner to **2.5-Y** using **2.1-Dy** (0.124 g, 0.164 mmol) and IMes (0.1 g, 0.328 mmol). Yield: (0.175 g, 86 %). Crystals suitable for X-ray diffraction were grown by slow evaporation of a toluene solution at RT. Elemental analysis; found/% (calculated)/%: C, 50.67 (50.86); H, 6.02 (6.14). IR (solid) ν_{max} (cm^{-1}); 2962 (w), 2922 (w), 2895 (w), 2857 (w), 1587 (w), 1569 (w), 1488 (w), 1459 (w), 1445 (w), 1392 (w), 1380 (w), 1312 (w), 1298 (w), 1261 (m), 1241 (w), 1169 (w), 1096 (m), 1025 (s), 964 (w), 929 (w), 872 (m), 858 (m), 809 (s), 778 (s), 769 (s), 752 (s), 735 (s), 684 (w), 660 (w), 623 (w), 581 (w), 566 (m), 549 (w), 519 (w), 495 (w), 465 (w).

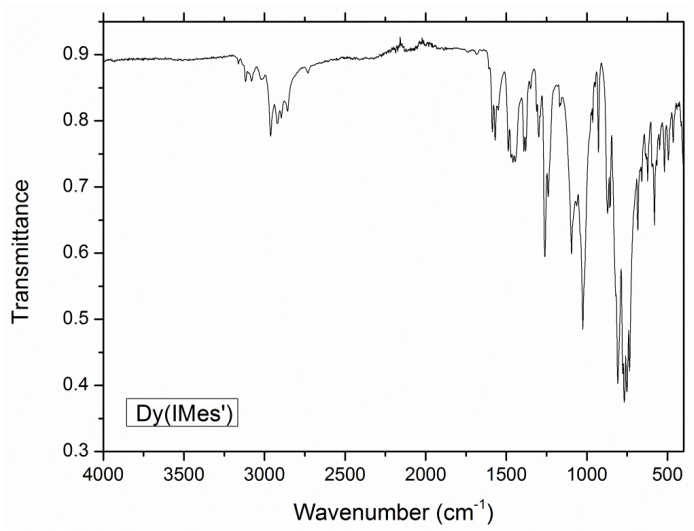

Figure 6.12. IR spectrum of **2.5-Dy**

[Cp^{Me}_3Y(aIMes)]· C_6H_6 (2.6-Y) IMes (0.239 g, 0.785 mmol) was dissolved in benzene (3 mL) and added dropwise to a solution of Cp^{Me}_3Y (0.256 g, 0.785 mmol) in benzene (3 mL) at RT. The reaction mixture was left to stand for 5 d during which time colourless crystals formed. The solution was decanted and the crystals washed with benzene to afford the product (0.453 g, 81 %). **^{1}H NMR** (C_6D_6, 298.15 K, δ/ppm): 6.78 (s, 2 H, ArC-*H*); 6.77 (d, $^3J_{HH}$ = 1.47 Hz, 1 H, N-C(*H*)-N); 6.64 (s, 2 H, ArC-*H*); 6.10 (d, $^3J_{HH}$ = 1.47 Hz, 1 H, N-C(*H*)-C-Y); 5.85 (t, 6 H, CpC-*H*); 5.60 (t, $^3J_{HH}$ = 1.59 Hz, 1 H, CpC-*H*); 2.37 (s, 9 H, Ar-CH_3); 2.11 (s, 3 H, Cp-CH_3); 2.10 (s, 3 H, Cp-CH_3); 1.81 (s, 6 H, Ar-CH_3). **Elemental analysis**, found/% (calculated)/%; C, 71.38 (76.2); H, 6.52 (7.25); N, 4.10 (3.95). **IR** (solid) ν_{max} (cm^{-1}); 3052 (w), 2919 (w), 2857 (w), 1480 (w), 1457 (w), 1377 (w), 1226 (w), 1080 (w), 930 (w), 870 (w), 851 (w), 771 (s), 617 (w).

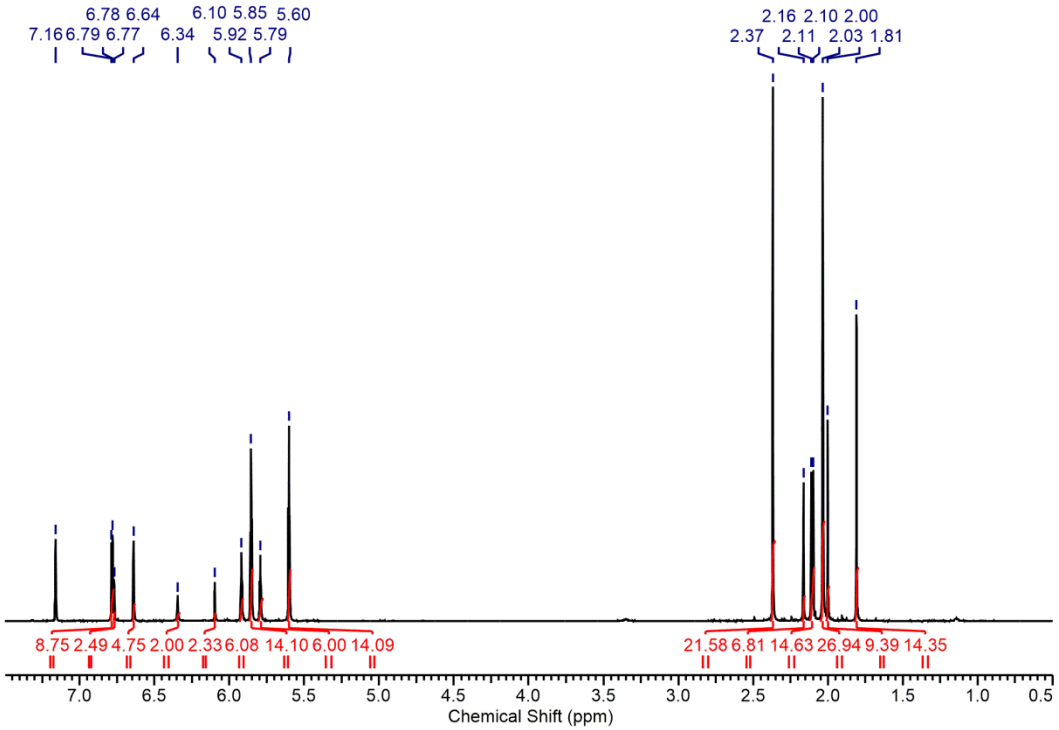

Figure 6.13. ^{1}H NMR spectrum of a mixture of $(Cp^{Me})_3$Y, IMes and **2.6-Y_Y** in benzene-d_6, recorded 576 hours after mixing.

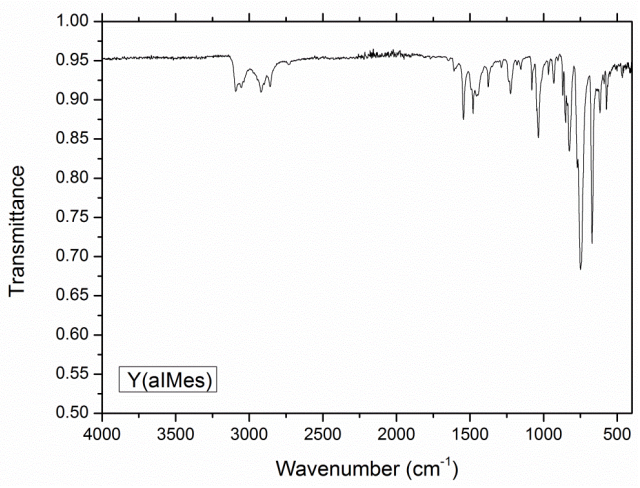

Figure 6.14. IR spectrum of **2.6-Y**.

[Cp^{Me}_3Dy(aIMes)]· C_6H_6 (2.6-Dy) was synthesised in an identical manner to **2.6-Y** using Cp^{Me}_3Dy (0.1 g, 0.25 mmol) and IMes (0.076 g, 0.25 mmol). Yield: 0.132 g, 68 %. Elemental analysis, found/% (calculated)/%; C, 68.89 (69.08); H, 6.72 (6.57); N, 3.60 (3.58). IR (solid) ν_{max} (cm^{-1}); 3092 (w), 2919 (w), 2859 (w), 1545 (w), 1479 (w), 1376 (w), 1225 (w), 1080 (w), 1035 (w), 967 (m), 929 (w), 869 (w), 850 (w), 825 (m), 745 (s), 671 (s), 616 (w), 565 (w).

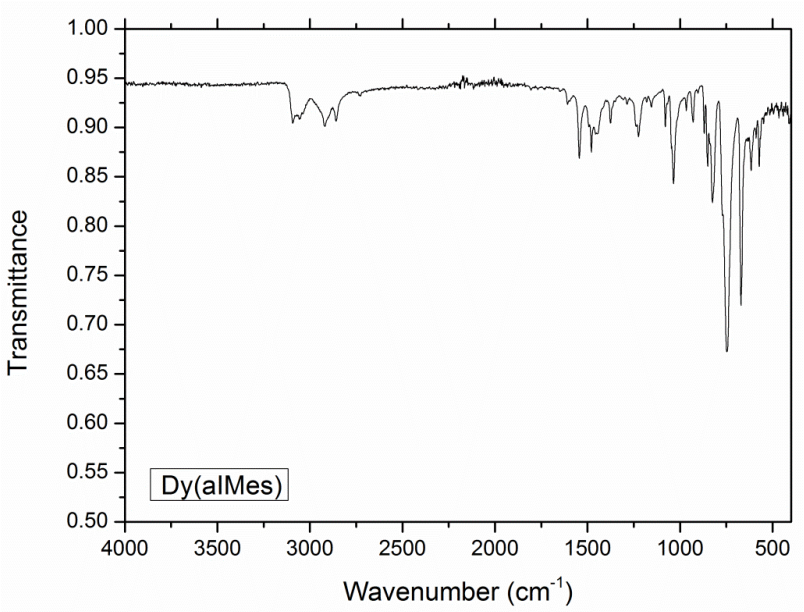

Figure 6.15. IR spectrum of **2.6-Dy**.

6.3 Synthesis for Chapter 3

[$Cp^{Me}_{10}Y_6(\mu_3\text{-}S_3)_2(\mu_4\text{-}S_2)$] (3.11-Y): Toluene (2.5 mL) was added to a mixture of **2.1-Y** (150 mg, 0.246 mmol) and sulfur (32 mg, 0.123 mmol) at room temperature and stirred until all the solid was dissolved. The solution was left to stand at RT for 2 d, during which time the product crystallised out (102 mg, 53 % based on S). **^{1}H NMR** (500 MHz, THF-d_8): δ (ppm) 5.84 (s, 40 H, CpC-*H*); 2.17 (s, 30 H, Cp-CH_3). **Elemental analysis**: found/% (calculated)/%: %C – 35.73 (35.42), % H – 3.41 (3.48).

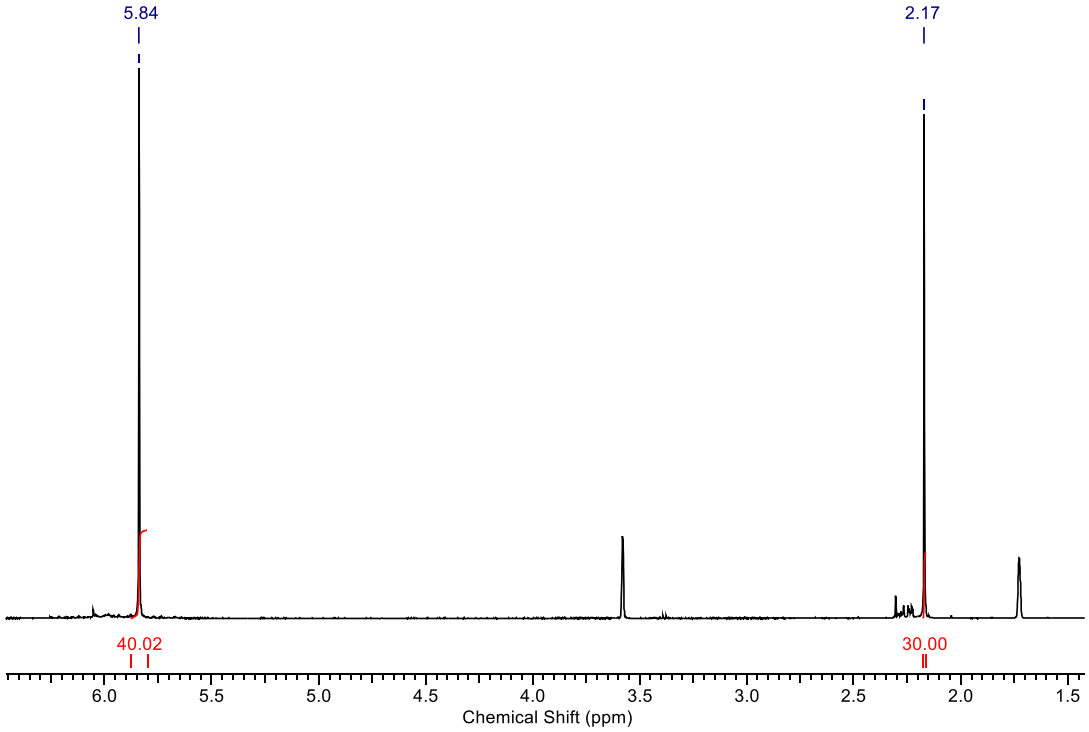

Figure 6.16. ^{1}H NMR spectrum of **3.11-Y**.

[$Cp^{Me}_{10}Dy_6(\mu_3\text{-}S_3)_2(\mu_4\text{-}S_2)$] (3.11-Dy): As for **1** with **2.1-Dy** (200 mg, 0.264 mmol) and sulfur (34 mg, 0.132 mmol). Yield: 140 mg, 52 % based on S. **Elemental analysis**; found/% (calculated)/%: %C – 35.73 (35.42), % H – 3.41 (3.48). **IR** (solid) ν_{max} (cm^{-1}): 3066 (w), 2920 (w), 2894 (w), 2856 (w), 1493 (w), 1456 (w), 1440 (w), 1375 (w), 1045 (w), 1029 (m), 929

(w), 842 (m), 828 (m), 816 (m), 786 (s), 773 (s), 766 (s), 759 (s), 746 (s), 694 (m), 631 (m), 625 (m), 617 (m), 473 (w).

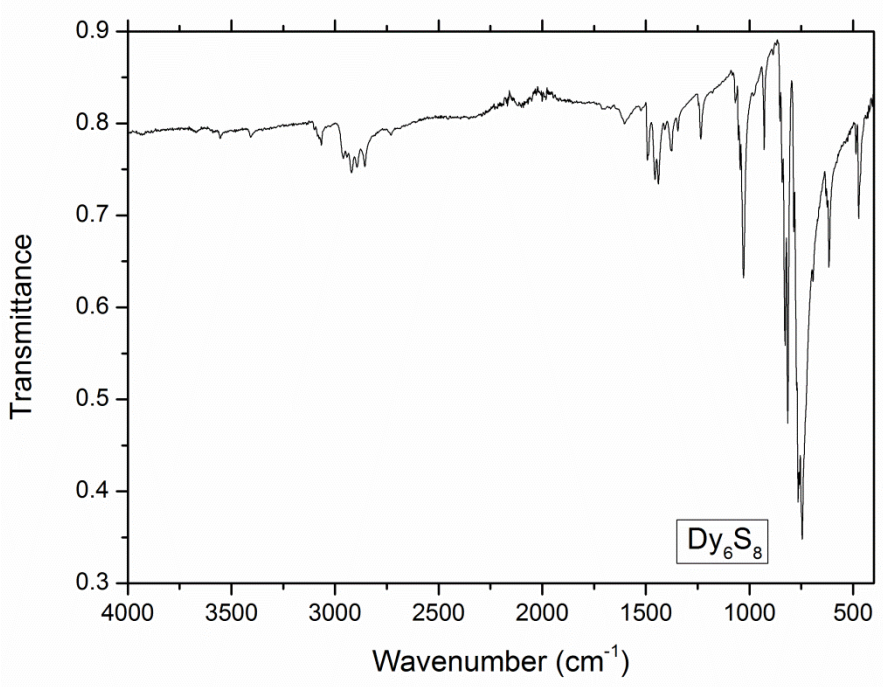

Figure 6.17. IR spectrum of **3.11-Dy**

[$Cp^{Me}_{10}Y_6(\mu_3\text{-}Se_3)_2(\mu_4\text{-}Se_2)$] (3.12-Y): Toluene (4 mL) was added to a mixture of **2.1-Y** (100 mg, 0.164 mmol) and selenium (52 mg, 0.657 mmol) at room temperature. The mixture was then heated without stirring at 80°C overnight, during which time the product crystallises in a layer over unreacted selenium. **Cannot be separated from excess Se – Characterised by XRD only.** ^{1}H NMR spectrum of the reaction mixture shown below (Figure 5.15).

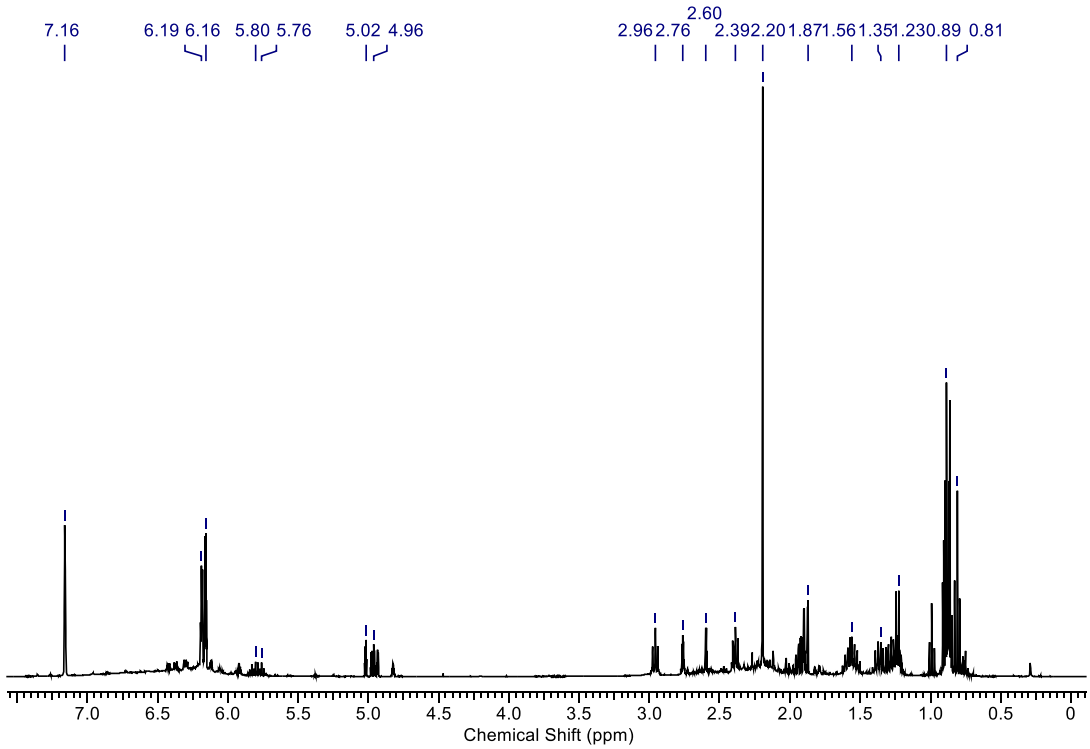

Figure 6.18. ^{1}H NMR spectrum of the reaction mixture containing **2.1-Y** and excess selenium in C_6D_6 after heating for 18 h.

[$Cp^{Me}_{10}Dy_6(\mu_3\text{-}Se_3)_2(\mu_4\text{-}Se_2)$] (3.12-Dy): Toluene (4 mL) was added to a mixture of **2.1-Dy** (200 mg, 0.264 mmol) and selenium (83 mg, 1.056 mmol) at room temperature. The mixture was then heated without stirring at 80°C overnight, during which time the product crystallises in a layer over unreacted selenium. **Cannot be separated from excess Se – Characterised by XRD only.**

6.4 Synthesis for Chapter 4

[{(thd)$_3$Dy}$_3$HAN]·3(C$_7$H$_8$) (4.12) Toluene (10 mL) was added to a mixture of Dy(thd)$_3$ (1.00 g, 1.40 mmol) and HAN (0.18 g, 0.47 mmol) at room temperature. The solution immediately turned dark red, with a small amount of yellow solid remaining, and the reaction was stirred at room temperature for 40 minutes until all of the yellow solid had been consumed. The mixture was filtered and concentrated to approximately 5 mL. The resulting precipitate was re-dissolved with gentle heating. Dark red crystals formed overnight upon storage at 2.5°C. A second crop of crystals was isolated after concentrating the supernatant solution (total isolated yield: 1.01 g, 86 %). **Elemental analysis** (%): found/% (calculated)/%: C – 58.66 (58.59), H – 7.45 (7.31), N – 3.22 (3.33). **IR** (solid) ν_{max} (cm^{-1}): 2951 (w), 2902 (w), 2863 (w), 1603 (m), 1588 (s), 1573 (s), 1537 (s), 1504 (s), 1450 (s), 1401 (s), 1385 (s), 1355 (s), 1244 (m), 1225 (m), 1178 (m), 1140 (m), 1086 (m), 868 (m), 792 (m), 757 (m), 733 (m), 615 (m), 604 (m), 474 (m), 409 (m).

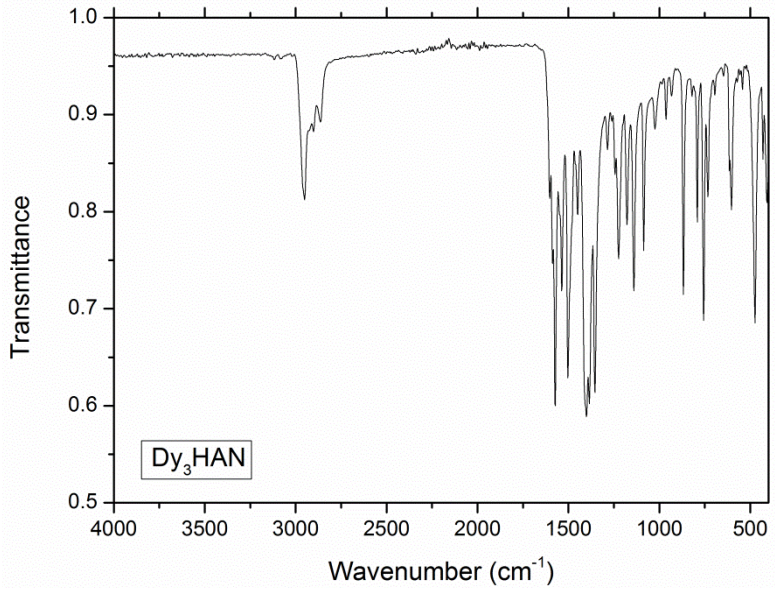

Figure 6.19. IR spectrum of **4.12**.

6.5 Crystallographic details

Crystal data and Structure Refinement for Compound 2.1-Y

Identification code	aral305
Empirical formula	$C_{32}H_{46}Y_2$
Formula weight	608.51
Temperature/K	150.02(10)
Crystal system	orthorhombic
Space group	$P2_12_12$
a/Å	14.4805(4)
b/Å	15.4640(3)
c/Å	13.0556(2)
α/°	90
β/°	90
γ/°	90
Volume/Å^3	2923.49(11)
Z	4
ρ_{calc}g/cm^3	1.383
μ/mm^{-1}	3.967
F(000)	1264.0
Crystal size/mm^3	0.15 × 0.15 × 0.1
Radiation	MoKα (λ = 0.71073)
2Θ range for data collection/°	6.74 to 50.69
Index ranges	-17 ≤ h ≤ 17, -18 ≤ k ≤ 18, -15 ≤ l ≤ 15
Reflections collected	38521
Independent reflections	5363 [R_{int} = 0.0515, R_{sigma} = 0.0312]
Data/restraints/parameters	5363/208/359
Goodness-of-fit on F^2	1.047
Final R indexes [I>=2σ (I)]	R_1 = 0.0532, wR_2 = 0.1214
Final R indexes [all data]	R_1 = 0.0641, wR_2 = 0.1278
Largest diff. peak/hole / e Å^{-3}	0.98/-0.88
Flack parameter	0.45(2)

Crystal data and Structure Refinement for Compound 2.2-Y

Identification code	oral312
Empirical formula	$C_{44}H_{46}Fe_2Y_2$
Formula weight	864.33
Temperature/K	150
Crystal system	monoclinic
Space group	$P2_1/n$
a/Å	11.4603(11)
b/Å	8.7867(8)
c/Å	17.6568(17)
α/°	90
β/°	105.777(10)
γ/°	90
Volume/Å^3	1711.0(3)
Z	2
ρ_{calc}g/cm^3	1.678
μ/mm^{-1}	4.221
F(000)	880.0
Crystal size/mm^3	0.3 × 0.2 × 0.2
Radiation	MoKα (λ = 0.71073)
2Θ range for data collection/°	6.966 to 52.74
Index ranges	-14 ≤ h ≤ 14, -10 ≤ k ≤ 10, -22 ≤ l ≤ 18
Reflections collected	7617
Independent reflections	3454 [R_{int} = 0.0464, R_{sigma} = 0.0722]
Data/restraints/parameters	3454/0/219
Goodness-of-fit on F^2	1.027
Final R indexes [I>=2σ (I)]	R_1 = 0.0413, wR_2 = 0.0861
Final R indexes [all data]	R_1 = 0.0629, wR_2 = 0.0944
Largest diff. peak/hole / e Å^{-3}	1.11/-0.51

Crystal Data and Structure Refinement for Compound 2.2-Dy

Identification code	oral318
Empirical formula	$C_{44}H_{46}Dy_2Fe_2$
Formula weight	1011.51
Temperature/K	150
Crystal system	monoclinic
Space group	$P2_1/n$
a/Å	11.4410(5)
b/Å	8.8007(3)
c/Å	17.6498(7)
α/°	90
β/°	105.794(4)
γ/°	90
Volume/Å^3	1710.04(12)
Z	2
ρ_{calc}g/cm^3	1.964
μ/mm^{-1}	5.183
F(000)	988.0
Crystal size/mm^3	0.838 × 0.751 × 0.42
Radiation	MoKα (λ = 0.71073)
2Θ range for data collection/°	7.142 to 52.788
Index ranges	-14 ≤ h ≤ 14, -11 ≤ k ≤ 10, -18 ≤ l ≤ 21
Reflections collected	10803
Independent reflections	3477 [R_{int} = 0.0356, R_{sigma} = 0.0392]
Data/restraints/parameters	3477/0/219
Goodness-of-fit on F^2	1.096
Final R indexes [I>=2σ (I)]	R_1 = 0.0285, wR_2 = 0.0629
Final R indexes [all data]	R_1 = 0.0315, wR_2 = 0.0642
Largest diff. peak/hole / e Å^{-3}	1.94/-1.48

Crystal Data and Structure Refinement for Compound 2.5-Y

Identification code	xral89
Empirical formula	$C_{33}H_{37}N_2Y$
Formula weight	550.55
Temperature/K	150.01(12)
Crystal system	monoclinic
Space group	$P2_1/c$
a/Å	17.8886(16)
b/Å	14.8409(10)
c/Å	22.412(2)
α/°	90
β/°	110.351(10)
γ/°	90
Volume/Å^3	5578.7(9)
Z	8
ρ_{calc}g/cm^3	1.311
μ/mm^{-1}	2.114
F(000)	2304.0
Crystal size/mm^3	0.5 × 0.4 × 0.15
Radiation	MoKα (λ = 0.71073)
2Θ range for data collection/°	6.674 to 50.7
Index ranges	-21 ≤ h ≤ 20, -17 ≤ k ≤ 17, -13 ≤ l ≤ 26
Reflections collected	10178
Independent reflections	10178 [R_{int} = ?, R_{sigma} = 0.1094]
Data/restraints/parameters	10178/6/664
Goodness-of-fit on F^2	1.119
Final R indexes [I>=2σ (I)]	R_1 = 0.0922, wR_2 = 0.2118
Final R indexes [all data]	R_1 = 0.1318, wR_2 = 0.2279
Largest diff. peak/hole / e Å^{-3}	2.02/-1.62

Crystal Data and Structure Refinement for Compound 2.5-Dy

Identification code	oral347
Empirical formula	$C_{33}H_{37}DyN_2$
Formula weight	624.14
Temperature/K	150
Crystal system	monoclinic
Space group	$P2_1/c$
a/Å	17.9045(7)
b/Å	14.8465(5)
c/Å	22.4149(10)
α/°	90
β/°	110.370(4)
γ/°	90
Volume/Å^3	5585.7(4)
Z	8
ρ_{calc}g/cm^3	1.484
μ/mm^{-1}	2.699
F(000)	2520.0
Crystal size/mm^3	1.094 × 1.048 × 0.729
Radiation	MoKα (λ = 0.71073)
2Θ range for data collection/°	6.958 to 52.798
Index ranges	-22 ≤ h ≤ 20, -18 ≤ k ≤ 18, -13 ≤ l ≤ 28
Reflections collected	11385
Independent reflections	11385 [R_{int} = ?, R_{sigma} = 0.0582]
Data/restraints/parameters	11385/0/664
Goodness-of-fit on F^2	1.135
Final R indexes [I>=2σ (I)]	R_1 = 0.0718, wR_2 = 0.1571
Final R indexes [all data]	R_1 = 0.0842, wR_2 = 0.1632
Largest diff. peak/hole / e Å^{-3}	4.34/-1.97

Crystal Data and Structure Refinement for Compound 2.6-Y

Identification code	aral439
Empirical formula	$C_{90}H_{102}N_4Y_2$
Formula weight	1417.57
Temperature/K	100.02(10)
Crystal system	monoclinic
Space group	$P2_1/c$
a/Å	15.5723(8)
b/Å	12.8913(8)
c/Å	37.4502(14)
α/°	90
β/°	90.982(4)
γ/°	90
Volume/Å^3	7516.9(7)
Z	4
ρ_{calc}g/cm^3	1.253
μ/mm^{-1}	1.585
F(000)	2992.0
Crystal size/mm^3	0.49 × 0.19 × 0.15
Radiation	MoKα (λ = 0.71073)
2Θ range for data collection/°	6.52 to 50.7
Index ranges	-18 ≤ h ≤ 18, -15 ≤ k ≤ 12, -45 ≤ l ≤ 42
Reflections collected	37268
Independent reflections	13751 [R_{int} = 0.0677, R_{sigma} = 0.1093]
Data/restraints/parameters	13751/350/982
Goodness-of-fit on F^2	1.045
Final R indexes [I>=2σ (I)]	R_1 = 0.0786, wR_2 = 0.1714
Final R indexes [all data]	R_1 = 0.1332, wR_2 = 0.1962
Largest diff. peak/hole / e Å^{-3}	1.76/-0.74

Crystal Data and Structure Refinement for Compound 2.6-Dy

Identification code	oral353
Empirical formula	$C_{45}H_{51}DyN_2$
Formula weight	782.38
Temperature/K	150
Crystal system	monoclinic
Space group	$P2_1/c$
a/Å	15.6469(6)
b/Å	12.9702(7)
c/Å	37.5845(12)
α/°	90
β/°	91.221(3)
γ/°	90
Volume/Å^3	7625.8(5)
Z	8
ρ_{calc}g/cm^3	1.363
μ/mm^{-1}	1.992
F(000)	3208.0
Crystal size/mm^3	0.761 × 0.326 × 0.287
Radiation	MoKα (λ = 0.71073)
2Θ range for data collection/°	6.496 to 50.696
Index ranges	-18 ≤ h ≤ 17, -12 ≤ k ≤ 15, -45 ≤ l ≤ 45
Reflections collected	49837
Independent reflections	13634 [R_{int} = 0.0717, R_{sigma} = 0.0855]
Data/restraints/parameters	13634/662/983
Goodness-of-fit on F^2	1.212
Final R indexes [I>=2σ (I)]	R_1 = 0.0893, wR_2 = 0.1593
Final R indexes [all data]	R_1 = 0.1168, wR_2 = 0.1705
Largest diff. peak/hole / e Å^{-3}	2.48/-1.76

Crystal Data and Structure Refinement for Compound 3.11-Y

Identification code	aral410abscor
Empirical formula	$C_{60}H_{70}S_8Y_6$
Formula weight	1581.10
Temperature/K	150.02(10)
Crystal system	monoclinic
Space group	$P2_1/n$
a/Å	12.3952(6)
b/Å	12.1669(7)
c/Å	20.0344(10)
α/°	90
β/°	93.341(4)
γ/°	90
Volume/Å^3	3016.3(3)
Z	2
ρ_{calc}g/cm^3	1.741
μ/mm^{-1}	6.020
F(000)	1584.0
Crystal size/mm^3	0.6202 × 0.524 × 0.2451
Radiation	MoKα (λ = 0.71073)
2Θ range for data collection/°	7.11 to 52.738
Index ranges	-15 ≤ h ≤ 12, -13 ≤ k ≤ 15, -23 ≤ l ≤ 25
Reflections collected	14320
Independent reflections	6151 [R_{int} = 0.0530, R_{sigma} = 0.0793]
Data/restraints/parameters	6151/0/339
Goodness-of-fit on F^2	1.024
Final R indexes [I>=2σ (I)]	R_1 = 0.0424, wR_2 = 0.0811
Final R indexes [all data]	R_1 = 0.0622, wR_2 = 0.0889
Largest diff. peak/hole / e Å^{-3}	0.83/-0.84

Crystal Data and Structure Refinement for Compound 3.11-Dy

Identification code	oral341abscor2
Empirical formula	$C_{60}H_{70}S_8Dy_6$
Formula weight	2022.64
Temperature/K	150
Crystal system	monoclinic
Space group	$P2_1/n$
a/Å	12.4207(4)
b/Å	12.1656(4)
c/Å	20.0395(7)
α/°	90
β/°	93.241(3)
γ/°	90
Volume/Å^3	3023.23(17)
Z	2
ρ_{calc}g/cm^3	2.222
μ/mm^{-1}	7.634
F(000)	1908.0
Crystal size/mm^3	0.6908 × 0.6697 × 0.314
Radiation	MoKα (λ = 0.71073)
2Θ range for data collection/°	6.968 to 52.74
Index ranges	-15 ≤ h ≤ 15, -15 ≤ k ≤ 15, -25 ≤ l ≤ 23
Reflections collected	26321
Independent reflections	6159 [R_{int} = 0.0546, R_{sigma} = 0.0551]
Data/restraints/parameters	6159/0/339
Goodness-of-fit on F^2	1.098
Final R indexes [I>=2σ (I)]	R_1 = 0.0335, wR_2 = 0.0751
Final R indexes [all data]	R_1 = 0.0420, wR_2 = 0.0781
Largest diff. peak/hole / e Å^{-3}	2.51/-1.26

Crystal Data and Structure Refinement for Compound 3.12-Dy

Identification code	aral409
Empirical formula	$C_{60}H_{70}Dy_6Se_8$
Formula weight	2397.84
Temperature/K	150.03(10)
Crystal system	monoclinic
Space group	C2/c
a/Å	29.088(2)
b/Å	9.6050(4)
c/Å	24.1207(16)
α/°	90
β/°	110.934(8)
γ/°	90
Volume/Å^3	6294.3(7)
Z	4
ρ_{calc}g/cm^3	2.530
μ/mm^{-1}	11.694
F(000)	4392.0
Crystal size/mm^3	0.1 × 0.06 × 0.025
Radiation	MoKα (λ = 0.71073)
2Θ range for data collection/°	7.45 to 52.742
Index ranges	-36 ≤ h ≤ 36, -12 ≤ k ≤ 11, -29 ≤ l ≤ 30
Reflections collected	26058
Independent reflections	6403 [R_{int} = 0.0433, R_{sigma} = 0.0430]
Data/restraints/parameters	6403/0/339
Goodness-of-fit on F^2	1.051
Final R indexes [I>=2σ (I)]	R_1 = 0.0294, wR_2 = 0.0521
Final R indexes [all data]	R_1 = 0.0405, wR_2 = 0.0560
Largest diff. peak/hole / e Å^{-3}	0.77/-0.79

Crystal Data and Structure Refinement for Compound 4.12

Identification code	oral253rered
Empirical formula	$C_{144}H_{207}Dy_3N_6O_{18}$
Formula weight	2797.64
Temperature/K	100
Crystal system	monoclinic
Space group	$P2_1/c$
a/Å	30.2821(16)
b/Å	13.7793(5)
c/Å	34.9863(9)
α/°	90
β/°	96.055(3)
γ/°	90
Volume/Å^3	14517.1(10)
Z	4
ρ_{calc}g/cm^3	1.280
μ/mm^{-1}	1.590
F(000)	5820.0
Crystal size/mm^3	0.1 × 0.1 × 0.05
Radiation	MoKα (λ = 0.71073)
2Θ range for data collection/°	5.944 to 50.7
Index ranges	-36 ≤ h ≤ 32, -16 ≤ k ≤ 16, -25 ≤ l ≤ 42
Reflections collected	54065
Independent reflections	26550 [R_{int} = 0.0464, R_{sigma} = 0.0760]
Data/restraints/parameters	26550/876/1699
Goodness-of-fit on F^2	1.075
Final R indexes [I>=2σ (I)]	R_1 = 0.0633, wR_2 = 0.1406
Final R indexes [all data]	R_1 = 0.0962, wR_2 = 0.1600
Largest diff. peak/hole / e Å^{-3}	1.64/-1.02

Chapter 7

References

1. M. E. Fieser, M. R. MacDonald, B. T. Krull, J. E. Bates, J. W. Ziller, F. Furche and W. J. Evans, *J Am Chem Soc*, 2015, **137**, 369-382.
2. G. Wilkinson and J. M. Birmingham, *J Am Chem Soc*, 1954, **76**, 6210-6210.
3. G. Wilkinson, M. Rosenblum, M. C. Whiting and R. B. Woodward, *J Am Chem Soc*, 1952, **74**, 2125-2126.
4. M. F. Lappert and R. Pearce, *J Am Chem Soc, Chem Comm*, 1973, 126-126.
5. H. Schumann, D. M. M. Freckmann and S. Dechert, *Z anorg allg Chem*, 2002, **628**, 2422-2426.
6. J. D. Masuda, K. C. Jantunen, B. L. Scott and J. L. Kiplinger, *Organometallics*, 2008, **27**, 1299-1304.
7. J. D. Masuda, K. C. Jantunen, O. V. Ozerov, K. J. T. Noonan, D. P. Gates, B. L. Scott and J. L. Kiplinger, *J Am Chem Soc*, 2008, **130**, 2408-2409.
8. K. C. Jantunen, B. L. Scott, P. J. Hay, J. C. Gordon and J. L. Kiplinger, *J Am Chem Soc*, 2006, **128**, 6322-6323.
9. K. R. D. Johnson and P. G. Hayes, *Organometallics*, 2013, **32**, 4046-4049.
10. J.-L. Liu, Y.-C. Chen, Y.-Z. Zheng, W.-Q. Lin, L. Ungur, W. Wernsdorfer, L. F. Chibotaru and M.-L. Tong, *Chem Sci*, 2013, **4**, 3310-3316.
11. J. Liu, Y.-C. Chen, J.-L. Liu, V. Vieru, L. Ungur, J.-H. Jia, L. F. Chibotaru, Y. Lan, W. Wernsdorfer, S. Gao, X.-M. Chen and M.-L. Tong, *J Am Chem Soc*, 2016, **138**, 5441-5450.
12. Y.-C. Chen, J.-L. Liu, L. Ungur, J. Liu, Q.-W. Li, L.-F. Wang, Z.-P. Ni, L. F. Chibotaru, X.-M. Chen and M.-L. Tong, *J Am Chem Soc*, 2016, **138**, 2829-2837.
13. M. Zimmermann and R. Anwander, *Chem Rev*, 2010, **110**, 6194-6259.
14. T. M. Cameron, J. C. Gordon and B. L. Scott, *Organometallics*, 2004, **23**, 2995-3002.
15. T. M. Cameron, J. C. Gordon, B. L. Scott and W. Tumas, *Chem Comm*, 2004, 1398-1399.
16. D. Cui, M. Nishiura and Z. Hou, *Angew Chem Int Ed*, 2005, **44**, 959-962.
17. P. L. Watson, *J Chem Soc, Chem Commun*, 1983, 276-277.
18. C. L. Webster, J. W. Ziller and W. J. Evans, *Organometallics*, 2014, **33**, 433-436.
19. P. L. Watson, *J Am Chem Soc*, 1983, **105**, 6491-6493.
20. W. J. Evans, J. M. Perotti and J. W. Ziller, *J Am Chem Soc*, 2005, **127**, 3894-3909.
21. M. R. MacDonald, R. R. Langeslay, J. W. Ziller and W. J. Evans, *J Am Chem Soc*, 2015, **137**, 14716-14725.
22. M. E. Thompson, S. M. Baxter, A. R. Bulls, B. J. Burger, M. C. Nolan, B. D. Santarsiero, W. P. Schaefer and J. E. Bercaw, *J Am Chem Soc*, 1987, **109**, 203-219.
23. W. J. Evans, T. A. Ulibarri and J. W. Ziller, *J Am Chem Soc*, 1990, **112**, 2314-2324.
24. W. J. Evans, S. A. Kozimor, J. C. Brady, B. L. Davis, G. W. Nyce, C. A. Seibel, J. W. Ziller and R. J. Doedens, *Organometallics*, 2005, **24**, 2269-2278.
25. W. J. Evans, S. E. Lorenz and J. W. Ziller, *Chem Comm*, 2007, 4662-4664.
26. S. Demir, T. J. Mueller, J. W. Ziller and W. J. Evans, *Organometallics*, 2011, **30**, 3083-3089.
27. W. J. Evans, C. A. Seibel and J. W. Ziller, *J Am Chem Soc*, 1998, **120**, 6745-6752.
28. C. J. Weiss and T. J. Marks, *Dalton Trans*, 2010, **39**, 6576-6588.
29. D. G. H. Ballard, A. Courtis, J. Holton, J. McMeeking and R. Pearce, *J Am Chem Soc, Chem Comm*, 1978, 994-995.
30. P. L. Watson and D. C. Roe, *J Am Chem Soc*, 1982, **104**, 6471-6473.
31. P. L. Watson, *J Am Chem Soc*, 1982, **104**, 337-339.
32. J. Gromada, J.-F. Carpentier and A. Mortreux, *Coord Chem Rev*, 2004, **248**, 397-410.
33. K. H. Den Haan, Y. Wielstra, J. J. W. Eshuis and J. H. Teuben, *J Organomet Chem*, 1987, **323**, 181-192.

34. C. P. Casey, J. A. Tunge, T.-Y. Lee and M. A. Fagan, *J Am Chem Soc*, 2003, **125**, 2641-2651.
35. G. Jeske, H. Lauke, H. Mauermann, P. N. Swepston, H. Schumann and T. J. Marks, *J Am Chem Soc*, 1985, **107**, 8091-8103.
36. J.-F. Pelletier, A. Mortreux, X. Olonde and K. Bujadoux, *Angew Chem Int Ed*, 1996, **35**, 1854-1856.
37. L. Lukesova, B. D. Ward, S. Bellemin-Laponnaz, H. Wadepohl and L. H. Gade, *Dalton Trans*, 2007, 920-922.
38. Z. Jian, D. Cui and Z. Hou, *Chem Eur J*, 2012, **18**, 2674-2684.
39. K. N. Harrison and T. J. Marks, *J Am Chem Soc*, 1992, **114**, 9220-9221.
40. P.-F. Fu, L. Brard, Y. Li and T. J. Marks, *J Am Chem Soc*, 1995, **117**, 7157-7168.
41. S. D. Wobser, C. J. Stephenson, M. Delferro and T. J. Marks, *Organometallics*, 2013, **32**, 1317-1327.
42. R. A. Layfield, J. J. W. McDouall, S. A. Sulway, F. Tuna, D. Collison and R. E. P. Winpenny, *Chem Eur J*, 2010, **16**, 4442-4446.
43. J. D. Rinehart and J. R. Long, *Chem Sci*, 2011, **2**, 2078-2085.
44. R. A. Layfield, *Organometallics*, 2014, **33**, 1084-1099.
45. O. Kahn, *Molecular magnetism*, Wiley-VCH Verlag GmbH & Co. KGaA, 1994.
46. D. Gatteschi, *Molecular Nanomagnets*, Oxford University Press, 2006.
47. F. Tuna, C. A. Smith, M. Bodensteiner, L. Ungur, L. F. Chibotaru, E. J. L. McInnes, R. E. P. Winpenny, D. Collison and R. A. Layfield, *Angew Chem Int Ed*, 2012, **51**, 6976-6980.
48. T. Pugh, F. Tuna, L. Ungur, D. Collison, E. J. L. McInnes, L. F. Chibotaru and R. A. Layfield, *Nat Comms*, 2015, **6**, 7492.
49. T. Pugh, A. Kerridge and R. A. Layfield, *Angew Chem Int Ed*, 2015, **54**, 4255-4258.
50. T. Pugh, V. Vieru, L. F. Chibotaru and R. A. Layfield, *Chem Sci*, 2016, **7**, 2128-2137.
51. T. Pugh, N. F. Chilton and R. A. Layfield, *Chem Sci*, 2017.
52. T. Pugh, N. F. Chilton and R. A. Layfield, *Angew Chem Int Ed*, 2016, **55**, 11082-11085.
53. M. P. Blake, N. Kaltsoyannis and P. Mountford, *J Am Chem Soc*, 2011, **133**, 15358-15361.
54. S. Demir, J. M. Zadrozny, M. Nippe and J. R. Long, *J Am Chem Soc*, 2012, **134**, 18546-18549.
55. S. Demir, M. Nippe, M. I. Gonzalez and J. R. Long, *Chem Sci*, 2014, **5**, 4701-4711.
56. E. O. Fischer and H. Fischer, *Angew Chem Int Ed*, 1964, **3**, 132-133.
57. E. O. Fischer and H. Fischer, *J Organomet Chem*, 1965, **3**, 181-187.
58. W. Klemm, *Z anorg allg Chem*, 1929, **184**, 345-351.
59. W. Klemm and W. Schüth, *Z anorg allg Chem*, 1929, **184**, 352-358.
60. P. Girard, J. L. Namy and H. B. Kagan, *J Am Chem Soc*, 1980, **102**, 2693-2698.
61. H. B. Kagan, J. L. Namy and P. Girard, *Tetrahedron*, 1981, **37**, 175-180.
62. J. L. Namy, J. Souppe and H. B. Kagan, *Tetrahedron Lett*, 1983, **24**, 765-766.
63. J. Souppe, L. Danon, J. L. Namy and H. B. Kagan, *J Organomet Chem*, 1983, **250**, 227-236.
64. W. J. Evans, T. S. Gummersheimer and J. W. Ziller, *J Am Chem Soc*, 1995, **117**, 8999-9002.
65. M. N. Bochkarev, I. L. Fedushkin, A. A. Fagin, T. V. Petrovskaya, J. W. Ziller, R. N. R. Broomhall-Dillard and W. J. Evans, *Angew Chem Int Ed*, 1997, **36**, 133-135.
66. M. N. Bochkarev and A. A. Fagin, *Chem Eur J*, 1999, **5**, 2990-2992.
67. M. N. Bochkarev, I. L. Fedushkin, S. Dechert, A. A. Fagin and H. Schumann, *Angew Chem Int Ed*, 2001, **40**, 3176-3178.
68. W. J. Evans, N. T. Allen and J. W. Ziller, *J Am Chem Soc*, 2000, **122**, 11749-11750.

69. D. H. Woen, G. P. Chen, J. W. Ziller, T. J. Boyle, F. Furche and W. J. Evans, *Angew Chem Int Ed*, 2017, **56**, 2050-2053.
70. F. Nief, D. Turcitu and L. Ricard, *Chem Comm*, 2002, 1646-1647.
71. F. Jaroschik, F. Nief and L. Ricard, *Chem Comm*, 2006, 426-428.
72. M. C. Cassani, D. J. Duncalf and M. F. Lappert, *J Am Chem Soc*, 1998, **120**, 12958-12959.
73. M. C. Cassani, Y. K. Gun'ko, P. B. Hitchcock and M. F. Lappert, *Chem Commun*, 1996, 1987-1988.
74. P. B. Hitchcock, M. F. Lappert, L. Maron and A. V. Protchenko, *Angew Chem Int Ed*, 2008, **47**, 1488-1491.
75. M. R. MacDonald, J. W. Ziller and W. J. Evans, *J Am Chem Soc*, 2011, **133**, 15914-15917.
76. W. J. Evans, M. Fang, G. Zucchi, F. Furche, J. W. Ziller, R. M. Hoekstra and J. I. Zink, *J Am Chem Soc*, 2009, **131**, 11195-11202.
77. M. R. MacDonald, J. E. Bates, M. E. Fieser, J. W. Ziller, F. Furche and W. J. Evans, *J Am Chem Soc*, 2012, **134**, 8420-8423.
78. M. R. MacDonald, J. E. Bates, J. W. Ziller, F. Furche and W. J. Evans, *J Am Chem Soc*, 2013, **135**, 9857-9868.
79. C. M. Kotyk, M. R. MacDonald, J. W. Ziller and W. J. Evans, *Organometallics*, 2015, **34**, 2287-2295.
80. P. Voth, S. Arndt, T. P. Spaniol, J. Okuda, L. J. Ackerman and M. L. H. Green, *Organometallics*, 2003, **22**, 65-76.
81. Y. Li, C. Pi, J. Zhang, X. Zhou, Z. Chen and L. Weng, *Organometallics*, 2005, **24**, 1982-1988.
82. H. Schumann and G. Jeske, *Angew Chem Int Ed*, 1985, **24**, 225-226.
83. M. Adam, U. Behrens and R. D. Fischer, *Acta Cryst C*, 1991, **47**, 968-971.
84. H. M. Dietrich, C. Zapilko, E. Herdtweck and R. Anwander, *Organometallics*, 2005, **24**, 5767-5771.
85. K. H. den Haan and J. H. Teuben, *J Chem Soc, Chem Comm*, 1986, 682-683.
86. S. E. Lorenz, B. M. Schmiege, D. S. Lee, J. W. Ziller and W. J. Evans, *Inorg Chem*, 2010, **49**, 6655-6663.
87. M. D. Rausch and D. J. Ciappenelli, *J Organomet Chem*, 1967, **10**, 127-136.
88. H. Gornitzka, A. Steiner, D. Stalke, U. Kilimann, F. T. Edelmann, K. Jacob and K.-H. Thiele, *J Organomet Chem*, 1992, **439**, C6-C10.
89. K. Jacob, I. Pavlik and F. T. Edelmann, *Z anorg allg Chem*, 1993, **619**, 1957-1961.
90. K. Jacob, M. Schäfer, A. Steiner, G. M. Sheldrick and F. T. Edelmann, *J Organomet Chem*, 1995, **487**, C18-C20.
91. W. Clegg, E. Crosbie, S. H. Dale-Black, E. Hevia, G. W. Honeyman, A. R. Kennedy, R. E. Mulvey, D. L. Ramsay and S. D. Robertson, *Organometallics*, 2015, **34**, 2580-2589.
92. W. Clegg, K. W. Henderson, A. R. Kennedy, R. E. Mulvey, C. T. O'Hara, R. B. Rowlings and D. M. Tooke, *Angew Chem Int Ed*, 2001, **40**, 3902-3905.
93. P. L. Arnold and S. T. Liddle, *Chem Comm*, 2006, 3959-3971.
94. S. Long, B. Wang, H. Xie, C. Yao, C. Wu and D. Cui, *New J Chem*, 2015, **39**, 7682-7687.
95. A. J. Arduengo, M. Tamm, S. J. McLain, J. C. Calabrese, F. Davidson and W. J. Marshall, *J Am Chem Soc*, 1994, **116**, 7927-7928.
96. T. Mehdoui, J.-C. Berthet, P. Thuery and M. Ephritikhine, *Chem Comm*, 2005, 2860-2862.
97. P. L. Arnold and I. J. Casely, *Chem Rev*, 2009, **109**, 3599-3611.

98. Z. R. Turner, R. Bellabarba, R. P. Tooze and P. L. Arnold, *J Am Chem Soc,* 2010, **132**, 4050-4051.
99. P. L. Arnold, Z. R. Turner, R. Bellabarba and R. P. Tooze, *J Am Chem Soc*, 2011, **133**, 11744-11756.
100. P. L. Arnold, Z. R. Turner, A. I. Germeroth, I. J. Casely, G. S. Nichol, R. Bellabarba and R. P. Tooze, *Dalton Trans*, 2013, **42**, 1333-1337.
101. Y. Wang, Y. Xie, M. Y. Abraham, P. Wei, H. F. Schaefer, P. v. R. Schleyer and G. H. Robinson, *J Am Chem Soc*, 2010, **132**, 14370-14372.
102. R. A. Musgrave, R. S. P. Turbervill, M. Irwin and J. M. Goicoechea, *Angew Chem*, 2012, **124**, 10990-10993.
103. R. A. Musgrave, R. S. P. Turbervill, M. Irwin, R. Herchel and J. M. Goicoechea, *Dalton Trans*, 2014, **43**, 4335-4344.
104. D. R. Armstrong, S. E. Baillie, V. L. Blair, N. G. Chabloz, J. Diez, J. Garcia-Alvarez, A. R. Kennedy, S. D. Robertson and E. Hevia, *Chem Sci*, 2013, **4**, 4259-4266.
105. A. J. Martínez-Martínez, M. Á. Fuentes, A. Hernán-Gómez, E. Hevia, A. R. Kennedy, R. E. Mulvey and C. T. O'Hara, *Angew Chem Int Ed*, 2015, **54**, 14075-14079.
106. P. L. Arnold, I. J. Casely, Z. R. Turner and C. D. Carmichael, *Chem Eur J*, 2008, **14**, 10415-10422.
107. W. Fegler, T. P. Spaniol and J. Okuda, *Dalton Trans*, 2010, **39**, 6774-6779.
108. W. Fegler, T. Saito, K. Mashima, T. P. Spaniol and J. Okuda, *J Organomet Chem*, 2010, **695**, 2794-2797.
109. Z. Mo, D. Chen, X. Leng and L. Deng, *Organometallics*, 2012, **31**, 7040-7043.
110. Z. Ouyang and L. Deng, *Organometallics*, 2013, **32**, 7268-7271.
111. C. E. Cooke, M. C. Jennings, R. K. Pomeroy and J. A. C. Clyburne, *Organometallics*, 2007, **26**, 6059-6062.
112. G. C. Fortman, N. M. Scott, A. Linden, E. D. Stevens, R. Dorta and S. P. Nolan, *Chem Comm*, 2010, **46**, 1050-1052.
113. M. Nishio, *CrystEngComm*, 2004, **6**, 130-158.
114. P. L. Arnold and S. T. Liddle, *Organometallics*, 2006, **25**, 1485-1491.
115. B. M. Day, T. Pugh, D. Hendriks, C. F. Guerra, D. J. Evans, F. M. Bickelhaupt and R. A. Layfield, *J Am Chem Soc*, 2013, **135**, 13338-13341.
116. M. Uzelac, A. Hernan-Gomez, D. R. Armstrong, A. R. Kennedy and E. Hevia, *Chem Sci*, 2015, **6**, 5719-5728.
117. G. Schnee, O. Nieto Faza, D. Specklin, B. Jacques, L. Karmazin, R. Welter, C. Silva López and S. Dagorne, *Chem Eur J*, 2015, **21**, 17959-17972.
118. H.-X. Li, Y.-J. Zhu, M.-L. Cheng, Z.-G. Ren, J.-P. Lang and Q. Shen, *Coord Chem Rev*, 2006, **250**, 2059-2092.
119. W. J. Evans, G. W. Rabe, M. A. Ansari and J. W. Ziller, *Angew Chem Int Ed*, 1994, **33**, 2110-2111.
120. W. J. Evans, G. W. Rabe, J. W. Ziller and R. J. Doedens, *Inorg Chem*, 1994, **33**, 2719-2726.
121. J. H. Melman, T. J. Emge and J. G. Brennan, *Chem Comm*, 1997, 2269-2270.
122. D. Freedman, T. J. Emge and J. G. Brennan, *J Am Chem Soc*, 1997, **119**, 11112-11113.
123. D. R. Cary, G. E. Ball and J. Arnold, *J Am Chem Soc*, 1995, **117**, 3492-3501.
124. Z.-X. Zhang, Y.-R. Li, R.-T. Liu, Z.-X. Chen, L.-H. Weng and X.-G. Zhou, *Polyhedron*, 2007, **26**, 4986-4992.
125. M.-L. Cheng, H.-X. Li, W.-H. Zhang, Z.-G. Ren, Y. Zhang and J.-P. Lang, *Eur J Inorg Chem,* 2007, **2007**, 1889-1896.
126. M. Kuhling, R. McDonald, P. Liebing, L. Hilfert, M. J. Ferguson, J. Takats and F. T. Edelmann, *Dalton Trans*, 2016, **45**, 10118-10121.

127. F. Zhang, J. Zhang and X. Zhou, *Inorg Chem*, 2017, **56**, 2070-2077.
128. D. E. Smiles, G. Wu and T. W. Hayton, *Inorg Chem*, 2014, **53**, 12683-12685.
129. D. E. Smiles, G. Wu and T. W. Hayton, *Inorg Chem*, 2016, **55**, 9150-9153.
130. J. F. Corbey, M. Fang, J. W. Ziller and W. J. Evans, *Inorg Chem*, 2015, **54**, 801-807.
131. D. N. Woodruff, F. Tuna, M. Bodensteiner, R. E. P. Winpenny and R. A. Layfield, *Organometallics*, 2013, **32**, 1224-1229.
132. C. R. Ganivet, B. Ballesteros, G. de la Torre, J. M. Clemente-Juan, E. Coronado and T. Torres, *Chem Eur J*, 2013, **19**, 1457-1465.
133. L. F. Chibotaru, L. Ungur and A. Soncini, *Angew Chem Int Ed*, 2008, **47**, 4126-4129.
134. L. Ungur, S.-Y. Lin, J. Tang and L. F. Chibotaru, *Chem Soc Rev*, 2014, **43**, 6894-6905.
135. L. Ungur, S. K. Langley, T. N. Hooper, B. Moubaraki, E. K. Brechin, K. S. Murray and L. F. Chibotaru, *J Am Chem Soc*, 2012, **134**, 18554-18557.
136. A. Cornia, D. Gatteschi and R. Sessoli, *Coord Chem Rev*, 2001, **219**, 573-604.
137. P.-H. Guo, J.-L. Liu, Z.-M. Zhang, L. Ungur, L. F. Chibotaru, J.-D. Leng, F.-S. Guo and M.-L. Tong, *Inorg Chem*, 2012, **51**, 1233-1235.
138. J. Tang, I. Hewitt, N. T. Madhu, G. Chastanet, W. Wernsdorfer, C. E. Anson, C. Benelli, R. Sessoli and A. K. Powell, *Angew Chem Int Ed*, 2006, **45**, 1729-1733.
139. Y.-X. Wang, W. Shi, H. Li, Y. Song, L. Fang, Y. Lan, A. K. Powell, W. Wernsdorfer, L. Ungur, L. F. Chibotaru, M. Shen and P. Cheng, *Chem Sci*, 2012, **3**, 3366-3370.
140. G. Novitchi, G. Pilet, L. Ungur, V. V. Moshchalkov, W. Wernsdorfer, L. F. Chibotaru, D. Luneau and A. K. Powell, *Chem Sci*, 2012, **3**, 1169-1176.
141. I. J. Hewitt, J. Tang, N. T. Madhu, C. E. Anson, Y. Lan, J. Luzon, M. Etienne, R. Sessoli and A. K. Powell, *Angew Chem Int Ed*, 2010, **49**, 6352-6356.
142. S.-Y. Lin, W. Wernsdorfer, L. Ungur, A. K. Powell, Y.-N. Guo, J. Tang, L. Zhao, L. F. Chibotaru and H.-J. Zhang, *Angew Chem Int Ed*, 2012, **51**, 12767-12771.
143. X.-L. Li, J. Wu, J. Tang, B. Le Guennic, W. Shi and P. Cheng, *Chem Comm*, 2016, **52**, 9570-9573.
144. S. Biswas, S. Das, T. Gupta, S. K. Singh, M. Pissas, G. Rajaraman and V. Chandrasekhar, *Chem Eur J*, 2016, **22**, 18532-18550.
145. C. Das, S. Vaidya, T. Gupta, J. M. Frost, M. Righi, E. K. Brechin, M. Affronte, G. Rajaraman and M. Shanmugam, *Chem Eur J*, 2015, **21**, 15639-15650.
146. S. Kitagawa and S. Masaoka, *Coord Chem Rev*, 2003, **246**, 73-88.
147. S. R. Marshall, A. L. Rheingold, L. N. Dawe, W. W. Shum, C. Kitamura and J. S. Miller, *Inorg Chem*, 2002, **41**, 3599-3601.
148. J. R. Galan-Mascaros and K. R. Dunbar, *Chem Comm*, 2001, 217-218.
149. H. Grove, J. Sletten, M. Julve and F. Lloret, *J Chem Soc, Dalton Trans*, 2001, 1029-1034.
150. P. S. Szalay, J. R. Galán-Mascarós, B. L. Schottel, J. Bacsa, L. M. Pérez, A. S. Ichimura, A. Chouai and K. R. Dunbar, *Journal of Cluster Science*, 2004, **15**, 503-530.
151. J. O. Moilanen, B. M. Day, T. Pugh and R. A. Layfield, *Chem Comm*, 2015, **51**, 11478-11481.
152. J. O. Moilanen, N. F. Chilton, B. M. Day, T. Pugh and R. A. Layfield, *Angew Chem Int Ed*, 2016, **55**, 5521-5525.
153. R. Grindell, V. Vieru, T. Pugh, L. F. Chibotaru and R. A. Layfield, *Dalton Trans*, 2016, **45**, 16556-16560.
154. K. Qian, J. J. Baldovi, S.-D. Jiang, A. Gaita-Arino, Y.-Q. Zhang, J. Overgaard, B.-W. Wang, E. Coronado and S. Gao, *Chem Sci*, 2015, **6**, 4587-4593.
155. G.-J. Chen, C.-Y. Gao, J.-L. Tian, J. Tang, W. Gu, X. Liu, S.-P. Yan, D.-Z. Liao and P. Cheng, *Dalton Trans*, 2011, **40**, 5579-5583.
156. S. C. M. Calculation, *version 2.1*, Universitat de Barcelona, **2013**.
157. V. Vieru, L. Ungur and L. F. Chibotaru, *J Phys Chem Lett*, 2013, **4**, 3565-3569.

158. R. Layfield, F.-S. Guo, B. Day, Y.-C. Chen, M.-L. Tong and A. Mansikamäkki, *Angew Chem Int Ed*, 2017, Accepted article.
159. J. D. Rinehart, M. Fang, W. J. Evans and J. R. Long, *J Am Chem Soc*, 2011, **133**, 14236-14239.
160. L. T. Reynolds and G. Wilkinson, *J Inorg Nucl Chem*, 1959, **9**, 86-92.
161. X. Bantreil and S. P. Nolan, *Nat. Protocols*, 2011, **6**, 69-77.
162. J. W. Runyon, O. Steinhof, H. V. R. Dias, J. C. Calabrese, W. J. Marshall and A. J. Arduengo, *Aust J Chem*, 2011, **64**, 1165-1172.
163. S. Barlow, Q. Zhang, B. R. Kaafarani, C. Risko, F. Amy, C. K. Chan, B. Domercq, Z. A. Starikova, M. Y. Antipin, T. V. Timofeeva, B. Kippelen, J.-L. Brédas, A. Kahn and S. R. Marder, *Chem Eur J*, 2007, **13**, 3537-3547.
164. G. M. Sheldrick, *Acta Cryst C, Struct Chem*, 2015, **71**, 3-8.
165. G. Sheldrick, *Acta Cryst A*, 2015, **71**, 3-8.
166. O. V. Dolomanov, L. J. Bourhis, R. J. Gildea, J. A. K. Howard and H. Puschmann, *J Appl Crystallogr*, 2009, **42**, 339-341.
167. F. Aquilante, J. Autschbach, R. K. Carlson, L. F. Chibotaru, M. G. Delcey, L. De Vico, I. Fdez. Galván, N. Ferré, L. M. Frutos, L. Gagliardi, M. Garavelli, A. Giussani, C. E. Hoyer, G. Li Manni, H. Lischka, D. Ma, P. Å. Malmqvist, T. Müller, A. Nenov, M. Olivucci, T. B. Pedersen, D. Peng, F. Plasser, B. Pritchard, M. Reiher, I. Rivalta, I. Schapiro, J. Segarra-Martí, M. Stenrup, D. G. Truhlar, L. Ungur, A. Valentini, S. Vancoillie, V. Veryazov, V. P. Vysotskiy, O. Weingart, F. Zapata and R. Lindh, *J Comput Chem*, 2016, **37**, 506-541.